Origin of cranial sensory systems

By

Matthew N. McCarroll

A THESIS/DISSERTATION

Presented to the Department of Cell and Developmental Biology
and the Oregon Health & Science University
School of Medicine
in partial fulfillment of
the requirements for the degree of

Doctor of Philosophy

(January, 2014)

School of Medicine
Oregon Health & Science University
CERTIFICATE OF APPROVAL

_____

This is to certify that the PhD dissertation of

Matthew N. McCarroll has been approved

_____
Mentor/Advisor (Dr. Alex Nechiporuk)

_____
Member (Dr. Melissa Wong)

_____
Member (Dr. John Brigande)

_____
Member (Dr. Bruce Schnapp)

_____
Member (Dr. Mary Logan)

Table of Contents

LIST OF ABBREVIATIONS

AP –	**Anterior to posterior axis**
BAC –	**Bacterial artificial chromosome**
BMP –	**Bone morphogenetic protein**
CNS –	**Central nervous system**
Dsh –	**Disheveled**
Dkk -	**Dikkoph**
DV –	**Dorsal to ventral axis**
EB –	**Epibranchial**
EMT-	**Epithelial to mesenchymal transition**
ESC-	**Embryonic stem cell**
Fgf –	**Fibroblast growth factor**
gAll –	**Anterior lateral line ganglia**
GnRH –	**Gonadotrophin releasing hormone**
gVIII –	**Acoustic ganglia**
hESC-	**Human embryonic stem cell**
Hh -	**Hedgehog**
hiPSC-	**Human induced pluripotent stem cell**
hpf –	**Hours post fertilization**
MHB –	**Midbrain hindbrain boundary**
MO –	**Morphilino**
neurog –	**Neurogenin**
NLS –	**Nuclear localization signal**

NNE – **Non-neural ectoderm**

OEPD – **Otic epibranchial placode domain**

PDGF – **Platelet derived growth factor**

PKC – **Protein kinase c**

PNS – **Peripheral nervous system**

PPA – **Posterior placodal area**

PPE – **Pan-placodal ectoderm**

RA – **Retinoic acid**

SAG – **Statoacoustic ganglion**

Shh – **Sonic hedgehog**

LIST OF FIGURES

ACKNOWLEDGEMENTS

I would like to thank my thesis advisor Dr. Alex Nechiporuk for his continuous help and commitment to the success of my projects, scientific development, and future career. I would also like to thank members of my thesis committee: Dr. Melissa Wong (chair), Dr. John Brigande, and Dr. Bruce Schnapp for their knowledgeable input and encouragement throughout my graduate training. I would like to acknowledge ad hoc member Dr. Mary Logan for her contribution reviewing and providing useful criticism of my academic work. I would like to thank the current Nechiporuk lab members: Molly Harding, Hillary McGraw, Catherine Drerup, Austin Forbes and Chris Riso for all creating a dynamic, friendly, productive environment in which I have been able to hone my skills in research, scientific writing, presentations, and journal clubs. I would also like to thank former lab members, and co-authors: Zack Lewis and Maya Culbertson, both contributing to the material in Chapter 3 of this dissertation, for their continued support and friendship. Their hard work and dedication to scientific research has been a huge influence on my own approach to life science. I would like to exhibit a special thanks to my colleague and good friend Jude Parman for critical discussions pertaining to developmental and neurological processes. This dissertation is dedicated to my father, Nicholas F. McCarroll who passed away too soon while I was in graduate school.

ABSTRACT

In the developing vertebrate head, essential structures that constitute the paired sensory organs arise from discrete regions of sensory epithelium, known as cranial placodes. These regions reside outside the axial ectoderm of the forming central nervous system (CNS). Cranial placodes are morphologically defined as transient ectodermal thickenings, with columnar or pseudostratified epithelial cell morphology; on a molecular level, placodal cells exhibit a unique expression profile of transcription factors. Through physical interactions with neighboring tissues and in response to extrinsic signals, cells of the ectodermal placodes delaminate and/or invaginate to form structures as diverse as the optic lens, the otic vesicle, and neurons of the cranial ganglia. My studies have focused on the more posterior placodes, the otic and epibranchial (EB) placodes. The otic placode gives rise to all inner ear structures, including the sensory epithelia and its associated neurons. The EB placodes form the sensory neurons of the EB ganglia, including the facial, glossopharyngeal, and vagal ganglia. EB neurons act as a relay for information from the sensory organs (e.g. taste buds of the gustatory system, baroreceptors of the heart, and sensory enteric nerves of the gut) to the CNS. Initially, the EB placode precursors are intermingled with other pan-placodal cell populations in a single domain called pan-placodal ectoderm (PPE). Subsequently, cells within this domain undergo multiple sorting steps in order to segregate into distinct placodes. The molecular and cellular mechanisms that govern the segregation and the subsequent migration of precursors are largely unknown. In zebrafish, precursors for the EB and otic

placodes segregate from the PPE and form a posterior domain called the posterior placodal area (PPA) shortly after gastrulation. This domain is marked by expression of the transcription factors Pax2a, Pax8, and Sox3. Specification of both the otic and EB placodes requires extrinsic signaling from Fibroblast growth factors (Fgf), which in turn controls Pax2a, Pax8 and Sox3 expression. In this work, we used lineage tracing and live imaging analyses to show that cells of the PPA become biased towards certain fates as early as 12 hours post fertilization (hpf). Ablation studies verified the requirement of the PPA to form the otic and EB placodes, and support a spatial correlation bias with final structure contribution. We also discovered that levels of Pax2a expression correlate to cell fate: high Pax2a+ cells segregate into the otic placode and low Pax2a+ cells segregate into the EB placodes. Pax2a overexpression and suboptimal morpholino knockdown of Pax2a together with Pax8 confirm that high levels of Pax expression bias cells towards an otic fate, while low levels of Pax expression bias cells toward an EB fate. Final, we found the Wnt signaling from the neural tube is responsible for inducing high levels of Pax2a in a subset of cells of the PPA to enforce an otic identity.

Once EB placode precursors segregate from the nascent otic placode, their subsequent differentiation requires continuous Fgf signaling. When Fgf receptor signaling is globally inactivated between 12 and 24 hpf the EB placodes are lost, while other placode derived structures (like the otic vesicle) remain relatively intact. Notably, activation of local Fgf signaling through Fgf ligand soaked beads implanted near forming EB placodes expands placodal Pax2a

expression. Analysis of various Fgf ligands during this critical period revealed that Fgf3 and Fgf10a are responsible for maturation of the EB placodes. Injection of *fgf10a* morpholino in *fgf3*-/- embryos resulted in loss of the EB placodes as marked by Pax2a and *sox3*, a reduction in the glossopharyngeal and vagal placodes at 24 hpf, and a loss of the respective ganglia at 72 hpf. Loss of Fgf3/10a did not result in an otic deficit, indicating a process specific to EB placode development. We find that the endoderm is the tissue source of Fgf3 responsible for EB placode maturation, and provide evidence that the lateral line system and possibly the anterior otic vesicle is the signaling center of Fgf10a. Our studies contribute to a better understanding of sensory organ development and early neural progenitor cell induction and specification in a unique setting outside of the CNS.

CHAPTER 1: INTRODUCTION

Chapter 1.5 modified from: Harding, M. J., McCarroll, M. N., McGraw, H. F. and Nechiporuk, A. V. (2013). Ear and Lateral line Development of Vertebrates: Organization and Development. *Encyclopedia of Life Sciences.*

1.1 Placodes are innovations of the vertebrate head

During the course of evolution, innovations to the body plan of Chordates have arisen in response to the increasing demand for survival. As animals progressed from simple filter feeders to active predation, new anatomical features evolved to accommodate a new existence. This predatory feeding behavior appears to have been favored by evolution, given that Vertebrates are the overwhelming majority of the phylum Chordata. Members of this subphylum are uniquely endowed with anatomical advancements enabling their participation and survival in the predatory world. The Vertebrate posses a highly specialized head containing an elaborate brain (composed of a forebrain, midbrain and hindbrain) enclosed in a skull of cartilage or bone and complex paired sensory organs such as the eyes, nose, and ears. Perhaps most interestingly, the latter of the aforementioned innovations to the vertebrate head arise from just two cell populations during embryonic development: the cranial placodes and the cranial neural crest.

The cranial placodes and the cranial neural crest are specialized regions of embryonic ectoderm that develop in close proximity to each other (near the neural plate border) and have potential to give rise to numerous different cell types, undergo complex cellular morphological changes, and have motile capacity. However, these cell populations both have their own unique cellular characteristics; the neural crest gives rise to a more extensive repertoire of tissues. While both placodes and neural crest contribute to secretory, mechanosensory, and neuronal cell types; the neural crest has less constraint on

its potency and can also give rise to cartilage, bone, smooth muscle, and pigment cells. In addition, the neural crest can give rise to glia including peripheral Schwann cells (Barraud et al., 2010); however, it is unclear whether placodes have the potential to form glial type cells (Harden et al., 2012; Ramón-Cueto and Avila, 1998).

The cranial placodes were first described in the late 1800's by classical embryologists: Drs. van Wihje, von Kupffer, Froriep, Beard, and Stone to name a few (Beard, 1885; Schlosser, 2006; von Kupffer, 1891). These placode pioneers focused on the development of the sensory organs including the cranial nerves and lateral line systems, describing their origins as intimate connections to the skin, "the participation of elements of the epidermis in the formation of the nerves might be regarded as certain" (Beard, 1885). Sensory ectodermal elements were morphologically described as a "thickened mass of epidermis that reaches deep into the ganglion so that the two cannot be definitely separated from each other" (Beard, 1885). These early accounts remain a valuable resource to the placode development field, describing the timing of placode formation across numerous different vertebrate species. However, they depended primarily on morphology and histological descriptions, which cannot explain early placodal specification and induction, or the molecular players involved during this process.

Despite early efforts to unravel the mystery of cranial placode development, these embryonic entities have been neglected. Recent discovery of intrinsic and extrinsic molecules involved in various stages of cranial placode development has initiated resurgence in interest and much progress has been made in the

field during the past 20 years. Currently, cranial placodes are defined as transient focal thickenings of embryonic ectoderm that contribute critical components to the paired sensory organs of the vertebrate head (Baker and Bronner-Fraser, 2001; Nechiporuk et al., 2006; Schlosser, 2006; Streit, 2004a). These structures are discrete entities, fully formed after the closure of the neural tube. These distinct placodes, named in approximate anterior to posterior order are: adenohypophysial, olfactory, lens, trigeminal, otic, epibranchial, hypobranchial (only described in amphibians), and a varying number of lateral line placodes (absent in terrestrial organisms; Figure 1). After formation, the placodes will undergo delamination, invagination, and/or morphological changes as they differentiate to contribute components to their respective tissues (Schlosser, 2006).

1.2 The Fgf and Wnt signaling pathways

Cellular signaling is a critical mechanism by which neighboring and distal tissues can communicate with each other to control transcriptional programs required to orchestrate the complexities of embryonic development, and to maintain normal function during adult homeostasis. The Wnt signaling pathway and the fibroblast growth factor (Fgf) signaling pathway are two of a small number of signaling pathways widely conserved throughout evolution and implemented repeatedly during the development of numerous morphologically and functionally distinct tissues (Itoh and Ornitz, 2004; Siegfried and Perrimon, 1994; Thisse and Thisse, 2005). With temporal and spatial precision, these

pathways can control a verity of cellular functions including changes in cell shape, endogenous transcriptional programs, cell migration, differentiation, proliferation, cell survival and/or apoptosis (Chien et al., 2009; Hoppler and Kavanagh, 2007; Itoh, 2007; Itoh and Konishi, 2007). In the adult organism these same pathways will control different aspects of tissue homeostasis and play a role in adult stem cell maintenance and differentiation (Hoppler and Kavanagh, 2007; Thisse and Thisse, 2005). It follows that perturbation of these signaling pathways can lead to a myriad of different pathologies including congenital defects and other diseases including cancer. We focus on how these pathways are used under normal developmental conditions to build sensory organs of the vertebrate head.

The first Wnt signaling pathway genes were discovered in two separate systems in the early 1980s. The Int-1 gene discovered by its preferential integration site of the murine mammary tumor virus in a mouse model of breast cancer and the wingless gene described as a segment polarity gene in *Drosophila* (Nusse and Varmus, 1982; Nüsslein-Volhard and Wieschaus, 1980). The resultant name “Wnt” is a fusion of these two names and refers to the extracellular ligands of the Wnt signaling module. The *Drosophila* animal model continued to be crucial for the discovery of many of the downstream signaling components of the Wnt pathway, while studies in Xenopus were instrumental for a further understanding of how these molecules act on the developing embryo (McMahon and Moon, 1989; Siegfried and Perrimon, 1994). A brief summary of canonical Wnt signaling is as follows: the canonical Wnt signaling pathway is

activated through the binding of the Wnt ligand to the single pass transmembrane protein LRP5/6 and the 7 pass transmembrane protein Frizzled to activate cytoplasmic Disheveled (Dvl). In the absence of active Wnt signaling cytoplasmic β-catenin is targeted for degradation by phosphorylation of Gsk3β a component of the β-catenin destruction complex. During active Wnt signaling, Dvl can phosphorylate and inhibit Gsk3β activity thus allowing accumulation of cytoplasmic β-catenin which subsequently translocates to the nucleus and forms the β-catenin-Tcf/Lef complex to activate Wnt responsive genes (Figure 2) (Hoppler and Kavanagh, 2007).

Regulation of the Wnt signaling pathway occurs at multiple levels. At the extracellular level, the secreted factors of the Dikkoph (Dkk) family can bind to the membrane proteins Kremen and LRP5/6 to inhibit Wnt signaling by blocking Wnt induced Frizzled/LRP6 complex formation (Wang et al., 2008). Also the Wnt signaling core complex (Tcf/Lef) has multiple different family members each with different isoforms that all affect their transcriptional role to provide various outcomes during Wnt signaling (Hoppler and Kavanagh, 2007). These core complex proteins are also amenable to various posttranslational modifications including SUMOylation (a ubiquitination like mechanism) to mediate nuclear and subnuclear localization (Yamamoto et al., 2003). The cytoplasmic molecular gateway to the canonical Wnt signaling pathway is β-catenin, which in itself is a complex protein capable of many different functions. In addition to its role in Wnt signal transduction, β-catenin is critical component of adherens junctions, where it can tether transmembrane cadherins to the actin cytoskeleton via α-catenin

(Figure 2) (Valenta et al., 2012). In this context β-catenin is positioned to act as a mechanical sensor to respond to changes in tension force imposed on the cell by changes in its immediate surroundings. The Hippo pathway is a critical regulator of cell and tissue size. Cross talk between the Wnt pathway and the Hippo pathway has been demonstrated where β-catenin interacts with the Hippo effector YAP to integrate developmental programs with control of tissue size (Tsai et al., 2012).

The first Fgf ligands to be discovered (Fgf1 and Fgf2) were purified from brain tissue. These factors were initially described for their mitogenic influence on cultured fibroblast cells (Gospodarowicz and Moran, 1975). Since this time, Fgfs and their receptors have been described to be important during numerous biological processes, and misregulated in many diseases including cancer (Itoh, 2007). The influence that these factors have on cells goes beyond the initially described mitogenic effects. Fgf signaling can also control cell fate specification, cell survival, cell motility, and cell shape.

Fgf ligands are conserved throughout all multicellular organisms, however single cell organisms such as E. Coli and S. cerevisiae do not posses Fgf like genes. The human and mouse Fgf gene family is comprised of 22 genes, with 4 Fgf receptors (Fgfr). All of these Fgf ligands with exception of Fgf11-14 function extracellularly by binding to activate the cell surface tyrosine kinase Fgfrs (Goldfarb, 2005). Fgf11-14 function intracellularly independent of Fgfrs (Goldfarb, 2005). The zebrafish genome contains homologues of all the known human Fgfs with exception of Fgf9. In addition the zebrafish genome contains at least 27 Fgf

members; this excess of Fgf genes is partially due to the zebrafish partial genome duplication resulting in occasional “a” and “b” paralogs (Itoh and Konishi, 2007). All the ligands in the Fgf family contain a homologous core amino acid sequence, flanked by variable C and N-terminal ends. Upon binding of the Fgf ligand to the receptor, dimerization of two tyrosine kinase receptors followed by trans phosphorylation of specific intracellular tyrosine residues is required for activation of cytoplasmic signal transduction pathways including the Akt pathway, protein kinase C (PKC) pathways, or the Ras/ERK pathway (Thisse and Thisse, 2005). While the end result of Fgf signaling will vary depending on context, expression of its direct transcriptional targets, Pea3 and Erm, is indicative of an active Fgf pathway (Raible and Brand, 2001). A simplified summary of the Fgf signaling pathway is illustrated in Figure 3.

Fgf signaling is known to instruct an overwhelming number of biological processes, and depending on context the same signaling pathway can be reiterated continuously to result in incredibly diverse outcomes. The 22 (more or less depending on species) different Fgf ligands and the 4 receptors alone are not responsible for this magnitude of outcomes (Itoh, 2007). Activation of both the tyrosine kinase receptors and the ligands are reliant on heparin sulfate binding, and the ligands are post-translationally modified through different glycosylation states making this mode of cell signaling highly dependent on the cell’s surrounding milieu and varying modifications to the ligand (Burgess and Maciag, 1989). Thus fine-tuning of this pathway occurs even at the level of tissue environment before the pathway has even been activated. Modifications of the 4

different receptors also occur, by alternative splicing of receptor mRNA, resulting in “b” and “c” isoforms changing the composition of the extracellular Ig domains; this gives added specificity of the receptor to discrete ligands (Zhang et al., 2006). In addition, different combinations of Fgfrs can dimerize, adding another level of regulation (Belov and Mohammadi, 2013). Downstream of receptor activation, different cytoplasmic signal transduction arms can be utilized. The Akt or PI3K pathway alone is a powerful branching network that has been associated with cell survival among other processes (Dailey et al., 2005). PKC is a family of protein kinase enzymes that can control many other proteins in the cell through phosphorylation of hydroxyl groups on serine or threonine residues and is positioned to influence many different signal transduction pathways. PKC has been shown to play a role in orchestrating changes in cellular architecture and cell migration (Schlessinger, 2000). The Ras/ERK/MAPK pathway is a cascade of protein kinases that results in regulation of gene transcription and translation and has been associated with cell proliferation and differentiation (Mohammadi et al., 2005). Some of the Fgf pathway target genes are members of the sprouty family, a family of signaling modulators that can interact with tyrosine kinase receptors to inhibit specific kinase events including inhibition of the Ras/ERK pathway (Hanafusa et al., 2002) (Figure 3).

It is astounding that the Fgf and Wnt signal transduction pathways can perform such a plethora of biological processes. However, with a closer analysis of the vast number and variety of molecular components involved and the countless ways in which each member can be regulated, a clearer understanding

comes into focus of how a few signaling pathways can execute such a vast number of developmental programs. The further investigation of these pathways provides an intriguing model in which to better understand the many ways that evolution has used a small handful of signaling modules repeatedly to create new innovations during the development of multicellular organisms.

1.3 Cranial Placodes

As mentioned above, the cranial placodes are discrete thickenings of epithelium with potential to give rise to different cell types of the paired sensory organs of the vertebrate head (Figure 4). The lens and adenohypophysis placodes are the only two cranial placodes that do not have neurogenic potential. Ectodermal thickenings that give rise to feathers and teeth are named placodes as well. However, we have focused on the sensory cranial placodes that contribute components to the cephalic sensory organs in vertebrates. A brief description of individual cranial placodes is given below in anterior to posterior order (Figure 1).

1.3.1 Olfactory placode

The anterior most olfactory placode originates in close proximity to the anterior neural plate and the forming neural crest. This placode invaginates to form epithelia of the olfactory and vomeronasal organs (Zeiske et al., 2003). The olfactory placode is an especially plastic placode with respect to the number of

different cell types that it can produce; it even maintains stem cells in the adult structure capable of replenishing regions of the epithelium throughout the life of the adult (Beites et al., 2005; Schwob, 2002). The olfactory placode will contribute support cells, mucus secreting cells, and primary sensory cells to the sensory epithelium. The aforementioned sensory cells possess chemoreceptors that respond to odorants for the olfactory component or phermones for the vomeronasal component. These sensory cells and their projections are congregated together to form both the olfactory and vomeronasal ganglia.

Until recently, the source of glial cells that ensheathe the axons of the olfactory nerve has been controversial. It was initially thought that the olfactory placode had potential to give rise to a migratory group of cells that would later result in specialized types of glial cells that ensheathe the olfactory nerve (Ramón-Cueto and Avila, 1998). However, a recent study by Harden et al., took advantage of genetically encoded distinct reporters for cells of both placode and neural crest lineage and showed that olfactory associated glia were of neural crest origin (Harden et al., 2012). Furthermore, another study involving both fate mapping experiments in chicken embryos and genetic lineage tracing in mouse clearly illustrates a neural crest origin for the olfactory nerve ensheathing cells (Barraud et al., 2010). Developmentally, it is consistent with the idea that the neural crest is the exclusive source of all glia in the peripheral nervous system (PNS), as there has been no demonstration of other placodes possessing glial potential. Neural crest derived stem cells are maintained in adults and it has been suggested that patient derived neural crest stem cells could be an

accessible, plentiful source of therapeutic glia for an injured nervous system (Barraud et al., 2010).

The close apposition of the anterior most placodes, neural crest and anterior neural plate has hampered earlier experiments aimed at understanding cell contribution of these early primordial populations to the mature sensory organs and PNS. Current technologies now allow genetic lineage experiments with temporal control and fine fate mapping using genetically encoded photoconvertable molecules. Well-executed studies employing these methodologies will unequivocally determine origins of many tissue types.

Studies have shown that diverse populations of secretory cells arise from the olfactory placode. These secretory cells release neuropeptides such as neuropeptide Y, FMRFamide, and gonadotropin-releasing hormone (GnRH) (Metz and Wray, 2010; Northcutt and Muske, 1994; Wray, 2002; Wray et al., 1989). The olfactory and vermonasal nerves act as tracts on which these neuroblasts migrate towards and into the brain (Northcutt and Muske, 1994; Wray, 2002; Wray et al., 1989). Placodally derived GnRH cells contribute to different structures including the terminal nerve as well as a group of septo-preoptic nuclei to control the release of gonadotropins (luteinizing hormone and follicle-stimulating hormone) from the andenohypophysis (Eisthen et al., 2000; Von Bartheld, 2004). These neuroblasts have to migrate a surprisingly long distance crossing multiple tissue boundaries in order to reach their final destination. It has been shown that the chemokine (Cxcl12) and its receptors (Cxcr4 and Cxcr7) are required for the proper migration and guidance of the

GnRH precursors to their target organ (Memi et al., 2013). It is remarkable that secretory cells whose purpose is to control reproductive behavior in an organism have their origins in the olfactory anlagen.

1.3.2 Adenohypophysis placode

The adenohypophysis placode is the only cranial placode that is not involved in the development of a sensory structure. Rather this placode will give rise to the anterior lobe of the pituitary gland, while it has no neurogenic potential, it will give rise to systemic hormone secreting cells (Chapman et al., 2005; Herzog et al., 2003). Interestingly the anterior lobe of the pituitary gland develops from a placode in fish, while in birds and mammals it originates from a placode which then migrates to form an invagination of oral ectoderm under the ventral forebrain known as Rathke's pouch (Dutta et al., 2005; Takuma et al., 1998). In all species the anterior pituitary gland is derived from the anterior neural ridge, and specification is characterized by expression of specific LIM homeobox transcription factors *Lhx3* and *Lhx4* in mice and the *Lhx3* homologue *lim3* in zebrafish (Glasgow et al., 1997).

Studies in both mice and zebrafish have indicated the Sonic hedgehog (Shh) signaling pathway as one of the earliest positive mediators of andenohypophyseal formation. It is continuously required throughout multiple stages of its development. Late developmental roles have also been assigned to signaling of the transforming growth factor β (TGFβ) super family factors such as Nodal and BMP4 (Davis and Camper, 2007). During early stages, both the lens

and the andenohypophysis placodes develop in close proximity to each other, and studies have illustrated that Shh signaling is sufficient to alter fate of other anterior placodes to an adenohypophysis fate at early stages of placode induction (Herzog et al., 2003), illustrating critical requirement of this pathway for adenohypophysial development.

1.3.3 Lens placode

The lens placode is one of two placodes (aside from the adenohypophysis) that does not generate neurons. This placode will invaginate to form the lens vesicle, which will give rise to the crystalline-accumulating cells in the mature lens of the eye (McAvoy et al., 1999). The optic cup that will give rise to the retina is not a placodally-derived structure, but rather originates from neural ectoderm in the region of the anterior neural plate. These two structures develop in close proximity to each other. The father of embryonic induction, Dr. Hans Spemann, performed early studies to better understand optic development. Using hot needles to ablate optic primordia in frog embryos, Dr. Spemann investigated whether the lens and optic vesicle development are solely dependent on each other. Such that the forming optic cup was responsible for the induction of the lens placode, and the lens placode was responsible for the proper cellular reorganizations required for invagination of the optic cup (Spemann, 1901). It is now clear, however, that these structures are not entirely dependent on each other's early development. Signals (Fgfs and TGFβ family members, BMP4 and BMP7) from the mesoderm and the neural plate are

required for the induction of the lens placode (Faber et al., 2001; Sjödal et al., 2007; Wawersik et al., 1999). Additionally recent in vitro cultures of embryoid bodies under specific medium conditions have been shown to spontaneously form optic cups in the absence of placodal ectoderm, and a lens (Eiraku et al., 2011), suggesting that morphogenetic cell reorganizations of the optic cup is intrinsic to the optic epithelium and not solely dependent on cues from the lens.

Pax6, a transcription factor known to be one of the most striking examples of a master regulator, has the capacity to induce ectopic eyes in both invertebrates and vertebrates. Pax6 alone has been shown to induce ectopic eyes in both drosophila and Xenopus (Chow et al., 1999; Halder et al., 1995), and even the human Pax6 gene is capable of inducing ectopic eyes in drosophila (Halder et al., 1995) indicating high levels of evolutionary conservation. Pax6 is also important for early olfactory placode formation (Quinn et al., 1996). Although the function of Pax6 as a master regulator has been known for sometime, upstream regulators of Pax6 have been identified only recently by Lleras-Forero et al. This study showed the anterior mesendoderm is the source of the neuropeptide somatostatin which in turn activates nociceptin in the overlying anterior placode progenitor domain to regulate Pax6 expression (Lleras-Forero et al., 2013). This is a surprising finding because other neuropeptides have not yet been described to play a role in more posterior placode induction, perhaps due to the close apposition of this domain with the anterior neural ridge neuropeptides have been co-opted to induce nearby ectoderm.

1.3.4 Trigeminal placodes

The trigeminal placodes have their origins from the non-neural ectoderm lateral to the forming midbrain and the caudal hindbrain. These placodes will give rise to a fused trigeminal ganglion that is composed of the ophthalmic lobe and the maxillomandibular lobe in amniotes and in anamniotes the profundal and trigeminal placodes will respectively give rise to ganglia of the same name (Begbie et al., 2002; McCabe et al., 2009). These placodes will give rise to neuronal precursors that delaminate from the placodal ectoderm and congregate in the underlying mesenchyme where they coalesce with neural crest derived neurons and glia to form their respective ganglia. Thus the trigeminal ganglia have dual origins from both the cranial placodes and the cranial neural crest. In amniotes, placodal origins of the ophthalmic lobe have been less studied due to a lack of specific molecular markers and a delay in development relative to the maxillomandibular placode (McCabe and Bronner-Fraser, 2009). The nerves of the trigeminal ganglia transmit somatosensory information such as temperature and pain from the oral cavity and the anterior face (McCabe et al., 2009).

The platelet derived growth factor (PDGF) family of signaling factors has been implicated in the induction of the ophthalmic trigeminal placode in chick (McCabe and Bronner-Fraser, 2008). The signaling of PDGF through the receptor PDGFRβ was required for optothalmic induction as shown through pharmacological inhibition studies. When PDGF signaling was absent, Pax3 and CD151 (two markers of the ophthalmic trigeminal placode) were not expressed and subsequent neurogenesis was inhibited. However, later inhibition of PDGF

after initial placode induction did not result in a significant loss of trigeminal neurons, indicating that this pathway was likely involved in inductive stages and not responsible for neurogenesis (McCabe and Bronner-Fraser, 2008).

The Wnt signaling pathway is an important mediator of trigeminal placode development, both at specification and subsequent neurogenesis stages (Lassiter et al., 2007). Overexpression of Wnt3a results in premature differentiation of the trigeminal placode. Additionally, Wnt3a has the ability to induce Pax3 expression in chick ectodermal explants; however it should be noted that explant cultures were incubated in a complex tissue culture medium with other undefined factors, potentially convoluting results (Lassiter et al., 2007).

1.3.5 Otic placode

The otic placode will invaginate to form the otic vesicle containing sensory epithelium of the vertebrate inner ear and associated neurons of the statoacoustic ganglion (SAG). This placode gives rise to a wide variety of cell types, including endolymph secreting cells, support cells, neurons, and the mechanosensory hair cells of the vestibular and auditory portions of the inner ear. The mechanosensory hair cells of the vestibular and auditory regions of the ear are isolated in distinct sensory regions of the ear that vary between taxa. More information on the specific sensory territories of the ear can be found in Chapter 1.5.

The otic placode is induced adjacent to the forming hindbrain from a region of ectoderm known as the otic epibranchial placode domain (OEPD), also

known as the posterior placodal area or PPA (Ohyama and Groves, 2004a; Streit, 2002). In chick a broad region of posterior placodal ectoderm expresses the transcription factor Pax2. Fate mapping studies using vital dyes in chick indicate that both the otic and epibranchial placodes arise from this region of ectoderm (Streit, 2002). However, my studies in zebrafish have challenged this view. Using fine fate mapping, expression analysis, and genetically encoded lineage methods we demonstrated that the early Pax2 domain gives rise to the anterior lateral line and the otic vesicle, but contributes very few, if any, cells to the epibranchial placodes (McCarroll et al., 2012). It is also possible that the development of these placodes could vary between species, making it important not to generalize the process of placode development for all vertebrates. The origin of the epibranchial placodes in zebrafish is presently under active investigation in the Nechiporuk lab.

Early specification and induction of otic placode in all species analyzed to date depends on active Fgf signaling. Experiments in zebrafish show that Fgf3 and Fgf8 from the hindbrain and mesoderm are required at early stages for the specification of posterior placodal precursors (Ladher, 2005; Léger and Brand, 2002; Maroon et al., 2002; Nechiporuk et al., 2006; Park and Saint-Jeannet, 2008; Phillips et al., 2001). Loss of these two factors results in the absence of the otic vesicle and the epibranchial (EB) placodes. In chick, Fgf3 and Fgf19 acting from the mesoderm activate a cascade of events needed for otic induction (Freter et al., 2008a; Ladher, 2000). Finally, in mouse Fgf3 and Fgf10 are required for otic induction (Alvarez et al., 2003; Wright and Mansour, 2003). After

initial specification of the otic precursors, subsequent attenuation of Fgf signaling combined with active Wnt signaling from the hindbrain is required for assigning an otic fate to the PPA, while continued Fgf signaling is needed for an EB fate (Freter et al., 2008b; Ohyama et al., 2006).

1.3.6 Epibranchial placodes

The EB placodes are comprised of the geniculate, petrosal, and nodose placodes that contribute neurons to the facial, glossopharyngeal, and vagal ganglia respectively. The later naming convention will be used in this dissertation for both the EB placodes and the EB ganglia. The EB placodes are named such due to their positional development at the dorsal aspect of the branchial arches. In amniotes, the EB placodes will give rise to the distal roots of the EB ganglia, while the more proximal roots are neural crest derived (D'Amico-Martel and Noden, 1983). In zebrafish, however, it appears that at early larval stages of development the entire EB ganglia consist of placode derived neurons, while EB associated Schwann cells are from the neural crest (unpublished data). It is possible in zebrafish that during juvenile stages of development neural crest-derived Schwann cells transdifferentiate into EB neurons. Recent studies in other regions of the PNS have shown that this Schwann cell transdifferentiation can occur to generate neurons (Enomoto, 2013). More studies are needed to determine whether EB ganglia in lower vertebrates, like zebrafish, contain neural crest-derived neurons.

Initial development of the EB placodes appears to dependent on the same early Fgf signals as the otic placode. In chick, blocking specific Fgf ligands using short hairpin RNA to Fgf3 and Fgf19 at Hamburger-Hamilton (HH) stage 4 severely inhibits EB placode development at HH stage 13 (Freter et al., 2008b). Additionally, in zebrafish loss of Fgf3 and Fgf8 (also required for otic placode induction) results in a loss of the EB placodes as well (Nechiporuk et al., 2006). Interestingly, in zebrafish the EB placodes are not detected as discrete morphological structures until 24 hpf, which is much later than otic placode induction (14 hpf). This timing difference indicates that additional factors, possibly distinct from those required for otic placode induction, may be involved in EB placode development.

Lateral to the epibranchial placodes another pair of neurogenic placodes has been described, albeit, only in amphibians (Schlosser and Northcutt, 2000). These placodes give rise to the hypobranchial ganglia, which are small ganglia of unknown function (Schlosser, 2003). Dr. Schlosser hypothesized that both the hypobranchial and the EB placodes share early origins, suggesting that the hypobranchial placodes are merely ventrally misplaced EB placodes that generate viscerosensory neurons. While these ganglia have not been described in other vertebrates, one group reports the presence of placode structures ventral to the branchial arches that are later eliminated by apoptosis in *Tupaia belangeri* commonly known as the northern tree shrew (Washausen et al., 2005). It will be interesting to determine what the specific functions (if any) these ganglionic

bodies provide and if they are conserved in other aquatic vertebrates, such as zebrafish.

1.3.7 Lateral line placodes

The lateral line placodes are the source of all components of the lateral line system, a mechanosensory system responsible for detection of electrical fields and water movements in aquatic vertebrates (Ghysen and Dambly-Chaudière, 2004; Gibbs, 2004; Modrell et al., 2011; Winklbauer, 1989). This sensory system endows fish and amphibians with their ability to sense “touch at a distance” necessary for many of their behaviors including schooling, mating, finding food, and evading predators (Ghysen and Dambly-Chaudière, 2004; Gibbs, 2004; Winklbauer, 1989). Sensory neurons of the lateral line ganglia will innervate mechanosensory structures responsible for transducing water movements, called neuromasts, or electro-receptive structures (ampullary or tuberous organs) (Modrell et al., 2011; Winklbauer, 1989). Neuromasts contain mechanosensory hair cells, which are very similar to mechanosensory hair cells of the vestibular system. Little is known of the initial inductive processes of lateral line placode formation, including required signaling pathways and intrinsic transcriptional players (Schlosser, 2006). After the initial induction of the lateral line placode, the neuroblasts will leave the placodal ectoderm to congregate and condense in the underlying mesenchyme to form lateral line sensory ganglia. Meanwhile, the remaining placode cells will segregate from the neurogenic region of the placode to form the lateral line primordium, a migratory group of

cells that will travel along the basement membrane just under the ectoderm. Different taxa of aquatic vertebrates have varying numbers of later line placodes. In the zebrafish there are two anterior lateral line primordia (called sensory ridges) and a posterior lateral line primordium. As the primordium migrates either through the head (anterior lateral line) or trunk (posterior lateral line) of the embryo, the neuronal processes of the associated ganglia extend to follow the migrating primordium. As the primordium migrates, it deposits rosette structures in a stereotyped fashion; these rosettes will then differentiate to form the support cells and mehanosensory hair cells of the neuromasts, which are innervated by the tracking neurites of the lateral line ganglia (Harding and Nechiporuk, 2012). The lateral line system will elaborate during juvenile and adult stages of life (Wada et al., 2013). Finally the neuromasts are known to have regenerative capacity making them an attractive model to study mechanisms of hair cell regeneration (Harris et al., 2003).

1.4 The pan-placodal ectoderm

The cranial placodes give rise to a diverse array of sensory systems and critical components of the PNS (Streit, 2004b). Because of this broad diversity it has long been argued as to whether the cranial placodes share a common embryonic origin. Despite the differences in cell types and tissue contribution, there is a convincing body of evidence arguing that all cranial placodes do indeed originate from a common field of embryonic ectoderm, the pan-placodal ectoderm or PPE (Bailey et al., 2006; Bhattacharyya et al., 2004; Schlosser and

Ahrens, 2004). This region of ectoderm is a continuous domain of presumably homogeneous progenitor cells possessing a generic placodal ground state from which all placodes can be generated.

1.4.1 Evidence of the pan-placodal domain

It has been stated that in order for the PPE to exist there are two criteria that must be met. First the PPE must be a continuous region of embryonic ectoderm sharing a common origin, specific molecular markers and homogeneity of cellular composition (Ahrens and Schlosser, 2005; Streit, 2004b). Second, this continuous region of ectoderm would have related developmental history resulting in the acquisition of exclusive properties, a “placode ground state” or generic placodeness where given the proper signals, all cranial placodes can be generated (Schlosser, 2006; Streit, 2004a). These exclusive properties would be different from other ectodermal derived tissues, such as the epidermis or the CNS.

After gastrulation, during the early neurula stages a horseshoe-shaped domain emerges which contains a presumably homogeneous population of placode precursors (Bhattacharyya et al., 2004; Streit, 2004a). This domain abuts the forming neural plate and is lateral to the forming neural crest. The PPE is characterized by the expression of specific factors (Eya1, Six4b, Dlx3b, Dach) unique to this region of ectoderm, distinguishing it from the neural plate and neural crest (Figure 1). In addition to expression profiles, fate-mapping studies in chick, zebrafish, and amphibian showed that all the cranial placodes arise from

the PPE (Bhattacharyya et al., 2004; Dutta et al., 2005; Streit, 2002; Whitlock and Westerfield, 2000). These studies (particularly the fate map studies performed in chick) indicate that at early neural plate stages precursors for individual placodes are comingled with a substantial degree of mixing; it is not until later that placode precursors begin to adopt their own fate and segregate into distinct territories only after directed large scale cellular rearrangements occur. A recent, impressively detailed fate map of the PPE in Xenopus embryos at early neural plate stages further provides evidence that the PPE is indeed the source of all cranial placodes (Pieper et al., 2011). Interestingly, this study found only modest degrees of cell mixing between individual placode precursors, and this group found no evidence for large scale cell sorting (Pieper et al., 2011). Indeed, fate map results presented in this dissertation indicate that precursors of the otic and EB placodes in zebrafish embryos at early neurula stages (12 hpf) occupy their own territories and undergo only minimal cellular reorganization, with occasional larger cell movements (Chapter 3.3.1).

Identification of transcription factors that are unique to the PPE and conserved between species provides evidence for the hypothesis that all placodes are derived from a territory of ground state placode potential. Perhaps the most specific of these factors are members of the Six1/2, Six4/5 and Eya families (Grocott et al., 2012). Expression profiles of these factors reveal their presence in the horseshoe-shaped domain of the PPE and their expression persists after maturation of individual placodes (Litsiou et al., 2005; Schlosser and Ahrens, 2004). In addition, mutant analysis of these factors in human and

mouse, and mutant/morphant analysis in zebrafish reveal a loss or deficit in the cranial placodes or their subsequent structures, although it appears that different combinations of these factors are more important for one group of placodes over others (Grifone et al., 2005; Zhang et al., 2004). Also there is the possibility of compensation between members of the same Six or Eya gene family during placode development (Grocott et al., 2012).

Deficits in the eye, ear, cranial ganglia and olfactory epithelium have been reported during loss of function in the Six1, Six5, Eya1, and/or Eya4 genes (Ruf et al., 2004; Xu et al., 1999). Patients with defects in the aforementioned genes are associated with Branchio-Oto-Renal syndrome; these patients have renal defects, hearing deficits, branchial abnormalities and present late onset deafness and formation of lens cataracts. Studies analyzing loss of function of Six1 reveal a requirement of this factor for the formation of placodal precursors at the neural plate border, where a gain in function of Six1 expanded the PPE at the expense of the nearby neural crest and the epidermis (Brugmann et al., 2004a). Together these studies argue that factors of the Six and Eya family define a unique territory of pro-sensory ectoderm.

Continued expression of Eya and Six genes is seen throughout development of the placodes, as the neural tube starts to close, the PPE begins to be subdivided into distinct regions, and specific Pax factors begin to be expressed in unique territories (Pax6 anterior, Pax3 middle, and Pax2/8 posterior). It is at this time that cells of a generic placodal identity undergo regional transcriptional regulation to promote a more distinct placode program.

1.4.2 Defining boundaries of the pan-placodal ectoderm

Gastrulation is the embryonic process by which the three germ layers of an embryo are derived: endoderm, mesoderm and ectoderm. Initially the future ectoderm encompasses regions of neural and non-neural territories of considerable overlap. Even before the process of gastrulation commences (late blastula stage) precursors for the neural and non-neural fate are already being specified. Borders of neural specific markers: Sox3, Erni1, Gemenin are blurred with the NNE specific expression of Dlx genes, Gata2/3, Foxi1/3 (Grocott et al., 2012). By the end of gastrulation, these broad neural and non-neural territories are refined to specific domains. The BMP signaling pathway has been shown to promote a non-neural fate over a neural fate in early embryos, with BMP inhibition sufficient to give rise to only neural ectoderm (Wilson and Hemmati-Brivanlou, 1995). Thus it has been stated that the default program of ectoderm is neural (Weinstein and Hemmati-Brivanlou, 1997). A mediolateral BMP gradient is important for setting up the initial ectodermal boundaries, where high BMP resulting in epidermis, mid levels for PPE and neural crest, and low BMP for neural ectoderm (Brugmann et al., 2004a). However, a simple BMP gradient model for ectoderm patterning is not sufficient to explain the complexities of this process. For instance, simple attenuation of BMP is not sufficient for induction of PPE specific marker (Litsiou et al., 2005).

Fgf signaling appears to have a role in early ectodermal patterning as well. While this signaling pathway is a positive mediator of more medial populations of ectoderm (neural, neural crest, PPE) it is not sufficient on its own to induce

neural or PPE fate from distant tissue. Fgf2 has been demonstrated to induce Eya in competent ectoderm, but not the Six factors (Litsiou et al., 2005). However, treatment of grafts with the Fgf inhibitor SU5402 results in the loss of PPE markers (Litsiou et al., 2005) indicating that this factor is necessary but not sufficient to define the PPE.

Inhibition of BMP on its own is not sufficient to form PPE from distant tissues, and active Fgf signaling alone cannot induce PPE (Ahrens and Schlosser, 2005; Litsiou et al., 2005). However, a proper integration of these two signaling pathways can induce a subset of PPE markers. High Fgf in concert with attenuated BMP signaling can induce PPE markers (Ahrens and Schlosser, 2005; Kwon et al., 2010; Litsiou et al., 2005). Studies also indicate that proper timing of these signaling events is important. Although it seems that regulation of these two signaling pathways have some potential to induce PPE, not all markers are detected (Grocott et al., 2012). Integration of high Fgf, BMP inhibition in conjunction with antagonizing Wnt can efficiently induce PPE markers (Brugmann et al., 2004b; Litsiou et al., 2005). Inhibition of Wnt in chick and Xenopus embryos causes an expansion of the PPE boarders into future epidermis and extension of its posterior boarders (Brugmann et al., 2004b; Litsiou et al., 2005). Endogenous expression of Wnt ligands reveals the presence of these factors lateral and anterior to the PPE boarder (Litsiou et al., 2005). Interestingly active Wnt signaling expands the medially located neural crest tissue (Knecht and Bronner-Fraser, 2002). From these studies a model emerges

where an orchestration of appropriately timed signaling gradients will define the boarders of early embryonic ectodermal territories (Figure 6).

1.4.3 Subdivision of the pan-placodal ectoderm

During the early neurula stage, shortly after the boundaries of the PPE have been defined, placode precursors undergo a process of segregation and acquisition of unique regulatory states. This process of segregation occurs initially through the subdivision of generalized anterior and posterior placodal territories. After this initial line is drawn, individual placodes will progressively become more defined through specific transcriptional networks and physical separation.

In the nascent neuroectoderm, mutual repression between a pair of transcription factors results in the partitioning of neural territories along an anterior-posterior axis. This partitioning is important for proper localization of factors involved in the formation of the midbrain hindbrain boundary (MHB) (Glavic et al., 2002). The factor Gbx2 is expressed in the posterior portion of the neuroectoderm while Otx2 is restricted in the anterior region; these two factors mutually repress each other to form a defined boundary (Acampora et al., 2001; Simeone et al., 1992). The interface at which these two factors meet will be the location of the future MHB. Recently, a similar mechanism was tested for the partitioning of cranial placodes from the uniform PPE to anterior and posterior placode forming regions (Steventon et al., 2012) (Figure 6D). Similar to the neuroectoderm, these factors also were involved in formation of an anterior-

posterior boundary in the PPE, with Gbx2 required for otic specification and Otx2 involved in specification of the olfactory, lens, and trigeminal (the line drawn between the trigeminal and otic placodes). This is the earliest described partitioning of the PPE into progressively more discrete regions. A role for Gbx2 in the formation of other posterior placodes (EB and lateral line) has not yet been determined.

As the anterior portion of the PPE becomes further segregated, it begins to express Pitx3, Lens1 and Pax6 (Figure 6D). This region contains progenitors for the lens, andenohypophysis, and olfactory placodes. There is some evidence for the presence of trigeminal precursors in this early anterior domain as well (Bailey et al., 2006). Very recently, neuropeptides from the mesendoderm have been shown to play a role during induction of Pax6 in the anterior placodal domain (Lleras-Forero et al., 2013). Caudal to the latter domain, Pax3 expression is seen in precursors of the trigeminal placode, and in the posteriormost region of the PPE, factors such as Pax2/8 mark precursors of the otic and EB placodes (and variably the lateral line placodes in aquatic vertebrates) (Figure 6D). It should be noted that exact timing of onset and duration in expression for these Pax factors varies between species.

At the onset of Pax6 and Pitx3 expression, the anterior placodal domain contains a homogeneous population of cells with the potential to give rise to any of the anterior placodes. Given the appropriate signal, fates of the anterior placodal area can be experimentally altered. In the embryo, specification of the anterior placodes occurs through the secretion of proper signals emitting from

neighboring tissues. These signals occur locally to induce anterior placodes at a precise location from a territory of equal potential. One such signal is Shh, which is emitted from the midline (Karlstrom et al., 1999). This signal plays a dual role both to induce the andenohypophysis placode and to inhibit lens and olfactory fates. Loss of Shh can expand lens and olfactory fates, while ectopic expression of Shh can inhibit lens formation (Dutta et al., 2005; Herzog et al., 2003). Olfactory precursors are defined through Fgf signaling from the neural ridge, increased Fgf signaling can expand the olfactory territory at the expense of lens (Bailey et al., 2006). The endoderm will secrete BMPs that are needed to specify lens fate, while the forming optic cup plays a role later during lens formation by emitting Fgf and BMP signals (Faber et al., 2001; Sjödal et al., 2007). Interestingly, as the lens and olfactory fates are being specified through local signals, intrinsic factors begin to be expressed in a mutually exclusive manner. Dlx5 and Pax6 initially overlap in the anterior placodal territory, however after the onset of placode specification Dlx5 segregates to future olfactory epithelia while expression of Pax6 is restricted to lens precursors (Bhattacharyya et al., 2004). In chick, this differential expression of intrinsic factors is dependent on Fgf8 signaling from the anterior neural plate, promoting the expression of Dlx5, that actively suppresses Pax6 (Bailey et al., 2006; Bhattacharyya et al., 2004). In fact, explant studies in chick indicate that a Pax6+ lens fate is default for all placodal precursors; as development continues, other pan-placodal regions receive signals to actively promote unique placodal fates (Bailey et al., 2006). However, in vivo the more posterior pre-placode territory (otic and EB) does not express

Pax6 under normal conditions (Li et al., 1994; Schlosser and Ahrens, 2004), suggesting an additional mechanism in specifying posterior fates.

The trigeminal placodal precursors are positioned between the anterior placodal area and the more posterior otic, EB and lateral line precursors. While the majority of this domain initially expresses Otx2 and Pax6, indicating early origins in the anterior PPE (Bailey et al., 2006; Bhattacharyya et al., 2004), one study indicates a subset of trigeminal precursors may originate from the more posterior Pax2+ territory (Xu et al., 2008). At early neurula stages the trigeminal domain will define itself through the expression of Pax3 (Dude et al., 2009; Schlosser and Ahrens, 2004). This factor has the ability to repress expression of both the more anterior Pax6 (Wakamatsu, 2011) and posterior Pax2 (Dude et al., 2009), and positively regulates itself to define a trigeminal specific, intermediate placodal territory (Dude et al., 2009). Little is known about early trigeminal specification. Local inductive cues include neural tube derived Wnts that cooperate with the Fgf pathway to promote Pax3 expression (Canning et al., 2008). PDGF signaling has also been shown to be important, although it cannot promote Pax3 expression on its own (McCabe and Bronner-Fraser, 2008).

Similar to the refinement of the anterior placodal fates from a broad territory of competence, the posterior placodes undergo a stepwise process of placodal fate decisions determined by intrinsic regulatory networks and external inductive cues from local sources. Before the Six/Eya PPE network turns on, Gbx2 is expressed throughout the posterior ectoderm, and has been shown to positively regulate PPA specific factors (Li et al., 2009; Steventon et al., 2012).

Shortly after, Irx1-3 becomes expressed in the PPA (Glavic et al., 2002). In addition members of the Dlx and Foxi transcription factors initially show broad expression through out the NNE and the PPE then become restricted to the PPA (Nissen et al., 2003; Ohyama and Groves, 2004b; Solomon and Fritz, 2002; Solomon et al., 2003; Solomon et al., 2003). These factors differ between species: Dlx3b/4b and Foxi1 in fish (Solomon et al., 2003)(Solomon and Fritz, 2002), Dlx5/6 and Foxi3 in chick and mouse (Brown et al., 2005) (Ohyama and Groves, 2004b). Together these factors will form a transcriptional program necessary for expression of PPA-specific Pax factors, Pax2/8 and another important PPA factor, Sox3 (Hans et al., 2004a; Hans et al., 2007).

The regulation of Foxi1 and Dlx3b/4b seems to be dependent on each other and are regulated by Fgfs in the PPA (Figure 6). These factors will form a broad region of posterior placodal competence, from which the posterior placodes will form in more discrete regions. It is thought that these factors form a positive feedback loop and work in concert to induce the expression of Pax2/8 and Sox3. Pax8 and Sox3 are among the earliest otic and EB placode specific factors, with the expression of Pax2 slightly later. Dlx3b/4b has been shown to regulate Pax2 while Foxi1 is required for Pax8 and Sox3, both of these pathways however are dependent on Fgf signaling (Hans et al., 2004b; Hans et al., 2007; Nissen et al., 2003). In chick and mouse, studies show that subsequent Wnt signaling from the neural tube then enforces an otic fate over an EB fate, while continued Fgf signaling is needed to promote the EB placodes (Freter et al., 2008a; Ladher, 2000; Ohyama et al., 2006). However this mechanism of otic

formation is still under debate in the zebrafish (Phillips et al., 2004). After initial induction of the otic placode, the Pax2/8 factors cooperate to downregulate Sox3 and Foxi1 in the otic placode, a process required for further otic development (Mackereth et al., 2005; Padanad and Riley, 2011). Subsequently, these factors are confined to the future EB territory (Padanad and Riley, 2011).

In multiple species Pax2/8 has been shown to be essential for proper otic and EB placode formation. Knockdown of both these factors in mouse and zebrafish results in severe loss of otic specific markers. Interestingly the avian genome has lost the Pax8 homologue and only possesses Pax2, important for the PPA formation in birds. Expression of these factors is seen in the otic and EB placodes, however a role for the posterior Pax factors during otic and EB placode segregation has not been reported previously.

Otic placode development is initially dependent on Fgfs and then subsequently on Wnt signaling. Fgf ligands differ between species with Fgf3/10 required in mouse, Fgf3/19 in chick and Fgf3/8 in zebrafish. It has also been demonstrated that Fgf3/8 is required for initial specification of the EB placodes. In addition, subsequent EB development is also dependent on Fgf signaling, but the nature of Fgf ligand(s) required is unknown (Nechiporuk et al., 2006).

1.5 The Vertebrate inner ear

The vertebrate inner ear is comprised of 3 different sensory organs in one: the cochlea, the maculae, and the cristae (Figure 5A). These systems are responsible for integrating different stimuli such as sound waves (the cochlea),

angular acceleration (the cristae) and acceleration due to gravity or vertical acceleration (the maculae) (Rinkwitz et al., 2001). The mechanosensory information transduced by these structures is initially processed by sensory neurons of the statoacoustic ganglion (SAG) and subsequently relayed to the CNS where it is perceived as sound/motion (Vemaraju et al., 2012).

1.5.1 The Cochlea

The auditory portion of the mammalian inner ear is a bony spiral shaped structure appropriately named the cochlea after the Greek word for snail, *kokhlias*. The cochlea is lined with a delicate epithelial layer and contains three different fluid filled chambers; the scala vestibuli and scala tympani contain the sodium rich perilymph (similar in composition to the cerebral spinal fluid) and the scala media containing the potassium-enriched endolymph. The auditory sensory epithelium of the cochlea is called the organ of Corti (Figure 5D; also known as the papilla in non-mammals) (Groves and Fekete, 2012). Mechanosensory hair cells in this compartment will project into the nutrient, ion rich endolymph. The hair cells of the organ of Corti will translate fluid vibrations of sound into electrical signals processed by the SAG, with the apex of the sensory epithelium detecting low frequencies and the higher frequencies resonating near the basal aspect of the structure. Non-mammal vertebrates have an auditory structure sometimes referred to as the cochlea, however it lacks the spiral shaped morphology in these organisms.

1.5.2 The Maculae

The vertebrate inner ear also contains a vestibular component composed of semicircular canals filled with perilymph positioned dorsal to the cochlea. The sensation of gravitational or vertical acceleration is achieved by specialized mechanosensory hair cells located in specialized sensory tissue of the utricle and saccule known as the maculae (Figure 5B) (Purves et al., 2001). These hair cells are overlayed by the otolithic membrane, a thick gel containing calcium carbonate crystals known as otoliths (Stooke-Vaughan et al., 2012). These otoliths will reorient as the head moves which in turn stimulates the hair cells of the maculae in reference to gravity. The movement of the otolithic membrane is sufficient to displace stereocillia of the maculae hair cells resulting in the opening of ion channels and the resultant depolarization of the hair cells (Purves et al., 2001).

1.5.3 The Cristae

Sensing angular acceleration is achieved by the three cristae: sensory organs that are located at the base of three orthogonally arranged semi-circular canals. This arrangement allows these sense organs to detect motion in all three axes (Reisine et al., 1988). Swellings at the base of each of the canals called ampullae house the cristae sense organ (Figure 5C). The stereocilia of the mechanosensory hair cells of the cristae protrude into a gelatinous milieu known as the cupula. Fluid movement during angular acceleration results in displacement of the cupula, which bends the enclosed hair cell stereocilia

resulting in a subsequent depolarization of the sensory hair cells (Reisine et al., 1988).

1.5.4 Induction of the otic placode and early development of the inner ear

The vestibular and auditory system of the vertebrate inner ear along with sensory neurons of the SAG arise from an early embryonic structure know as the otic placode. As mentioned previously, a growing body of evidence supports a model that all cranial placodes are initially derived from a homogenous group of cells known as the pan-placodal ectoderm (PPE), a horseshoe-shaped region of cells that abuts the neural plate and is lateral to the developing neural crest (Figure 6A).

Shortly after the initial PPE is defined, its posterior most region begins to express the transcription factors Foxi1 and Dlx3/4 in both otic and epibranchial placode precursors (Ohyama and Groves, 2004b) (Figure 6B; the epibranchial placodes contribute neurons to the VII, IX, and X^{th} cranial nerves). These factors impart placodal competence to this region of the ectoderm, and allow cells to respond to placode inducing factors such as Fgfs (Hans et al., 2007). Once the otic placode is induced, it begins to express the paired box transcription factors Pax8 and shortly after Pax2 (McCarroll et al., 2012) as well as the SRY-related HMG-box Sox3 (Padanad and Riley, 2011) (Figure 6C). The otic placode will then condense and begin to invaginate to form the otic vesicle. This structure will ultimately give rise to the complex labyrinth of the inner ear as well as the related vestibular and acoustic neurons.

Fgfs have been shown to be indispensible during multiple stages of otic placode formation, and subsequent patterning (Figure 6B'). These factors signal from the hindbrain and cranial mesoderm to induce the expression of early otic markers like Pax2, however the specific Fgfs involved vary between species. Zebrafish embryos deficient for both Fgf3 (mesoderm derived) and Fgf8 (hindbrain) are incapable of turning on Pax2/8 in the posterior PPE, leading to a loss of the otic placode (Nechiporuk et al., 2006). Similarly in mouse, loss of mesodermal Fgf3 or loss of neural Fgf10 leads to a reduction in Pax2 expression and smaller otic vesicles, while simultaneous loss of either Fgf3/10 or Fgf3/8 results in a complete loss of Pax2, Pax8 and the otic vesicle (Zelarayan et al., 2007a). In chick, similar results are observed during loss of either Fgf19 or Fgf3 (Freter et al., 2008b). Conversely misexpression of Fgf3, 10 or 19 in chick and mouse is sufficient to induce Pax2 expression, and in some instances ectopic otic vesicles (Vendrell et al., 2000). In fish, misexpression of a constitutively active Fgfr1 is sufficient to expand the Pax2/8 domain (McCarroll et al., 2012). Importantly only PPE cells are capable of responding to Fgfs to expand the early otic territory.

The hierarchy of transcriptional regulators involved in early otic specification has been extensively studied in zebrafish. At the top of this hierarchy are the Foxi1 and Dlx3/4 transcription factors that become restricted to the posterior most region of the PPE before the Pax2/8 and Sox3 factors are expressed (Hans et al., 2007). While Fgf signaling is required for proper expression of Pax2/8, Foxi1 and Dlx3/4 are still expressed when Fgf signaling is

abrogated; instead, these early competence factors are dependent on BMP signaling (Furthauer, 2004). Loss of Foxi1 or Dlx3/4 alone results in developmentally impaired otic vesicles, and a loss of both these factors leads to a complete absence of the otic vesicle, with a concomitant loss of Pax2/8 expression (Hans et al., 2004b). Studies in both zebrafish and Xenopus indicate that Pax2 is initiated downstream of Dlx3/4 while the expression of Pax8 mostly relies on Foxi1 (Hans et al., 2004b; Hans et al., 2007; Saint-Germain, 2004).

While early Fgf signaling is required for initial otic and epibranchial placode induction, subsequent attenuation of this signaling pathway coordinated with increased Wnt signaling is required for proper segregation of the otic precursors from epibranchial progenitors (Figure 6C'). In mouse, Fgf inhibitors such as the Sproutys are upregulated in the otic placode shortly after induction (Mahoney Rogers et al., 2011); during this time, Wnt expression can be detected in the hindbrain, while downstream effectors begin to be expressed in otic placode precursors. It is thought that high Wnt and low Fgf signaling is required to commit early placode precursors to an otic fate, while low Wnt and high Fgf will commit precursors to an epibranchial fate (Freter et al., 2008b; Ohyama et al., 2006). This mechanism is conserved from zebrafish to mammals. Pharmacological experiments overactivating the Wnt pathway during otic induction results in high levels of Pax2 with a concomitant dramatic increase in the size of the otic vesicle at the expense of the epibranchial placodes; blocking Wnt signaling has the opposite effect (McCarroll et al., 2012). A reciprocal

interaction between Notch and Wnt signaling has also been shown in multiple species to further commit cells to an otic fate (Abelló et al., 2007).

1.5.5 Early regionalization of the inner ear

The vertebrate inner ear is a morphologically complex organ composed of highly specialized and regionalized structures. In order for the vertebrate embryo to execute a high level of specialization, complex molecular programs responsible for the patterning of the inner ear are initiated at early stages. After the otic placode is induced it undergoes invagination to form a spherical otocyst, or otic vesicle. At this stage, molecular asymmetries are evident based on differential gene expression patterns. Studies in early amphibian indicate that initially the otic vesicle patterning is not fixed, as mirror image duplications of anterior or posterior morphologies occur after surgical rotations (Harrison, 1936). Over time these markers become more established. Different extrinsic and intrinsic signals are responsible for setting up these axes; this is suggested by the observation that anterior to posterior (AP) patterning is fixed before dorsal to ventral (DV) patterning. Interestingly amniotes compared to non-amniotes have both shared and differing mechanisms to establish AP and DV patterning.

In amniotes, hedgehog (Hh) signaling is the primary otic ventralizing factor. This factor is expressed in the notocord and floor plate situating this morphogen in an appropriate region for activating ventral specific genes in the otic vesicle (Riccomagno et al., 2005) (Figure 6E). In conditional Smoothened or Smo (the Hh receptor) mouse mutants the ventral otic structures (cochlea and

saccule) are lost while the more dorsal structures (semicircular canals, criste and utricle) develop normally (Brown and Epstein, 2011). It should be noted that Hh also functions during DV neural tube axis establishment as well as mesenchymal tissue polarization and presumably can affect otic axis establishment both directly and indirectly as it helps to shape the surrounding tissues. Wnt signaling from the hindbrain has been shown across species to be the primary dorsalizing agent of the otic vesicle. Overactivation of Wnt results in the expansion of dorsal markers, like Dlx5, and a reduction of the ventral markers such as Otx2 (Riccomagno, 2005) (Figure 6E, E'). In summary, the current model for DV otic patterning in amniotes is one where opposing Hh and Wnt gradients set up the DV axis.

In zebrafish, Fgf3 is in part responsible for the induction of anterior markers such as Pax5 and Hmx2, whereas *fgf3* mutants show a partial reduction of anterior identity. Pharmacological inhibition of Fgf receptors shows a complete loss of Pax5 and Hmx2 with a concomitant mirrored expression of posterior marker, Fst1 (follistatin a) along the AP axis (Hammond and Whitfield, 2011) (Figure 6E, E'). Because global abrogation of all Fgf signaling has more severe effects than loss of Fgf3 alone, it follows that another Fgf ligand, in addition to Fgf3, is responsible for defining the anterior otic identity. The opposite phenotype is seen when Fgf3 is globally overexpressed (Hammond and Whitfield, 2011). In zebrafish and Xenopus, Hedgehog (Hh) signaling is responsible for posterior otic identity (Hammond et al., 2003; Hammond et al., 2010; Waldman et al., 2007). This is revealed by studies analyzing Smo mutants that display a loss of posterior

markers, and a partial mirrored duplication of anterior markers. In zebrafish the opposite is seen upon global activation of the Hh pathway by mRNA overexpression. Interestingly, in amniotes Hh signaling plays a role in setting up the DV axes while retinoic acid (RA) and not Hh will set up AP identity. High levels of RA in mouse and chick, as shown by treatment with RA, resulted in an expansion of posterior identity, while chemical inhibition of RA synthesis had the opposite effect (Bok et al., 2011) (Figure 6E, E'). Recent studies in fish have shown that Hh and RA also have a role on DV and AP patterning respectively, however it appears that these pathways act independently of the previously discussed Fgf/Hh, to mediate otic axis establishment (Hammond et al., 2010; Radosevic et al., 2011).

In summary, the establishment of early otic identity from a region of homogeneous ectoderm to the early axial patterning that ultimately results in a complex labyrinth of highly specialized sensory and support cells of the vertebrate ear is orchestrated by a collection of extrinsic signaling factors. These are reiterated during multiple stages of the development of the inner ear. During distinct developmental stages, the same signaling factors can specify, pattern and specialize the developing tissue. This is accomplished through the induction of specific transcriptional networks that take the inner ear on a journey from a simple epithelium to the adult sensory organ.

1.6 The epibranchial ganglia

Vital components of the reflex circuitry important in governing homeostasis of the body's viscera involve related neurons located centrally and in the periphery. Efferent pathways that emanate from the hindbrain and spinal tract control motor impulses for the digestive tract and control blood pressure and respiratory rhythm. The afferent pathways required for sensing the internal status of the viscera originate in the epibranchial ganglia known as the geniculate, petrosal, and nodose ganglia or commonly referred to as the facial (VII), glossopharyngeal (IX) and vagal (X) cranial ganglia, respectively (Schlosser, 2006). Afferents from these ganglia will relay sensory information about chemoreception (including taste) as well as baroreception and osmoreception from the vasculature, back to the hindbrain. For instance, the petrosal ganglia (glossopharyngeal) is postsynaptic with the glomus cells of the carotid body, a group of chemosensitive and support cells located near the site of bifurcation of the carotid artery (the artery that runs on either side of the throat). The carotid body is responsible for sensing levels of oxygen, carbon dioxide, glucose, pH and temperature (Gonzalez et al., 1994; Katz et al., 1987; Pardal and López-Barneo, 2002). The geniculate or facial nerve afferents will synapse on the taste buds of the gustatory system, while the nodose or vagal nerve will relay sensory information from a myriad of internal organs in the cardiovascular, gastrointestinal and even reproductive systems (Brunet and Pattyn, 2002; Clancy et al., 2012; Coppola et al., 2010; Matteoli and Boeckxstaens, 2012). Thus the

epibranchial ganglia are positioned strategically in this autonomic visceral circuit to modulate function of numerous internal organs.

1.6.1 Transcriptional cascades that control epibranchial development

The epibranchial ganglia originate from the transient epibranchial placodes, named for their positional development at the dorsal aspect of the branchial arches. Along with the otic (and lateral line placodes in aquatic vertebrates) the EB placodes are part of the PPA, and as a group share many of the early specification cues that the otic placode requires, discussed earlier in this chapter. Briefly, initial signaling factors, in particular Fgfs, are emitted from local tissues and a cascade of transcriptional events will begin to give identity to the PPA from the PPE. After this early specification event, differences in gene regulation are seen as the more lateral cells take on an EB program and the medial cells an otic fate. Despite these similarities in early specification and inductive signals, formation of the EB placodes and subsequent ganglia have been largely understudied in comparison to otic development.

Multiple transcription factors expressed during various stages play distinct roles in EB placode development. Foxi1 is a winged helix transcription factor that is important for development of the otic and EB placodes; this factor is thought to impart placodal competence to the ectoderm. While Foxi1 is a broadly expressed competence factor, other PPA factors, Sox3 and Pax8 are more specifically expressed in the otic anlage and Sox3 is among the first known factors to be detected in the EB placode precursors. Foxi1 and Sox3 are initially expressed in

precursors for both the otic and EB placodes; however, shortly after the onset of Pax2 expression in the developing otic placode, Foxi1 and Sox3 expression needs to be attenuated in the otic placode for proper development to proceed. Sox3 and Foxi1 expression then resolves to the developing EB placodes and is maintained in the mature EB placodes (Abu-Elmagd et al., 2001a; Nikaido et al., 2007a; Padanad and Riley, 2011). Similar to Foxi1 in fish, Pax2 and Sox3 is broadly expressed in the PPA in chick embryos, labeling both otic and EB precursors, and only at later stages of placode development does the expression pattern of both factors become restricted to individual placodes (Abu-Elmagd et al., 2001a; Streit, 2002; Tripathi et al., 2009). This difference in expression between species could in part account for differences in lineage studies between species. Pax2 expression in zebrafish appears to be much more dynamic (Nechiporuk et al., 2006), however, detailed temporal expression analysis has not yet been conducted. Currently there are no known factors to be specific to the EB placodes alone; the known markers are typically also expressed in the otic vesicle, promiscuously label the surrounding ectoderm, or extensively label the neural tube. Identification of EB placode specific markers would be invaluable to better understand EB cell dynamics including epithelial polarization and subsequent delamination.

After EB placodes have formed, delaminating cells will downregulate Sox3 and Pax2 so that transient expression of the basic helix-loop-helix factor Neurogenin1 (Neurog1) can ensue (Abu-Elmagd et al., 2001a; Andermann et al., 2002; Nechiporuk et al., 2006). In amniotes the specific basic helix-loop-helix

factor required for this process differs. Neurog1 is required for EB neurogenesis and Neurog2 for trigeminal neurogenesis in chick (Abu-Elmagd et al., 2001b). Interestingly, the opposite is observed in mouse with Neurog2 in the EB and Neurog1 in trigeminal (Fode et al., 1998; Ma et al., 1998). In zebrafish, Neurog1 is required in general for neurogenesis of the entire developing PNS, and is transiently upregulated in placodal cells as well as delaminating neuroblasts. Once migrating neuroblasts begin to condense into the EB ganglia in the underlying mesenchyme, they begin to express the neurodifferentiation factor NeuroD (Andermann et al., 2002; Nechiporuk et al., 2005; Nechiporuk et al., 2006). Downstream of NeuroD, another family of neurogenic factors will begin to be expressed, the paired-like homeobox 2 (Phox2) factors that marks differentiated EB neurons (Dauger et al., 2003; Nechiporuk et al., 2005). Phox2a appears to be upstream of Phox2b during EB ganglia maturation.

Interestingly all the neurons involved in the autonomic visceral reflex circuit, of which the EB ganglia is an integral component express the transcription factor Phox2b (Dauger et al., 2003). Although this circuit is composed of different classes of neurons and cellular sensors (motor neurons and sensory neurons located both peripherally and centrally) the same transcriptional regulator is seen in cell bodies of the entire circuit, including the chemosensing cells of the carotid body. This is a unique scenario where the circuit itself, not the subtype of cell involves the conserved expression of a specific factor, Phox2b. It has been hypothesized that Phox2b could regulate specific cellular adhesion factors

involved during path finding and circuit connectivity of the entire visceral autonomic system (Coppola et al., 2010; Dauger et al., 2003).

This factor also has clinical importance. In the human, heterozygous mutations in the Phox2b gene correlates with the complex dysautonomic syndrome known as congenital central hypoventilation syndrome (Amiel et al., 2003). One of the more notable symptoms is severe sleep apnea, where the afflicted may quit breathing and decease in their sleep without the aide of mechanical ventilators. This disease has also been termed Ondine's curse after the mythological water nymph whose unfaithful lover swears that his every waking breath will be a testament of his undying love. When the infidel is caught, Ondine curses him that if he should ever fall asleep he will forget to breathe (Nannapaneni et al., 2005).

1.6.2 Placode and neural crest interactions during epibranchial development

Recent studies have illustrated an important interaction between the developing cranial placodes and the cranial neural crest at multiple stages of EB placode development. In amniotes the EB ganglia is composed of both a proximal and a distal root. Lineage studies show that the proximal sympathetic and parasympathetic roots are of neural crest origin and the distal sensory roots arise from the EB placodes. Interestingly, this might not be the case in zebrafish, where it appears that at least during the larval stage the EB ganglia arise entirely from the EB placodes (Chapter 6.2). A single zebrafish study asserted that numerous neurons of the facial ganglia were of neural crest origin. This work was

performed using a *sox10:cre* transgenic crossed to a red to green reporter to permanently label all *sox10*+ cells. Peripheral neurons were assessed using the pan-neuronal marker anti-Hu (Elavl) (Kague et al., 2012). However, many neuroanatomical structures are present and overlap in the early zebrafish head near the site of the facial ganglia, and it is difficult to decipher individual structures without specific markers or experienced knowledge of zebrafish cranial ganglia. Detailed studies need to be conducted in order to unequivocally determine an early neural crest contribution of EB neurons in zebrafish. Notably, in the murine enteric nervous system, neural crest derived Schwann cells have been shown to transdifferentiate into enteric neurons during normal development (Enomoto, 2013). Given that EB ganglion-associated Schwann cells are neural crest derived, it is plausible that during juvenile development of the zebrafish, these Schwann cells could transdifferentiate into EB neurons.

In addition to direct cellular contribution, the neural crest and the cranial placodes are dependent on each other for proper development and organization. Initially interaction between early progenitors of these two tissues will help to define boarders between NNE, PPE, neural crest and neural plate (Figure 6A). After the initial boundaries are decided, cranial placodes will begin to segregate and the neural crest will migrate from the neural tube to invade the underlying mesenchyme. These two tissues again will interact providing guidance cues and contact inhibition of locomotion to orchestrate cellular movements resulting in proper segregation of the cranial placodes (Theveneau et al., 2013). This phenomenon was recently described as a chase-and-run behavior where the

migrating neural crest will chase early placode precursor cells which in turn run from the neural crest (Theveneau et al., 2013). After the EB placodes have segregated and begin delaminating from the ectoderm and undergo neurogenesis, neural crest derived tissues are again important. Studies in chick and mouse describe embryonic structures of neural crest origin that extend between the hindbrain and the branchial arches. These structures have been described to have corridor like architecture that acts as a physical pathway for delaminating neuroblasts to traverse into the mesenchyme from the EB placodal ectoderm (Freter et al., 2013). While analogous corridors have not been described in zebrafish, genetic ablation of the neural crest does result in disorganization and reduction of the placode-derived cranial ganglia (Culbertson et al., 2011). Altogether, these studies provide strong evidence for the importance of interactions between placode and neural crest populations to achieve correct migration and patterning of the cranial placodes and subsequent ganglia.

1.6.3 Signaling pathways involved in epibranchial development

While the majority of investigations have indicated a primary role for Fgfs during multiple stages of EB development, two studies indicate that BMPs from the endoderm are also necessary for EB ganglia formation in both chick and zebrafish (Begbie et al., 1999; Holzschuh et al., 2005). Explant studies in chick indicate that the EB placodal ectoderm is dependent on endoderm for the formation of Phox2b+ tissue. They determine that the Tgfβ superfamily factor

BMP7 plays a role in this process due to its expression in the endoderm and a reduction in Phox2b+ neurons when BMP signaling is blocked using follistatin soaked beads (Begbie et al., 1999). Interestingly they co-cultured explants in the absence of neural crest and saw no effect on the number of neurons induced from the EB ectoderm, indicating no role of neural crest for neurogenesis. In vivo analysis of endoderm and BMP's role during EB neurogenesis in zebrafish yielded similar results, showing a requirement of endoderm derived Bmp2b and Bmp5 for Phox2b expression in the glossopharyngeal and 3 small vagal ganglia (Holzschuh et al., 2005). After projections of the EB ganglia are established, another TGFβ related factor glial cell-derived neurotrophic factor (GDNF) is required for survival of these neurons (Buj-Bello et al., 1995). These studies, however, only analyzed later EB markers (NeuroD and Phox2b) that are expressed during neurogenesis and did not assess early EB placode formation. Also, only a reduction in EB neurogenesis was detected and not a complete loss, indicating that other factors must be involved during EB neurogenesis. It is possible that both BMP and Fgf signaling work in parallel to promote EB neurogenesis.

Signaling through Fgfs is essential during multiple stages of placode progression from the early homogeneous precursor stage to formation of discrete placodes and subsequent neurogenesis (Ladher et al., 2010; Nechiporuk et al., 2005). In zebrafish, a combined action of Fgf3 and Fgf8 (expressed during early neurula stages in the mesoderm and forming hindbrain) is responsible for specification of the early PPA, a combined loss of these factors results in an

abnormal *foxi1* distribution and the absence of otic and EB placodes (Léger and Brand, 2002; Maroon et al., 2002; Maroon et al., 2002; Nechiporuk et al., 2006; Phillips et al., 2001). Fgfs are also important in amniotes during EB and early otic formation, although the specific Fgf ligands involved varies between species (Freter et al., 2008b; Kil et al., 2005; Ladher, 2005). Zebrafish studies show that subsequent EB development is dependent on endoderm-derived Fgf3 for neurogenesis of the glossopharyngeal and three small vagal ganglia, interestingly the facial and large vagal ganglia appear unaffected in *fgf3* deficient embryos (Nechiporuk et al., 2005). The specific signaling factor (most likely an Fgf) required for facial and large vagal development is currently unknown. Notably, the EB ganglia develop at the dorsal aspect of the branchial arches, and Fgf3 is also important for the proper development of the endodermal pouches (Nechiporuk et al., 2005; Crump et al., 2004). These pouches are populated with chondrogenic NC cells that give rise to mature branchial arches. In *fgf3* mutants, NC derived chondrogenic precursors migrate to their destination, however they are not properly maintained, do not undergo a chondrogenic program and will eventually undergo cell death (Crump et al., 2004). These studies illustrate the complexity of tissue interactions and convergent signaling pathways involved during placode development and subsequent neurogenesis.

1.7 Summary and Hypothesis

The cranial placodes arise from a horseshoe shaped homogeneous region of ectoderm known as the PPE. This domain abuts the forming neural plate

anteriorly and the forming neural crest laterally. The PPE is then subdivided into an anterior pan-placodal domain containing precursors for the andenohypophysis, olfactory, and lens placodes; an intermediate domain with trigeminal precursors; and the PPA including the otic, EB, and lateral line placodes in aquatic vertebrates. Formation of the cranial placodes is a multi-step process involving local signaling from neighboring tissues that activates intrinsic transcriptional networks, resulting in the subsequent segregation and maturation of individual placodes from this initial domain of equivalent potential.

While placodes were initially described nearly 150 years ago, recent molecular and technological advances in the field have provided a new platform to study the specification, induction, maturation, and ultimate differentiation of these embryonic structures. Our current view of cranial placode development came into focus from studies involving detailed temporal and spatial expression analysis of placode specific factors in multiple species; the discovery of signaling factors and neighboring tissues required for placode specification, induction, and differentiation; and lineage or fate mapping studies aimed to define embryonic domains from which these structures arise. While much advancement has been made, many outstanding questions still remain including:

1) Are the precursors of EB, lateral line and otic placodes intermixed within the PPA or do these precursors occupy discrete domains?

2) Is the Pax2+ PPA required for the development of the otic and EB placodes?

3) What are the intrinsic and extrinsic factors required for the proper development of the otic and EB placodes? These questions are the focus of this dissertation.

Previous fate mapping studies have provided a general layout of the PPE and the placode derivatives of this domain. Many of the initial lineage studies were conducted in chicken embryos where injection of DiI and DiO vital dyes was used to construct fate maps. While these studies have provided the field with valuable information, there are limitations to such an approach. This includes the possibility of accidentally labeling neighboring tissues such as neural crest or NNE. Also the chick model organism lacks the genetic tools to enable tissue specific labeling. To date the most detailed lineage study of the entire PPE was conducted in the Xenopus embryo, where numerous examples of multiple time points and placodal territories were analyzed (Pieper et al., 2011). Again these fate maps relied on injection of vital dyes into PPE tissues, and the authors admittedly stated that a high frequency of co-labeling of adjacent placodal fields occured resulting in a fate map with broad regions of overlap between different placode territories. The limitations of vital dye injection studies results in a placodal fate map of low resolution, suggesting high degrees of placodal precursor mixing when the true nature and timing of placode segregation might not be fully appreciated.

Similar experimental approaches were utilized in chick embryos to study development of the otic and EB placodes from the PPA (Streit, 2002). Fate maps constructed from this study indicated that otic and EB placode precursors intermingle extensively. While time-lapse analysis suggested that the forming otic

placode undergoes extensive cellular movements and reorganizations before assembling into the otic vesicle. From this data a model emerged where cells in the PPA are at one point bi-potent for either otic or EB fates, and by some cell sorting and fate assignment mechanism distinct placodes will resolve. However, this model has not been tested directly.

Further experiments to construct fate maps of the PPA were conducted in mouse using a genetically encoded lineage approach. Here transgenic mice were generated using knock in technology to generate a Pax8Cre allele to constitutively drive Cre recombinase in Pax8+ tissue, these mice were crossed to a Z/AP reporter line (Bouchard et al., 2004). The otic and EB placodes were two of the embryonic tissues labeled by Pax8 cre expression. From these studies it was concluded that the otic and EB placodes originate from a common territory. However, because Pax8 is continuously expressed in both the developing otic and EB placodes and this particular Pax8Cre driver was not conditional, it is not clear whether these results reflect a common lineage of otic and EB placodes.

Due to the limitations that arise from relying on injectable dyes to construct fate maps and the use of tissue specific drivers in the absence of temporal control to genetically label placode derivatives we propose that the current model of posterior placode formation is not fully resolved. To better understand otic and EB placode origins, we have conducted fate mapping experiments using the genetic and high resolution imaging advantages of the zebrafish model system. In addition to these adavantages, zebrafish develop ex-utero, making this an ideal system to perform embryonic manipulations during gastrula and early

neurula stages. We used a genetically encoded *pax2a:GFP* transgenic in conjunction with the expression of photoconvertable fluorescent molecules to construct a fine fate map with 3-cell labeling resolution of the PPA as marked by Pax2a at the 12 hpf (early neurulation) stage. To better understand cellular behavior involved during otic vesicle formation we have conducted time-lapse imaging using similar techniques. From these experiments we have constructed a high fidelity, detailed fate map of the PPA. We also determined if the PPA is necessary for the formation of the otic and EB placodes through two-photon ablation experiments.

Another outstanding question in the field of placode formation is the mechanisms by which placodes gain their own identity from a common territory. Our preliminary studies analyzing Pax2a expression in the otic and EB placodes revealed that differential levels of this factor were expressed in these placodes, with high levels of Pax2a in the otic placode and low levels of Pax2a in the EB placodes. We hypothesize that these differential levels of Pax2a (and the redundant factor Pax8) are instructive during placode fate assignment, with high levels important for otic and low levels for EB development. Gain and loss of function experiments were employed to determine the validity of this hypothesis (Chapter 3.3.4)

If indeed differential levels of Pax factors are important, then there must be an extrinsic signaling pathway involved to regulate Pax levels. A likely candidate for controlling Pax2a levels is the Wnt signaling pathway. This pathway has previously been implicated in enforcing an otic fate from precursor cells in

the PPA in chick and mouse (Freter et al., 2008b; Ohyama et al., 2006). However, its role in otic development in zebrafish is still unclear (Phillips et al., 2004). Here we propose that Wnt signaling from the hindbrain is required to induce high levels of Pax2a in a subset of the PPA cells to promote otic development. To test this hypothesis, modulation of the Wnt signaling pathway was performed during developmental stages critical for early otic formation using pharmacological and genetic approaches (Chapter 3.3.8 & 3.3.9).

Previous studies have shown a requirement for Fgf signaling during early stages of otic and EB placode precursor specification, and again during later stages of EB neurogenesis (Nechiporuk et al., 2005; Nechiporuk et al., 2006), however the signaling factors required for intermediate stages of EB placode development and maturation are currently unknown. Preliminary work suggests that Fgf signaling is required again during formation and maturation of the EB placodes, independent of otic vesicle formation. Loss of Fgf signaling between 14 and 22 hpf in zebrafish using an inducible dominant negative Fgf receptor shows a loss or reduction in the EB placodes (as measured by loss of Pax2a expression) while the otic vesicle remains relatively unaffected (Nechiporuk et al., 2006). Based on this preliminary work, we hypothesize that Fgf signaling is necessary and sufficient to promote EB placode development. This was tested through global gain and loss of function experiments during critical stages of EB placode development, and further assessed by local gain of function experiments. Also, the specific Fgf ligands responsible for EB placode development were determined through a combination of expression profile

analysis, and loss of function experiments. Specific sources that provide these Fgfs were determined as well through the use of expression profiling, tissue ablation, and mosaic analysis.

Knowledge on the origins of cranial sensory systems has progressed much in the past 20 years. However, much work remains, including the construction of highly resolved fate-maps, an understanding of cranial placode segregation mechanisms, revealing neighboring tissue signals that provide cues for placode development, and identifying additional intrinsic and extrinsic molecules involved. The data included in this dissertation provide advancements in all the aforementioned dimensions of placode formation, and is a contribution to the field as we progress to a better understanding of how the vertebrate head is formed.

CHAPTER 1 FIGURES

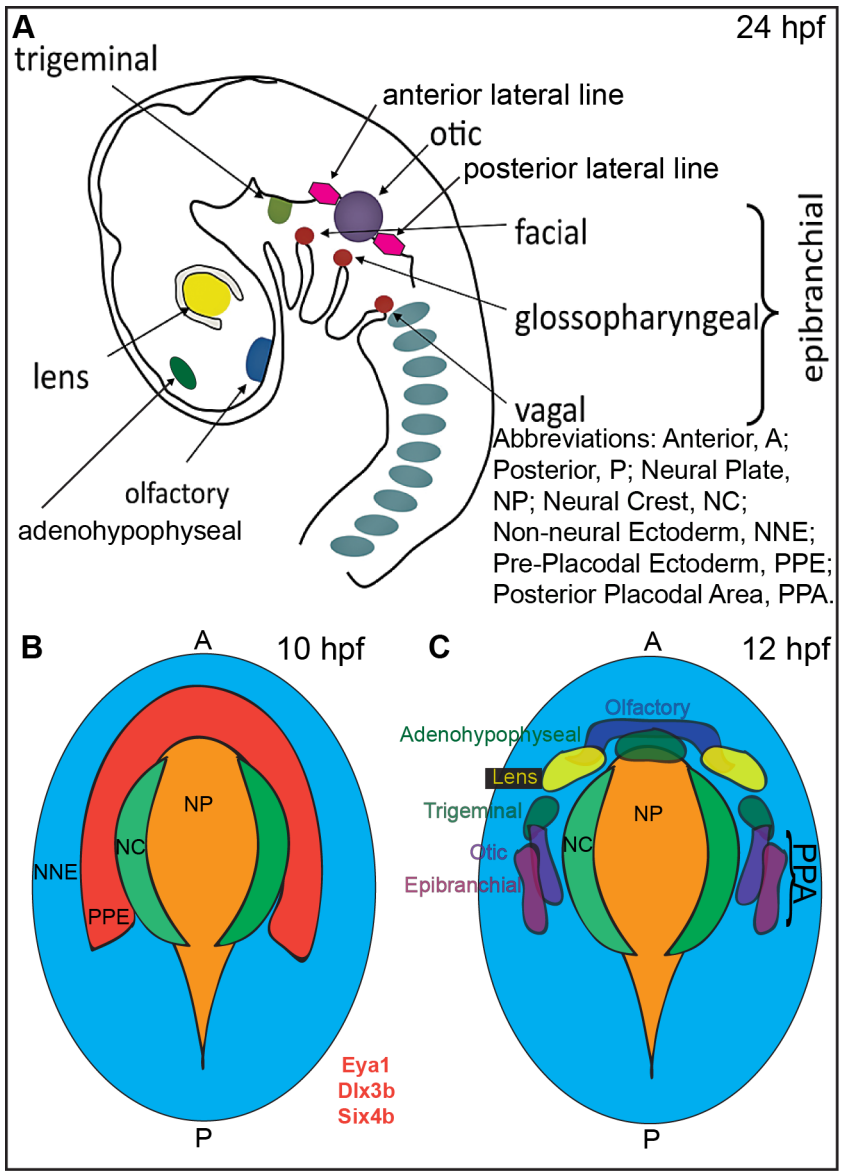

Figure 1: Schematized placode development

(A) 24 hpf zebrafish embryo, placodes are fully mature at this stage. **(B)** 10 hpf neural plate stage zebrafish embryo, PPE is a horseshoe shaped domain labeled in red, and can be marked by the factors Eya1, Dlx3b, and Six4b. **(C)** 12 hpf zebrafish embryo, individual placodes begin to segregate and the PPA can be identified broadly by *foxi1* and more specifically by *pax2a* expression.

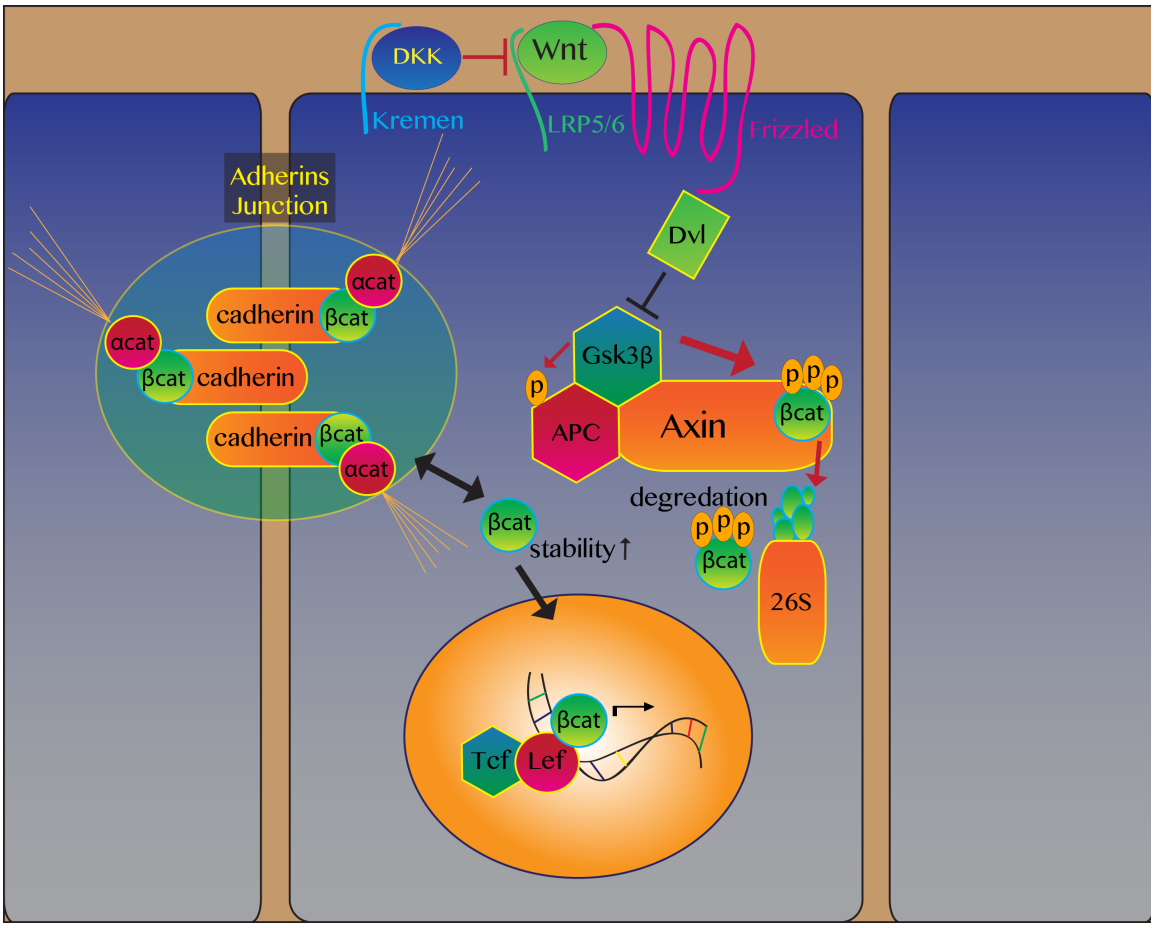

Figure 2: Canonical Wnt signaling
Simplified version of the generally accepted view of canonical Wnt signaling: Upon binding of a canonical Wnt ligand to Frizzled and LRP5/6 groups these receptors together to activate Dvl, which will in turn inhibit the Gsk3β mediated β-catenin destruction complex, resulting in an increase of cytoplasmic β-catenin which will interact with Wnt co-factors Tcf/Lef to activate transcription. The extracellular molecule DKK can inhibit Wnt signaling. In the absence of activated Wnt pathway Gsk3β can initiate the destruction of β-catenin through the 26S proteasome. Also included in this diagram is β-catenin's (βcat) role as a cytoskeleton intermediate in adherins junctions.

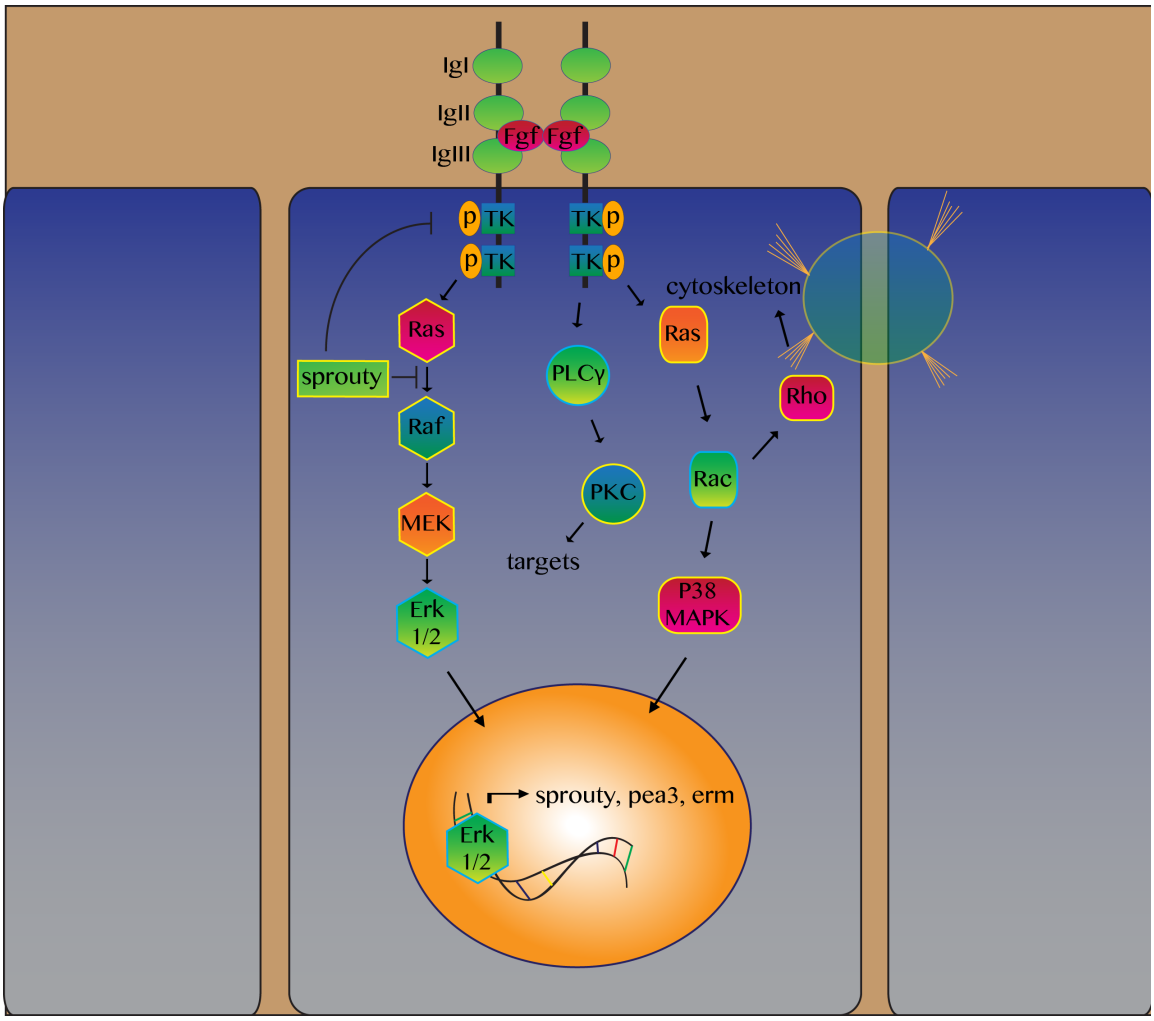

Figure 3: Signaling through the fibroblast growth factor receptors
Fgf signaling is initiated by the ligand dependent dimerization of Fgfrs which leads to transphosphorylation of tyrosine residues on the intracellular domain of the receptors, which results in binding of several specific cytoplasmic signaling factors that can initiate a multiplicity of signaling cascades including: Ras, Raf, MEK; PLCγ, PKC; and/or Ras, Rac, Rho. Abbreviations: Ig, Immunoglobulin domain; TK, tyrosine kinase.

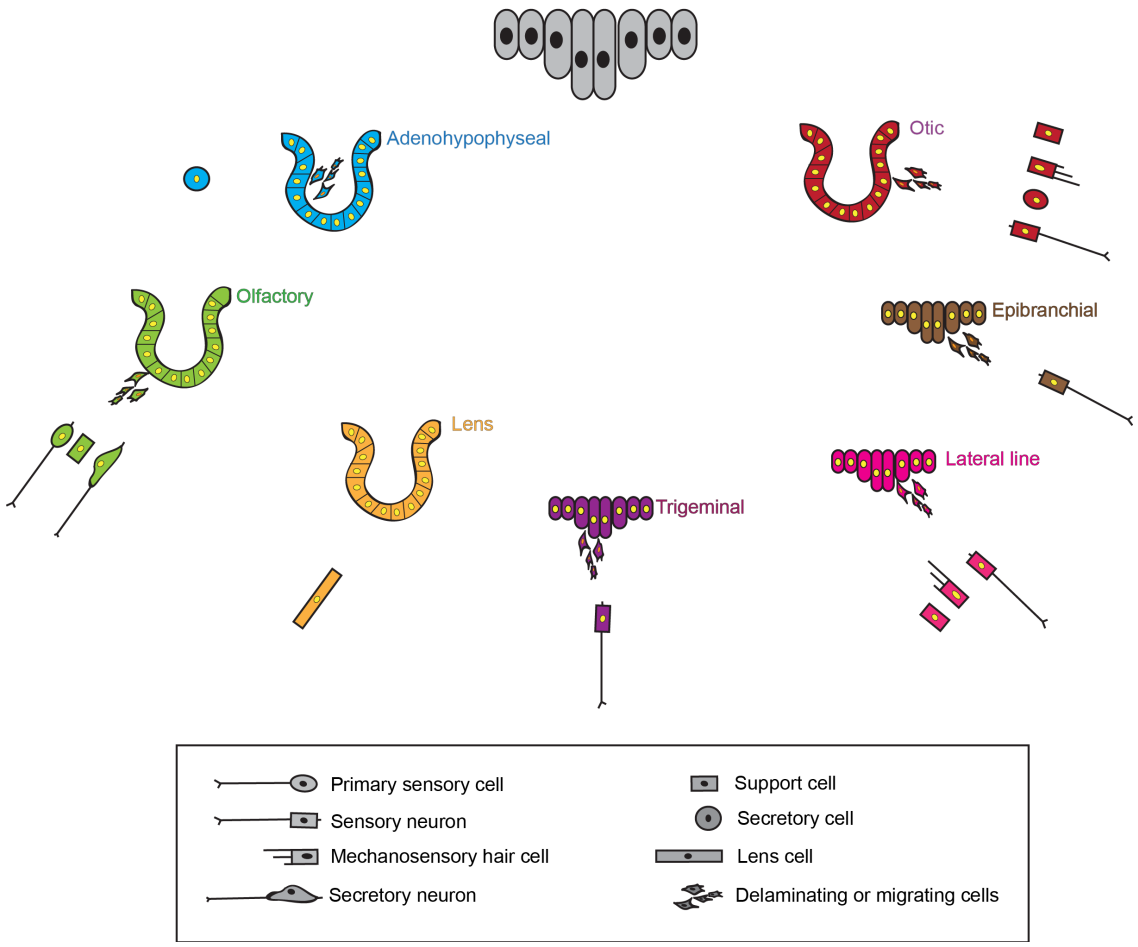

Figure 4: Cranial placode potential in vertebrates
Summaries of the different cellular derivatives cranial placodes are capable of generating and the morphogenetic movements (invagination delamination) involved. Modified from (Schlosser, 2005).

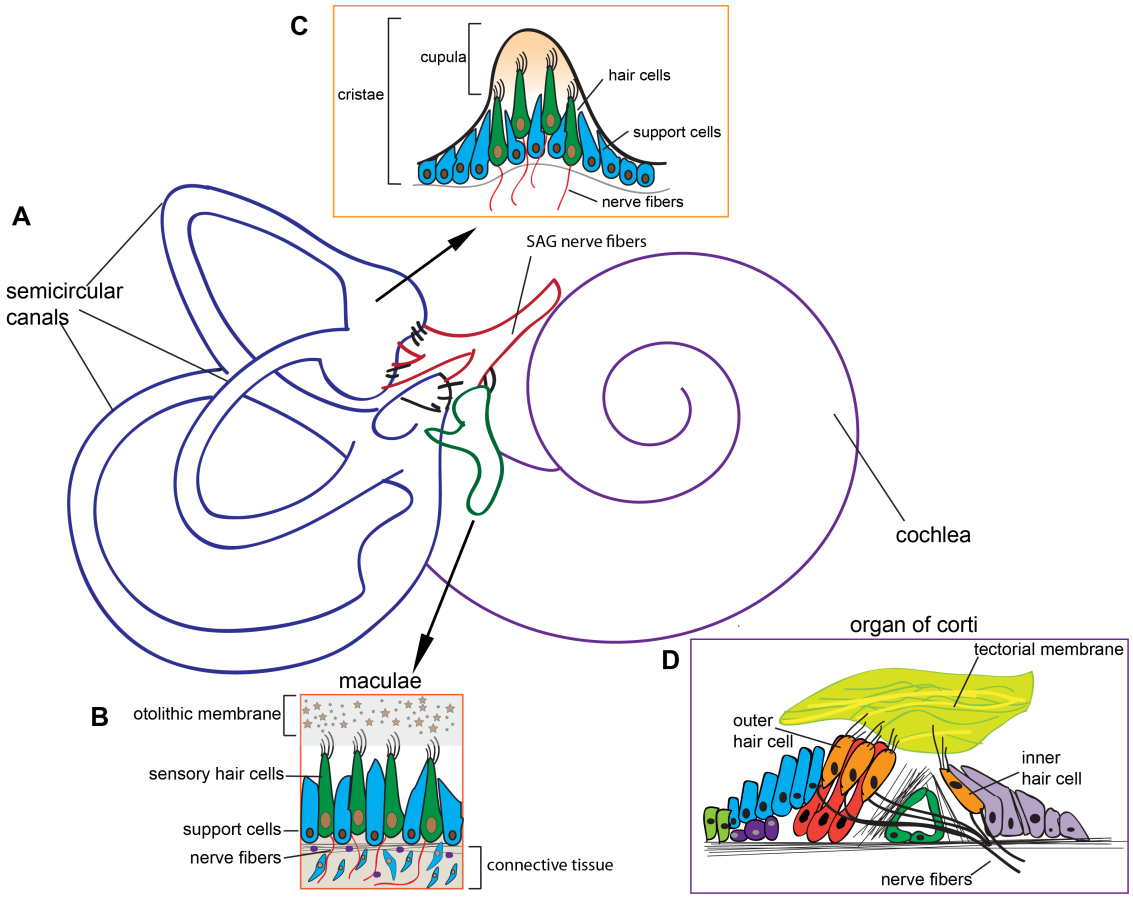

Figure 5: Schematic of the inner ear and its associated sensory structures, the maculae and the cristae.

(A) Depiction of the inner ear showing the three semicircular canals in blue. These canals contain vestibular sensory structures, the cristae. Illustrated in green is the vestibular region containing the utricle and saccule, which harbor the otolith organs, the maculae. Nerve fibers of the SAG are shown in red, and the auditory component of the inner ear, the cochlea, is depicted in purple. **(B)** Illustration of the maculae showing in detail the otolithic membrane which covers the stereocillia of the sensory hair cells, the associated support cells and nerve fibers. **(C)** Representative image of the cristae contained in the semicircular canals, stereocilia of the hair cells project into the cupula. **(D)** Illustration of the organ of corti found on the scala media side of the basilar membrane; two types of sensory cells are located in the organ of corti: inner hair cells and outer hair cells.

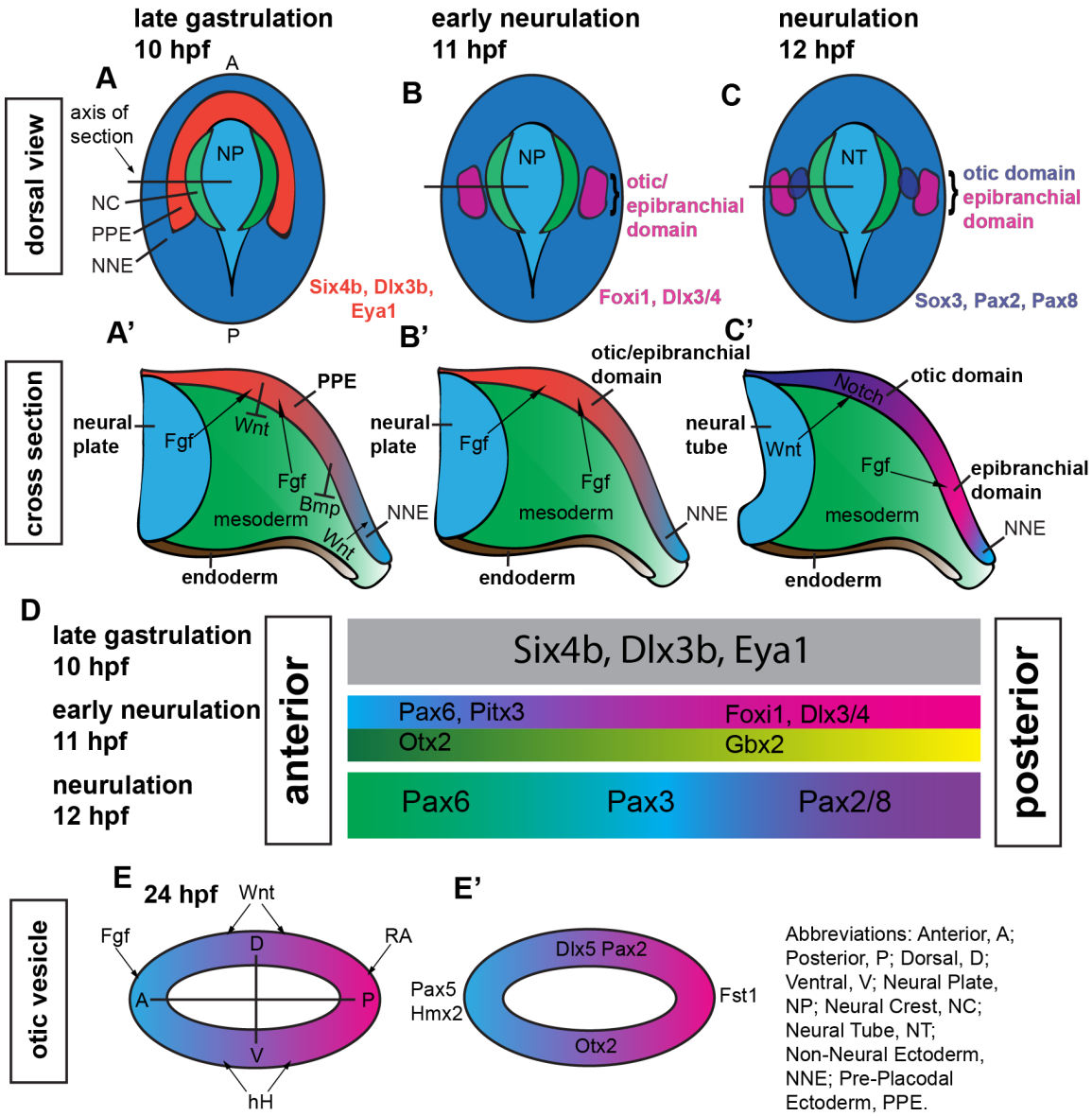

Abbreviations: Anterior, A; Posterior, P; Dorsal, D; Ventral, V; Neural Plate, NP; Neural Crest, NC; Neural Tube, NT; Non-Neural Ectoderm, NNE; Pre-Placodal Ectoderm, PPE.

Figure 6: Illustration of early PPE and PPA development and subsequent otic patterning.

(A) Dorsal view of a late-gastrulation embryo, the horseshoe shaped PPE domain is depicted in red. This domain adjoins the neural plate (light blue) and is lateral to the forming neural crest (green), lateral of the PPE is the non-neural ectoderm (blue). The PPE is defined at this stage by the expression of Six, Dlx, and Eya. **(A')** Unilateral cross-section at the indicated axis and same time point as in (A). The neural plate (blue) and the cephalic mesoderm (green) secrete Fgfs that induce the PPE (red); Wnt and BMP inhibitors are expressed in the PPE while lateral and posterior mesodermal Wnt defines PPE boundaries. **(B)** At early neurulation stage, precursors for both the otic and EB placodes are contained in a common domain (purple) defined by the expression of Foxi1 and Dlx3/4. **(B')** Cross-section of an early neurulation stage embryo at the indicated axis (B). Continued Fgf signaling from the neural tube and cephalic mesoderm induce the common otic/EB domain. **(C)** Neurulation stage embryo illustrating the segregation of the early otic placode in blue, defined by its expression of Sox3, Pax2, and Pax8. **(C')** Cross-section of a neurulation stage embryo at the indicated axis (C). At this stage, Wnt signaling from the neural tube works in conjunction with the Notch pathway to define the early otic domain, continued Fgf signaling from the cephalic mesoderm defines the epibranchial domain. **(D)** Anterior-posterior patterning of the PPE. Late gastrulation stage PPE factors are expressed along the entire A-P axis of the domain; by early neurula stage regionalization of anterior or posterior factors can be seen with Pax6, Pitx3, and Otx2 anterior and Foxi1, Dlx3/4, and Gbx2 posterior. By late neurula/early somitogenesis stage regionalized Pax factors emerge with Pax6 anterior most, Pax3 intermediate, and Pax2/8 posterior most. **(E)** Illustration of the signaling pathways involved in early otic regionalization. Fgf defines the anterior while an RA gradient is responsible for the posterior; Wnt signaling imparts dorsal identity while hH signaling sets up the ventral axis. **(E')** Factors that define molecular asymmetries during otic patterning: Dlx5, Pax2 for dorsal; Pax5, Hmx2 for anterior; Otx2 for ventral and Fst1 for posterior.

CHAPTER 2: GENERAL METHODS

2.1 Animal care, transgenics, and mutants.

Zebrafish husbandry was performed as previously described (Westerfield, 2000) and staged by hours post fertilization (Kimmel et al., 1995). The following zebrafish strains were used in this dissertation: *AB; Tg(*pax2a:GFP*)^{e1} (Picker et al., 2002); TgBAC(*phox2b:EGFP)*^{w37} (Nechiporuk et al., 2006); *pax2a*$^{b593/+}$ (Erickson et al., 2007); Tg*(hsp70:ca-fgfr1)*^{pd3} (Marques et al., 2008); Tg*(hsp70:dnfgfr1-EGFP)*^{pd1} (Lee et al., 2005); Tg(*hsp70:tcf∆C-EGFP)* (Martin and Kimelman, 2011); Tg*(hsp70:dkk1-GFP)*^{w32} (Stoick-Cooper et al., 2006); *lia*^{t26121} (Herzog, 2004); TgBAC*(foxi1:d2EGFP)*^{nl11}; Tg*(pax2a:Kaede)*^{nl12}; TgBAC*(neurog1:DSRed)*^{nl6} (Drerup and Nechiporuk, 2013); and*Tg*(*sox10*(*7.2*)*:mrfp*)^{vu234} (Kucenas et al., 2008).

2.2 Pharmacological, heat-shock and morpholino treatments

The gsk3-β inhibitor 6-bromoindirubin-3'-oxime (BIO, Sigma) was dissolved in Dimethyl sulfoxide (DMSO) at 10 mM as a stock and stored at 4˚C, and then further diluted to working concentrations in embryo medium (EM). Wildtype embryos were treated with 2.5 µM and 5.0 µM BIO; control embryos were treated with equal volume of DMSO in EM between 12-24 or 12-52 hpf. All heat-shock experiments were conducted in a Bio-Rad Tetrad-2 PCR machine in 100µl EM in 8 well pcr strips (BioExpress) at 11 hpf unless otherwise stated. Homozygous Tg*(hsp70:ca-fgfr1)*^{pd3} transgenic fish were crossed to wildtype fish to obtain heterozygous embryos that were heat-shocked at 36.9˚C to 38˚C for 45 minutes, then assayed for Pax2a+ cells between 12-24 hpf. As control, we

compared both un-heatshocked heterozygous Tg*(hsp70:ca-fgfr1)*^{pd3} and heat-shocked *Ab. Heterozygous Tg*(hsp70l:dnfgfr1-egfp)*^{pd1} transgenic fish were crossed to wildtype fish, heat-shocked at 35˚C to 37.2˚C for 30 minutes and then sorted for GFP under epifluorescence to identify transgene carriers. Heterozygous transgenic Tg(*hsp70:*Δ*tcf-gfp)* fish were crossed to wild-type fish, heat-shocked at 38˚C and 39˚C for 30 minutes and sorted for GFP under epifluorescence to identify transgene carriers. Heterozygous Tg*(hsp70l:dkk1-GFP)*^{w32} fish were in-crossed, embryos underwent two rounds of heat-shock at 39˚C for 40 minutes both at 11 hpf and 16 hpf and sorted for GFP under epifluorescence. For all heat-shock experiments that involved heterozygous transgene carriers, GFP negative siblings were used as controls. Antisense morpholino oligonucleotides (MO) were obtained from GeneTools (Corvalis, OR), diluted to working concentrations in H_2O and injected into *AB; TgBAC(*phox2b:EGFP)*^{w37}; TgBAC*(foxi1:d2EGFP)*^{nl11}; TgBAC*(neurog:dsRED)*^{nl6}; *Tg*(*sox10*(*7.2*)*:mrfp*); and *lia*^{t26121} embryos: *fgf3*-MO (5'-CATTGTGGCATGGCGGGATGTCGGC (Maroon et al., 2002); *fgf10*-MO (5'-GCTTTACTCACTGTACGGATCGTCC (Nechiporuk and Raible, 2008); *cas*-MO (5'-GCATCCGGTCGAGATACATGCTGTT (Sakaguchi et al., 2001); *pax2a*-MO (5'-ATATGGTGTCTCACCTATAGTGTGT; gift from Joshua Waxman, Cincinnati Children's Hospital), *pax8*E5/I5-MO+*pax8*E9/I9-MO (Hans et al., 2004b). Efficacy of *fgf3* and *fgf10*-MO were assessed by fusion of the otoliths at 2 dpf (Herzog, 2004) and loss of pectoral fins at 4 dpf (Norton et al., 2005), respectively. Efficacy of *pax2a*-MO was assessed by RT-PCR using the following primers:

pax2a-MO-F: 5'-GCAGAATACAAGCGGCAAAATC, *pax2a*-MO-R: 5'-CGTAAACTCTCCACACTACCCTGAG.

2.3 Whole-mount in situ hybridization and immunostaining

Whole-mount immunostaining and in-situ hybridization were performed as described previously (Andermann et al., 2002). The following antibodies and riboprobes were used in this dissertation: α-Pax2 (1:100, Covance); α-GFP (1:1000, Invitrogen); α-Fluorescein (1:1000, Roche); α-Elavl 3/4 (1:1000, Invitrogen; sold as α-Hu C/D); α-Dlx3b (1:100, Zirc); α-beta Catenin (1:100, Iowa Hybridoma bank); *pax2a* (Krauss et al., 1991); *pax8* (Pfeffer et al., 1998); *fgf3 (Kiefer et al., 1996)*; *fgf8* (Reifers et al., 1998); *fgf10* (Grandel et al., 2000); *pax5 (Hammond et al., 2003)*; *sox3* (Sun et al., 2007); *eya1* (Sahly et al., 1999); *foxi1* (Lee et al., 2003). Whole-mount fluorescent images were obtained using an upright Olympus FV1000 confocal microscope using a 20X (0.75 NA) air objective. Brightfield images were photographed using an Axio Imager Z1 compound microscope with an HRc digital camera controlled by Axiovision software (Zeiss). Assembly of Z-stack images, heat-map analysis, and measurements of mean fluorescence intensity were prepared using Image-J software (Abramoff et al., 2004). Experiments comparing mean fluorescence intensities between conditions were done in parallel using the same dilution of α-Pax2; care was taken to maintain consistency of confocal acquisition settings. Brightness and contrast were adjusted using Adobe Photoshop.

2.4 Statistical Analyses

Numerical data was organized and graphs were generated using Excel (Microsoft) or Prism (GraphPad). Standard error of mean (SEM) was used for error bars through out all studies. Student's t-tests were performed using Excel or Prism, while Chi-Square (χ^2), ANOVA multiple comparison with Bonferroni's correction or Sidak's correction, and Wilcoxon matched-pairs signed rank test were performed using Prism.

2.5 Generation of plasmids and BAC transgenesis

A previously published bi-directional heat-shock inducible construct was modified to contain the coding sequence of *pax2a* together with dTomato reporter (Bajoghli et al., 2004). The *pax2a* coding sequence was amplified from zebrafish cDNA using the following primers: Forward 5'-ACCGGTCTACATAATCAAGGCGAGACGG; Reverse 5'-TACGTACAGTTTGACTGGGCTGCGATGGT. Primers contained a 5' AgeI site and a 3' SnaBI site for incorporation into the expression construct to obtain the recombinant dTomato:HSE:Pax2a plasmid. The same bi-directional heatshock vector expressing dTomato and EGFP (dTomato:HSE:EGFP) was used as control. Plasmids were microinjected into wildtype single cell stage embryos at 20 ng/µl and heat-shocked at 11 hpf at 38˚C for 30 minutes. Embryos were assayed for efficiency of Pax2a induction at 3 hours post heat shock, and placodes were assayed at 24 hpf.

BAC recombination was performed according to published methods (Suster et al., 2011), with following modifications. Dy380 cells (a modified DH10B E. Coli strain) were used, because they can be efficiently transformed with BAC DNA and also contain a heat-shock inducible recombinase. Electro-competent cells were made according to the Suster et al., 2011 protocol; 2µg of BAC DNA extracted with the NeucleoBond BAC100 (Clontech) kit was electroporated into Dy380 cells in 0.1 mm Gene Pulser/E. Coli Pulser cuvetts (BioRad) at 1.5 kV. After BAC DNA is transformed into Dy380 cells, all incubations are performed at 32˚C or below except for when inducing recombinase expression (42˚C), this is because the cells can become unstable when exposed to higher temperatures for prolonged periods of time or activate recombinase at undesired times. Bacterial colonies take 48 hours to grow at 32˚C.

2.6 2-photon ablations of *EGFP*+ cells in the PPA

Ablation of specific regions of the early Pax2a domain in Tg(*pax2a:GFP*)^{e1} embryos was accomplished by modifying previously described methods (Sagasti et al., 2009). Tg(*pax2a:GFP*)^{e1} embryos were collected at 11-12 hpf and sorted for EGFP expression and embedded in 1% low melt agarose (GenePure) in EM in the bottom of a scored 30 mm petri dish (Falcon). Embryos were mounted such that the PPA was positioned for optimal imaging. We used a Ti:sapphire pulsed laser (Chameleon Ultra II; Coherent, Auburn, CA) powered by Prairie Technologies Ultima two-photon imaging system (Middleton, WI). Laser intensity was adjusted with a Pockels cell (350-80 LA; Conoptics, Danbury, CT). The laser frequency was adjusted to 910 nm. Target region was identified with a 60X (0.9

NA) water objective with the pockels cell adjusted to 2 and PTMs (photomultiplier) ~ 750, dwell time of 15 ms and a zoom of 1X. After ROI was identified, ablations were executed at 3 - 6X zoom, PMTs were decreased to zero, the pockels cell was adjusted between 50-60 with the dwell time increased to 30 ms. Post-ablation of the entire OED was scanned on an upright Olympus FV1000 confocal microscope using a 40X (0.8 NA) water objective to document ablated region. Embryos were then dissected out of agarose and allowed to develop to 24 hpf at 28.5˚C, fixed and stained with anti-Pax2a antibody as described above. Following Pax2 labeling, both sides were imaged to compare placode formation on ablated versus unablated sides of the embryo.

2.7 Fate mapping experiments

Small groups of cells (mean = 3.53±0.32) were labeled at 4 to 7 somite stages (12-13 hpf). At the time of labeling, the position of the cells within the Pax2a domain was recorded, along with the number of cells and the stage of the embryo. Labeling was achieved either with focal photoconversion of Kaede, or by fluorescein uncaging. For photoconversion or fluorescein uncaging experiments Tg(*pax2a:GFP*)*e1* embryos were injected at the 1-cell stage with 1 nL of 100 pg of NLS-Kaede capped mRNA or 1.25% caged fluorescein (Invitrogen) in 0.2M KCl (Sigma) with 0.167% Phenol Red. At 4-somite stage, embryos were mounted in 1% Low-Melt Agarose (GenePure) in EM on top of a coverslip, then immersed in embryo medium. Labeling was performed with an upright Olympus FV1000 confocal microscope with a 60x (1.20 NA) water objective using a small ROI in the Bleach function. Magnification was increased to approximately 30X and

selected cells were scanned with the 405 nm laser at 0.1% power setting. Care was taken to document the extent of labeling and ensure that no labeling occurred outside of the Pax2a domain. In Kaede experiments, the embryos were imaged live at 24 hpf to detect the location of the converted cells. In fluorescein uncaging experiments, embryos were fixed in 4% paraformaldehyde/1x PBS (PFA) at 24 hpf, stained with α-Fluorescein (Roche), α-Pax2 (Covance) antibodies and Alexa546 and Alexa647 secondary antibodies. Embryos were analyzed by taking z-series of the Pax2a-derived region and examining for labeled cells. Contribution to each of the Pax2a-derived placodes was quantified by dividing the number of labeling instances of a placode by the total number of labeling instances within each sub-region of the Pax2a domain.

CHAPTER 3: WNT CONTROLLED PAX LEVELS DURING OTIC AND EPIBRANCHIAL PLACODE DEVELOPMENT

Modified from: McCarroll, M. N., Lewis, Z. R., Culbertson, M. D., Martin, B. L., Kimelman, D. and Nechiporuk, A. V. (2012). Graded levels of Pax2a and Pax8 regulate cell differentiation during sensory placode formation. *Development*.

Author Contributions

Conceived and designed the photoconversion experiments: AVN ZRL MNM. Performed the photoconversion experiments: ZRL MNM. Analyzed the data for photoconversion experiments: AVN ZRL MNM. Performed cell death/proliferation assays and *fgf3/8* in situs: MDC. Conceived and designed all other experiments: AVN MNM. Performed all other experiments: MNM. Analyzed the data for all other experiments: AVN MNM. Generated the *hsp70:tcf∆C-EGFP* transgenic: BLM DK. Contributed other reagents/materials/analysis tools: AVN MNM ZRL. Wrote the manuscript: AVN MNM ZRL.

3.1 Abstract:

Pax gene haploinsufficiency causes a variety of congenital defects. Renal-coloboma syndrome, resulting from mutations in Pax2, is characterized by kidney hypoplasia, optic nerve malformation, and hearing loss. Although this underscores the importance of Pax gene dosage in normal development, how differential levels of these transcriptional regulators affect cell differentiation and tissue morphogenesis is still poorly understood. We show that differential levels of zebrafish Pax2a and Pax8 modulate commitment and behavior in cells that eventually contribute to the otic vesicle and epibranchial placodes. Initially, a subset of epibranchial placode precursors lie lateral to otic precursors within a single Pax2a/8+ domain; these cells subsequently move to segregate into distinct placodes. Using lineage-tracing and ablation analyses, we show that cells in the Pax2a/8+ domain become biased towards certain fates at the beginning of somitogenesis. Experiments involving either Pax2a overexpression or partial, combinatorial Pax2a and Pax8 loss of function reveal that high levels of Pax favor otic differentiation whereas low levels increase cell numbers in epibranchial ganglia. In addition, the Fgf and Wnt signaling pathways control Pax2a expression: Fgf is necessary to induce Pax2a, whereas Wnt instructs the high levels of Pax2a that favor otic differentiation. Our studies reveal the importance of Pax levels during sensory placode formation and provide a mechanism by which these levels are controlled.

3.2 Introduction:

The sensory organs of the vertebrate head develop from discrete regions of neurogenic epithelium known as cranial placodes. Placodes are transient ectodermal thickenings situated lateral to the forming central nervous system (CNS) and neural crest. Responding to extrinsic signals, cranial placode cells invaginate or delaminate, migrate, and condense to form diverse structures, including the otic vesicle, and neurons of the cranial ganglia. The EB placodes give rise to the EB ganglia, the facial, glossopharyngeal, and vagal (alternatively, the geniculate, petrosal, and nodose) ganglia that relay sensory information about taste and the visceral sensation to the CNS (Schlosser, 2006).

Cranial placodes are derived from the pan-placodal ectoderm (PPE; Streit, 2004; Schlosser, 2005) which develops during late gastrulation as a horseshoe-shaped region adjacent to the neural plate and lateral to the neural crest (Ahrens and Schlosser, 2005; Brugmann et al., 2004a; Litsiou et al., 2005). Once formed, the PPE is subdivided into distinct subdomains containing shared precursors for multiple placodes (Bailey et al., 2006; Schlosser, 2006). Previous studies suggest that otic and EB placode precursors might arise from a common subdomain of the PPE, the posterior placodal area (PPA; (Freter et al., 2008a; Ohyama and Groves, 2004a; Schlosser and Ahrens, 2004; Sun et al., 2007). However, one zebrafish study showed that glossopharyngeal and vagal (but not facial) placode precursors were induced from adjacent non-neural ectoderm via Fgf24 secreted from the PPA (Padanad and Riley, 2011). Thus, it is unclear whether the PPA contributes cells to the EB placodes.

The PPA is delineated by *Paired-box2* (*Pax2*) and *Pax8* expression at the onset of somitogenesis (Streit, 2002; Schlosser and Ahrens, 2004; Ohyama and Groves, 2004; Bouchard et al., 2004) with Pax8 and Pax2a acting redundantly in otic and EB placode development (Bouchard et al., 2004; Padanad and Riley, 2011). Humans with *Pax2* haploinsufficiencies exhibit renal hypoplasia, vesicoureteric reflux, and optic nerve coloboma (Alur et al., 2010; Schimmenti, 2011) whereas persistent expression of Pax2 causes a variety of cystic and dysplastic renal diseases (Cunliffe et al., 1998; Davis et al., 2011). This implies that levels of this transcriptional regulator must be strictly controlled (Eccles et al., 2002). However, whether different levels of Pax2a/8 play a role during sensory organ development is unknown.

Fgf and Wnt are both critical during otic and EB placode induction. In zebrafish and chick, hindbrain and mesoderm-derived Fgf signals act redundantly to induce EB placodes (Freter et al., 2008a; Nechiporuk et al., 2006; Nikaido et al., 2007b) and are required for initial otic placode induction. Attenuated Fgf signaling, coupled with increased hindbrain-derived Wnt8, subsequently leads to otic commitment and eventual inner ear patterning (Ohyama et al., 2006). While Wnt and Fgf signaling requirements for defining otic and EB fate have been demonstrated, it is unclear how these signals control Pax2a/8 expression during placode resolution.

We show that in zebrafish, as in mouse and chick, the otic placode arises from a Pax2a+ PPA precursor domain that also contributes to the EB placodes. Through loss-of-function and overexpression analyses, we find that relative

Pax2a/8 expression levels correlate with distinct placodes: high Pax2a/8 levels promote otic differentiation while cells with low Pax2a/8 levels acquire an EB bias. We show that Wnt pathway activation promotes high levels of Pax2a expression, biasing PPA cells toward otic commitment. We propose that Wnt directs PPA cell segregation, in part, by altering Pax2a/8 expression levels.

3.3 Results:

3.3.1 Pax2a+ PPA precursors are spatially biased at the four-somite stage

Previous studies indicate that the EB and otic placodes arise from a common domain, the PPA, consisting of Pax2/8+ precursors (Bouchard et al., 2004). However, a study in zebrafish showed that glossopharyngeal and vagal placode precursors arose from non-neural ectoderm lateral to the PPA (Padanad and Riley, 2011). We asked whether the PPA contained both EB placode and otic precursors and whether these populations were segregated or intermingled. To address this, we utilized a Tg(*pax2a:GFP*) line with GFP driven by a 5.3 kb portion of the *pax2a* promoter (Picker et al., 2002). By comparing expression of Tg(*pax2a:GFP*) with Pax2a immunolabeling, we found that the transgene largely recapitulated endogenous early-stage Pax2a expression in the PPA. At 11 hpf, the transgene is expressed at low levels in a small population of cells lateral to the neural plate (data not shown). By 12 hpf, the GFP+ and Pax2a+ cells

aggregate lateral to rhombomeres 5 and 6 (Figure 7A-A'' and Figure 8). While at 24 hpf the transgene was expressed in all otic vesicle cells, it marked only a small subset of Pax2a+ cells in the facial and glossopharyngeal/vagal placodes (Figure 7B-B''). We concluded that the transgene contains necessary regulatory elements to mark PPA cells during early development, but is insufficient to drive GFP expression in most of the EB placodes.

We utilized early Tg(*pax2a:GFP*) expression to mark specific cells within the PPA. Using a nuclear-localized Kaede protein (NLS-Kaede; 119 out of 139 specimens), caged fluorescein-dextran (20 of 139), small groups of cells were labeled in discrete regions of the PPA (Figure 9A,C). The initial location of the cells at 12 hpf was recorded and assigned to one of 12 domains (Figure 9E). Importantly, we saw little variability in either cell number or dimensions of the GFP+ domain (107.8±2.16 cells; n=11; 1,186 cells), indicating consistency of this domain between labeled embryos (Figure 7C,D). Additionally, few cells were added to this domain after 12 hpf (data not shown), which imparted little variation between labeled embryos. This is in contrast to a previous study suggesting that additional cells are recruited to this domain after 12 hpf (Bhat and Riley, 2011). This difference could be attributed to the more sensitive confocal detection technique used in our study which allowed visualization of the most lateral, low-expressing Tg(*pax2a:GFP*)+ cells as early as 12 hpf. At 24 hpf, the fate of labeled cells was determined based on morphology and location of Kaede-labeled cells, and on Pax2a antibody labeling for fluorescein+ cells (Figure 9B-E).

The resulting fate map revealed a strong spatial bias within the PPA at 12 hpf. The subdomains of the PPA that contributed to the facial and glossopharyngeal/vagal placodes exhibited minimal overlap and corresponded to their respective anterior or posterior locations (Figure 9E), suggesting a subset of cells from the PPA contribute to the EB placodes (22 out of 139 labeling events).

In contrast to the spatial bias observed for the EB placode precursors, cells contributing to the otic vesicle were distributed throughout the Pax2a domain. However, anterolateral labeling events were more likely to label the acoustic (gVIII) and anterior lateral line (gAll) ganglia while posteromedial labeling marked the otic vesicle (Figure 9F). We never observed labeled cells in the posterior lateral line ganglion. We found that otic vesicle patterning is based on the initial location of precursor cells in the PPA: cells from the anterior PPA preferentially segregated to the anterolateral otic vesicle (Figure 10C) while cells from the posterior and posteromedial regions were distributed throughout the posterior and posteromedial aspects (Figure 10C,D). The bias of anterior contributions to the anterolateral otic vesicle is consistent with previous observations indicating that the anterior neurogenic region is established prior to otic placode formation (Abello et al., 2010).

Our fate-mapping experiments implied that most PPA cells did not undergo extensive re-arrangements after 12 hpf; however, a subset can contribute to more distal locations (e.g., anterior PPA cells contributed to the otic vesicle; Figure 9F). To visualize this, we labeled small clusters of PPA cells at 12 hpf and analyzed their behavior using live imaging. These analyses confirmed

that while PPA cells generally retained their A-P position, cells occasionally exhibited extensive movement (Figure 11). Cells not incorporated into the otic vesicle were also found migrating towards EB placodes (Figure 12).

Our fate mapping data support the assertion that not all cells of the EB placodes arise from the PPA (Padanad and Riley, 2011). However, a subset of PPA contributes to the EB placodes; at 12 hpf, these cells exhibited a spatial bias for EB placode precursors. In addition, the bulk of the otic vesicle arises from the posteriomedial regions of the PPA, with anterior regions contributing to the neurogenic anterolateral portion of the otic vesicle and the gAll/gVIII.

3.3.2 Cells of the Pax2a domain are required for normal development of the epibranchial and otic placodes

Our fate-mapping demonstrated spatial restriction within the PPA by 12 hpf. To confirm this, we unilaterally ablated different regions of the PPA in 12 hpf transgenic *Tg(pax2a:GFP)* embryos. Embryos were then immunostained for Pax2 at 24 hpf to visualize EB placodes and otic vesicles on the ablated and unablated (contralateral) sides. Ablating the anterior PPA yielded dramatic reductions in the facial placode versus the contralateral side (Figure 13A,C,D) without affecting the otic vesicle or glossopharyngeal/vagal placodes. Interestingly, anterior ablations also resulted in a loss of the early anterior lateral line as marked by *Tg(pax2a:GFP)* expression (data not shown). Conversely, ablating the posterior PPA resulted in a near-complete loss of the otic vesicle and a marked reduction in the glossopharyngeal/vagal placodes while the facial

placode was unaffected (Figure 13B,E,F). Thus, consistent with our fate-map, cells exhibit co-linearity between their initial positions in the PPA and their destinations within resolved placodes.

3.3.3 Differential expression of Pax2a in the PPA

As the PPA is defined by the expression of Pax2a, we next asked whether different levels of Pax2a affect differentiation of the otic and EB placodes. At 11 hpf, PPA cells exhibited low and uniform levels of Pax2a (Figure 14A,A'). However, by 12 hpf, Pax2a+ progenitors had assumed different expression levels with a significant increase in the number of high-expressing cells in the posteromedial region (Figure 14B,B',D). These differential levels of Pax2a persisted in PPA-derived structures; cells in the EB placodes expressed Pax2a at low levels, while the otic vesicle expressed Pax2a at high levels in the medial-most aspect and at lower levels in the lateral-most aspect (Figure 14C,C'). We also observed differential levels of *pax2a* mRNA that mirrored differential protein levels in PPA cells at 12 hpf and in the otic vesicle and EB placodes at 24 hpf, indicating that differences in Pax2a protein originate at the transcriptional level (Figure 15A-C).

Another *pax* gene, *pax8*, has been described as functionally redundant to *pax2a* during otic and EB placode formation (Padanad and Riley, 2011). Unfortunately, levels of Pax8 protein cannot be examined due to the lack of a zebrafish-compatible antibody. *pax8* transcripts are seen in zebrafish as early as 8 hpf in presumptive PPA (Pfeffer et al., 1998). We found that *pax8* expression

was discernable in the PPA at 11 and 12 hpf as well as in EB placodes and discrete foci of the otic vesicle at 24 hpf (Figure 15D-F). Thus, like *pax2a*, levels of *pax8* transcripts were also differentially regulated in PPA cells. These observations suggest that heterogeneous levels of Pax2a and Pax8 expression may reflect early cell biases toward specific placodal destinations.

3.3.4 High levels of Pax2a instruct an otic placode bias

Since Pax2a expression levels correlate with PPA cell identity, we asked whether overexpression or reduction of Pax2a would alter precursor commitment or differentiation. We conducted overexpression experiments using a bi-directional heat-shock-inducible promoter driving Pax2a (or EGFP control) in one direction and the dTomato reporter in the other. DNA was injected into wildtype embryos followed by heat-shock at 12 and 14 hpf, resulting in mosaic expression. The construct induced Pax2a expression comparable to high endogenous levels; 96% of cells that were positive for dTomato also expressed high levels of Pax2a at 15 hpf (Figure 16). Induced Pax2a was quickly turned over and was undetectable in most dTomato+ cells by 24 hpf (Figure 17B); at this stage, we assessed relative numbers of dTomato+ cells in the EB placodes and otic vesicle (Figure 17A,B). Following induction at 12 hpf and 14 hpf, 57% and 65% of dTomato+ cells contributed to the ear versus 44% and 45% in control embryos, respectively (Figure 17C). There was also a significant decrease in facial placode cell contribution in Pax2a overexpression embryos (11% and 10% versus 20% and 17% in controls). We also observed a significant progressive

decrease in cells populating the glossopharyngeal/vagal placodes in both induction conditions (controls: 36% and 38%; Pax2a overexpression: 32% and 25%; Figure 17C). To examine this bias, we used live imaging to follow Pax2a overexpressing cells in *Tg(pax2a:GFP)* embryos. We observed that Pax2a+ overexpressing cells from the lateral non-neural ectoderm moved medially to join the forming otic vesicle; dTomato+ cells that did not integrate died off more frequently versus GFP+ controls (Figure 18 and Figure 19). These data indicate that high levels of Pax2a alter cell behavior resulting in preferential segregation to the otic placode versus the EB placodes.

3.3.5 Partial knockdown of pax transcripts increases cell numbers in the epibranchial ganglia

We posited that if raising levels of Pax2a biases precursor cells toward otic commitment, reducing Pax2a levels might affect commitment or differentiation of PPA cells to EB placodes. Previous studies indicate that both Pax2a and Pax8 are required during otic and EB placode development (Padanad and Riley, 2011). However, whether differential levels of these factors bias cell commitment is unknown. Injection of 1 ng of *pax8* morpholino (*pax8*-MO) into zygotes from a heterozygous *pax2a*+/- incross resulted in severe reductions of EB ganglia (Figure 20A,B) in ~25% of progeny, supporting gene redundancy during EB development. We subsequently examined the effect of partial combinatorial reductions in Pax2a and Pax8 on the otic vesicle and EB ganglia.

The *pax8*-MO used in our studies was characterized previously (Hans et al., 2004b). Doses of *pax2a* splice-blocking MO that yield partial knockdown were estimated based on Pax2a expression levels in the PPA at 12 hpf and using RT-PCR (Figure 21 and Figure 20I). Injections of partial knockdown concentrations of *pax2a*-MO (3.0 ng) into wildtype embryos markedly reduced levels of Pax2a in the PPA versus controls at 12 hpf. Transgenic zygotes were injected with either *pax2a*-MO or *pax8*-MO alone, or in combination at increasing concentrations. The numbers of cells in the forming cranial ganglia were quantified at 50 hpf using TgBAC(*phox2b:EGFP)*^{w37} expression (Nechiporuk et al., 2006). Suboptimal concentrations of individual *pax* morpholinos alone yielded no change in cranial ganglion cell numbers versus controls (Figure 20). However, when partial knockdown concentrations were co-injected, we saw a significant increase in the numbers of Phox2b+ neurons in the facial, glossopharyngeal, and anteriormost small vagal ganglia. As dosages increased, ganglion sizes decreased (Figure 22A-C), indicating loss of precursor differentiation (Padanad and Riley, 2011). We also observed a concomitant reduction (albeit not statistically significant) in the size of the otic vesicle (Figure 22D). Therefore, relative levels of Pax2a/8 expression instruct cell commitment during subsequent placode segregation, with low levels favoring EB placode differentiation and higher levels favoring otic differentiation.

3.3.6 Fgf regulates the number of Pax2a positive progenitors but does not control levels of Pax2a

Previous studies demonstrated that FGF signaling was necessary for Pax2 expression to initiate otic and EB development (Ladher et al., 2010); however, FGF must be attenuated during later stages for continued otic development (Freter et al., 2008a). We asked whether similar Fgf signaling requirements exist in zebrafish and whether Fgf levels bias PPA cell behavior. We examined Pax2a expression in transgenic embryos carrying Tg*(hsp70:ca-fgfr1),* a heat-shock-inducible form of constitutively-active Fgfr1 (Marques et al., 2008). The transgene was differentially induced using a range of heat-shock temperatures (36.9-38˚C). Transgenic embryos were heat-shocked at 10 hpf and Pax2a expression analyzed at 24 hpf (Figure 23A,B). At the highest heat-shock induction temperature, Pax2a+ cell numbers increased more than 3-fold in the facial placode, while Pax2a+ cell numbers in the otic vesicle and the glossopharyngeal/vagal placodes decreased significantly (Figure 23D). Time-lapse imaging of Tg(*pax2a:GFP*) revealed that Pax2a+ cells were continuously generated from non-neural ectoderm lateral to the PPA between 14 and 18 hpf in induced Tg(*hsp70:ca-fgfr1)* embryos, but not in wildtype controls (Figure 8 and Figure 24). Increased facial placode size is likely explained by this dramatic increase in Pax2a+ precursors and not higher proliferation levels (Figure 23F).

Consistent with the live imaging and previous studies (Hans et al., 2007; Padanad et al., 2012), the overall number of otic cells (as measured by Dlx3b

expression) increased at 18 hpf following Tg*(hsp70:ca-fgfr1)* induction, although these cells appeared more dispersed than in controls (Figure 25). This increase in cell number was also accompanied by a significant increase in apoptosis after 18 hpf (Figure 23G), which accounts for smaller otic vesicles in Tg*(hsp70:ca-fgfr1)* embryos at 24 hpf. However, we cannot rule out the possibility that the observed increase in cell death was due to persistently high levels of transgene expression. In summary, our data indicate that high levels of Fgf activity favor the formation of facial and otic, but not glossopharyngeal/vagal, placodes.

We also conditionally inhibited Fgf signaling using Tg(*hsp70:dnfgfr1-EGFP)*: a heat-shock inducible dominant-negative form of Fgfr1 (Lee et al., 2005). The transgene was induced at 10 hpf using a range of heat-shock conditions (35-37.2˚C); Pax2a expression was analyzed at 24 hpf (Figure 23A,C). Here, the facial placode was severely reduced or completely absent, while the glossopharyngeal/vagal placodes failed to form. At higher induction temperatures the otic vesicle was severely reduced (Figure 23E), confirming a requirement for Fgf during placode formation.

We then asked if modulating Fgf alters otic vesicle and EB placode size via Pax2a. Tg(*hsp70:dnfgfr1-EGFP)* and Tg*(hsp70:ca-fgfr1)* embryos were heat-shocked at 10 hpf at 36.3˚C and 37.5˚C, respectively, and levels of Pax2a expression were analyzed at 12 hpf (Figure 23N). We found that the distribution of Pax2a intensity levels were similar between experimental conditions and control. We conclude that Fgf signaling is sufficient to induce Pax2a+ precursors from non-neural ectoderm and that persistent Fgf favors formation of the facial

and otic placode, but not glossopharyngeal/vagal placodes. However, Fgf does not establish heterogeneous Pax2a levels in PPA progenitors.

3.3.7 Overactivation of Wnt biases PPA cells to an otic commitment.

Studies in chick, *Xenopus* and mouse demonstrated that canonical Wnt activation is required to restrict a subset of posteromedial PPE cells to an otic fate (Freter et al., 2008; Park and Saint-Jeannet, 2008; Ohyama et al., 2006). Based on this and our observation that high-expressing Pax2a cells segregate to the otic placode, we hypothesized that Wnt might influence otic differentiation by inducing high levels of Pax2a within the PPA. To test this, embryos were treated from 11 hpf with BIO, which inhibits GSK3-β-mediated degradation of β-catenin, overactivating canonical Wnt signaling (Sato et al., 2003). At 12 hpf, we observed dramatic Pax2a level increases in treated embryos (Figure 26A-C). These increases were dose-dependent, with average fluorescence intensities of 107.1 and 151.6 for 2.5 and 5.0 μM BIO conditions, respectively (88.4 for control). The proportion of PPA cells expressing high levels of Pax2a increased in the presence of 5.0 μM BIO ($p<0.001$, χ^2-test; Figure 26G). Pax2a expression analyses at 24 hpf revealed dramatic increases in otic vesicle Pax2a+ cell numbers (2.5 fold increase for 2.5 μM BIO and 1.5 fold increase for 5.0 μM BIO), with a concomitant 80% reduction in the facial placode at 2.5 μM BIO (Figure 26D-F and I). At 5.0 μM BIO, the otic vesicle was enlarged and the EB placodes completely absent. The increase in otic cells correlated with higher Pax2a expression levels in the otic vesicle (Figure 26H). Loss of EB placodes was not

due to developmental delay, as EB ganglia were either severely reduced or completely absent at 50 hpf in TgBAC(*phox2b:EGFP)* embryos treated with BIO between 11 and 24 hpf (Figure 27). Importantly, BIO-induced effects were specific to the canonical Wnt pathway, as these phenotypes were lost when the Wnt pathway was blocked downstream of GSK3-β via Tg(*hsp70:tcf∆C-EGFP)* activation (Martin and Kimelman, 2012; Figure 28).

Next, we endeavored to determine the cellular bases of the BIO-induced phenotype. Cell proliferation was not responsible for increased Dlx3b+ otic progenitors (Figure 26J; Figure 25B,E), while decreased EB placodal progenitors was not due to increased cell death (Figure 26K). Live imaging of *Tg(pax2a:GFP)* embryos treated with BIO between 11 and 24 hpf revealed that anterior PPA cells failed to move rostrally, remaining in the presumptive otic region (Figure 29). This demonstrates that Wnt activation alters PPA cell behavior toward otic differentiation, possibly through high levels of Pax2a expression.

3.3.8 Inhibition of Wnt signaling reduces Pax2a expression levels and favors formation of the facial placode

We next determined whether inhibiting the canonical Wnt pathway affects Pax2a levels and PPA progenitor cell behavior. We used Tg(*hsp70:tcf∆C-EGFP)*: a heat-shock-inducible dominant-negative form of the Wnt effector Tcf7 fused to EGFP (Martin and Kimelman, 2012). We heat-shocked transgenic embryos for 30 minutes at 38˚C and 39˚C at 10 hpf, using EGFP-negative siblings as controls. At 12 hpf, with Wnt signaling loss, we observed dose-dependent

decreases in PPA Pax2a expression levels (χ^2-test, p<0.001; Figure 30A-C,G). The otic vesicle was dramatically reduced by 24 hpf, with significant concomitant facial placode expansion (Figure 30D-F). We measured Pax2a protein levels in the otic placode and observed decreases of 63% at 38˚C and 75% at 39˚C (Student's t-test: p<0.0033, p<0.0017; Figure 30H). We also observed fewer Pax2a-expressing cells in the otic placode in both conditions: 75% and 91% reductions (p<<0.001) with concurrent 1.4- and 2.5-fold increases (p<0.05, p<0.005) in facial placodes (Figure 30I). The glossopharyngeal/vagal placode was reduced significantly under both conditions (71% reduction; Figure 30I). These effects were recapitulated by the conditional induction of the Wnt antagonist Dkk1 using the Tg*(hsp70:dkk1-GFP)* line (Figure 31). Wnt signaling loss did not alter levels of cell proliferation or cell death in the otic/EB precursors (Figure 30J,K). Interestingly, we observed a more modest reduction in Dlx3b+ otic cells (25%) versus Pax2a+ cells (61%) at 18 hpf, confirming that a subset of otic vesicle cells either do not express Pax2a or express Pax2a at low levels (Figure 25D,E). These results indicate that the absence of Wnt signaling promotes low Pax2a levels in the PPA and favors facial placodal development; conversely, high levels of Wnt signaling induce high Pax2a levels and promote otic development.

3.3.9 Wnt activation is cell-autonomously required for otic development

Wnt regulation of Pax2a in the PPA may be direct or indirect. Direct activation of Wnt signaling leads to otic commitment in chick and mouse (Freter

et al., 2008; (Ohyama et al., 2006). However, a previous zebrafish study suggested that canonical Wnt signaling does not directly affect otic development; rather, Wnt maintains hindbrain expression of *fgf3* and *fgf8*, both of which are required for otic induction (Phillips et al., 2004). However, in our hands, modulating Wnt activity did not disrupt *fgf3/8* expression in the hindbrain (Figure 32). To further explore whether intracellular Wnt activity drives high levels of Pax2a expression and subsequent otic commitment, we employed the Tg(*hsp70:tcf*Δ*C-EGFP)* line to perform mosaic analyses. A small number of Tg(*hsp70:tcf*Δ*C-EGFP)*+ (or wildtype) donor cells were transplanted into wildtype hosts. Mosaic embryos were heat-shocked at 10 hpf, and Pax2a expression examined at 24 hpf (Figure 33). We reasoned that if intracellular activation of the Wnt pathway is required for otic development, then PPA cells deficient for Wnt activity (TcfΔC-EGFP+ cells) should be excluded from the otic vesicle. Indeed, the vast majority of Tg(*hsp70:tcf*Δ*C-EGFP)*+ donor cells (92%) contributed to the EB placodes (Figure 33B,C,D) versus 42% in controls (χ^2-test: $p<<0.001$; Figure 33A,D). Interestingly, while very few Tg(*hsp70:tcf*Δ*C-EGFP)*+ donor cells were found in the otic vesicle, a substantial number of donor cells contributed to the presumptive gAll/gVIII (Figure 33C, D). These data reveal a cell-autonomous requirement for Wnt signaling in PPA cells for otic development.

3.4 Discussion

Our study, in context with prior work, suggests a new model for the patterning of the PPA into distinct placodes (Figure 34). During early

somitogenesis, Fgf signals from the neural tube and head mesoderm promote formation of the multipotent Pax2a/8+ PPA domain that gives rise to the otic placode and contributes cells to EB placodes. Shortly after the PPA is specified, Wnt signaling from the neural tube promotes otic commitment in the posteromedial PPA, potentially by driving high levels of Pax2a/8 expression. We speculate that, in parallel with other factors, these differential levels of Pax2a/8 modulate cellular behaviors that contribute to segregation and subsequent morphogenesis of otic or EB progenitors. Signals from the PPA, including Fgf24 for glossopharyngeal/vagal (Padanad and Riley, 2011) and an unknown signal for the facial placode, induce additional EB placode cells from non-neural ectoderm.

3.4.1 PPA cell segregation is biased during early somitogenesis

Our fate mapping and ablation experiments show that only a subset of PPA cells contribute to EB placodes; however, PPA formation is required for proper EB placode induction. Fate mapping indicated that EB placode precursors within the PPA are axially restricted, corresponding to the future antero-posterior position of their respective placodes. However, only 16% of labeling events marked EB placodes, indicating a limited contribution of the PPA to the EB placodes. Live-imaging experiments revealed that PPA contribution to EB placodes was limited (Figure 12). In contrast, labeling large regions of non-neural ectoderm immediately adjacent to the PPA resulted in labeling within both EB placodes and intervening ectoderm (data not shown), supporting the notion that

additional EB placode contributors are derived through induction from the non-neural ectoderm, lateral to the forming otic vesicle and anterior lateral line system. Recent work showed PPA-derived Fgf24 signals to the lateral ectoderm were required to induce glossopharyngeal/vagal placodal precursors (Padanad and Riley, 2011). In our hands, however, knock down of Fgf24 using a splice blocking MO showed no phenotype in the EB placodes or subsequent ganglia, bringing into question the actual role of Fgf24 during placode development. Regardless of Fgf24's role, our ablation experiments do indicate that the PPA provides some signal required for EB placode development, as loss of the posterior PPA yielded a marked reduction in the glossopharyngeal/vagal placodes. Interestingly, ablation of the anterior PPA led to near-complete loss of the facial placode, indicating that other PPA-derived signals are required for facial placode formation. Our present and previous work suggest that this signal is an Fgf, as inhibition of Fgf receptor activity between 11.5 and 16 hpf completely blocked formation of the facial placode without affecting the otic placode (Nechiporuk et al., 2006). These findings prompted the work described in Chapter 4 where we determined the specific Fgf ligands required for EB placode maturation and subsequent neurogenesis.

Unlike EB placode precursors, otic vesicle precursors are found throughout the Pax2a domain. However, labeling posteromedial regions resulted in contributions throughout the otic vesicle, while labeling of anterolateral regions yielded a majority of labeled cells within the anterolateral side of the otic vesicle: a neurogenic region that gives rise to the acoustic ganglion (Bricaud and Collazo,

2006). Consistent with our fate mapping, posterior PPA ablation yields near-complete loss of the otic vesicle, indicating that most otic precursors lie in the posterior region of this domain. By contrast, previous work in chick indicated extensive cell mixing of otic and EB precursors; however, the labeling was performed at earlier embryonic stages (3 somites and earlier vs. 5-6 somites in present study) and much larger regions of ectoderm were labeled using DiI or DiO dyes (Streit, 2002). A more recent study in frog indicated that progressively less cell mixing occurred between the otic and EB precursors when they were labeled at later developmental stages (Pieper et al., 2011). The anterolateral-posteromedial bias suggests that positional information (perhaps a morphogen gradient) confers otic fates. Reinforcing this idea, it has been shown that Fgf3 determines anterior otic characteristics while Hedgehog (Hh) defines lateral/posterior identity (Hammond and Whitfield, 2011; Hammond et al., 2010). Other factors subsequently assign neurogenic fate to anterior PPA cells. This is consistent with chick studies showing that FGF8 expression is sufficient to induce PPA expression of Sox3, a key factor in specifying the neurogenic region of the otic placode (Abello et al., 2010).

3.4.2 Pax2a levels regulate PPA cell behaviors

Through loss- and gain-of-function experiments, we determined that changes in Pax2a and Pax8 levels influence otic and EB precursor segregation. Importantly, the PPA can form in the absence of Pax2a/8 activity, as previous studies showed that *pax2a* transcript was expressed in the PPA of Pax2a

mutants injected with *pax8* morpholino (Hans et al., 2004b; Mackereth et al., 2005). Thus, differential levels of Pax2a/8 likely affect cellular behaviors/differentiation after the PPA is specified. Modulation of Pax2a/8 levels lead to modest (but statistically significant) changes in otic and EB segregation. We attribute this to several factors. First, during Pax2a overexpression experiments only a subset of transgenic cells was able to intercalate within the otic vesicle, while the remainder of high-expressing Pax2a cells underwent cell death. Second, the partial depletion experiments led to a 20-30% increase in EB ganglia, consistent with the limited contribution of the PPA to the EB domain. It is notable that the otic vesicle was composed of both high (medial) and low Pax2a (lateral) expressing cells, suggesting that other factor(s), in addition to Pax2a/8, contributes to segregation of otic and EB precursors in the PPA. In summary, while Pax2a/8 levels clearly influence commitment/differentiation of cells within the otic or EB domain, further experiments are needed to determine how Pax2a/8 levels modulate cellular behaviors of the PPA.

3.4.3 Roles of Fgf and Wnt pathways in regulating Pax2a expression

Our previous study demonstrated that Fgf signaling is necessary to induce Pax2a in PPA cells (Nechiporuk et al., 2006). Corroborating this idea, we observed that Fgf could impart placodal identity to non-neural ectoderm by inducing Pax2a expression. Wnt can subsequently act upon these cells to induce high Pax2a (and possibly Pax8) expression levels, influencing cellular behavior. Surprisingly, not all EB placodes exhibited the same responses to modulating Fgf

and Wnt signaling pathways. We observed that the number of Pax2a+ cells contributing to the facial placode related directly to levels of Fgf signaling, while increased Wnt activity resulted in facial placode loss. However, a measurable reduction of the glossopharyngeal/vagal placode was seen under both of these conditions. The reduction following decreased Wnt activity may be secondary to otic domain reductions (fewer Pax2a+ and Dlx3a+ otic cells); this would lead to a drop in the Fgf24 signaling necessary for posterior EB placode formation. Reinforcing this idea, we observed that absence or low levels of intracellular Wnt did not prevent cells from contributing to glossopharyngeal/vagal placodes in mosaic embryos, as Tg(*hsp70:tcf∆C-EGFP)*+ donor cells readily contributed to the these placodes.

Our mosaic experiments showed that, in contrast to previous work (Phillips et al., 2004), Wnt signaling is directly activated in a subpopulation of the PPA to drive high levels of Pax2a expression; biasing these cells to otic vesicle formation. It is likely that both Fgf and Wnt pathways are playing multiple roles during placode resolution. For example Fgf could be both initiating Pax2a expression and involved in placodal segregation by imparting regional identity or a motile cellular behavior to progenitors of low Pax2a expression. Wnt is also a demonstrated dorsalizing signal during otic placode morphogenesis (Ohyama et al., 2006). Indeed, when Wnt was overactivated using the BIO inhibitor, otic vesicle cells became supernumerary, and all expressed high levels of Pax2a. Furthermore, mediolateral extension of the otic vesicle was expanded versus activated Fgf and wildtypes.

3.5 Methods:

3.5.1 Fish strains, maintenance, BIO, and heat-shock treatments

Zebrafish husbandry was performed as described (Westerfield, 1995), and staging expressed in hours post fertilization (hpf; (Kimmel et al., 1995). The following lines were used in this study: *AB; Tg(*pax2a:GFP*)^{e1} (Picker et al., 2002); TgBAC(*phox2b:EGFP)*^{w37} (Nechiporuk et al., 2006); *pax2a*$^{b593/+}$ (Erickson et al., 2007); Tg*(hsp70:ca-fgfr1)*^{pd3} (Marques et al., 2008); Tg*(hsp70:dnfgfr1-EGFP)*^{pd1} (Lee et al., 2005); Tg(*hsp70:tcf*Δ*C-EGFP)* (Martin and Kimelman, 2011); and Tg*(hsp70:dkk1-GFP)*^{w32} (Stoick-Cooper et al., 2006). Heterozygous *pax2a*$^{b593/+}$ were used to generate homozygous offspring, identified by midbrain-hindbrain boundary loss. The GSK3-β inhibitor 6-bromoindirubin-3'-oxime (BIO; Sigma) was dissolved in DMSO at 10 mM and diluted to working concentrations in embryo medium. All heat-shock experiments were conducted at 10 hpf. Transgene expression (via EGFP reporter) was visible 45-60 min post heat-shock. Wildtype controls and heterozygous embryos obtained by outcrossing Tg*(hsp70:ca-fgfr1)*^{pd3} to *AB were heat-shocked between 38˚C and 36.9˚C for 45 minutes. Tg*(hsp70:dnfgfr1-EGFP)*^{pd1} were outcrossed to *AB and heat-shocked between 35˚C and 37.2˚C for 30 minutes. Tg(*hsp70:*Δ*tcf-EGFP)/*+ fish were crossed to wildtypes and heat-shocked at 38˚C and 39˚C for 30 minutes. Tg*(hsp70:dkk1-GFP)*^{w32}*/*+ fish were incrossed and embryos were heat-shocked at 39˚C for 40 minutes. Following heat-shock, GFP+ embryos were identified under epifluorescence; GFP- embryos were used as controls.

3.5.2 Fate-mapping experiments

For photoconversion or fluorescein uncaging, Tg(*pax2a:GFP*)^{e1} embryos were injected with 100 pg of NLS-Kaede mRNA, 250 pg of patagRFP mRNA (Subach et al., 2010) or 1 nl of 1.25% caged fluorescein (Invitrogen) in 0.2 M KCl. At 11.5 hpf, embryos were mounted and labeling performed with an FV1000 confocal microscope under a 60x/NA=1.20 water objective (Olympus) using a small ROI in the Bleach function. Zoom was increased to 30X and selected cells excited with a 405 nm laser at 0.1% output. Only embryos with labeling entirely contained within the Pax2a domain were analyzed. Kaede-expressing, embryos were live-imaged at 24 hpf to locate converted cells. In fluorescein uncaging experiments, embryos were fixed in 4% paraformaldehyde/1x PBS at 24 hpf and assayed for Pax2a expression.

3.5.3 Whole-mount in-situ hybridization and immunostaining

Immunostaining and in-situ hybridization were performed as described (Andermann et al., 2002). The following antibodies and riboprobes were used: α-Pax2 (1:100, Covance); α-GFP (1:1000, Invitrogen); α-Fluorescein (1:1000, Roche); α-Elavl 3/4 (1:1000, Invitrogen; sold as α-Hu C/D); α-Dlx3b (1:100, Zirc); *pax2a* (Krauss et al., 1991); *pax8* (Pfeffer et al., 1998); *fgf3 (Kiefer et al., 1996)*; and *fgf8* (Reifers et al., 1998). It is unknown whether the Pax2 antibody recognizes both Pax2a and Pax2b paralogs; however, immunostains mirrored *pax2a* mRNA distribution. Whole-mount confocal images were obtained using an FV1000 (Olympus). Brightfield images were acquired with an AxioImager Z1

compound microscope (Zeiss). Assembly of Z-stack images, heat-map analysis, and mean fluorescence intensity measurements were performed using ImageJ (Abramoff et al., 2004). Comparisons of mean fluorescence intensities were done in parallel using the same dilution of α-Pax2; confocal settings were consistent for each acquisition. Brightness and contrast were adjusted using Photoshop (Adobe).

3.5.4 Cellular ablations

Specific regions of the PPA in Tg(*pax2a:GFP*)^{e1} embryos were ablated at 11 hpf using previously-described methods (Sagasti et al., 2009). Following ablations, the entire PPA was imaged. Embryos were then allowed to develop to 24 hpf, fixed and immunostained for Pax2a.

3.5.5 Pax2a misexpression

A bi-directional heat-shock-inducible construct was modified to contain the *pax2a* coding sequence (or *egfp* as control) with a dTomato reporter (Bajoghli et al., 2004). Twenty pg of each plasmid was injected into wildtype embryos, which were heat-shocked at 12 and 14 hpf at 38˚C for 30 minutes.

3.5.6 Morpholino microinjections

The following antisense morpholino oligonucleotides (MO; Corvalis, OR) were diluted to working concentrations in H_2O and injected into TgBAC(*phox2b:EGFP)*^{w37} embryos: *pax2a*-MO (5'-

ATATGGTGTCTCACCTATAGTGTGT; gift from Joshua Waxman, Cincinnati Children's Hospital), *pax8*E5/I5-MO+*pax8*E9/I9-MO (Hans et al., 2004b). Efficacy of *pax2a*-MO was assessed by RT-PCR using the following primers; *pax2a*-MO-F: 5'-GCAGAATACAAGCGGCAAAATC, *pax2a*-MO-R: 5'-CGTAAACTCTCCACACTACCCTGAG.

3.5.7 Transplantation experiments

Donor zygotes from Tg(*hsp70:tcf∆C-EGFP)/*+X*AB crosses were injected with 10 kD rhodamine-dextran (Invitrogen) in 0.2M KCl. Embryos were dechorinated and allowed to develop to sphere and shield stage for donors and wildtype hosts, respectively. Twenty donor cells were transplanted into the presumptive placodal domain of host embryos (Kozlowski et al., 1997). Mosaic embryos were heat-shocked at 10 hpf at 39˚C for 30 minutes, fixed at 24 hpf, and immunostained for Pax2a and EGFP.

CHAPTER 3 FIGURES

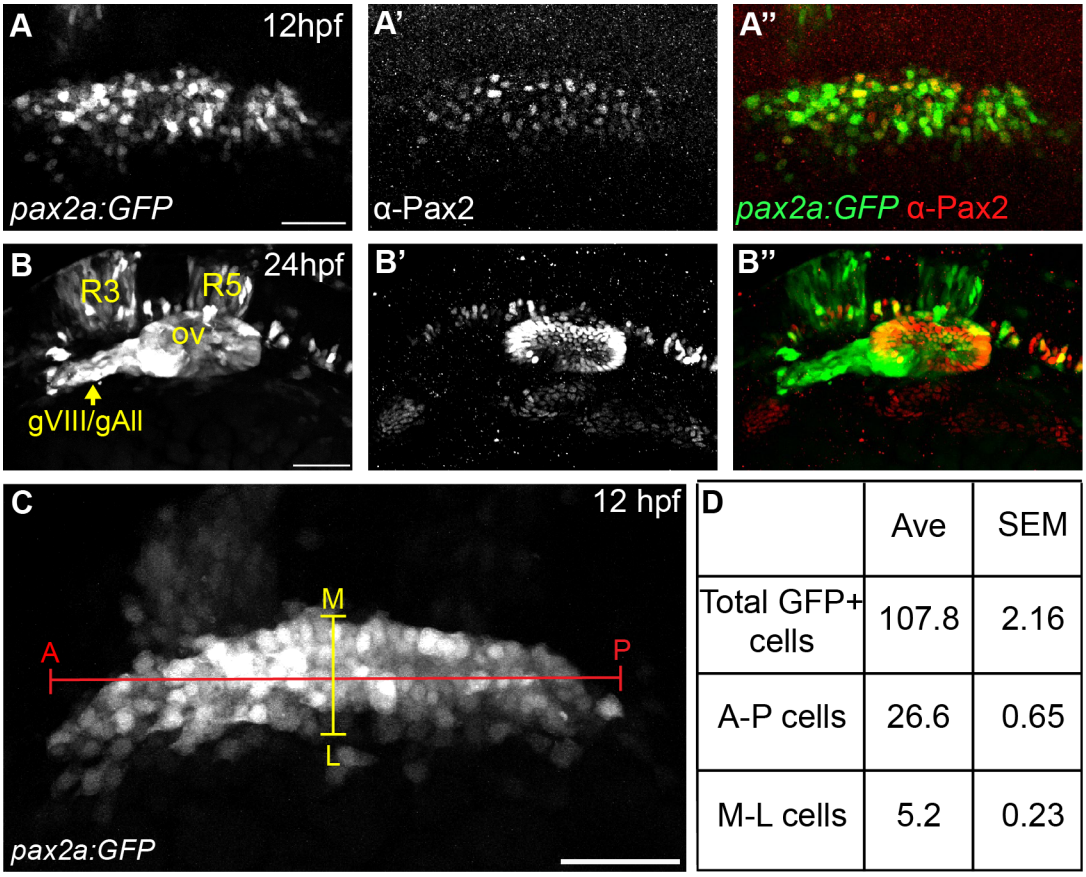

D	Ave	SEM
Total GFP+ cells	107.8	2.16
A-P cells	26.6	0.65
M-L cells	5.2	0.23

Figure 7: Characterization of the Tg(*pax2a:GFP*) PPA domain
(A) Confocal projection of a Tg*(pax2a:GFP)* embryo at 12 hpf immunostained for Pax2a. Significant overlap was seen between transgenic GFP and endogenous Pax2a; 97% of α-Pax2+ cells were GFP+ (N=380 cells from 5 embryos) and 87% of GFP+ cells were α-Pax2+ (N=420 cells from 5 embryos). **(B)** Confocal projection of a Tg*(pax2a:GFP)* embryo at 24 hpf co-stained with the Pax2 antibody. Few cells in the EB placodes are labeled with the transgene at this stage. Ectopic expression of transgene is seen in the acoustic and anterior lateral line ganglion (gVIII/gAll) and rhombomeres 3 and 5 (R3 and R5). **(C)** Confocal projection of a Tg*(pax2a:GFP)* transgenic embryo at 12 hpf, **(D)** Total number of cells of the PPA, in addition to number of cell diameters along the A-P (red marker) and M-L (yellow marker) axes, were counted in 11 embryos (1,186 cells total from 11 embryos) to determine variability in dimensions of this domain. Counts reveal a consistent average (Ave) with a small standard error of mean (SEM) for both total number of cells and cells across the A-P and M-L axis in the PPA of 12 hpf embryos. ov -otic vesicle; gVIII/gAll - acoustic/anterior lateral line ganglia; r3 and r5 - rhombomeres 3 and 5; A-P - anterior-posterior axis; M-L - medial-lateral axis. Scale bars = 50 μm.

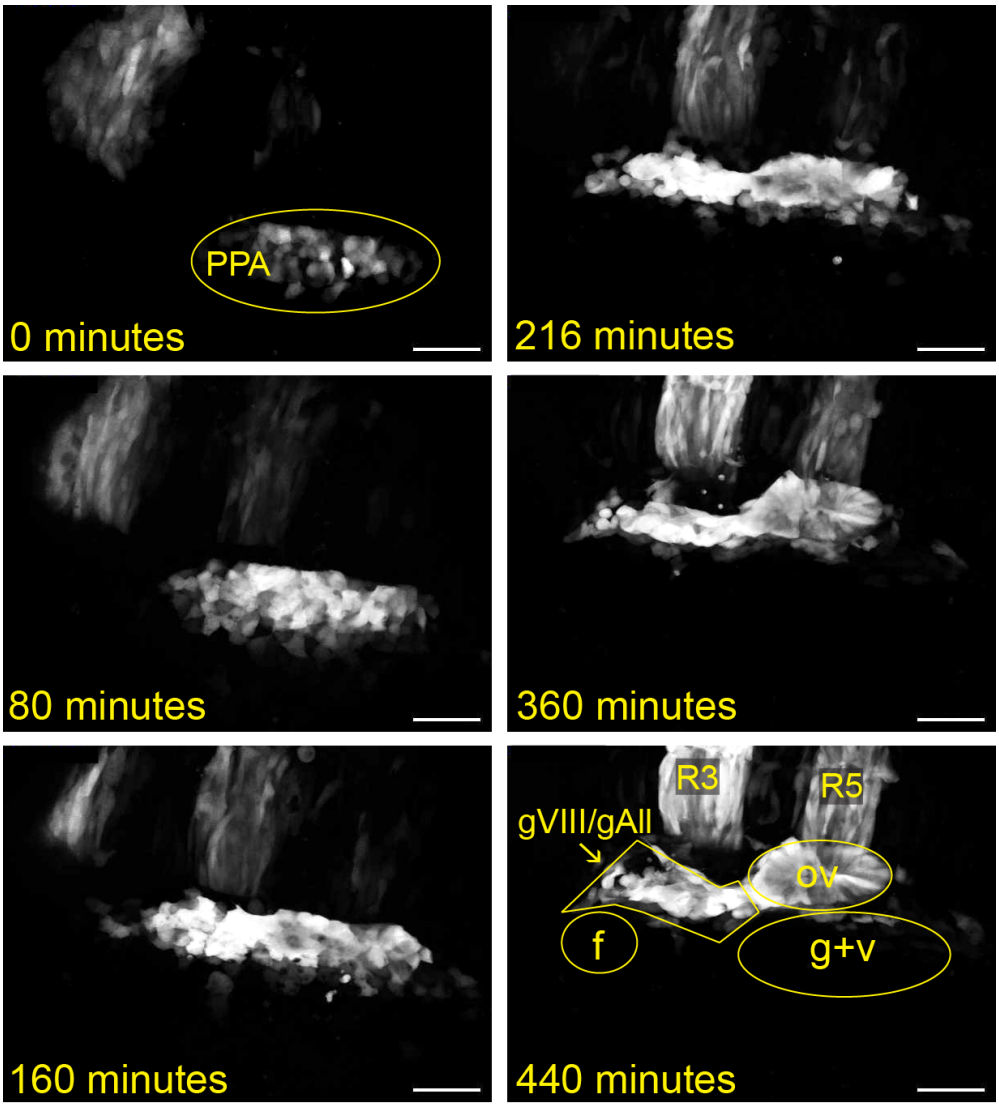

Figure 8: Time-lapse of wildtype Tg(pax2a:GFP) transgenic embryos during placode segregation and formation.

Stills from time-lapse of confocal projection images were acquired at labeled intervals over ~7.3 hours. First frame begins at 11 hpf with the PPA circled in yellow. Otic assembly commences ~17 hpf. Acoustic ganglion emanates from the forming otic vesicle during this time. Transgene is missing crucial regulator elements resulting in loss of expression in EB placodes and ectopic expression of GFP in rhombomeres 3 and 5. Note that the otic vesicle originates primarily from the posterior region of the PPE and the gVIII/gAll from the anterior region. Last frame highlights otic vesicle (ov), facial placode (f), glossopharyngeal/vagal placode (g+v), acoustic/All ganglia (gVIII/gAll), and rhombomeres 3 and 5 (R3, R5). Scale bar = 50 μm.

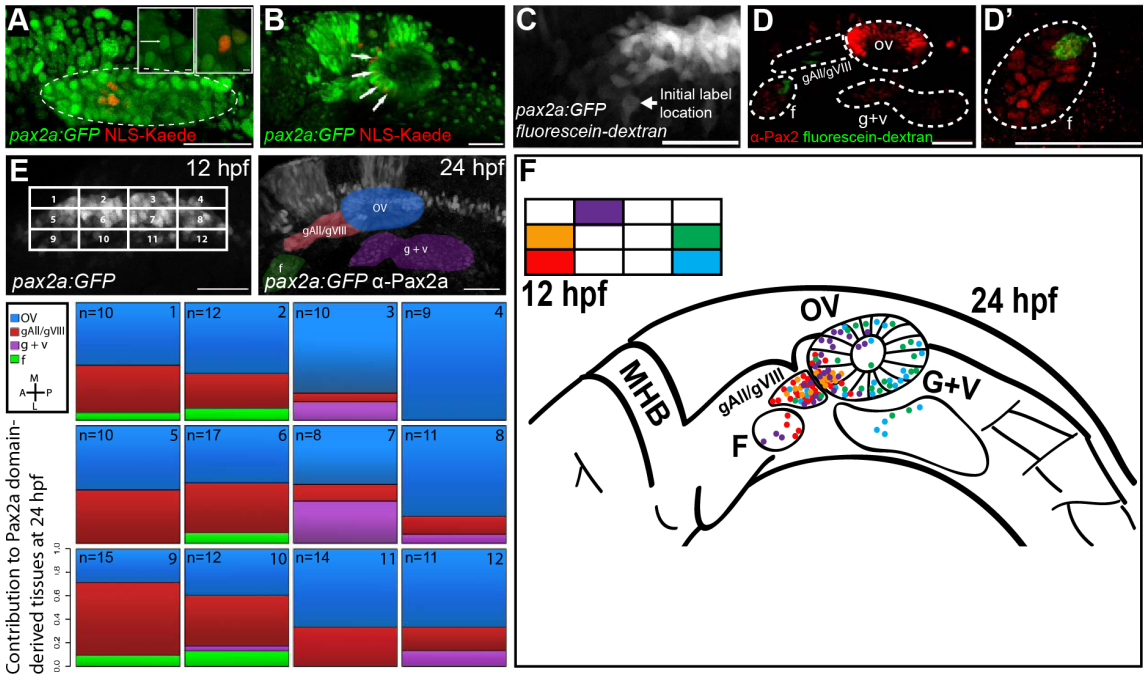

Figure 9: Posterior placodal area fate-map.
(A) NLS-Kaede photoconversion in the PPA (outlined) of a Tg*(pax2a:GFP)* transgenic embryo at 12 hpf. Insets show single z-planes at high magnification before (left; arrow) and after (right) photoconversion. The Pax2a domain is delineated by GFP expression (dashed outline). **(B)** Confocal projection showing labeled cells (red; arrows) at 24 hpf. Red nuclei outside the otic vesicle are incidentally-photoconverted epidermal cells. **(C)** Confocal projections of a caged fluorescein-dextran photoconversion in the PPA of a Tg*(pax2a:GFP)* transgenic embryo at 12 hpf. Arrow marks photoconverted area. **(D)** Confocal projection showing labeled cells (green) and Pax2a+ cells (red) at 24 hpf. **(E)** Fate map of the 12 hpf Pax2a domain, divided into 12 regions, each containing ~3x4 (12 total) cells except for corners where cell numbers vary. The location of labeled cells was assessed at 24 hpf and the proportion of labeling events recorded for each of the 12 regions. In instances where multiple tissues were labeled at 24 hpf, proportions were calculated by dividing the number of endpoint label instances by the total number of labeled tissues resulting from labeling each region. n=139 samples total; n for each quadrant shown in (E). **(F)** Fate map of all labeling events from 5 selected subregions (2, 5, 8, 9, and 12). Abbreviations: F=facial placode, gAll/gVIII=anterior lateral line ganglion/acoustic ganglion, G+V=glossopharyngeal /vagal placodes, OV=otic vesicle. Scale bars=50μm, inset scale bars=5μm.

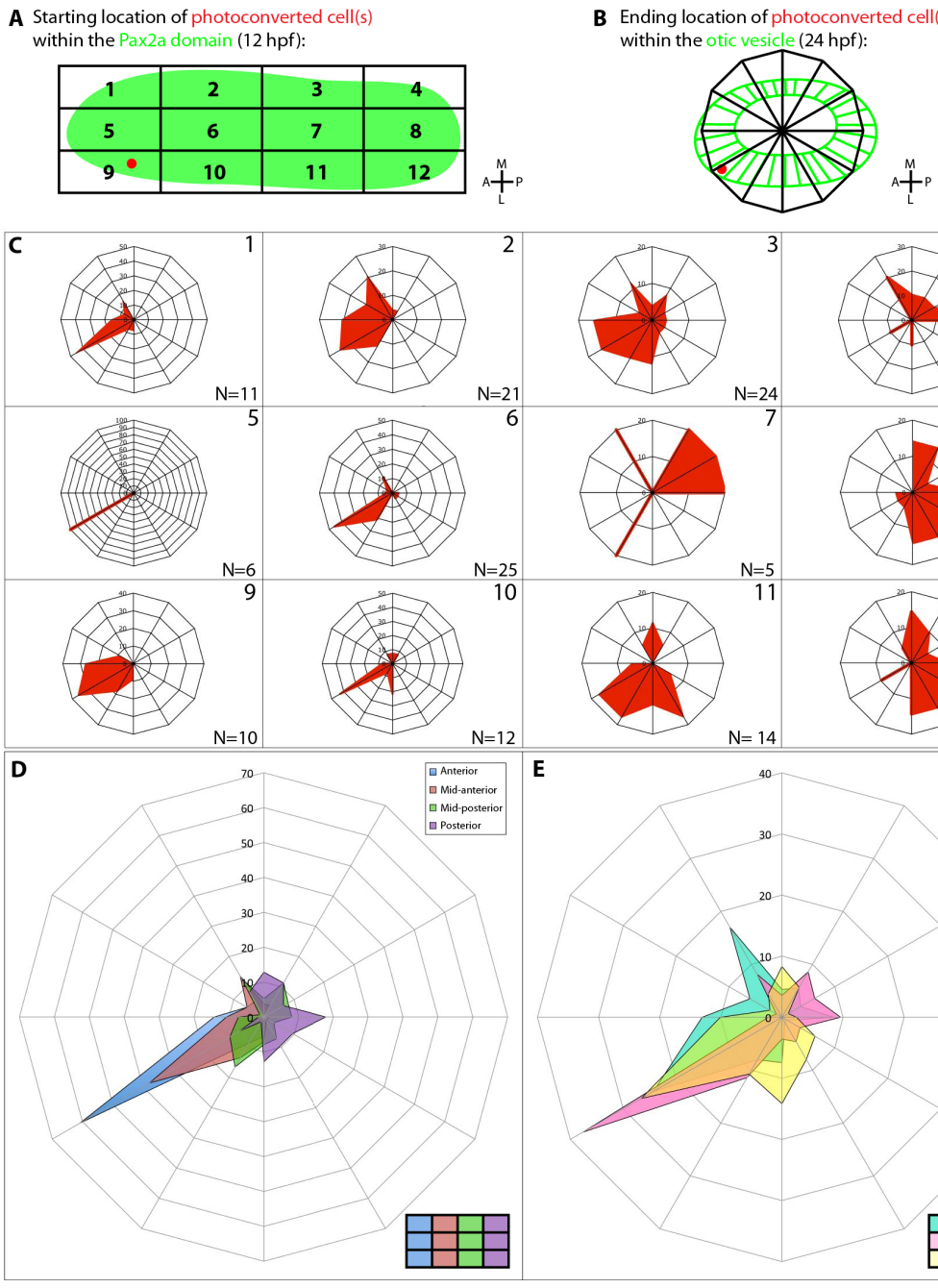
A Starting location of photoconverted cell(s) within the Pax2a domain (12 hpf):
1
2
3
4
5
6
7
8
9
10
11
12
M
A
P
L
B Ending location of photoconverted cell(s) within the otic vesicle (24 hpf):
M
A
P
L
C
1
N=11
2
N=21
3
N=24
4
N=10
5
N=6
6
N=25
7
N=5
8
N=20
9
N=10
10
N=12
11
N= 14
12
N=21
D
Anterior
Mid-anterior
Mid-posterior
Posterior
E
Medial
Middle
Lateral

Figure 10: Fate of Pax2a-expression cells in the otic vesicle
(A) Small groups of cells labeled within the PPA at 12 hours post-fertilization (hpf). **(B)** At 24 hpf, the location of labeled cells within the otic vesicle was recorded using polar coordinates transposed over the otic vesicle. Cells were cataloged by proximity to 1 of 12 markings (30 degree radial sectors, corresponding to hour marks on an analog clock). **(C)** Radial charts of the proportion of cells that ended up closest to each of the sectors for regions 1-12 of the Pax2a domain (A). Each concentric line represents 10 percent of all labeling instances. **(D)** Simplified fate map of Pax2a cells within the otic vesicle. The Pax2a domain is divided into four columns from anterior to posterior (colored grid) and position of cells from each column in the otic vesicle is mapped to a radial chart. Similar to the individual maps for regions 1-12 of the Pax2a domain (A), cells from the anterior portion of the Pax2a domain are strongly biased towards the anterolateral region of the otic vesicle. Cells from more posterior regions are more equally distributed around the otic vesicle. **(E)** Fate map of the Pax2a domain along the mediolateral axis. The pax2a domain is divided into three rows from medial to lateral. The anterolateral bias obscures the pattern, but cells from the medial, intermediate, or lateral regions of the Pax2a domain tend to remain in these positions as they are incorporated into the otic vesicle.

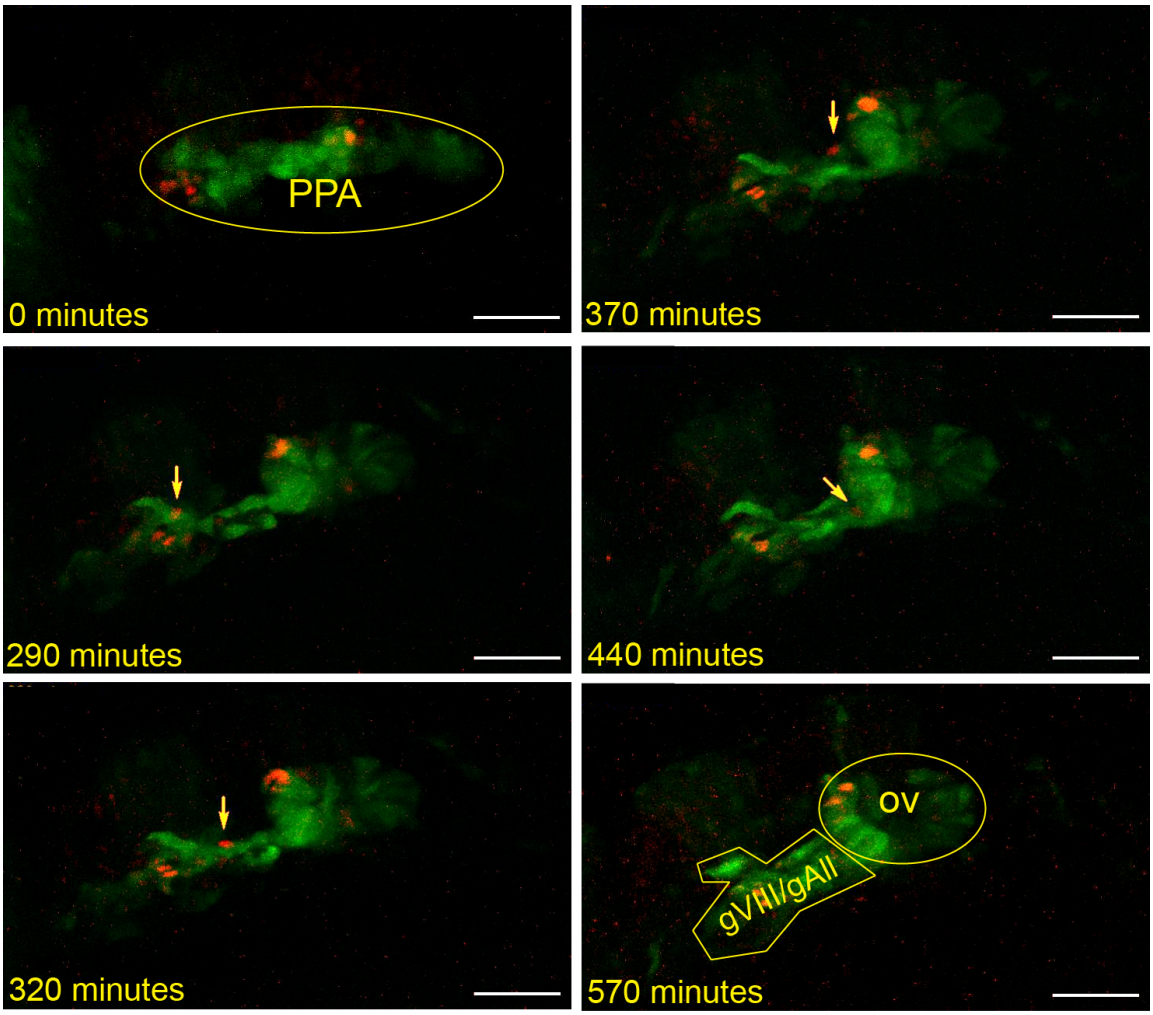

Figure 11: Extensive cell movements are rare in PPA cells
Stills from time-lapse of a Tg*(pax2a:GFP)* transgenic embryo injected with *pa-tagrfp* mRNA. One-cell stage embryos were microinjected with 250 pg of *pa-tagrfp* mRNA and a small number of cells in the anterior and middle regions of the PPA were photo-activated at 12 hpf. Confocal z-stacks were acquired at 10 minute intervals over ~9.5 hours. Time-lapse movie, consisting of z-projections, begins at 12.5 hpf with the PPA (green cells) circled in yellow. Note two clusters of photo-activated cells (red). The majority of photo-activated cells do not undergo extensive cell movements; however, at t=290 min one of the labeled anterior cells (arrow) undergoes extensive posterior movement from the presumptive acoustic and anterior lateral line ganglia (gVIII/gAll) region towards the forming otic placode. The gVIII/gAll ganglia and the otic vesicle (OV). Is marked in the last frame. Scale bar = 50 μm.

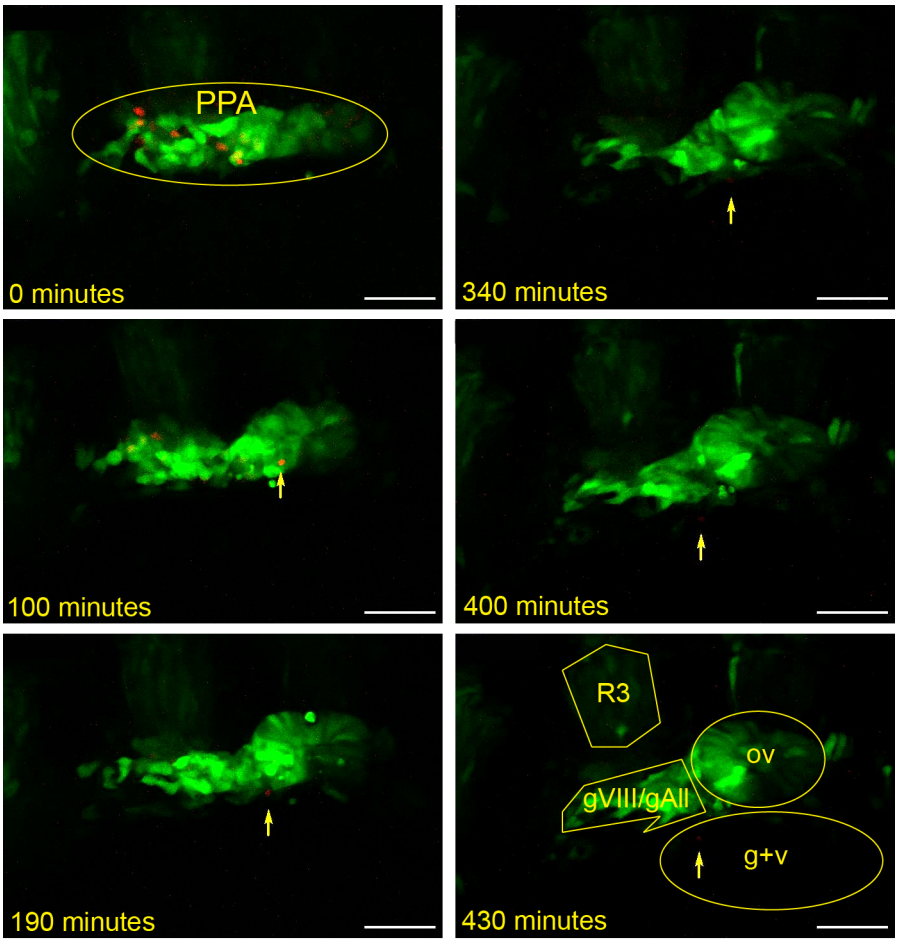

Figure 12: A small number of PPA cells move laterally and contribute to the EB placodes.
Stills from time-lapse of a Tg*(pax2a:GFP)* transgenic injected with 250 pg *pa-tagrfp* mRNA; a small subset of cells in the anterior and middle regions of the PPA were photo-activated at 12 hpf (red cells). Time-lapse of confocal z-stacks acquired at 10 minute intervals over ~7.2 hours beginning at 13 hpf. PPA (green cells) is circled in yellow. Most of the labeled cells exhibit little movement and maintain positions close to initial locations. Note a lateral cell in the middle of the PPA that did not integrate into the otic vesicle, migrated laterally to the G+V placode (yellow arrow). The acoustic/All ganglia (gVIII/gAll), glossopharyngeal/vagal placode (g+v), rhombomere 3 (R3) and the otic vesicle (ov) are marked on the last time frame. Scale bar = 50 μm.

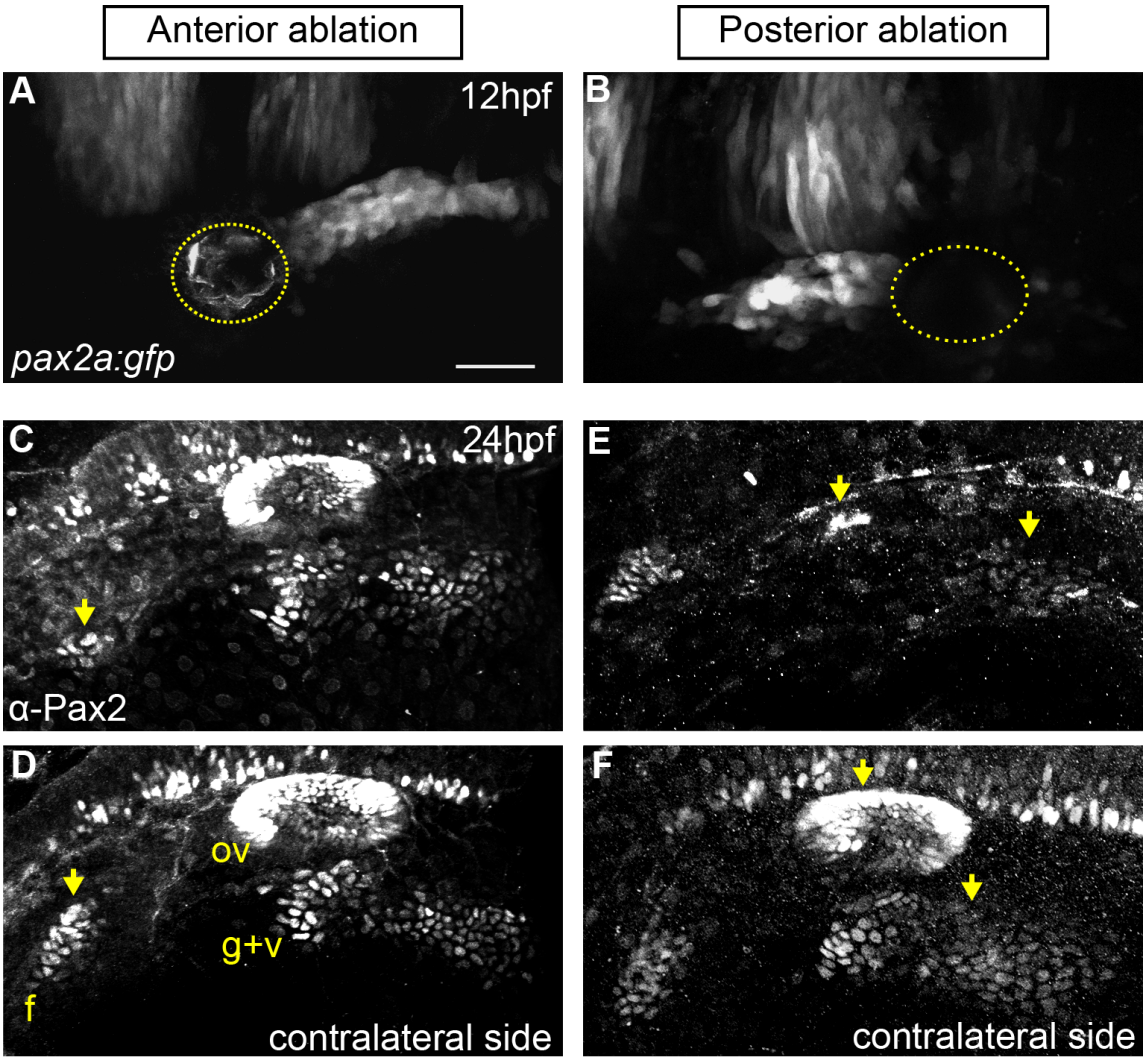

Figure 13: Posterior placodal area cells are required for normal epibranchial and otic placode development.
(A and B) Confocal projection of a Tg*(pax2a:GFP)*^{e1} transgenic embryo; anterior 1/4 (A) or posterior 1/3 (B) of the PPA was ablated at 12 hpf. **(C-F)** Twenty four hpf embryos shown in A and B were Pax2a immunolabeled, showing expression in otic vesicle and EB placodes. (C and D) Ablated and contralateral sides of the embryo in (A). Facial placode on the ablated side exhibits an 81% reduction versus contralateral control; otic and posterior EB placodes are unaffected. (E and F) Ablated and contralateral sides of the embryo in (B). Ablated side shows 95% loss of the otic vesicle and 72% reduction in the glossopharyngeal/vagal placodes versus control. Facial placode is unaffected. Arrows indicate corresponding placodes on ablated and control sides. Scale bar=50μm

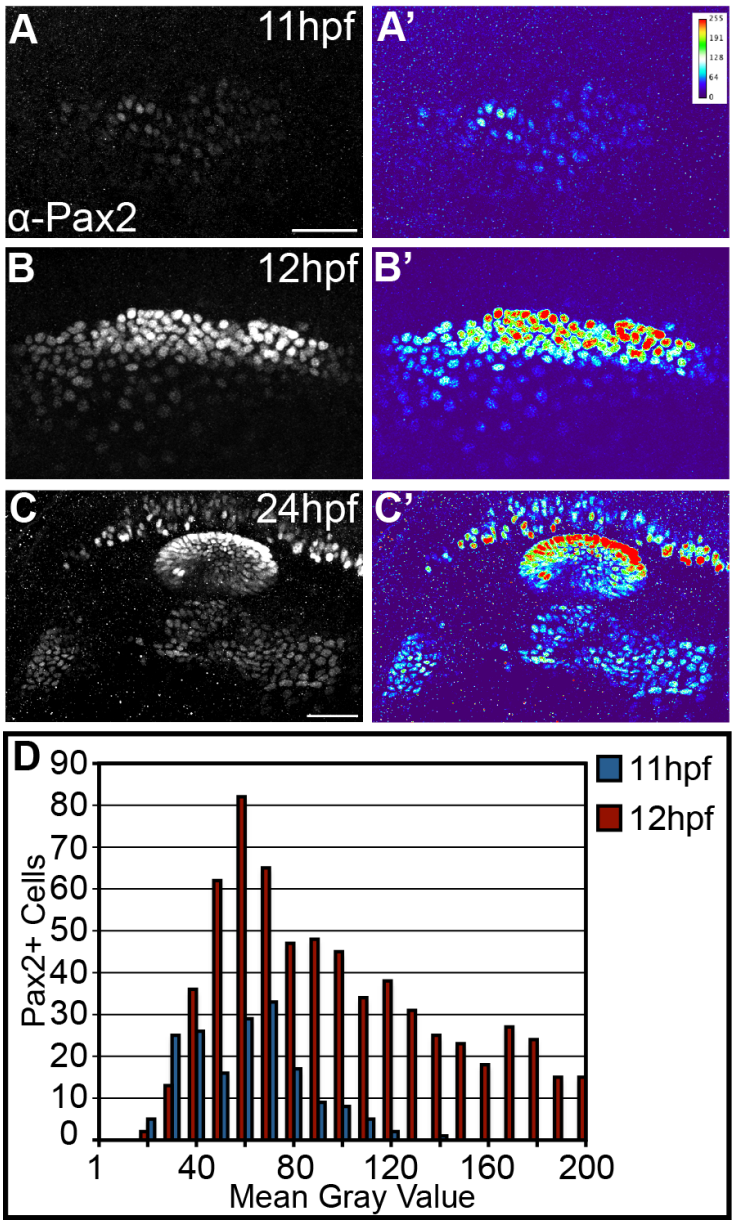

Figure 14: Differential levels of Pax2a expression in the posterior placodal area.

(A, A') Low, uniform Pax2a expression at 11 hpf. Heat map in A' shows fluorescence intensity. **(B, B')** At 12 hpf, Pax2a expression levels occur in a wider range. **(C, C')** Fully segregated placodal precursors with structures exhibiting differential Pax2a expression at 24 hpf. The otic placode exhibits high Pax2a expression; the EB placodes display low levels (C'). **(D)** Pax2a fluorescence mean gray value (MGV) distribution at 11 and 12 hpf ($n \geq 175$ cells, 7 embryos/time-point). Note significant increase in the number of cells with high Pax2a expression at 12 hpf (χ^2-test; $p << 0.001$). High Pax2a levels defined as MGV>100. Scale bar=50μm.

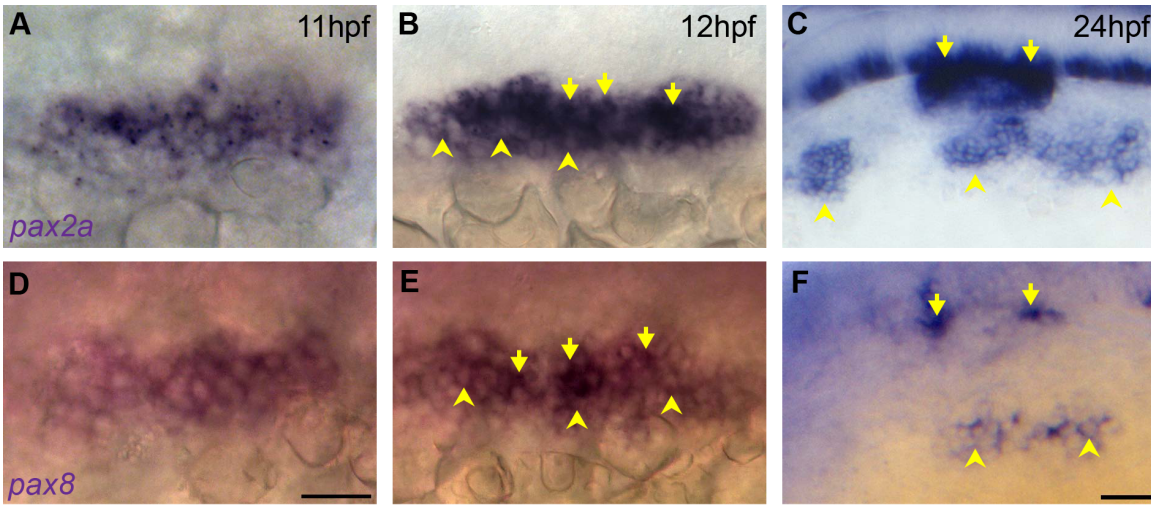

Figure 15: Differential levels of *pax2a/8* are observed in the PPA and mature placodes.
(A-C) In situ hybridization of *pax2a* reveals differential *pax2a* expression levels at both 12 (B) and 24 hpf (C). **(D-F)** In situ hybridization for *pax8* reveals presence of this transcript in the PPA at 11 (D) and 12 hpf (E); *pax8* is also expressed in the EB placodes and in distinct foci in the otic vesicle at 24 hpf (F). Note the differential expression levels of *pax8* at 12 and 24 hpf with low level *pax8* in the EB placode. Arrowheads indicate low expression; arrows indicate high *pax* expression. Scale bar = 50 μm.

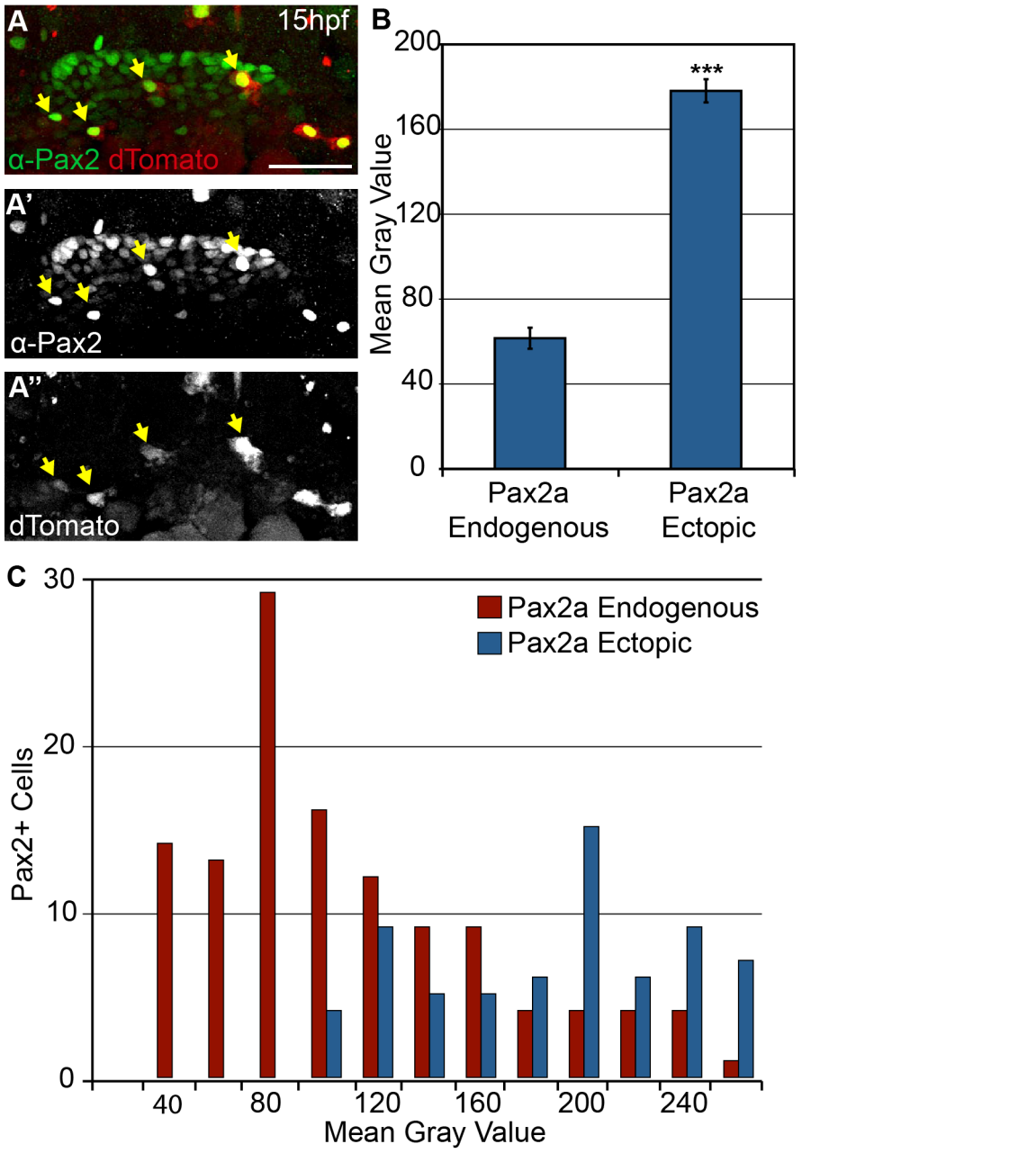

Figure 16: Injection of *hsp70-dTomato-pax2a* plasmid induces robust Pax2a expression following heat-shock

(A) Embryos injected with a heat-shock- inducible construct expressing both Pax2a and the dTomato reporter were heat-shocked at 12hpf. These embryos display mosaic Pax2a expression 3 hours post-heat-shock. **(B)** Quantification of induced Pax2a levels relative to endogenous Pax2a. Note that on average ectopic Pax2a levels are 2.9 fold higher than the endogenous levels (n=42 cells from 5 embryos; Student's *t*-test, ***$p<<0.001$). **(C)** Distribution of Pax2a fluorescence intensity comparing endogenous Pax2a to ectopically induced Pax2a. Note that overall intensity levels of the exogenous Pax2a fall within a high endogenous spectrum (n=198 cells from 5 embryos). Scale bar = 50 μm.

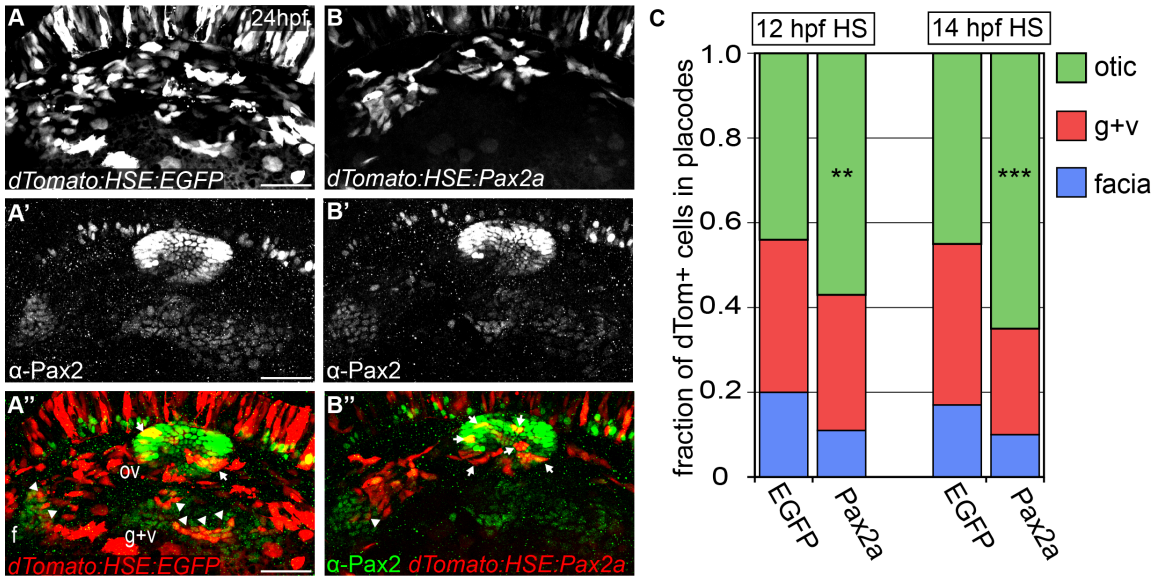

Figure 17: High levels of Pax2a bias otic contribution.
(A and B) Embryos expressing bi-directional heat-shock-inducible plasmid (heat-shocked at 12 and 14 hpf) driving *egfp* (A-A'') or *pax2a* (B-B'') in one direction and *dTomato* (*dTom*) in the other. Arrows indicate Pax2a misexpressing cells sequestered to otic placode. Arrowheads indicate cells segregated to EB placodes. **(C)** Relative contribution of dTomato+ cells to the otic vesicle and EB placodes at 24 hpf in EGFP (controls) and Pax2a (overexpression) embryos. Pax2a overexpressing cells are prone to otic contribution, segregating less frequently to EB placodes versus controls ($n \geq 192$ cells from 8-12 embryos/condition; χ^2-test; $^{**}p<0.016$, $^{***}p<0.001$). HS=Heat-Shock. Scale bar=50μm.

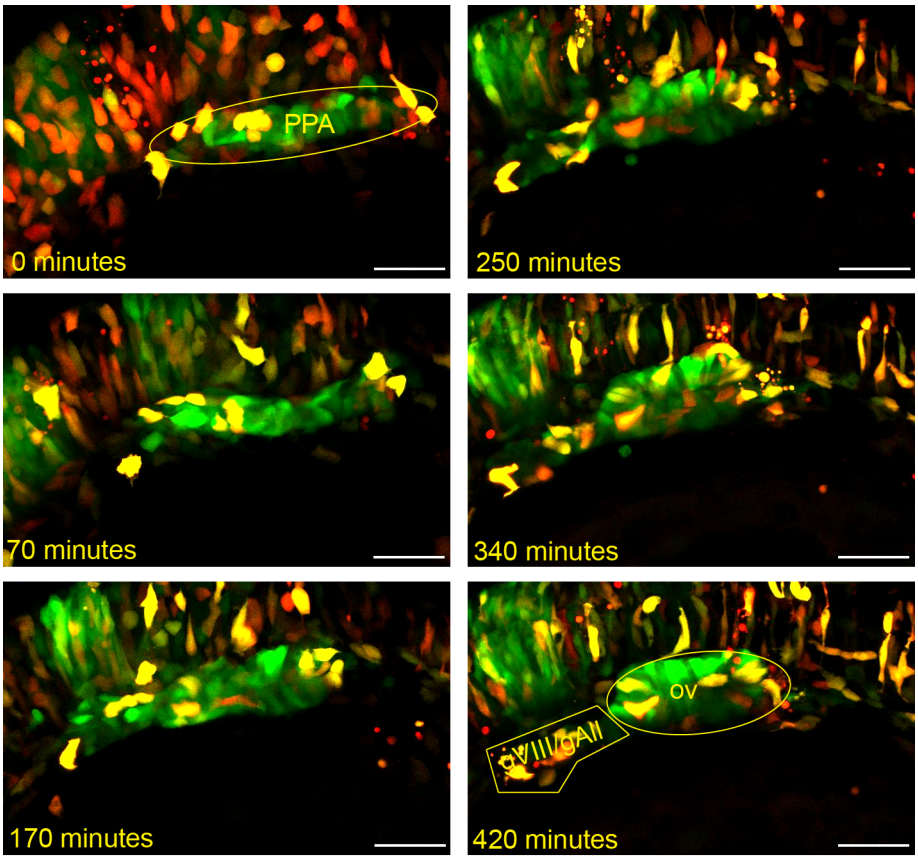

Figure 18: Transient expression of dTomato:HSE:EGFP transgene generates mosaic distribution of dTomato+ cells in the PPA.
Stills from time-lapse of a Tg*(pax2a:GFP)*^{e1} transgenic was injected with 25 pg of dTomato:HSE:EGFP DNA construct at 1-cell stage. The transgene was induced by heat-shock at 10 hpf and confocal z-stacks were acquired at 10 minute intervals over ~7 hours starting at 13 hpf. PPA (green cells) circled in yellow. Note a number of dTomato+ cells in the PPA (red). A small number of these cells undergo cell death during placode formation. Last frame highlights the acoustic/All ganglia (gVIII/gAll) and the otic vesicle (ov). Scale bar = 50 μm.

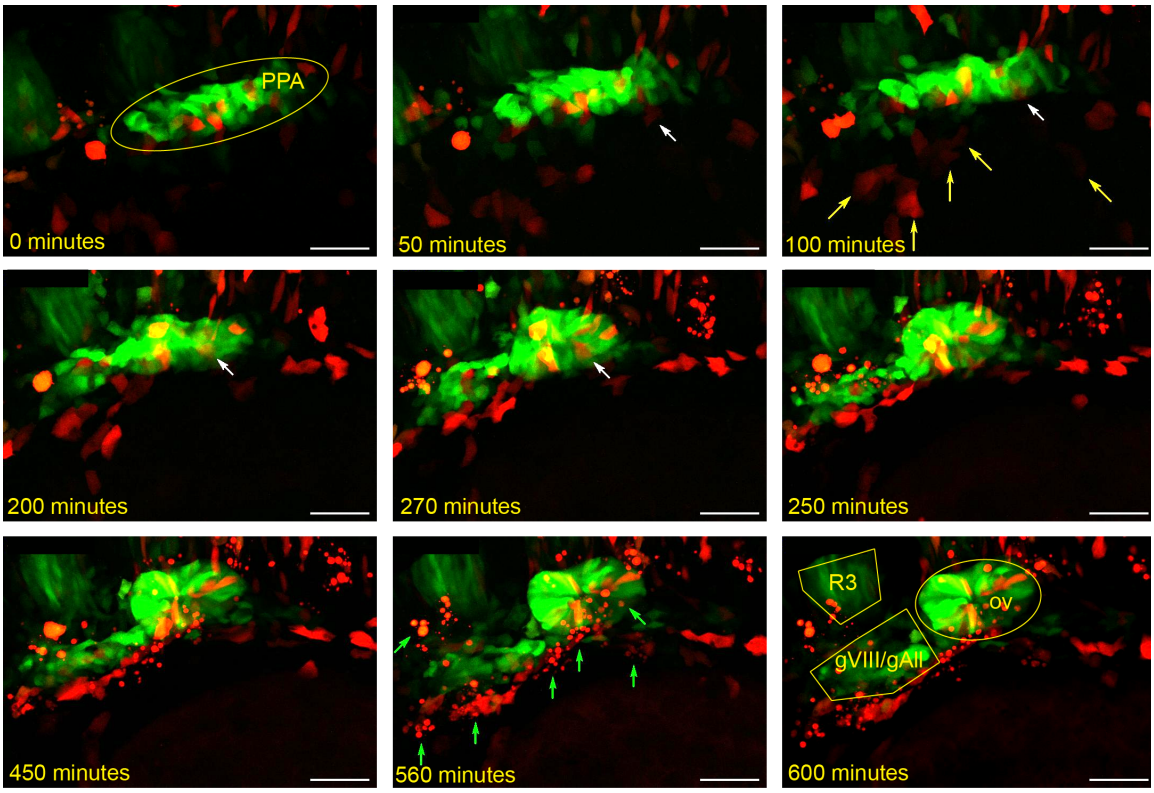

Figure 19: High levels of Pax2a induce formation of placodal precursors from the non-neural ectoderm and their subsequent incorporation into the otic placode.

One-cell stage Tg*(pax2a:GFP)* transgenic embryos were injected with 25 pg of dTomato:HSE:Pax2a DNA construct and heat-shocked at 10 hpf. Stills from time-lapse of confocal z-stacks acquired at 10 minute intervals over ~10.2 hours beginning at 12 hpf (PPA circled in yellow). Note mosaic expression of dTomato+ cells in red. Time-lapse reveals ectopic Pax2a-expressing cells appearing in the lateral non-neural ectoderm and migrating medially towards the forming otic placode (yellow and white arrows). Some of these cells are able to incorporate into the otic vesicle (white arrow), while a number of ectopic Pax2a cells that cannot incorporate undergo cell death (fragmented cells; green arrows). The acoustic/AII ganglia (gVIII/gAII), rhombomere 3 (R3) and the otic vesicle (OV) are marked on the last panel. Scale bar = 50 μm.

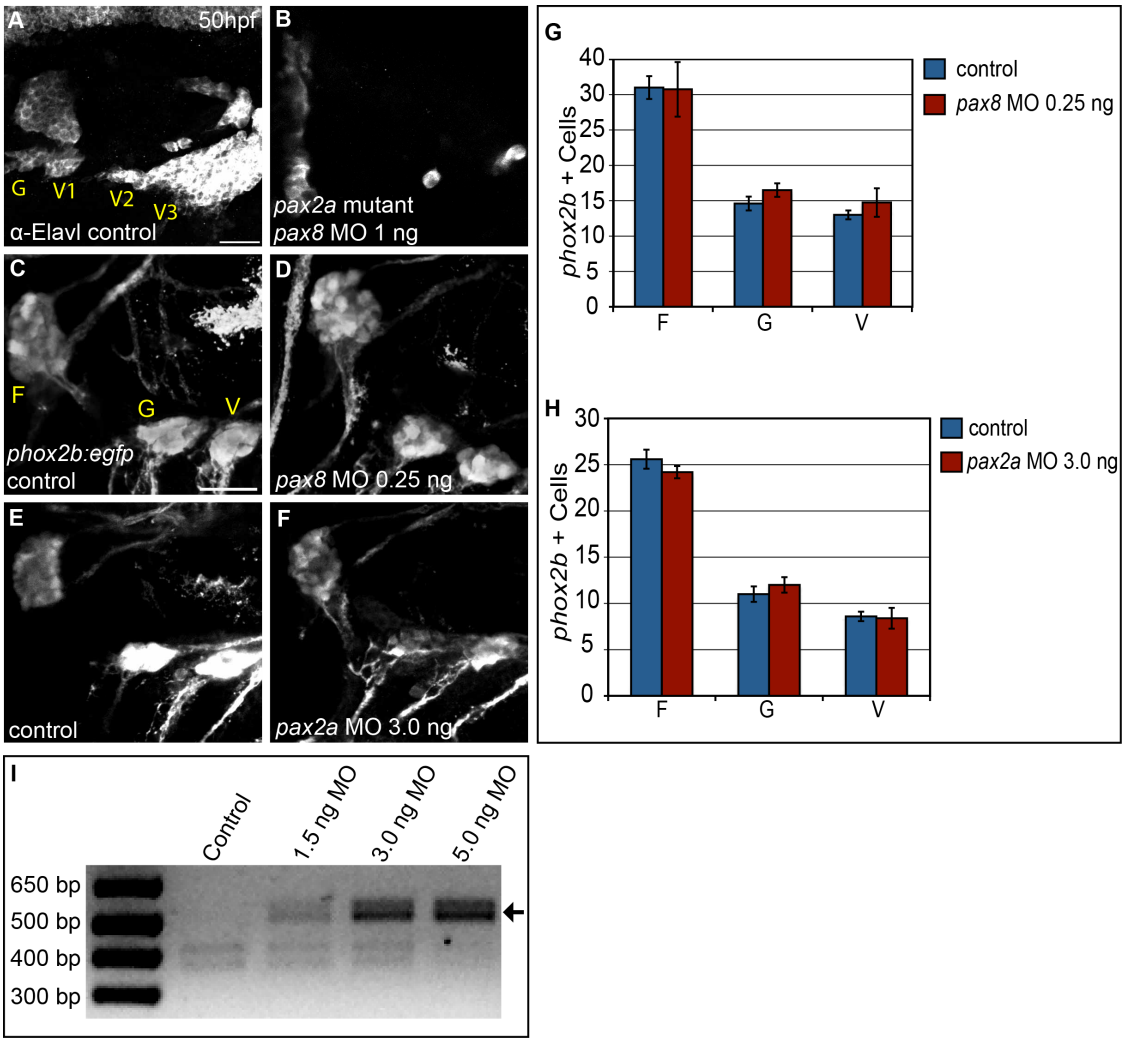

Figure 20: Combined activity of Pax2a and Pax8 is necessary for formation of the EB ganglia.
(A and B) Embryos derived from a *pax2a*$^{b593/+}$ incross immunolabeled with anti-Elavl3/4 to mark differentiated EB neurons in control (A) and embryos injected with 1 ng of *pax8*-MO (B). Note near-complete loss of Elavl3/4+ neurons in the EB ganglia of the *pax2a* mutant that also received *pax8*-MO (B). **(C-F)** Confocal projection from 50 hpf Tg*(phox2b:EGFP)*^{w37} embryos. Control embryos (C and E) were compared to embryos injected with either 0.25 ng of *pax8*-MO (D) or 3.0 ng of *pax2a*-MO (F). **(G and H)** Quantification of *phox2b*+ neurons at 50 hpf in the facial, glossopharyngeal, and most anterior small vagal ganglia in embryos injected with 0.25 ng of *pax8*-MO (G) and 3.0 ng *pax2a*-MO (H) versus controls (n≥34 cells from 5 embryos/condition). Note the lack of significant difference in ganglion sizes when MOs are singly injected at suboptimal concentrations. **(I)** RT-PCR of *pax2a* splice variant products from embryos that were injected with increasing amounts of *pax2a* MO. The amount of an RT-PCR product corresponding to an aberrant splice variant (arrow) increased with respect to injected *pax2a*-MO in a dose-dependent manner. Scale bar = 25 μm.

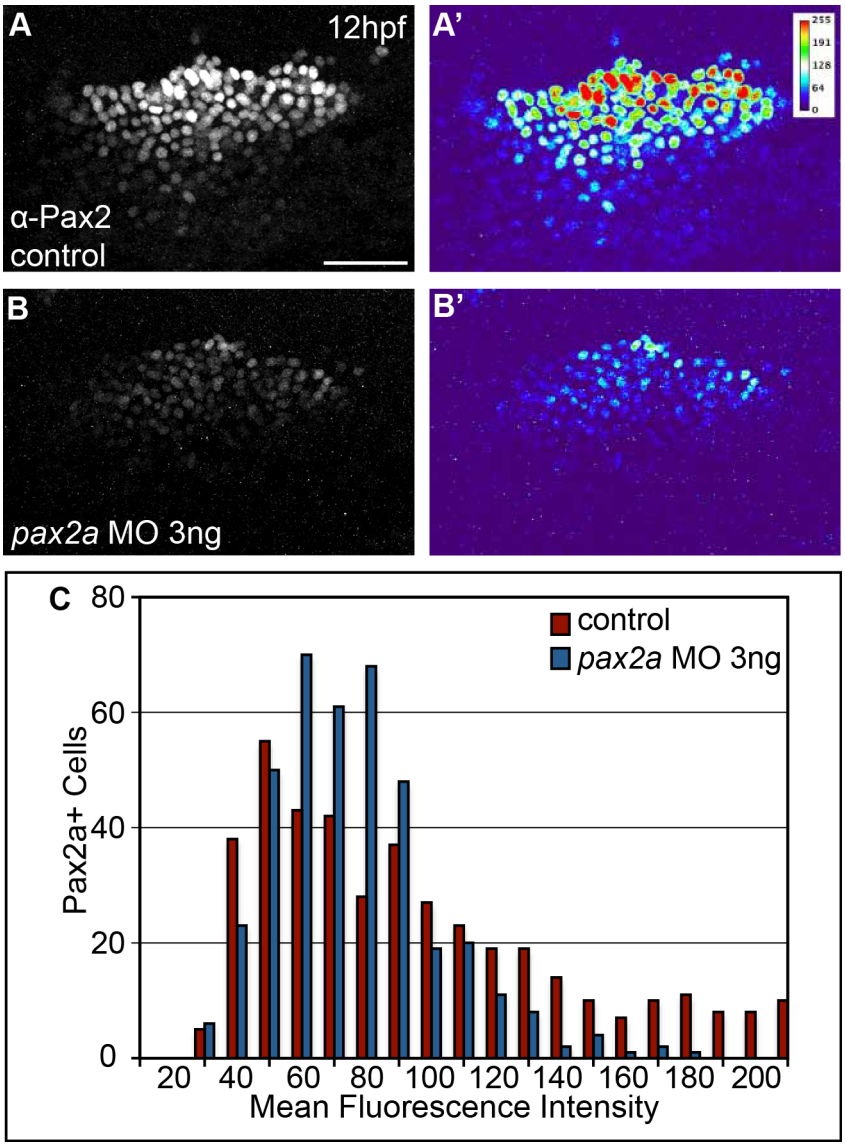

Figure 21: Injection of suboptimal amounts of *pax2a* MO results in a reduction in Pax2a protein levels in cells of the PPA at 12 hpf.
(A and B) Control embryos and embryos injected with 3 ng of *pax2a*-MO were immunolabeled with anti-Pax2 antibody at 12 hpf. Suboptimal MO levels were defined by titration experiments. Note that 3 ng of *pax2a* MO results in an overall reduction, but not complete absence, of Pax2a protein in the PPA (A' vs. B'). **(C)** Distribution of mean gray values of Pax2a levels in control and *pax2a*-MO injected embryos (n≥393 cells from 7 embryos/condition). Note the significant decrease (χ^2 - test, $p<<0.001$) in the number of cells with high Pax2a expression in embryos injected with *pax2a*-MO. Scale bar = 50 µm.

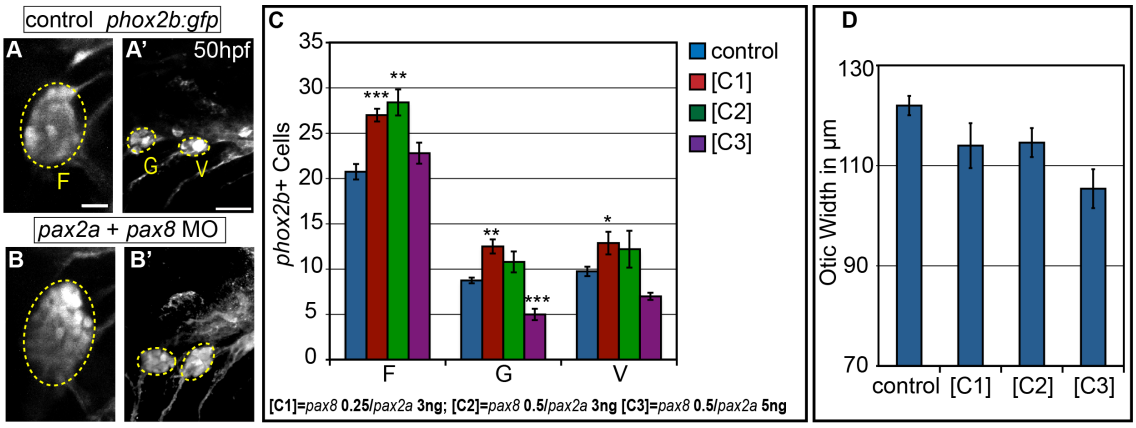

Figure 22: Partial knockdown of *pax2a* and *pax8* transcripts increases cell numbers in EB ganglia.

Zygotes carrying the TgBAC*(phox2b:EGFP)*^{w37} transgene were injected with different amounts of *pax2a+pax8* MOs; EB ganglion cell numbers were assayed at 50 hpf. **(A)** Confocal projection in uninjected control. Facial (F), glossopharyngeal (G) and vagal (V) ganglia (dashed ovals) contain 20, 8 and 9 EGFP+ cells, respectively. **(B)** Confocal projection of an embryo injected with 3+0.25 ng of *pax2a+pax8* MOs. Note increased size of G and small V ganglia (F=29, G=13, and V=13 cells). **(C)** Quantification of cells in F, G, and small V ganglia in controls and embryos that received increasing doses of *pax2a+pax8* MOs. Note significant size increase in all ganglia at [C1] (***p<0.001, **p<0.005, *p<0.05). **(D)** Quantification of otic width (longest A-P segment in µm) of controls and embryos receiving increasing doses of *pax2a+pax8* MOs (Student's t-test, p=0.056). Abbreviations: F=facial placode, gAll/gVIII=anterior lateral line ganglion/acoustic ganglion, G+V=glossopharyngeal /vagal placodes, OV=otic vesicle. n≥33 cells, 8 embryos/condition. Scale bar=10 µm (A) and 25µm (A').

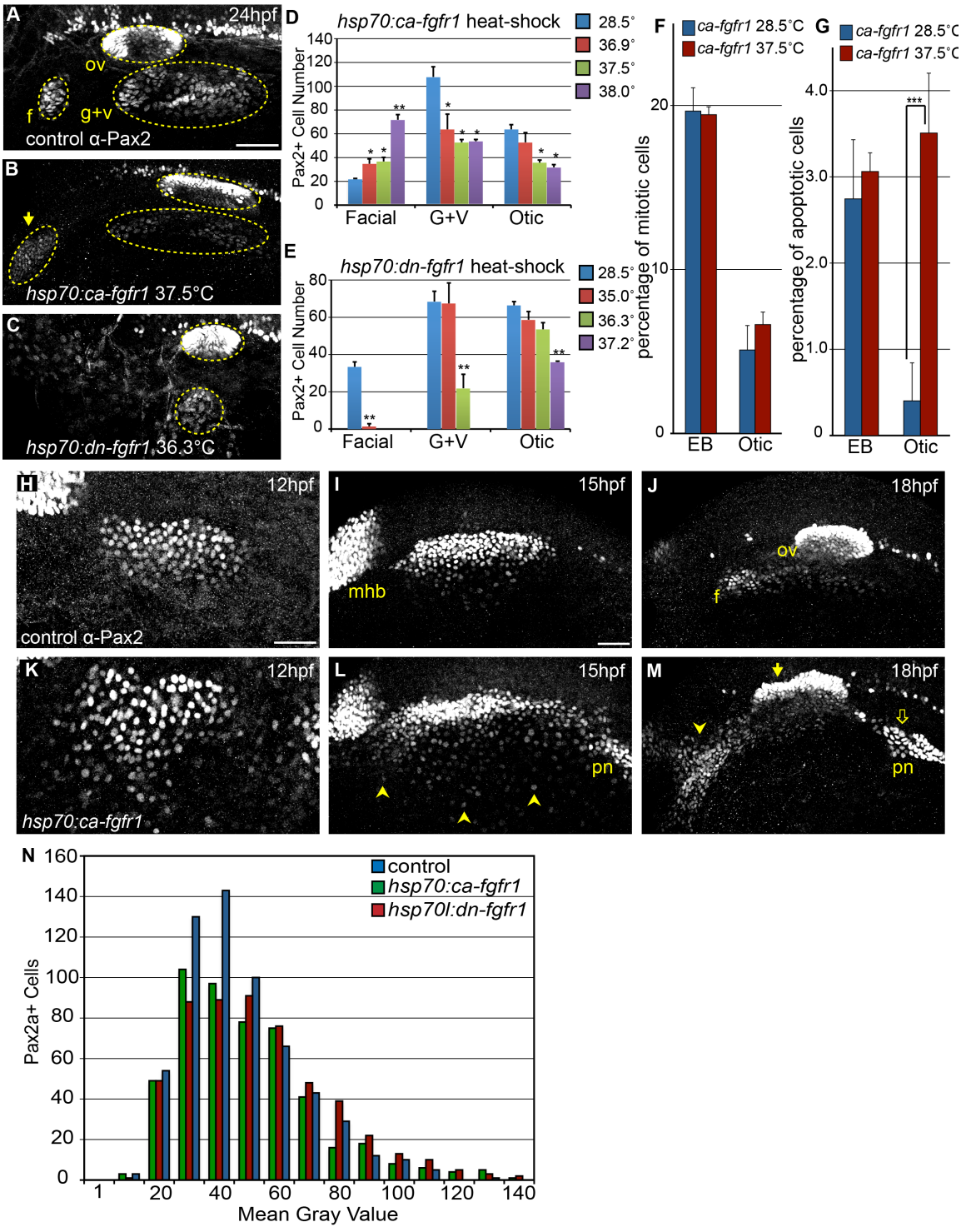
A
24hpf
ov
f
g+v
control α-Pax2
B
hsp70:ca-fgfr1 37.5°C
C
hsp70:dn-fgfr1 36.3°C
D
hsp70:ca-fgfr1 heat-shock
28.5°
36.9°
37.5°
38.0°
Pax2+ Cell Number
Facial
G+V
Otic
E
hsp70:dn-fgfr1 heat-shock
28.5°
35.0°
36.3°
37.2°
Pax2+ Cell Number
Facial
G+V
Otic
F
ca-fgfr1 28.5°C
ca-fgfr1 37.5°C
percentage of mitotic cells
EB
Otic
G
ca-fgfr1 28.5°C
ca-fgfr1 37.5°C
percentage of apoptotic cells
EB
Otic
H
12hpf
control α-Pax2
I
15hpf
mhb
J
18hpf
ov
f
K
12hpf
hsp70:ca-fgfr1
L
15hpf
pn
M
18hpf
pn
N
control
hsp70:ca-fgfr1
hsp70l:dn-fgfr1
Pax2a+ Cells
Mean Gray Value

Figure 23: Modulating Fgf signaling affects size of the otic and EB placodes.

(A-C) Representative confocal projections of embryos immunolabeled with anti-Pax2 antibody at 24 hpf including: control (A), constitutively-active Fgfr1 (Tg*(hsp70:ca-fgfr1)*^{pd3} transgene) (B) and dominant-negative Fgfr1 (Tg*(hsp70:dnfgfr1-EGFP)*^{pd1} transgene) (C). Heat shock induction for both constructs was carried out at 10 hpf. Note an increase in the number of Pax2+ cells in the facial placode (arrow in B) and concurrent reduction in the G+V placodes and dysmorphia in the otic vesicle following Fgf upregulation. By contrast, inhibition of Fgf results in loss of the facial placode with a concomitant reduction in the otic vesicle and G+V placodes (C). **(D)** Quantification of Pax2+ cells in the otic vesicle and EB placodes in control embryos (no heat-shock) and Tg*(hsp70:ca-fgfr1)*^{pd3} embryos heat-shocked at various temperatures (36.9, 37.5, and 38°C). Note the 3.4 fold increase in the number of Pax2+ cells in the facial placode following heat-shock at 38˚C, with concomitant decrease of the G+V placodes and otic vesicle (Student's *t*-test, ***p*<0.0075). **(E)** Quantification of Pax2+ cells in the otic vesicle and EB placodes in control embryos (no heat-shock) and Tg*(hsp70:dnfgfr1-EGFP)*^{pd1} embryos following heat-shock at various temperatures (35, 36.3, and 37.2°C). Note the ~95% reduction in the facial placode following 35° heat-shock (Student's *t*-test, ***p*<0.002), and complete loss of this placode at higher inductive temperatures. Whereas the G+V placodes are unaffected at lower inductive conditions, there is a 68% reduction (Student's *t*-test ***p*<0.004) and a complete loss of this domain following heat-shock at 36.3° and 37.2°, respectively. In contrast, the number of Pax2a+ cells in the otic vesicle is only reduced following heat-shock at the 37.2˚C (46% reduction; Student's *t*-test ***p*<0.001). **(F)** Percentage of Pax2a+ cells undergoing mitosis was measured by immunolabeling with a pH3 antibody at 18 hpf. There is no significant change in proliferation following 10 hpf heat-shock of Tg*(hsp70:ca-fgfr1)*^{pd3} embryos, compared to uninduced controls (n=12 embryos/condition). **(G)** Percentage of Pax2a+ cells undergoing apoptosis as measured by immunolabeling with Caspase-3 antibody at 18 hpf. There is a significant increase of cell death in the otic placode following 10 hpf heat-shock of Tg*(hsp70:ca-fgfr1)*^{pd3} embryos (n=12 embryos/condition). **(H-M)** Pax2a expression at 12, 15, and 18 hpf in control embryos (H, I, J) or Tg*(hsp70:ca-fgfr1)*^{pd3} transgenic embryos following heat-shock induction at 10 hpf (K, L, M). Note additional Pax2a+ cells lateral to the PPA at 15 hpf (L, arrowheads); and expansion and fusion of Pax2a+ cells in the pronephros (pn) with the PPA. By 18 hpf a striking expansion of the facial placode can be observed (arrowhead), concurrent with a dysmorphic otic vesicle (filled arrow) expansion and mislocalization of the pronephros (M, open arrow). **(N)** Distribution of Pax2a fluorescence intensity in PPA cells at 12 hpf in control, Tg*(hsp70:dnfgfr1-EGFP)*^{pd1}, and Tg*(hsp70:ca-fgfr1)*^{pd3} following 10 hpf heat- shock. Note that the overall distribution of Pax2a intensity levels is unchanged regardless of Fgf levels (n≥504 cells from 8 embryos per condition). Scale bar = 50 μm.

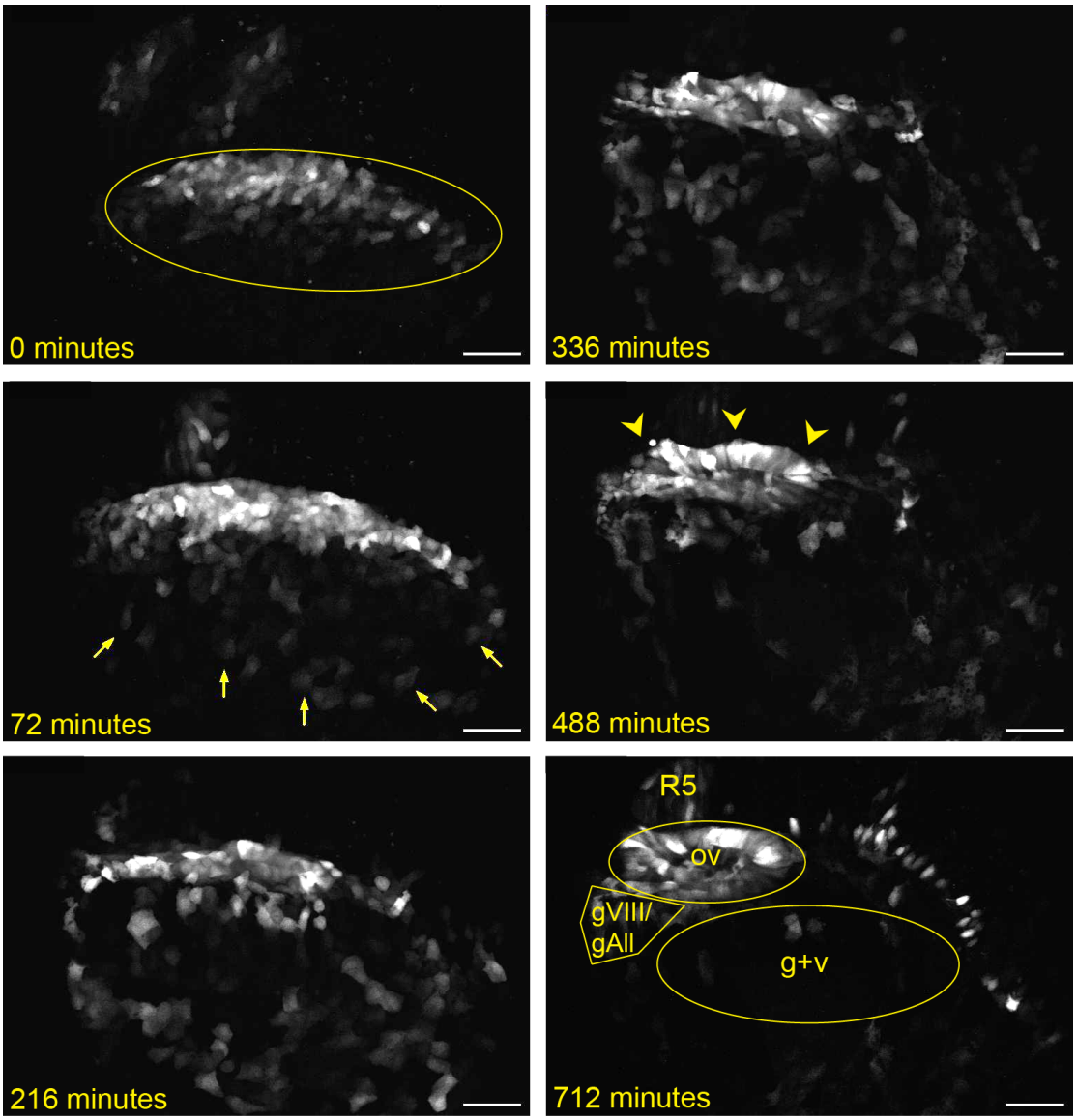

Figure 24: Activation of Fgf pathway results in recruitment of additional Pax2a+ cells into the PPA.
Time-lapse of an embryo derived from Tg*(hsp70:ca-fgfr1)* and Tg*(Pax2a:GFP)* cross during placode segregation and formation. Stills of confocal projections acquired at 8 minute intervals over ~12 hours. Embryos were heat-shocked at 10 hpf to induce transgene expression. First frame begins at 12 hpf with the PPA circled in yellow. By 14 hpf continuous ectopic induction of Pax2a is seen (yellow arrows) in the lateral non-neural ectoderm that continues until after otic placode assembly (~18 hpf). Note axial extension of the otic placode with concurrent failure of invagination (arrowheads). Otic vesicle (ov), glossopharyngeal/vagal placode (g+v), potential acoustic/AII ganglia (gVIII/gAII), and rhombomere 5 (R5) are marked in the last frame. Scale bar = 50 μm

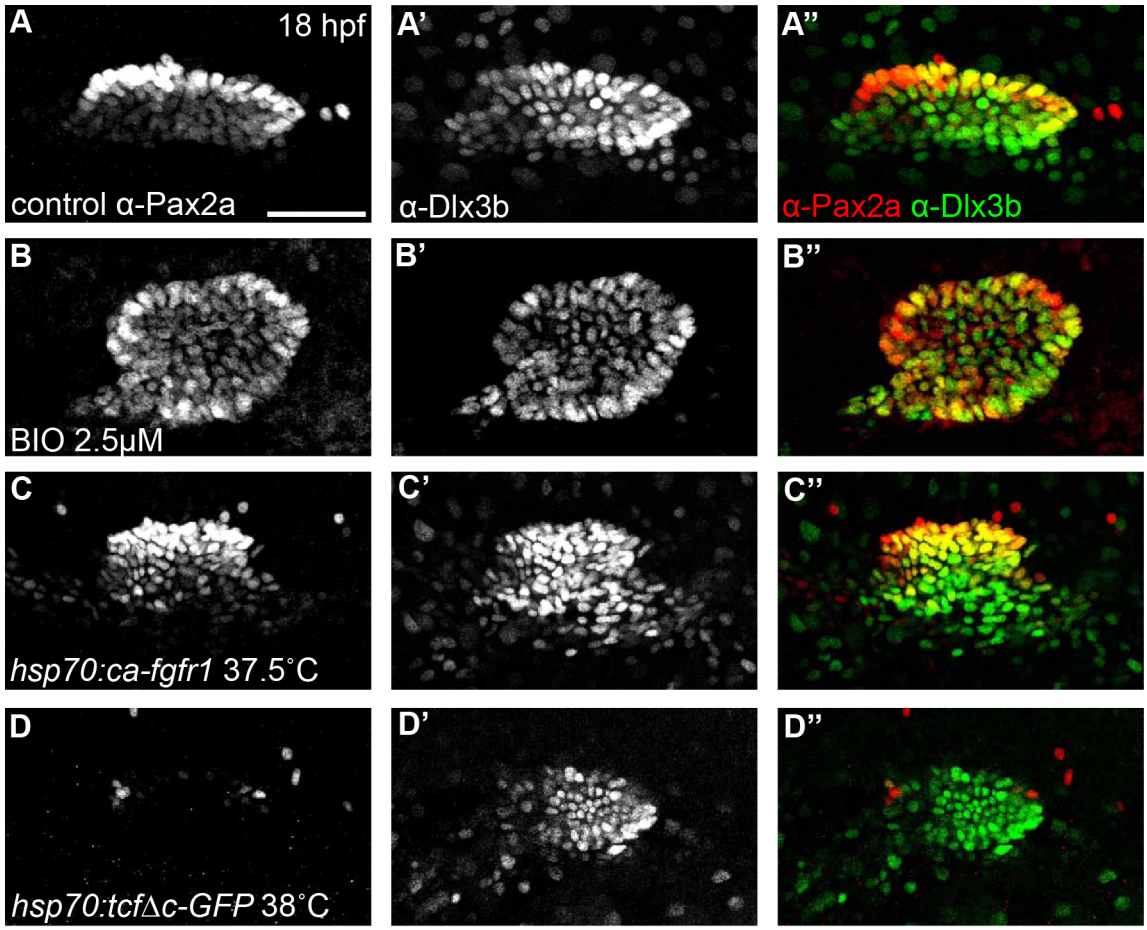
A
18 hpf
control α-Pax2a
A'
α-Dlx3b
A''
α-Pax2a α-Dlx3b
B
BIO 2.5μM
B'
B''
C
hsp70:ca-fgfr1 37.5˚C
C'
C''
D
hsp70:tcfΔc-GFP 38˚C
D'
D''

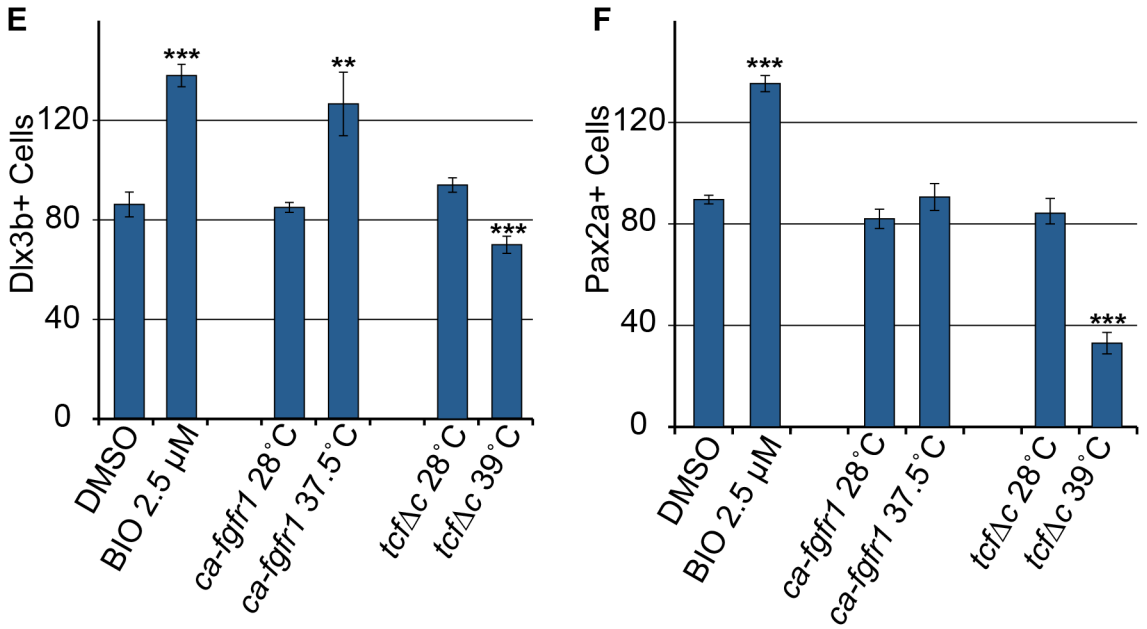
E
Dlx3b+ Cells
0
40
80
120
***
**
***
DMSO
BIO 2.5 μM
ca-fgfr1 28˚C
ca-fgfr1 37.5˚C
tcfΔc 28˚C
tcfΔc 39˚C
F
Pax2a+ Cells
0
40
80
120
***
***
DMSO
BIO 2.5 μM
ca-fgfr1 28˚C
ca-fgfr1 37.5˚C
tcfΔc 28˚C
tcfΔc 39˚C

Figure 25: Number of Dlx3b+ cells in the otic vesicle is altered when Fgf and Wnt pathways are modulated.

Confocal projections of 18 hpf embryos co-labeled with anti-Pax2a and anti-Dlx3b to assess expression in the developing otic vesicle. **(A)** Control embryos reveal that at 18 hpf Pax2a and Dlx3b exhibit extensive co-localization; however a number of lateral otic cells that either express very low Pax2a levels or do not express Pax2a at all are Dlx3b+. **(B)** Embryos treated with 2.5 μM BIO starting at 11 hpf show a concomitant increase in both Pax2a and Dlx3b+ cells. **(C)** 10 hpf heat-shock of Tg*(hsp70:ca-fgfr1)*^{pd3} embryos caused an increase in number of Dlx3b+ cells but also yielded a high level of cell disorganization. **(D)** Pax2a expression in the otic cells is completely lost following inhibition of Wnt signaling by 10 hpf heat-shock of Tg(*hsp70:tcf*Δ*C-EGFP)*. Otic cells retained Dlx3b expression; however the overall number of otic cells is reduced versus control. **(E)** Quantification of Dlx3b+ cells in the otic vesicle at 18 hpf following various treatments. This analysis revealed a 60% increase in Dlx3b+ cells in the otic vesicle after BIO treatment (Student's *t*-test ***p<<0.001) a 49% increase in Dlx3b+ cells after Tg*(hsp70:ca-fgfr1)*^{pd3} induction (Student's *t*-test **p<0.006), and a 25% reduction in the number of Dlx3b+ cells after induction of Tg(*hsp70:tcf*Δ*C-EGFP)* (Student's *t*-test ***p<<0.001; n=6 embryos/condition). **(F)** Quantification of Pax2a+ cells in the otic vesicle at 18 hpf following the above treatments. The analysis revealed a 51% increase in Pax2a+ cells in the otic vesicle after BIO treatment (Student's *t*-test ***p<<0.001), no significant change in Pax2a+ cells in Tg*(hsp70:ca-fgfr1)*^{pd3} induced embryos, and a 61% reduction in Pax2a+ cells after Tg(*hsp70:tcf*Δ*C-EGFP)* induction (Student's *t*-test ***p<<0.001; n=6 embryos/condition). Scale bar = 50 μm.

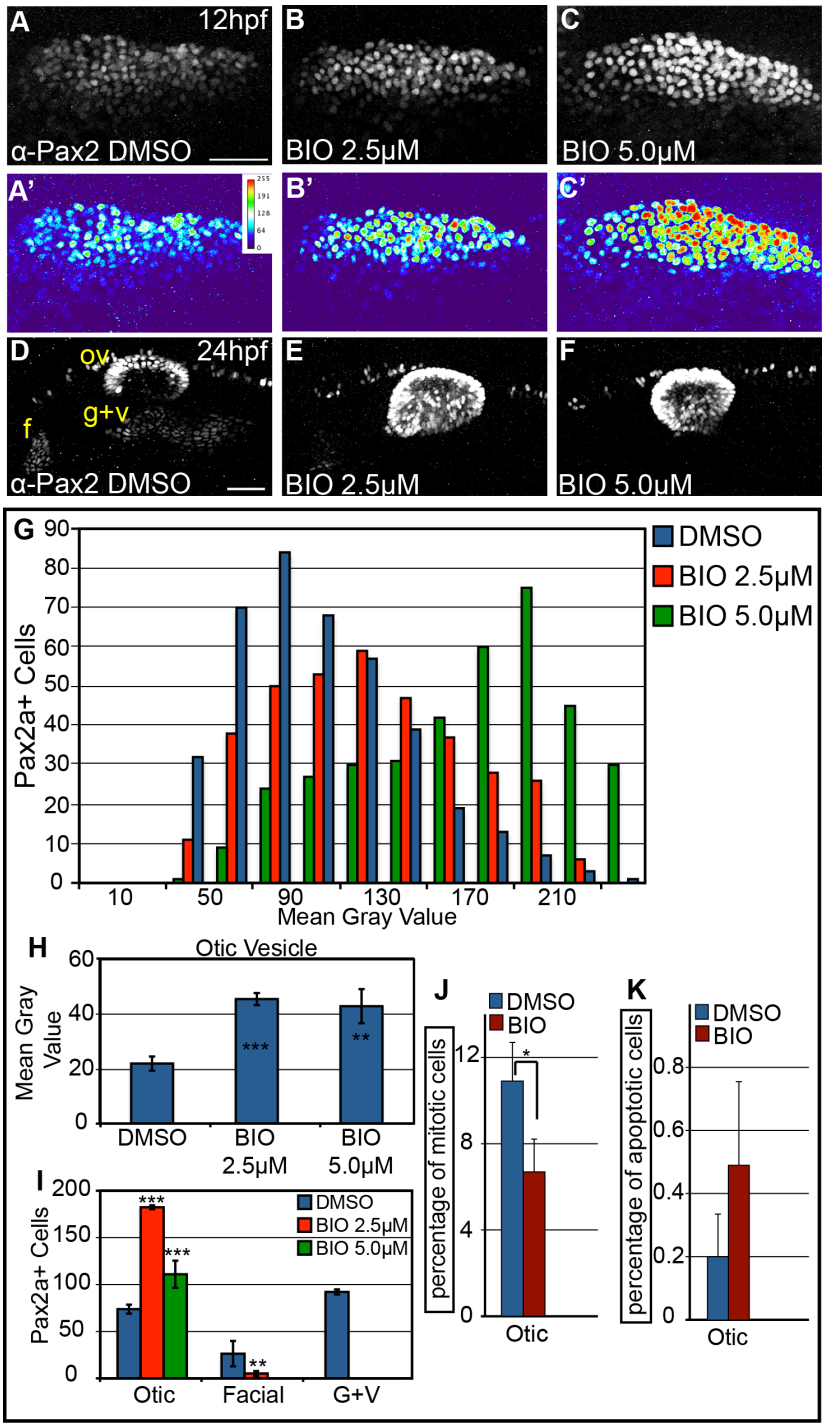
A
12hpf
α-Pax2 DMSO
B
BIO 2.5μM
C
BIO 5.0μM
A'
B'
C'
D
ov
g+v
f
24hpf
α-Pax2 DMSO
E
BIO 2.5μM
F
BIO 5.0μM
G
Pax2a+ Cells
Mean Gray Value
DMSO
BIO 2.5μM
BIO 5.0μM
H
Otic Vesicle
Mean Gray Value
DMSO
BIO 2.5μM
BIO 5.0μM
I
Pax2a+ Cells
Otic
Facial
G+V
J
percentage of mitotic cells
Otic
K
percentage of apoptotic cells
Otic

Figure 26: Overactivation of Wnt signaling increases levels of Pax2a expression and biases cells to an otic commitment.
(A-C) Confocal projections of DMSO- and BIO-treated embryos between 11 and 12 hpf and analyzed for Pax2a expression in the PPA. (A'-C') Heat maps show increased Pax2a levels after BIO treatment. **(D-F)** Confocal projection of DMSO- and BIO-treated embryos between 11 and 24 hpf. Otic vesicle and EB placodes visualized by Pax2a. In BIO-treated embryos, the otic vesicle is larger, while EB placodes are significantly reduced (80-100%.) **(G)** Analysis of PPA Pax2a+ cells in control and BIO-treated embryos (2.5 and 5.0 μM) at 12 hpf ($n \geq 354$ cells, 5 embryos/condition) shows dose-dependent increases in expression from low (MGV<120) to high (MGV>120) (χ^2, $p << 0.001$). **(H)** Comparison of MGVs for Pax2a fluorescence in the otic vesicle showed a significant increase in Pax2a expression levels following BIO treatment (Student's t-test; $^{**}p<0.007$). **(I)** Pax2a+ cell number in the otic vesicle showed a 2.47 fold increase in 2.5 μM BIO and a 1.5 fold increase in 5.0 μM BIO versus controls (Student's t-test; $^{***}p<0.001$). **(J)** Percentage of Pax2a+ mitotic cells in the otic vesicle dropped at 18 hpf following 10-hour-long BIO treatment ($^{*}p<0.05$; n=12 embryos/condition). **(K)** The percentage of Pax2a+ cells that were also Caspase-3+ at 18 hpf in embryos treated with BIO between 10-18 hpf (n=12 embryos/condition) was unchanged. Abbreviations: F=facial placode, gAll/gVIII=anterior lateral line ganglion/acoustic ganglion, G+V=glossopharyngeal /vagal placodes, OV=otic vesicle. MGV=mean gray value. Scale bar=50μm.

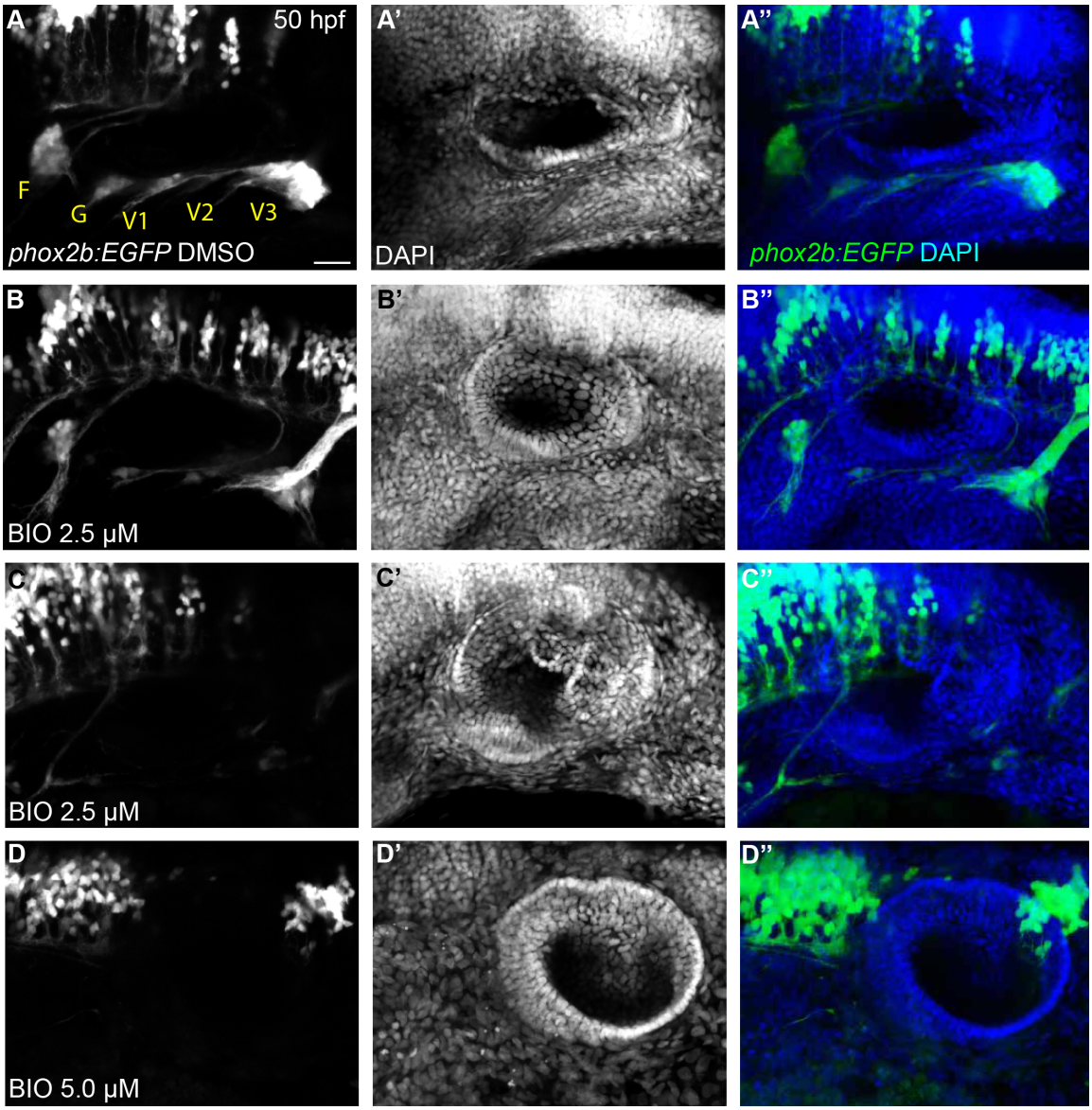

Figure 27: Overactivation of Wnt signaling severely reduces or blocks EB ganglia formation.
Confocal projection images of the otic vesicle and EB ganglia at 50 hpf. Tg*(phox2b:EGFP)*^{w37} embryos were treated with 2.5 and 5.0 µM BIO beginning 11 hpf, then washed out at 24 hpf. Embryos were allowed to develop until 50 hpf, at which time they were assessed for EB ganglion formation by *EGFP* expression and for otic vesicle formation by DAPI labeling. **(A-C)** While DMSO-treated control embryos had normal development of the otic vesicle and EB ganglia, approximately half of 2.5 µM BIO treated embryos had severely reduced EB ganglia and the remaining half had no EBs. **(D)** 5.0 µM BIO treated embryos resulted in a complete loss of EBs. Scale bar = 25 µm.

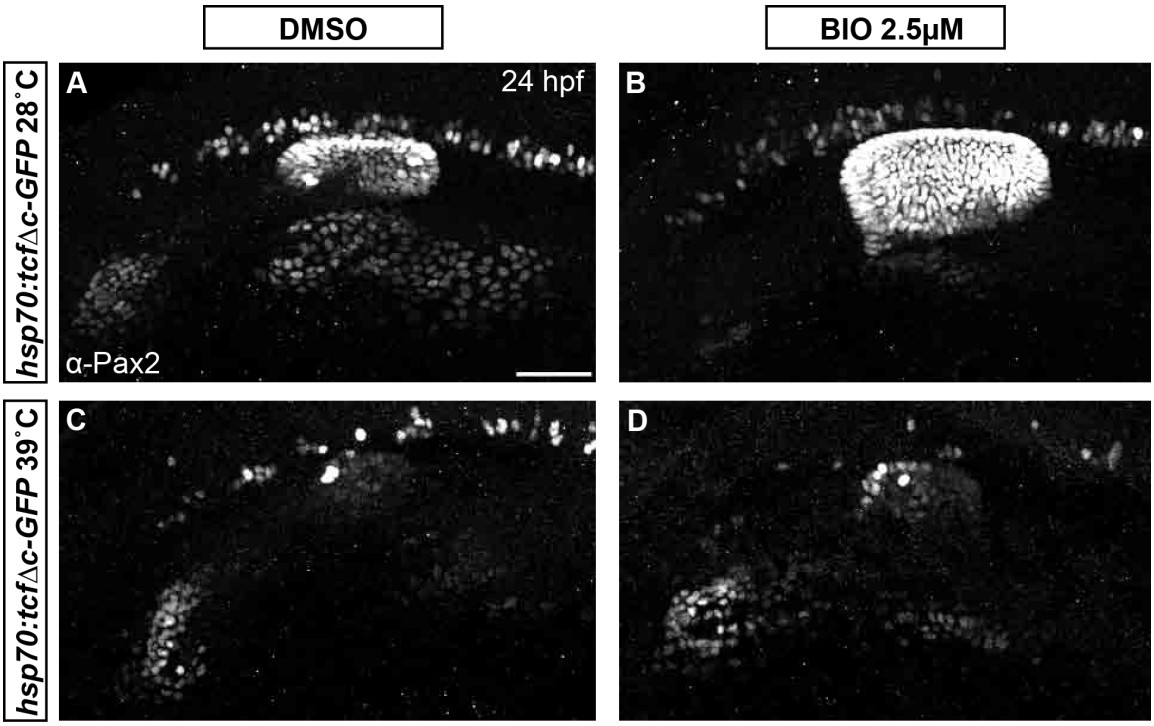

Figure 28: BIO treatment upregulates Pax2a levels and promotes otic cell commitment through the Wnt pathway.
(A,B) Tg(*hsp70:tcfΔC-EGFP)* embryos in which transgene was not activated were treated at 11 hpf with either DMSO (A) or 2.5μM BIO (B). In embryos treated with BIO we observed supernumerary Pax2+ cells in the otic vesicle and increased Pax2a levels. **(C,D)** Tg(*hsp70:tcfΔC-EGFP)* embryos that were heat-shocked at 10 hpf, yielded the same phenotype in both DMSO (C) and 2.5μM BIO (D) treated embryos, indicating that BIO is modulating Pax2 levels and otic fate via the canonical Wnt pathway (n=5 embryos/condition). Scale bar = 50 μm.

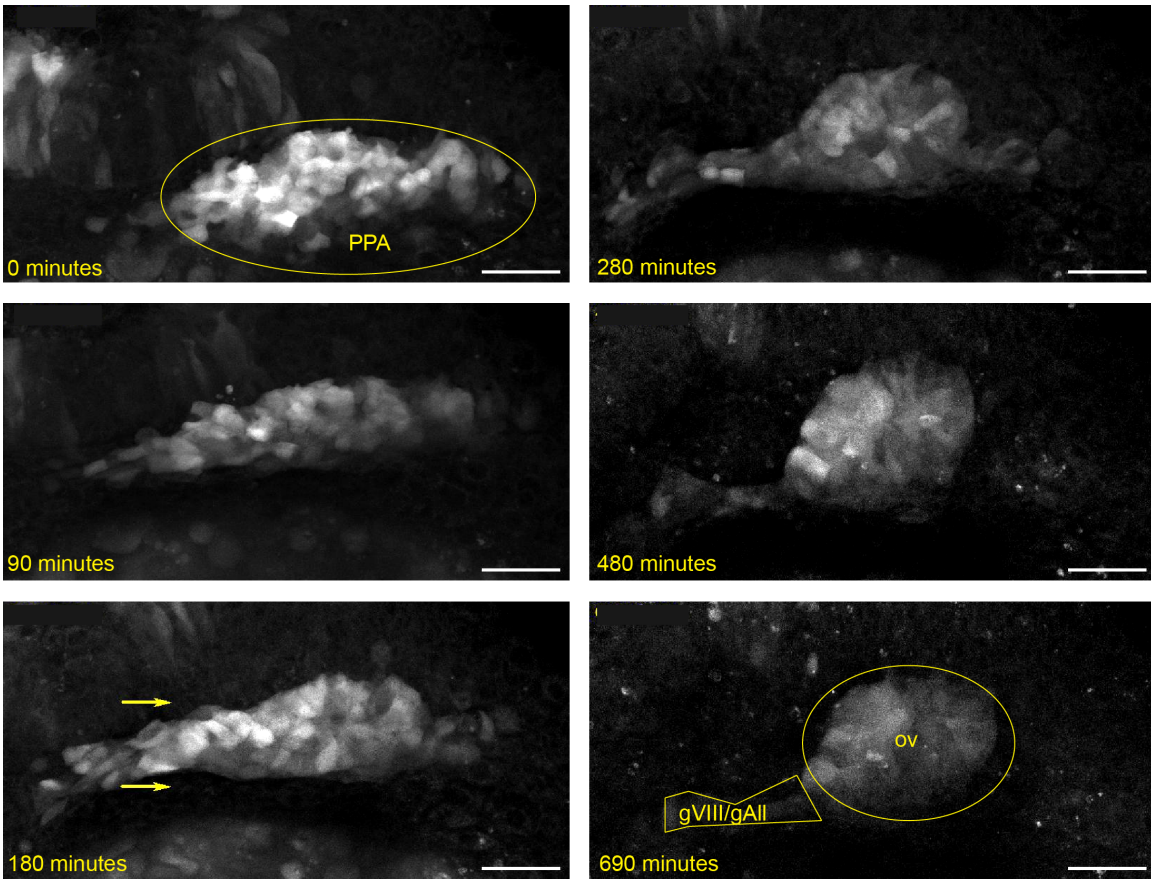

Figure 29: Anterior PPA cells contribute to the otic vesicle following over activation of Wnt signaling.
Time-lapse of a Tg*(pax2a:GFP)*^{e1} transgenic embryo treated with 2.5 µM BIO between 11 and 24 hpf (end of time lapse). Confocal z-stacks were acquired at 10 minute intervals over ~11.7 hours starting at 12 hpf. PPA is circled in yellow. By t=180 minutes, anterior cells of the prospective gVIII/gAll (marked by yellow arrows) begin to move posteriorly toward the forming otic vesicle. The reduced acoustic/All ganglia (gVIII/gAll) and the enlarged otic vesicle (OV) are marked in the last frame. There is a level of autofluorescence due to the presence of BIO inhibitor. Scale bar = 50 µm.

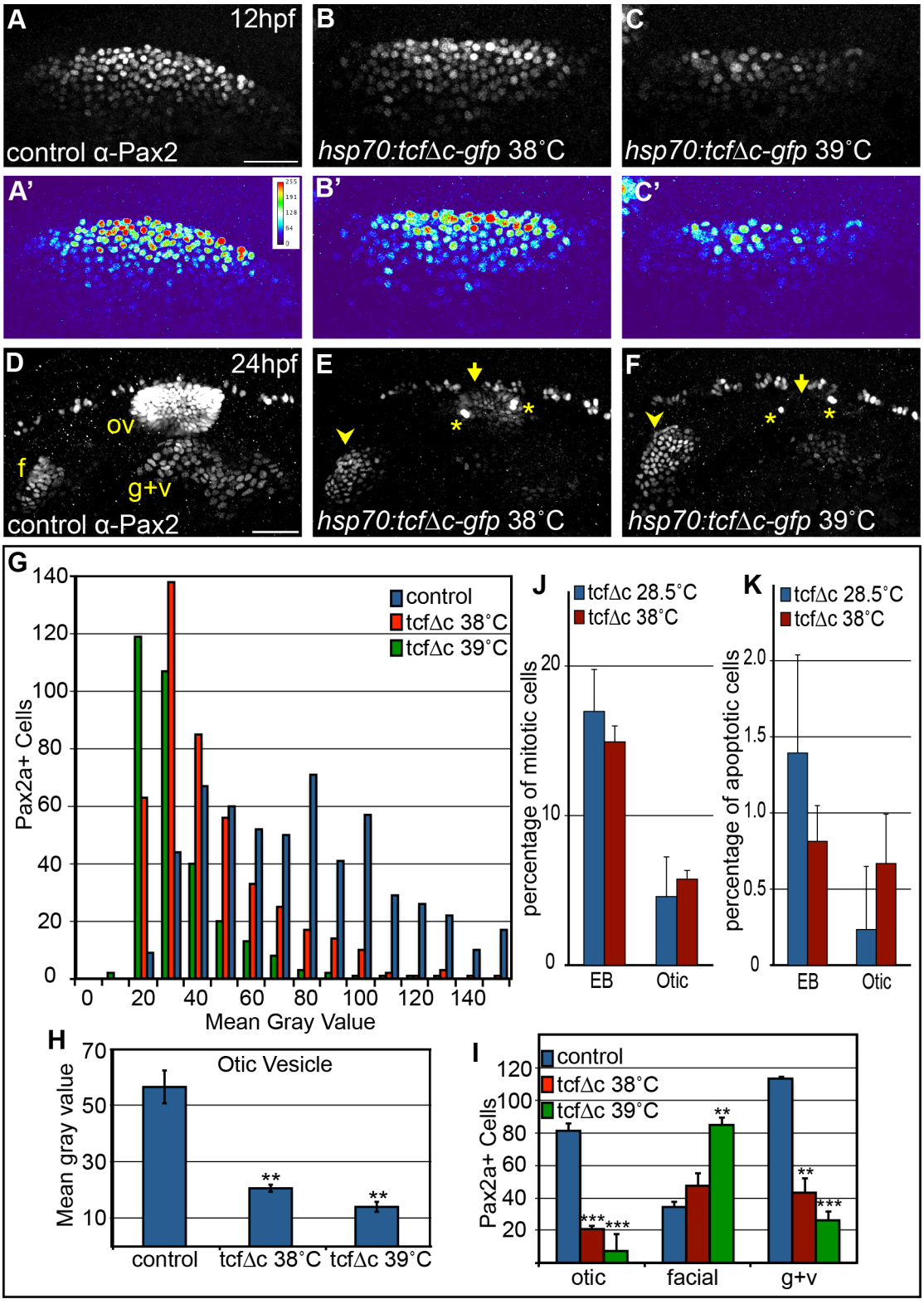
A
12hpf
control α-Pax2
B
hsp70:tcfΔc-gfp 38˚C
C
hsp70:tcfΔc-gfp 39˚C
A'
B'
C'
D
24hpf
ov
f
g+v
control α-Pax2
E
hsp70:tcfΔc-gfp 38˚C
F
hsp70:tcfΔc-gfp 39˚C
G
control
tcfΔc 38˚C
tcfΔc 39˚C
Pax2a+ Cells
Mean Gray Value
J
tcfΔc 28.5˚C
tcfΔc 38˚C
percentage of mitotic cells
EB
Otic
K
tcfΔc 28.5˚C
tcfΔc 38˚C
percentage of apoptotic cells
EB
Otic
H
Otic Vesicle
Mean gray value
control
tcfΔc 38˚C
tcfΔc 39˚C
I
control
tcfΔc 38˚C
tcfΔc 39˚C
Pax2a+ Cells
otic
facial
g+v

Figure 30: Inhibition of Wnt signaling reduces Pax2a levels resulting in a cell segregation shift from otic to facial placode.
(A-C) Confocal projections from control and Tg(*hsp70:tcf∆C-EGFP)* embryos heat-shocked at 10 hpf and analyzed for Pax2a expression at 12 hpf. Note decreased Pax2a levels in heat map images as heat-shock stringency increases (A'-C'). **(D-F)** Control and Tg(*hsp70:tcf∆C-EGFP)*+ embryos heat-shocked at 10 hpf and analyzed for Pax2a expression at 24hpf (arrowheads - facial placode, arrows - otic vesicle, and asterisks - putative otic sensory patches). **(G)** PPA Pax2a expression MGVs at 12 hpf. Note significant shift from high to low Pax2a levels with increased heat-shock stringency (χ^2-test; $p<<0.001$). **(H)** Average MGV of Pax2a expression in the otic vesicle was significantly reduced in Tg(*hsp70:tcf∆C-EGFP)*+ embryos (heat-shocked at 39˚C) versus controls (n≥317 cells from 5 embryos/condition; unpaired t-test; $^{**}p<0.003$). **(I)** Quantification of Pax2a+ cells in control and Wnt-inhibited embryos (heat-shocked at 39˚C) reveals significant otic vesicle and glossopharyngeal/vagal placode cell losses, with concurrent increases in facial placode ($^{***}p<0.001$; $^{**}p<0.01$). **(J)** Percentage of mitotic cells (by pH3 immunolabeling) at 18 hpf following heat-shock of Tg(*hsp70:tcf∆C-EGFP)* embryos at 10 hpf was unchanged versus uninduced controls (n=12 embryos/condition). **(K)** There is no significant change in Caspase-3+ cell percentage at 18 hpf following heat-shock of Tg(*hsp70:tcf∆C-EGFP)* embryos at 10 hpf (n=12 embryos/condition). Abbreviations: F=facial placode, gAll/gVIII=anterior lateral line ganglion/acoustic ganglion, G+V=glossopharyngeal /vagal placodes, OV=otic vesicle. Scale bar=50µm.

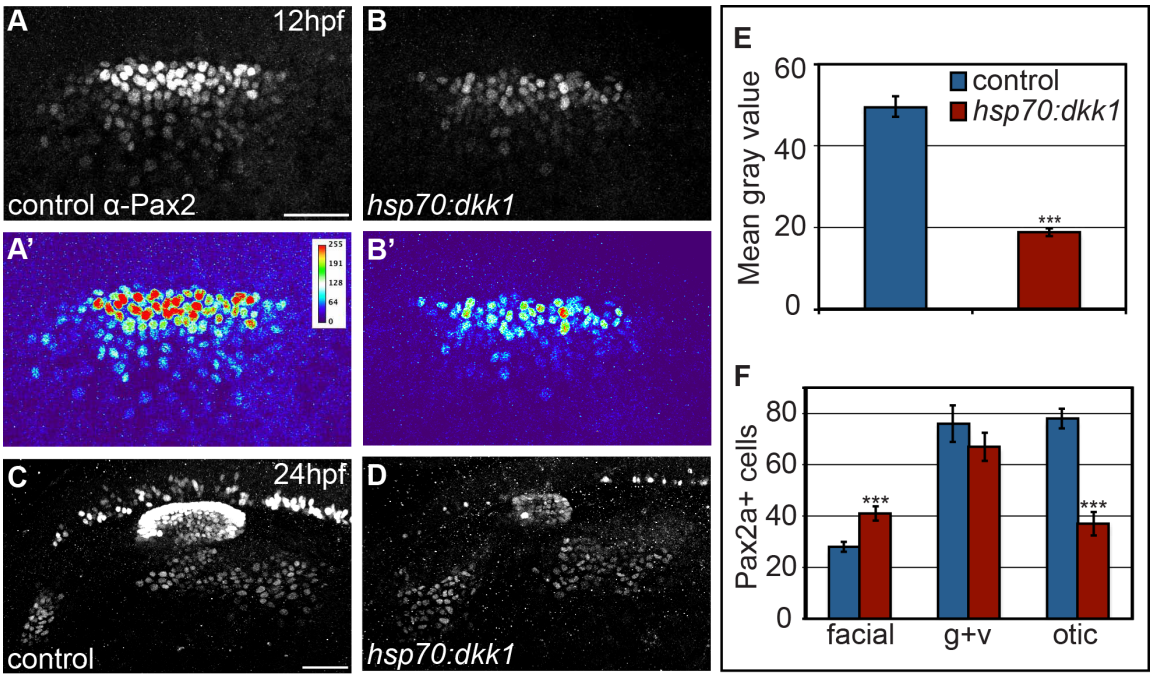

Figure 31: Global Wnt inhibition by Dkk1 expression attenuates Pax2a levels.

(A-D) Control and Tg*(hsp70:dkk1-GFP)*^{w32} embryos were heat-shocked at 10 hpf and assayed for Pax2a expression at 12 and 24 hpf. Heat maps generated from control (A') and transgenic embryos (B') reveal reduced Pax2a levels in the PPA at 12 hpf following heat-shock. Note that upregulation of Dkk1 caused an increase in facial placode size with a concurrent reduction in the size of the otic vesicle. **(E)** Mean gray values of Pax2a levels in the otic vesicle at 24 hpf revealed a 2.6 fold reduction in the Dkk1-induced embryos (Student's *t*-test, ***p<<0.001). **(F)** Control and Tg*(hsp70:dkk1-GFP)*^{w32} embryos were heat-shocked at 10 hpf, collected at 24 hpf and analyzed for Pax2a+ cell number in the otic vesicle and EB placodes. This analysis revealed a 48% increase in the number of cells that segregate to the facial placode (Student's t-test, ***p<0.001), with a concomitant 47% reduction in the number of cells in the otic placode (Student's *t*-test ***p<0.001). There was no significant difference in the number of cells in the glossopharyngeal/vagal placode in these experiments. Scale bar = 50 μm.

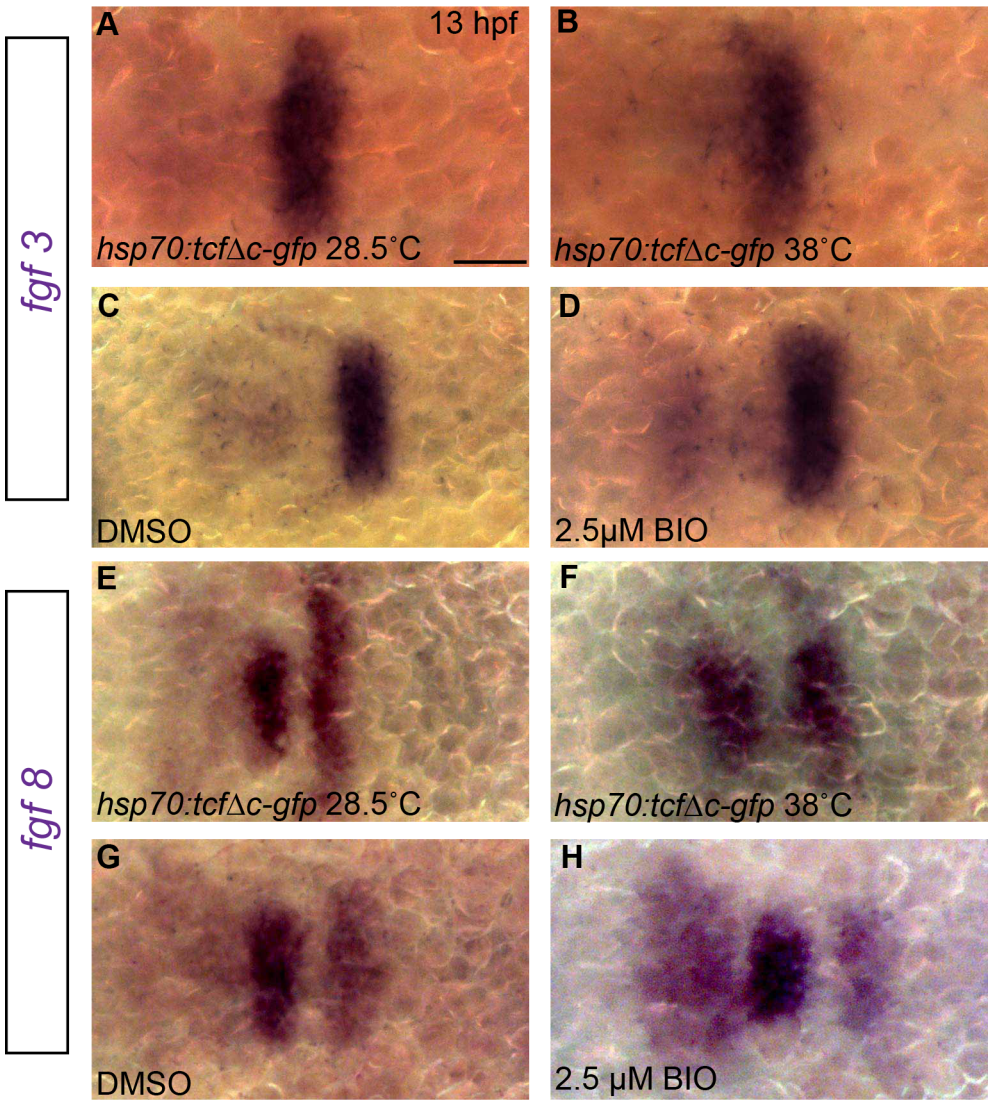

Figure 32: Modulation of Wnt signaling at early somitogenesis does not affect expression of *fgf3* and *fgf8* in the hindbrain.
fgf3 and *fgf8* expression were assayed by in-situ hybridization at 13 hpf after modulating Wnt signaling at 10 hpf. **(A-H)** Neither *fgf3* nor fgf8 expression is grossly altered when Wnt signaling is blocked by induction of Tg(*hsp70:tcf*Δ*C-EGFP)* transgene or overactivated by BIO treatment, compared to uninduced Tg(*hsp70:tcf*Δ*C-EGFP)* embryos or DMSO treated controls. Scale bar = 50 μm.

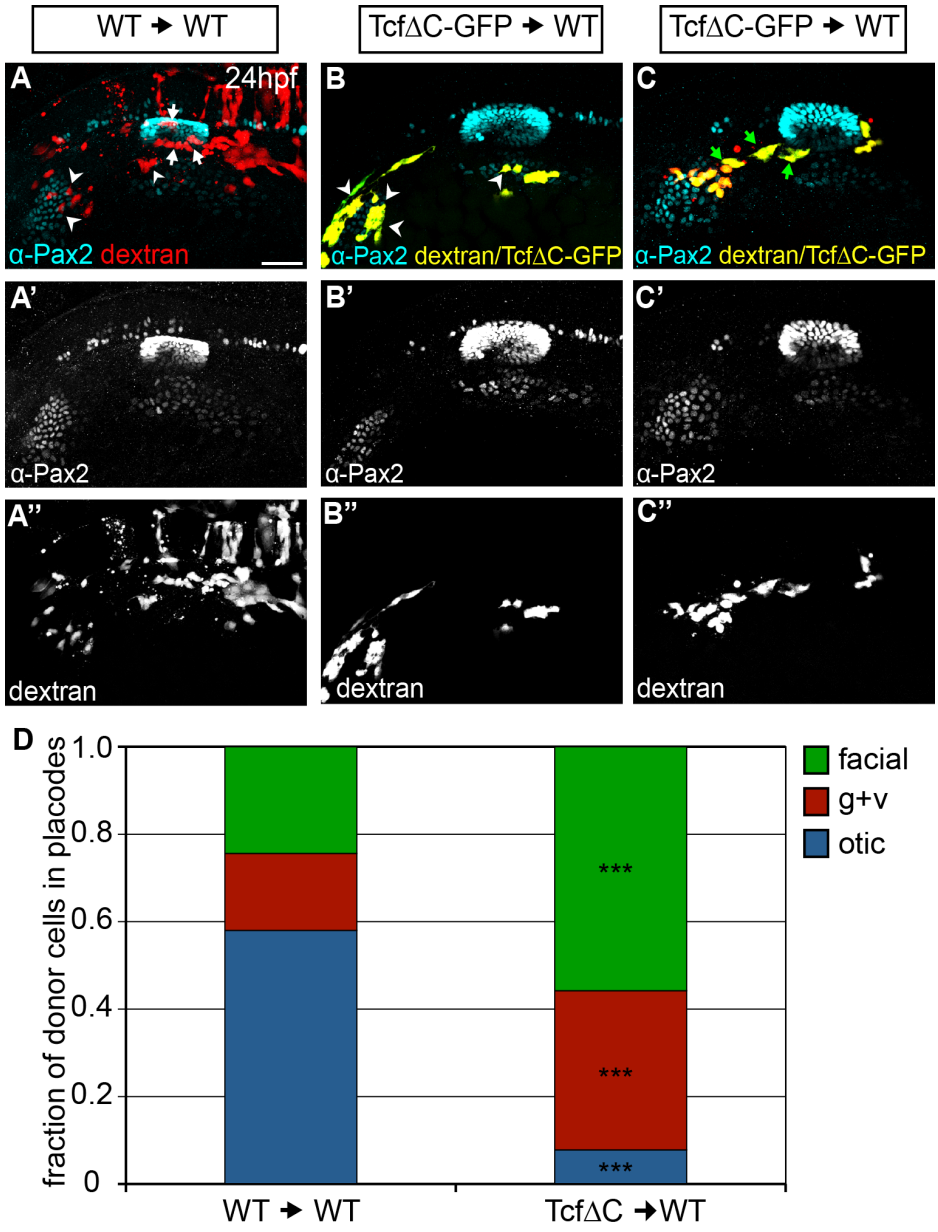

Figure 33: Wnt activation is required cell-autonomously for otic commitment.

(A-C) Wildtype hosts containing rhodamine-dextran positive cells from wildtype (red, A) or Tg(*hsp70:tcfΔC-EGFP)* (yellow, B,C) donors were heat-shocked at 10 hpf and immunolabeled for Pax2a (cyan) at 24 hpf. Cells derived from Tg(*hsp70:tcfΔC-EGFP)* donors appear yellow due to colocalization of EGFP and rhodamine-dextran. Arrowheads indicate donor cells in EB placodes; white arrows mark donor cells in the otic vesicle, green arrows mark donor cells in presumptive gAll/gVIII. **(D)** Relative contributions of donor cells to otic vesicle and EB placodes at 24 hpf in wildtype and Tg(*hsp70:tcfΔC-EGFP)* transplants. Tg(*hsp70:tcfΔC-EGFP)*+ cells are biased towards facial and glossopharyngeal/vagal placodes, rarely segregating to the otic vesicle (total of 77 and 131 donor cells counted from 11 Tg(*hsp70:tcfΔC-EGFP)* and 10 wildtype transplants, respectively; χ^2-test; ***p<<0.001). Scale bar=50μm.

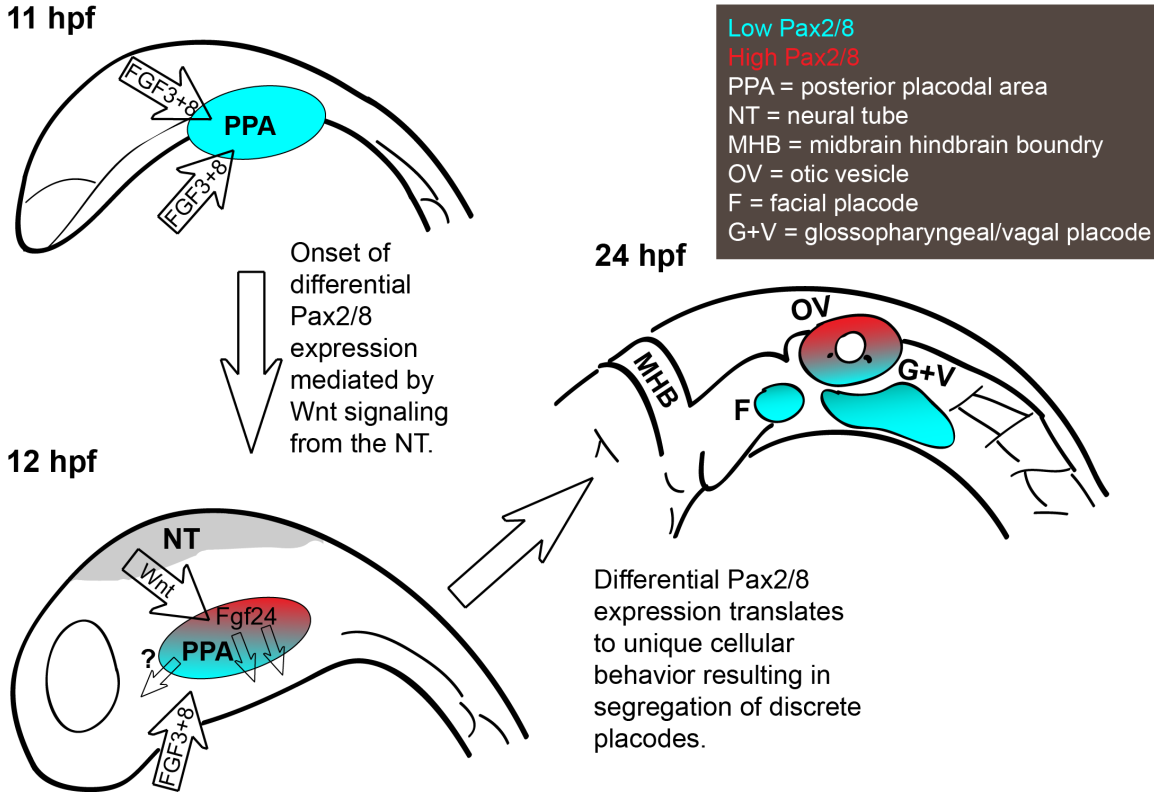

Figure 34: A model for PPA segregation into the otic vesicle and EB placodes.

At the onset of somitogenesis, Fgf signals emanating from the forming hindbrain and cephalic mesoderm induce the posteriormost region of the PPE to express basal levels Pax2a/8. This initial low expression of Pax2a/8 in conjunction with additional signals confers a general otic/EB identity. A subset of cells in the early PPA contribute to the EB placodes while the majority will give rise to the otic vesicle. Shortly after onset of Pax2a/8, Fgf24 expression (a known glossopharyngeal/vagal placode inducer) is seen in the medial aspect of the PPE. Simultaneously, a yet unidentified signal (designated by the '?' and most likely an Fgf ligand) emanates from the anteriormost region of the PPA to induce additional cells of the presumptive facial placode. During this time mesoderm-derived Fgf signals persist, while in the neural tube (NT) Fgf attenuation coupled with increased Wnt results in differential expression of Pax2a/8. At this time, cells of the PPA obtain unique cellular characteristics that are instructive to directional segregation of placodal progenitors in forming discrete placodes.

CHAPTER 4: ROLE OF FGF SIGNALING DURING THE DEVELOPMENT OF THE POSTERIOR PLACODAL AREA

Modified from: McCarroll, M. N. and Nechiporuk, A. V. (2013). Fgf3 and Fgf10a work in concert to promote maturation of the epibranchial placodes in zebrafish. *Plos One* **8**, e85087.

Author Contributions

Conceived and designed the experiments: AVN MNM. Performed the experiments: MNM. Analyzed the data: AVN MNM. Contributed reagents/materials/analysis tools: AVN MNM. Wrote the manuscript: AVN MNM.

4.1 Abstract

Essential cellular components of the paired sensory organs of the vertebrate head are derived from transient thickenings of embryonic ectoderm known as cranial placodes. The epibranchial (EB) placodes give rise to sensory neurons of the EB ganglia that are responsible for relaying visceral sensations form the periphery to the central nervous system. Development of EB placodes and subsequent formation of EB ganglia is a multistep process regulated by various extrinsic factors, including fibroblast growth factors (Fgfs). We discovered that two Fgf ligands, Fgf3 and Fgf10a, cooperate to promote EB placode development. Whereas EB placodes are induced in the absence of Fgf3 and Fgf10a, they fail to express placode specific markers Pax2a and Sox3. Expression analysis and mosaic rescue experiments demonstrate that Fgf3 signal is derived from the endoderm, whereas Fgf10a is emitted from the lateral line system and the otic placode. Further analyses revealed that Fgf3 and Fgf10a activities are not required for cell proliferation or survival, but are required for placodal cells to undergo neurogenesis. Based on these data, we conclude that a combined loss of these Fgf factors results in a failure of the EB placode precursors to initiate a transcriptional program needed for maturation and subsequent neurogenesis. These findings highlight the importance and complexity of reiterated Fgf signaling during cranial placode formation and subsequent sensory organ development.

4.2 Introduction

In the developing vertebrate head, essential cellular components of the paired sensory organs originate from anatomically distinct structures consisting of neurogenic epithelium called cranial placodes. Cranial placodes are morphologically defined as transient ectodermal thickenings, with columnar or pseudostratified epithelial cell morphology. Through physical interactions with neighboring tissues (i.e. neural crest, mesoderm and endoderm) and in response to extrinsic signals, cells of the cranial placodes delaminate and/or invaginate to form structures as diverse as the optic lens, the otic vesicle, and neurons of the cranial ganglia. Epibranchial (EB) placodes (comprised of the facial, glossopharyngeal, and vagal) give rise to sensory neurons of the EB ganglia. EB neurons act as a relay for information from the sensory organs (e.g. taste buds of the gustatory system, baroreceptors of the heart, and sensory enteric nerves of the gut) to the CNS (D'Amico-Martel and Noden, 1983; Schlosser and Northcutt, 2000).

Several lines of evidence from multiple vertebrate species indicate that placode development is a multi-phase process (Streit, 2004b). At the end of gastrulation, all cranial placode precursors reside in a horseshoe-shaped domain known as the pan-placodal ectoderm (Ahrens and Schlosser, 2005; Brugmann et al., 2004a; Litsiou et al., 2005; Schlosser, 2005). Shortly thereafter, regional cell fate specification begins. The most posterior portion of the pan-placodal ectoderm, the posterior placodal area (PPA), will undergo different stages of specification, induction and morphological changes to ultimately give rise to the

otic and EB placodes (Freter et al., 2008b; Ladher et al., 2010; Ohyama and Groves, 2004a). In aquatic vertebrates the PPA will also give rise to the lateral line system (Hans et al., 2013; McCarroll et al., 2012).

Recent studies have illustrated an important interaction between the developing cranial placodes and the cranial neural crest at multiple stages of EB placode development. These two tissues interact to orchestrate cellular movements by providing both guidance cues and contact inhibition of locomotion, recently described as a chase-and-run behavior where the NC will chase early placode precursor cells which in turn run from the NC, resulting in proper segregation of the cranial placodes (Theveneau et al., 2013). Once EB placodes form, the cranial neural crest is necessary for appropriate condensation of the cranial ganglia. In zebrafish, genetic ablation of the neural crest results in disorganization and reduction of the placode-derived cranial ganglia (Culbertson et al., 2011). A recent study in both chick and mouse has identified a neural crest derived structural corridor that is necessary for the migrating placodal neuroblasts to reach their final destination and form properly positioned ganglia (Freter et al., 2013). Altogether, these studies provide strong evidence for the importance of interactions between placode and neural crest populations to achieve correct migration and patterning of the cranial placodes and subsequent ganglia.

Multiple transcription factors expressed during various stages play distinct roles in cranial placode development. Foxi1 is a winged helix transcription factor that is important for development of the otic and EB placodes; this factor is

thought to impart placodal competence to the ectoderm (Hans et al., 2004a; Hans et al., 2007; Lee et al., 2003; Nechiporuk et al., 2006). While Foxi1 is a broadly expressed competence factor, another PPA factor, Sox3 is more specifically expressed in the otic anlage and is among the first known factor to be detected in the EB placode precursors. Sox3 expression is also maintained in the mature EB placodes (Nikaido et al., 2007a; Padanad and Riley, 2011). Pax2a is similarly expressed in the otic anlage, and later in maturing EB placodes (McCarroll et al., 2012). Finally cells of the fully mature EB placodal ectoderm express basic helix-loop-helix factor Neurogenin1 (Neurog1), which is required for neurogenesis (Andermann et al., 2002; Nechiporuk et al., 2006). Neurog1 is transiently upregulated in placodal cells as well as delaminating neuroblasts. Once migrating neuroblasts condense into EB ganglia, they begin to express another neurogenic factor, paired-like homeobox 2b (Phox2b) that marks differentiated EB neurons (Dauger et al., 2003; Nechiporuk et al., 2005).

Signaling through fibroblast growth factors (Fgfs) are essential during multiple stages of placode progression from the early homogeneous precursor stage to formation of discrete placodes and subsequent neurogenesis (Ladher et al., 2010; Nechiporuk et al., 2005). In zebrafish, mesoderm-derived expression of Fgf3 and Fgf8 are required for the specification of the early PPA, as a combined loss of these factors results in an abnormal distribution of *foxi1* and absence of the otic and EB placodes (Léger and Brand, 2002; Maroon et al., 2002; Maroon et al., 2002; Nechiporuk et al., 2006; Phillips et al., 2001). At later stages, endoderm-derived Fgf3 is required again for neurogenesis of the

glossopharyngeal and three small vagal ganglia, but the facial and large vagal ganglia appear unaffected in *fgf3* deficient embryos (Nechiporuk et al., 2005). Interestingly the EB ganglia develop at the dorsal aspect of the branchial arches, and Fgf3 is also important for the proper development of the endodermal pouches (Nechiporuk et al., 2005; Crump et al., 2004). These pouches are populated with chondrogenic NC cells that give rise to mature branchial arches. In *fgf3* mutants, NC derived chondrogenic precursors migrate to their destination, however they are not properly maintained, do not undergo a chondrogenic program and will eventually undergo cell death (Crump et al., 2004). These studies illustrate the complexity of tissue interactions and convergent signaling pathways involved during placode development and subsequent neurogenesis. However, after the initial specification of the PPA precursors, it is currently unknown what specific signals are needed for the proper development of the EB placodes.

Our data involving either disruption or over-activation of Fgf signaling provide strong evidence that an Fgf is required for EB placode maturation (McCarroll et al., 2012; Nechiporuk et al., 2006). When Fgf receptor signaling is globally inactivated between 12 and 22 hpf EB placode markers are lost or severely disrupted, while other placode-derived structures (like the otic vesicle) remain relatively intact. Close analysis of Fgf ligand expression revealed that two candidates, Fgf3 and Fgf10a, were temporally and spatially positioned for proper maturation and subsequent neurogenesis of the EB placodes. We find that injection of *fgf10a*-MO (morpholino) into *fgf3*$^{-/-}$ mutant embryos resulted in loss of

the facial placode, a nearly complete loss of the glossopharyngeal and vagal placodes at 24 hpf, and an absence of the respective ganglia at 72 hpf. We also find that Fgf3/10a deficient embryos exhibit a loss of anterior otic identity and a stalling of the anterior lateral line. Furthermore, we have identified the endoderm and the lateral line systems as the tissue sources of Fgf3 and Fgf10a, respectively, during this critical period. We determine that these factors do not control placode cell morphology, and only partially disrupt the placode neural crest interaction, but are required for EB placode precursors to express Pax2a and Sox3 necessary for cellular entry into a neurogenic program.

4.3 Results

4.3.1 Local Fgf activity is sufficient to expand the facial placode

We have previously demonstrated that Fgf activity is required for EB placode development during the second half of segmentation (McCarroll et al., 2012; Nechiporuk et al., 2006). Fgf target genes, *pea3* and *erm,* are expressed in the placodal ectoderm at 13 hpf (Nechiporuk et al., 2005) and *pea3* has also been detected at 24 hpf (Nechiporuk et al., 2005). Loss of Fgf signaling between 12 and 22 hpf abrogates EB placode development, without affecting gross morphology of the otic vesicle (Nechiporuk et al., 2006). In addition, global activation of Fgf signaling after 12 hpf can expand the EB placode domain (McCarroll et al., 2012). In this study, we asked whether local activation of Fgf

signaling is sufficient to enlarge the EB placodes. To accomplish this we unilaterally inserted recombinant Fgf8- or BSA- (control) soaked heparin beads into 12 hpf embryos near the site of early EB precursors. Embryos were assayed for placodes at 24 hpf using the anti-Pax2a antibody. Instances with Fgf8 beads near the site of the facial placode showed a significant increase in the number of Pax2a+ cells (Figure 35A, B, F) compared to contralateral control side (Figure 35C, F), whereas BSA beads showed no change in placodal cell numbers (Figure 35D-F). These data indicate that the EB placodes display active Fgf signaling and that local activation of Fgf signaling after 12 hpf is sufficient to significantly expand the EB placodes.

4.3.2 Fgf3 and Fgf10a are expressed during epibranchial placode formation

Our data indicate that Fgf signaling between 12 and 22 hpf is necessary and sufficient for EB placode development (McCarroll et al., 2012; Nechiporuk et al., 2006), however the actual Fgf ligand(s) responsible for this activity are unknown. To determine the specific Fgfs involved in EB placode development, we searched for Fgf ligands expressed in the proximity of developing EB placodes between 12 and 22 hpf. As demonstrated previously by our lab and others, *fgf3* is expressed in the mesoderm at 14 hpf, and then in the endoderm at later times (Figure 36A-C and (Crump et al., 2004; Nechiporuk et al., 2005). Another Fgf ligand, *fgf10a*, was expressed in the anterior portion of the developing otic vesicle, the anterior lateral line, and the posterior lateral line

during these time-periods (Figure 36D-F). Thus, both Fgf3 and Fgf10a are expressed in the proximity of developing EB placodes during the critical time window, suggesting their requirement for the development of the EB placodes (McCarroll et al., 2012; Nechiporuk et al., 2006).

4.3.3 Fgf3 and Fgf10a are required for maturation of epibranchial placodes and development of the epibranchial ganglia

Expression profiles of Fgf3 and Fgf10a indicated that these ligands could be involved in EB placode development. To test this, we injected the previously characterized *fgf10a*-MO (Nechiporuk and Raible, 2008), into embryos derived from heterozygous *fgf3+/-* crosses. At 24 hpf, we observed a slight reduction of Pax2a expression in the EB placodes of *fgf3-/-* mutants (Figure 37C, G). *fgf10a* morphants showed a partial loss of Pax2a+ cells, albeit more severe than *fgf3-/-* mutants (Figure 37D, G). In contrast, combined inactivation of Fgf3 and Fgf10a resulted in a complete loss Pax2a expression in the facial placode, and a near complete loss of Pax2a expression in the glossopharyngeal/vagal placode at 24 hpf (Figure 37F, G). In addition to Pax2a, we also observed a loss of *sox3* expression in Fgf3+10a deficient embryos at 24 hpf (Figure 38C, D). Importantly, combined loss of Fgf3+10a did not affect the *foxi1*+ expression domain (marks EB placode precursors; Figure 38A, B), indicating that the requirement for Fgf3 and Fgf10a was distinct from an earlier role of Fgf3+8b during EB placode specification.

To confirm that this phenotype is not due to developmental delay, we assayed the EB ganglia at 3 days post fertilization (dpf) using expression of TgBAC*(phox2b:EGFP)* (Nechiporuk et al., 2006). As reported previously, *fgf3-/-* mutants displayed a loss of the glossopharyngeal and three small vagal ganglia, however the facial and large vagal ganglia still formed (Figure 37J and (Nechiporuk et al., 2005)). We observed a complete or almost complete loss (occasionally we observed a few cells in the large vagal ganglion) of the EB ganglia in *fgf3-/-* embryos injected with *fgf10a*-MO (Figure 37M). These data reveal that Fgf3 and Fgf10a cooperate during development of the EB placodes; however their combined activity was not required for the development of EB placode precursors and gross development of the otic vesicle.

A previous study showed that Fgf signaling was required for anterior identity (marked by expression of *pax5*) of the otic vesicle (Hammond and Whitfield, 2011). Fgf3 was identified as a ligand in part responsible for regionalizing the otic vesicle, however only a partial loss of *pax5* mRNA was observed. Embryos treated with SU5402 showed a complete loss of anterior otic markers, indicating that an additional Fgf also acts with Fgf3 to impart anterior otic identity. We asked whether Fgf10a was another ligand responsible for assigning anterior otic identity. We found that combined inhibition of Fgf3 and Fgf10a resulted in a complete loss of *pax5* expression in the otic vesicle at 25 hpf (Figure 38E-H). While Fgf3 and Fgf10a in combination are not important for early otic placode specification or induction, we conclude that these ligands do play a role later to specify otic axial asymmetry.

4.3.4 Fgf10a and endodermally derived Fgf3 cooperate during EB placode formation.

As demonstrated previously, *fgf3* and *fgf10a* expression analyses revealed that Fgf3 is expressed in the endoderm and Fgf10a is expressed in the anterior portion of the otic vesicle, anterior lateral line, and posterior lateral line (Figure 36) (Nechiporuk and Raible, 2008; Nechiporuk et al., 2005). As reported previously (Nechiporuk et al., 2005), genetic ablation of the endoderm using MO against *casanova*, resulted only in a small reduction of the EB placodes as assayed by Pax2a immunostaining at 24hpf (Figure 39A, B). Consistent with these observations, *cas* morphants lacked expression of TgBAC*(phox2b:EGFP)* in the glossopharyngeal and small vagal ganglia, a phenotype very similar to the one observed in the *fgf3-/-* mutant (Figure 39D, E). However, co-injection of MOs against *cas* and *fgf10a* resulted in a near complete loss of the EB placodes (Figure 39C), phenocopying the *fgf3/10a* mutant/morphants. Moreover, we observed a complete loss of the EB ganglia (Figure 39F) in the *cas/fgf10a* double morphants, identical to that observed in the *fgf3/10a* mutant/morphant embryos (Figure 37L). We conclude that endodermally derived Fgf3 in cooperation with Fgf10a is responsible for EB placode maturation.

4.3.5 The anterior lateral line is the tissue source responsible for facial placode development.

We next addressed the tissue source of Fgf10a. Our analysis indicated this factor was expressed in the anterior otic vesicle, anterior lateral line and

posterior lateral line (Figure 36). For this study we specifically focused on Fgf10a's expression in the anterior lateral line during EB placode formation, due to the availability of transgenics that label anterior lateral line precursors. The anterior lateral line originates from the anterior portion of the PPA marked by Pax2a expression at 12 hpf (Hans et al., 2013; McCarroll et al., 2012). The anterior lateral line anlagen can be visualized by Tg(*pax2a:GFP*) which has an expression pattern similar to that of endogenous Pax2a between 12 and 14 hpf (Figure 40A inset and McCarroll et al., 2012). By 18 hpf, the anterior lateral line down regulates Pax2a, however the Tg(*pax2a:GFP*) maintains EGFP expression in this structure. The anterior lateral line is in close proximity to the condensing facial placode, which begins to express Pax2a at 14 hpf (Figure 40B). Notably, Tg(*pax2a:GFP*) is not expressed in EB placodes likely due to a lack of necessary enhancers (Figure 40D and McCarroll et al., 2012). The anterior lateral line maintains this close association to the facial placode as it matures and condenses between 14 and 24 hpf (Figure 40C, D).

Given the close association of the facial placode with the anterior PPA, we examined the role of the anterior PPA cells in facial placode development. Fate mapping analysis using a TG(*pax2a:Kaede),* in which the anterior portion of the Pax2a+ domain was photoconverted at 12 hpf (photoconverted, red fluorescent Kaede protein is stable for several days), revealed that this domain did not significantly contribute to the facial placode (Figure 40E, F). However, our previous study clearly demonstrated the anterior PPA was required for proper development of the facial placode, because ablation of these cells greatly

reduced the facial placode (McCarroll et al., 2012). Notably, anterior lateral line cells were still present in Fgf3+10a deficient embryos, albeit anterior lateral line neuromasts were not properly patterned in these embryos (Figure 40G,H). These results argue that the anterior lateral line precursors supply a signal necessary for the development of the facial placode.

Our previous fate mapping study showed that the anterior PPA cells contribute to both the anterior lateral line and anterior portion of the otic vesicle (McCarroll et al., 2012). Thus, we asked which of these structures is the source of the signal required for facial placode development. To accomplish this, we transplanted wild type cells into the presumptive placodal domain of Fgf3+10a morphants and assayed the resulting mosaic embryos for Pax2a expression at 24 hpf. We observed a partial rescue in embryos that contained wild type cells medial to the developing facial placode, a presumptive anterior lateral line domain (Figure 40I-L; Wilcoxon matched-pairs signed rank test: **P<0.01; n=8 embryos). The majority of our mosaic experiments contained wild-type cells in both anterior lateral line and the anterior otic vesicle. We did obtain a single embryo that only contained wild-type cells in the anterior portion of the otic vesicle; in that instance, we did not observe rescue of the facial placode. Overall, we did observe a minor increase in Pax2a+ cells in the glossopharyngeal and vagal placodes in our mosaic embryos (Figure 40L). Conversely, a case of wild-type cells in the presumptive anterior lateral line and not the otic vesicle resulted in a partial rescue of the facial placode. Taken together with our lineage, ablation,

and Fgf10a expression data, these data argue for a primary role of anterior lateral line derived Fgf10a during facial placode development.

4.3.6 Fgf3 and Fgf10a are required for placode maturation and neurogenesis.

We reasoned that Fgf3+10a activity could be required for one or more of the following steps during EB placode development: 1) placode induction, 2) placode NC interaction required for proper organization of the placodes and subsequent formation of ganglia, and/or 3) placode maturation and neurogenesis. To test the placode induction requirement, we assayed whether Fgf3+10a-deficient embryos displayed thickened ectoderm, a hallmark of placode morphology (Bancroft and Bellairs, 1977). TgBAC(*foxi1:d2EGFP)* positive embryos injected with *fgf3+10a*-MOs and uninjected controls were collected at 26 hpf, counterstained with anti-beta-Catenin antibody to visualize cell membranes and then transversely sectioned to reveal epithelial morphology. We observed no difference in the extent of EB *foxi1-EGFP* expression or in the height of ectodermal cells marked by transgene expression between wild type and *fgf3+10a* deficient embryos (Figure 41A-C). Moreover, neither proliferation nor cell death in EB placode precursors were affected by combined loss of Fgf3 and Fgf10a (Figure 41D, E). From these experiments, we conclude that Fgf3 and Fgf10a do not control changes in placode cell morphology and are not required for the EB placode induction.

Next, we asked if Fgf3 and Fgf10a control development of the chondrogenic neural crest that is required for the proper organization of the EB ganglia (Culbertson et al., 2011). To accomplish this, we visualized placode precursors and neural crest derived structures using TgBAC(*foxi1:d2EGFP)* and *Tg*(*sox10*(*7.2*)*:mrfp*) in *fgf3+10a* morphants and control embryos at 26 hpf. We observed a disruption of the posterior neural crest stream that populated branchial arches (arrow heads; Figure 41F, G). This is not surprising, as endoderm secreted *fgf3* is required for pharyngeal arch formation (Crump et al., 2004). However, the second neural crest stream and the posterior most aspect of the third stream were still present in *fgf3+10a*-deficient embryos. Despite their presence, the EB ganglia that develop in close association with these neural crest streams failed to form in *fgf3+10a*-deficient embryos. This observation indicates that Fgf3 and Fgf10a are unlikely to exert their effect through the disruption of chondrogenic neural crest. This is consistent with our previous study demonstrating that disruption of chondrogenic neural crest in zebrafish did not affect formation or neurogenesis of EB placodes, but instead disrupted condensation of the EB ganglia (Culbertson et al., 2011).

Lastly, we asked if the loss of Fgf3 and Fgf10a inhibits neurogenesis of the EB placodes. To accomplish this we injected *fgf10a*-MO into embryos derived from *fgf3+/-* parents that also carried TgBAC(*neurog1:DSRed)*, an early marker of EB placode neurogenesis (Andermann et al., 2002; Nechiporuk et al., 2006). Embryos were collected at 36 hpf and immunolabled for Pax2a to visualize placodes. In wildtypes, Pax2a+ cells of the EB placodes were arranged in linear

fashion (Figure 42A; dashed lines). At the dorsal most aspect of these Pax2a+ corridors, we observed *neurog1:DSRed*+ cells (Figure 42A, B), likely marking delaminating neuroblasts at the medial most aspect of placodes. This is consistent with our previous observations (Culbertson et al., 2011) using live analysis of TgBAC(*neuord:EGFP*), demonstrating similar arrangement of neuroblasts in EB placodes. In *fgf3-/-* mutants, we observe a loss of the Pax2a+ corridors for the prospective glossopharyngeal and 3 small vagal ganglia concurrent with a loss of neurogenesis (Figure 42C; bracket), however, the facial and large vagal placodes were present and undergoing neurogenesis (Figure 42C; arrowheads). Interestingly in embryos injected with *fgf10a*-MO, while the Pax2a+ placode structures were properly assembled, a subset of EB cells underwent ectopic neurogenesis ventral to the posterior most region of the vagal placode (Figure 42D; arrows). In Fgf3+10a deficient embryos, we observed a complete loss of the Pax2a+ placode structures and a near complete loss of neurogenesis in the region of the nascent EB ganglia, except for a small group of cells postero-ventral to the otic vesicle (Figure 42F; asterisk). These data demonstrate a combined requirement of Fgf3 and Fgf10a during placode maturation and subsequent neurogenesis.

4.4 Discussion

Our studies highlight the importance of reiterated Fgf signaling to promote specific transcriptional programs necessary during multiple stages of EB placode development. Previous work in zebrafish and other species has shown that Fgf

signaling is required to specify the early posterior placodal precursors (Figure 43). After EB placode formation, Fgf3 is required again to initiate neurogenesis of a subset of the EB placodes. However previous studies did not examine other Fgf ligands or a combinatorial requirement of various Fgf ligands during placode maturation and neurogenesis. In this study, we show that Fgf3 and Fgf10a work in concert to promote maturation and subsequent neurogenesis of the EB placodes. Our analyses revealed that Fgf3 and Fgf10a do not control placode cell morphology (Figure 41A-C). Instead, these factors affect the maturation of the EB placodes by controlling expression of Pax2a and Sox3 required for development and subsequent neurogenesis of the EB placodes.

4.4.1 Lateral line system is the tissue source of Fgf10a during EB placode formation

Whereas Fgf3 signal is endoderm-derived, as previously reported (Nechiporuk et al., 2005), we provide evidence through tissue ablations and transplantation studies, that the developing anterior lateral line is the source of Fgf10a responsible for formation of the facial placode (Figure 43). Only a partial rescue of the facial placode was observed in mosaic analysis, a reasonable result due to the additional requirement of Fgf3 from the endoderm. We propose that otic and posterior lateral line derived Fgf10a may be similarly required for development of the more posterior, glossopharyngeal and vagal placodes. In support of this role, *fgf10a* transcripts were expressed in the otic placode/vesicle and the posterior lateral line, both of which develop in close proximity to the

posterior EB placodes. We also demonstrated that ablation of the posterior portion of the Pax2a otic domain resulted in a loss of the otic vesicle and a large reduction of the glossopharyngeal/vagal placode (Figure 13B, E, F), supporting the role of the otic placode/vesicle in EB placode development. In addition, our mosaic analysis showed an increase in Pax2a positive cells on the transplanted side relative to the contralateral control side (Figure 40K, L). It may be difficult to completely discriminate whether anterior lateral line expression of Fgf10a is exclusively required for facial placode development, whereas the otic and posterior lateral line foci of Fgf10a are only responsible for the development of glossopharyngeal and vagal placodes. Because both the anterior lateral anlagen and the anterior portion of the otic placode are derived from the same source, rostral part of the PPA (Hans et al., 2013; and Figure 9), a vast majority of our mosaic embryos contained cells in these two regions. Nevertheless, together with our ablation data, mosaic analysis argues for a significant contribution of the lateral line derived Fgf10a in the development of the facial placode.

Of course, we cannot exclude the possibility that other otic expressed Fgf factors, in addition to Fgf10a, may play a role in EB placode development. However, our combined knockdown of Fgf3 and Fgf10a resulted in almost complete loss of Pax2a expression and a complete loss of *sox3* in the EB placodes and supports the argument for a major role of Fgf3 and Fgf10a during EB placode development.

Our finding that the anterior lateral line is the tissue source of Fgf10a required for EB placode development raises an interesting question about the

nature of a functionally equivalent signal in higher vertebrates. The anterior and posterior lateral line system is only present in aquatic vertebrates, however a homologous set of EB ganglia is present in terrestrial vertebrates. It is possible that during the course of evolution, different tissues took over as the primary source of necessary signals for EB placode formation. For example, endoderm is thought to be a primary signaling source for EB placode development and subsequent neurogenesis in chick (Begbie et al., 1999). In mouse, mesoderm derived Fgf3 and Fgf10 are required during early stages of PPA specification (Wright and Mansour, 2003), and again during otic induction, and subsequent inner ear formation (Zelarayan et al., 2007b). However, an additional role for these ligands during later stages of EB placode development and subsequent neurogenesis has not been addressed in the mouse. Future studies in other vertebrates will be necessary to determine if a conserved role exists for Fgf3 and Fgf10 during EB placode maturation.

4.5 Methods

4.5.1 Fish strains, maintenance, and Transgenesis

Breeding and maintenance of zebrafish were performed as described (Westerfield, 2000) and staged in hours post fertilization (hpf) (Kimmel et al., 1995). The following transgenic and mutant lines were used for this study: *AB; Tg(*pax2a:GFP*)^{e1} (Picker et al., 2002); TgBAC(*phox2b:EGFP)*^{w37} (Nechiporuk et al., 2006); *lia*^{t26121} (Herzog, 2004) TgBAC*(foxi1:d2EGFP)*^{nl11};

Tg*(pax2a:Kaede)*^{nl12}; TgBAC*(neurog1:DSRed)*^{nl6} (Drerup and Nechiporuk, 2013); *Tg*(*sox10*(*7.2*):*mrfp*)^{vu234} (Kucenas et al., 2008). Heterozygous *lia*^{t26121} were used to generate homozygous mutant offsprings that were identified by genotyping with the following primers: Fgf3 F: 5'-CCCATGAACTCATCTCGTACC, Fgf3 R: 5'-GCTTCTTGGATCCGAGTTTG.

4.5.2 Whole-mount in-situ hybridization and immunostaining

Whole-mount immunostaining and in-situ hybridization were performed as described (Andermann et al., 2002). The following antibodies and riboprobes were used: α-Pax2a (1:100, Covance); anti beta-Catenin (1:100, The Developmental Studies Hybridoma Bank, Iowa); *fgf3* (Kiefer et al., 1996); *fgf10* (Grandel et al., 2000); *pax5 (Hammond et al., 2003)*; *sox3* (Sun et al., 2007); *eya1* (Sahly et al., 1999); *foxi1* (Lee et al., 2003). Whole-mount fluorescent images were obtained using an Olympus FV1000 confocal microscope. Brightfield images were acquired with an AxioImager Z1 compound microscope and HRc digital camera (Zeiss). Assembly of Z-stack images was performed using ImageJ (Abramoff et al., 2004). Brightness and contrast were adjusted using Photoshop (Adobe).

4.5.3 Morpholino microinjections

Antisense morpholino oligonucleotides (MO) were obtained from GeneTools (Corvalis, OR), diluted to working concentrations in H_2O and injected into TgBAC(*phox2b:EGFP)*^{w37}, TgBAC*(foxi1:d2EGFP)*^{nl11},

TgBAC*(neurog:dsRED)*^{nl6}*, Tg*(*sox10*(*7.2*)*:mrfp*), and *lia*^{t26121} embryos: *fgf3*-MO (5'-CATTGTGGCATGGCGGGATGTCGGC (Maroon et al., 2002); *fgf10*-MO (5'-GCTTTACTCACTGTACGGATCGTCC (Nechiporuk and Raible, 2008); *cas*-MO (5'-GCATCCGGTCGAGATACATGCTGTT (Sakaguchi et al., 2001). Efficacy of *fgf3* and *fgf10*-MO was assessed by fusion of the otoliths at 2 dpf (Herzog, 2004) and loss of pectoral fins at 4 dpf (Norton et al., 2005) respectively.

4.5.4 Tissue Sections

TgBAC*(foxi1:d2EGFP)*^{nl11} embryos were injected with *fgf3* and *fgf10a*-MO were allowed to develop to 24 hpf and then fixed and probed with anti beta-Catenin. Embryos were then processed and cryosectioned as previously described (Culbertson et al., 2011). Sections were counterstained with DAPI and fluorescent images were obtained using an Olympus FV1000 confocal microscope.

4.5.5 Transplantation and bead experiments

Donor *AB embryos were microinjected at the one-cell stage with 10 kD fluorescein (Invitrogen) in 0.2M KCl. Embryos were dechorinated and allowed to develop to sphere and shield stage for donors and wild type hosts, respectively. Twenty to 30 donor cells were transplanted into the presumptive placodal domain of *fgf3/10*-MO injected host embryos (Kozlowski et al., 1997). Mosaic embryos were fixed at 24 hpf and immunostained for Pax2a. Heparin coated (5 mg/ml), polystyrene beads (Polysciences, Philadelphia) were incubated with either 250

μg/ml of recombinant mouse Fgf8 protein (R&D Systems, Minnesota) or 0.5% BSA (Fisher Scientific) in PBS. Following incubation, beads were rinsed in PBS and implanted into 12-14 hpf wild type embryos near the site of presumptive facial placodal precursors. Embryos were fixed at 24 hpf and immunostained for Pax2a.

CHAPTER 4 FIGURES

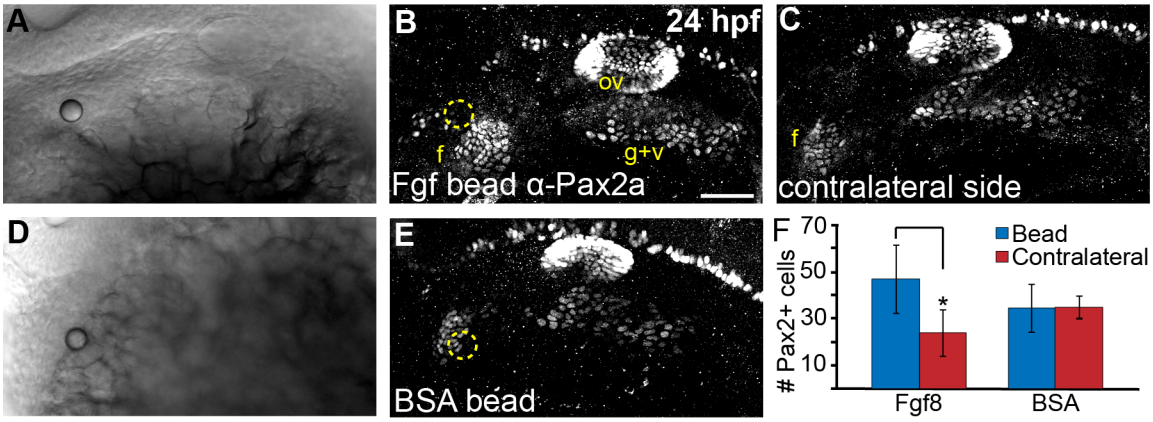

Figure 35: Local Fgf activity is sufficient to expand the facial placode.
(A-E) Twenty-four hour old zebrafish embryos that received heparin beads soaked in either recombinant Fgf8 (A-C) or BSA (D,E) were immunostained for Pax2a expression and imaged using either transmitted light (shows site of bead implantation in A, D) or confocal microscopy (bead is outlined in B, E). Note the expansion of the facial placode (f) near the Fgf8-soaked bead (B) compared to contralateral control of the same embryo (C). **(F)** Quantification of Pax2a+ cells in the facial placode revealed a 2 fold increase in the facial placode in embryos that received an Fgf8 soaked bead compared to the contralateral side (Wilcoxon matched-pairs signed rank test; *P<0.05; error bars: standard error of mean; n=5 embryos/condition).

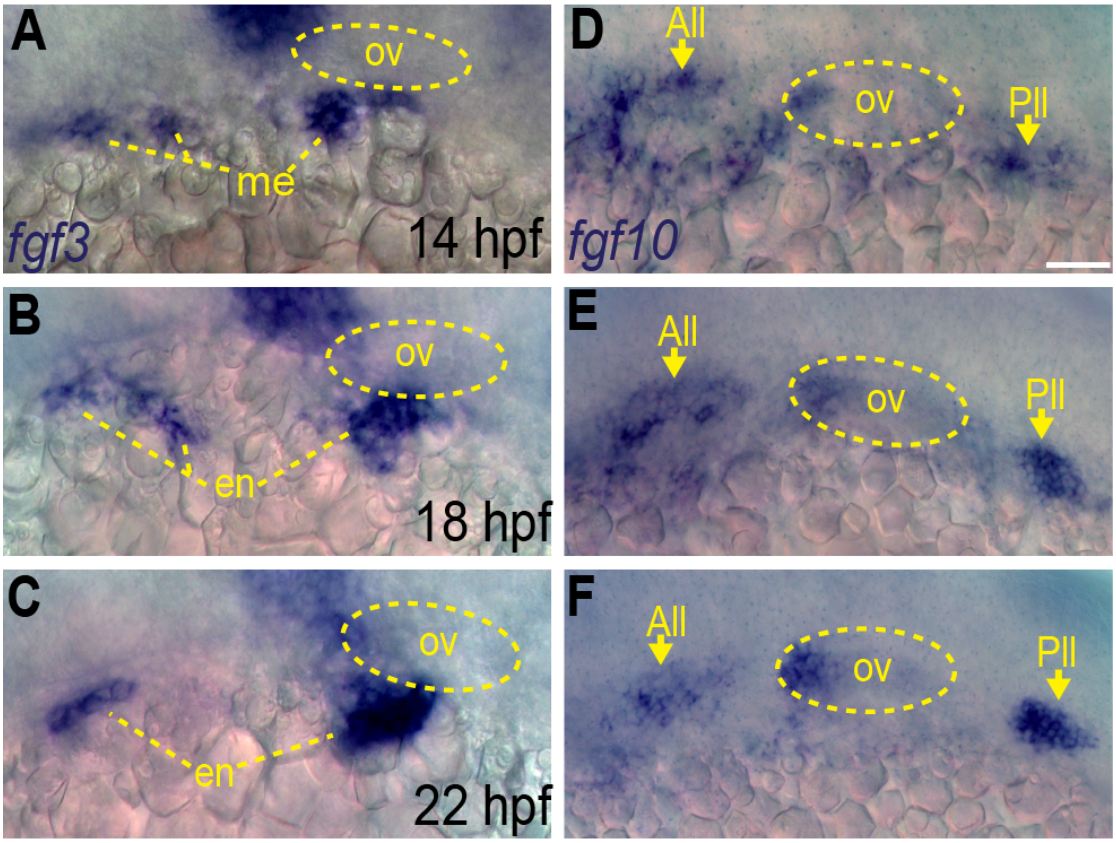

Figure 36: *fgf3* and *fgf10a* are expressed during epibranchial placode formation.
(A-C) In situ hybridization reveals presence of *fgf3* transcript in the mesoderm at 14 hpf (A), and then in the endoderm at 18 (B) and 22 hpf (C). **(D-F)** In situ hybridization reveals presence of *fgf10a* transcript in the anterior and posterior lateral line (arrows) and the anterior portion of the otic vesicle at 14 (D),18 (E) and 22 hpf (F). Otic vesicle is outlined by a dotted line in (A-F). Abbreviations: ov, otic vesicle; me, mesoderm; en, endoderm; AII, anterior lateral line; PII, posterior lateral line. Scale bar: 50 μm.

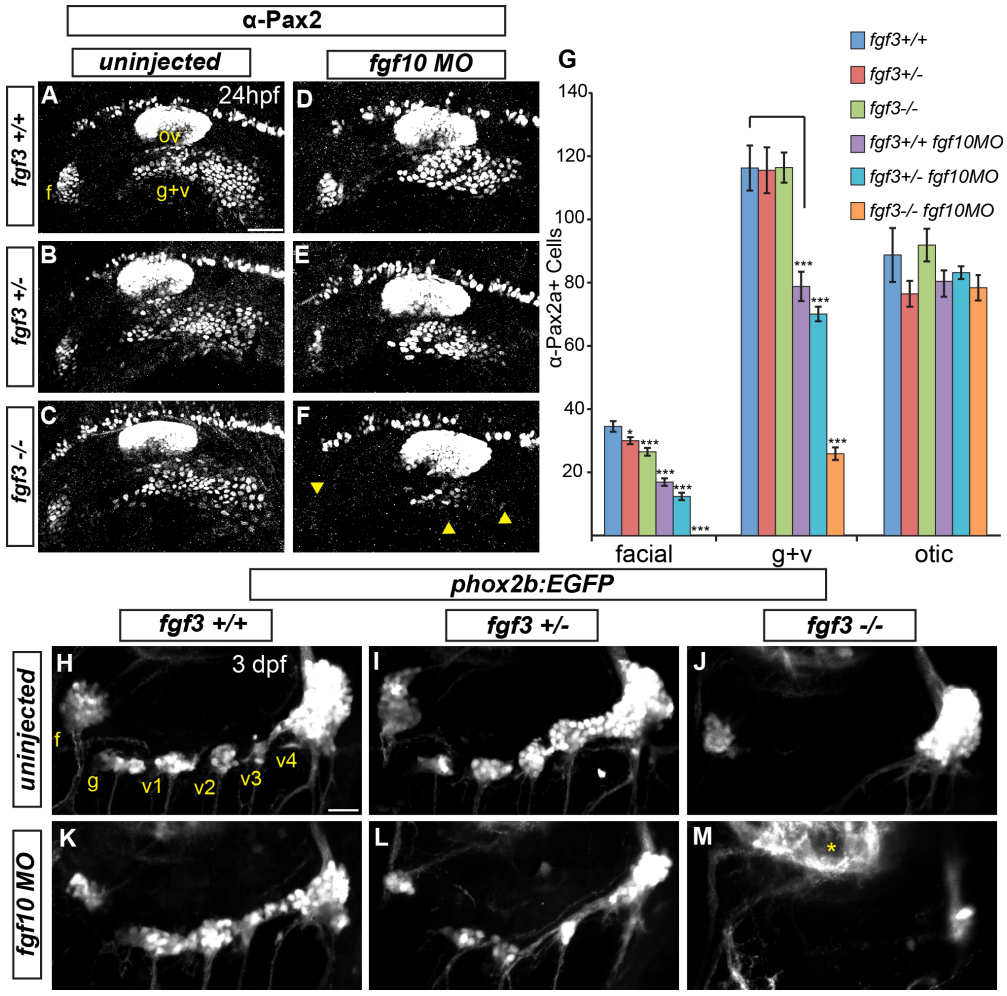

Figure 37: Fgf3 and Fgf10a are required for maturation of epibranchial placodes and development of the epibranchial ganglia.
(A-C) Confocal projections showing Pax2a expression in wild-type (A) *fgf3+/-* (B) and *fgf3-/-* (C) embryos at 24 hpf. **(D-F)** Confocal projections showing Pax2a expression in 24-hour old wild-type (D) *fgf3+/-* (E) and *fgf3-/-* (F) embryos injected with *fgf10a*-MO. Note the significant loss of Pax2a expression in the EB placodes (F; arrowheads). **(G)** Pax2a+ cell number in the facial, glossopharyngeal/vagal, and otic placodes for conditions in (A-F). Note the complete loss of Pax2a+ cells in the facial placode and a 4.5 fold reduction in the glossopharyngeal/vagal placode in *fgf3-/-;fgf10a*-MO embryos (ANOVA multiple comparison with Bonferroni's correction; *P<0.05; ***P<<0.001; Error bars: standard error of mean; n=11 embryos per condition). **(H-M)** Confocal projections of 3 dpf wild-type (H), *fgf3+/-* (I) and *fgf3-/-* (J) embryos and wild-type (K), *fgf3+/-* (L) and *fgf3-/-* (M) embryos injected with *fgf10a*-MO. All embryos contain TgBAC(*phox2b:EGFP*) that marks EB ganglia. Note the loss of EGFP expression in the glossopharyngeal and three small vagal ganglia in *fgf3-/-* embryos (J) and the complete loss of EGFP expression in all EB ganglia in *fgf3-/-*;*fgf10a*-MO with the exception of a few EGFP+ cells in the region of the large vagal ganglion (M). Asterisk marks hindbrain neurons also expressing TgBAC(*phox2b:EGFP*). Abbreviations: f, facial placode (A) or facial ganglia (H); ov, otic vesicle; g+v, glossopharyngeal/vagal placode; g, glossopharyngeal ganglia; v1-v3, small vagal ganglia 1-3; v4, large vagal ganglion. Scale bars: 50 μm (A); 25 μm (H).

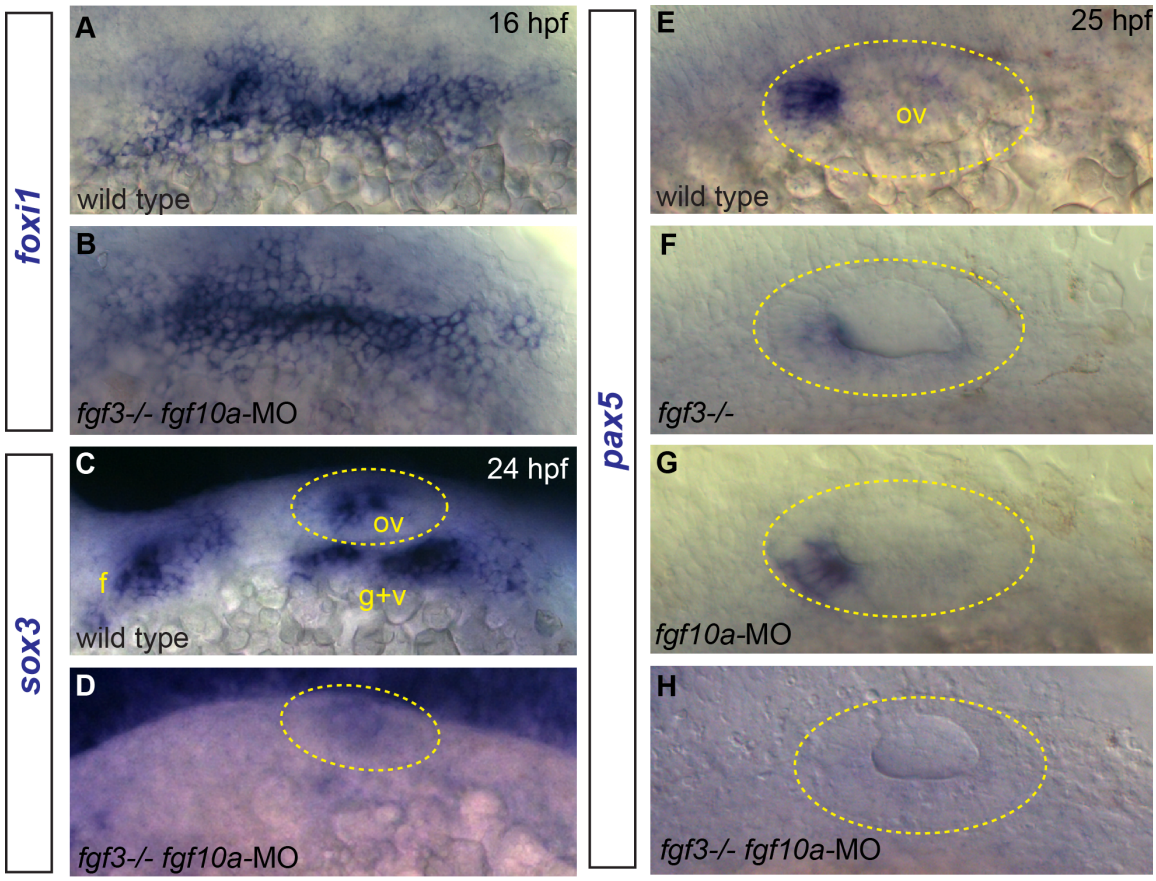

Figure 38: Effects of Fgf3+1-a loss on development of EB and otic placodes.

(A, B) *foxi1* expression detected by in situ hybridization in 16 hpf zebrafish embryos reveals no difference in distribution of EB placode precursors in control (A) and *fgf3-/-;fgf10a*-MO (B) conditions. **(C, D)** *sox3* expression detected by in situ hybridization in 24 hpf zebrafish embryos. Control shows expression of *sox3* transcripts in the otic vesicle (outlined in yellow), and the EB placodes (C); *sox3* expression is lost in these structures in the *fgf3-/-;fgf10a*-MO embryo (D). **(E-H)** *pax5* expression detected by in situ hybridization in 25 hpf embryos. Control conditions show expression of *pax5* in the anterior portion of the otic vesicle (E). Whereas only partial loss of *pax5* was observed in *fgf3-/-* (F) or *fgf10a*-MO (G) embryos, complete loss of *pax5* expression was observed in *fgf3-/-;fgf10a*-MO embryo (H). Abbreviations: f, facial placode; g+v glossopharyngeal/vagal placode; ov, otic vesicle.

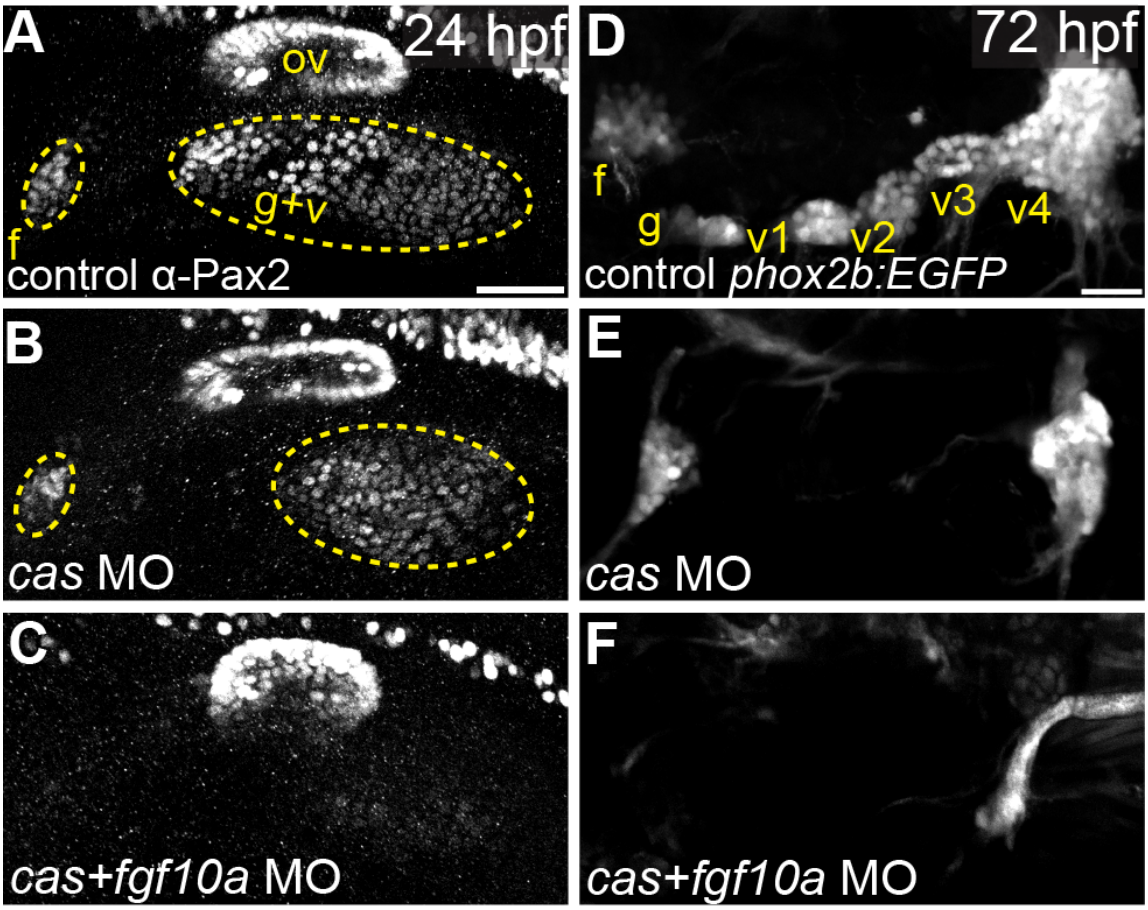

Figure 39: Fgf10a and endodermally derived Fgf3 cooperate during EB placode formation.
(A-C) Confocal projections of Pax2a expression in control (A), *casanova*-MO injected (B), or *casanova/fgf10a*-MO coinjected (C) embryos at 24 hpf. **(D-F)** Confocal projections of 72 hpf TgBAC(*phox2b:EGFP)* in control (D), *casanova*-MO (E), or *casanova/fgf10*-MO (F) embryos. Note a complete loss of Pax2a and EGFP expression in EB placodes and ganglia, respectively, in *casanova/fgf10a-MO* embryos (C and F). Abbreviations: f, facial placode (A) or facial ganglia (D); ov, otic vesicle; g+v, glossopharyngeal/vagal placode; *cas*, *casanova*; g, glossopharyngeal ganglia; v1-v3, small vagal ganglia 1-3; v4, large vagal ganglion. Scale bars: 50 μm (A); 25 μm (D).

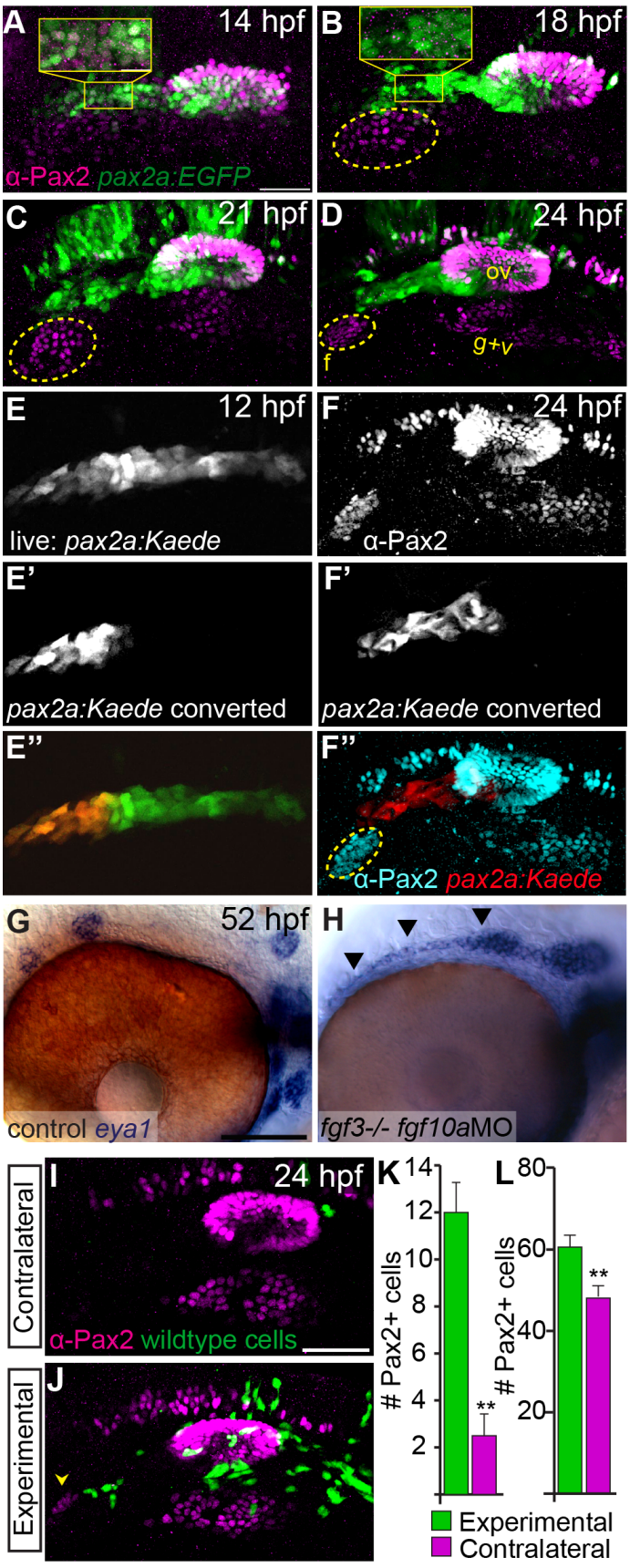
A
14 hpf
α-Pax2 pax2a:EGFP
B
18 hpf
C
21 hpf
D
24 hpf
ov
g+v
f
E
12 hpf
live: pax2a:Kaede
F
24 hpf
α-Pax2
E'
pax2a:Kaede converted
F'
pax2a:Kaede converted
E''
F''
α-Pax2 pax2a:Kaede
G
52 hpf
control eya1
H
fgf3-/- fgf10aMO
Contralateral
I
24 hpf
α-Pax2 wildtype cells
Experimental
J
K
Pax2+ cells
14
12
10
8
6
4
2
**
L
Pax2+ cells
80
60
40
20
**
Experimental
Contralateral

Figure 40: The anterior lateral line is the tissue source of Fgf10a responsible for facial placode development.
(A-D) confocal projections of Tg(*pax2a:EGFP*) zebrafish embryos (green) analyzed for Pax2a expression (magenta) at 14 (A), 18 (B), 21 (C), and 24 hpf (D). The presumptive facial placode is outlined in yellow as it condenses between 18 and 24 hpf. Insets show co-expression of Pax2a and Tg(*pax2a:EGFP*) at 14 hpf (A); by 18 hpf, however, Pax2a expression is absent in anterior lateral line precursors, while Tg(*pax2a:EGFP*) maintains expression in these cells (B). **(E-E'')** Live confocal projection of a 12 hpf Tg(*pax2a:Kaede*) zebrafish embryo (E) with the anterior portion of the *pax2a:Kaede*+ domain photoconverted from green to red emission (E') overlay (E''). **(F-F'')** Composite image of the same photoconverted embryo from (E) at 24 hpf analyzed for Pax2a expression (F) and cyan in (F'') and photoconverted Kaede (F') and red in (F''). Note absence of Kaede positive cells in the facial placode. **(G, H)** In situ hybridization of *eya1* in 52 hpf zebrafish embryos reveals proper neuromast deposition in control (G) and a failure of deposition and elongation of the anterior lateral line in *fgf3-/-;fgf10*-MO embryo (H; arrowheads). **(I, J)** Lateral views of the 24 hpf *fgf3+10* morphant embryo showing the side that received wild-type donor cells (green) as well as the contralateral control side that did not receive donor cells. Pax2a expression is visualized by immunolabeling (magenta). Note partial rescue of the facial placode when wild-type donor cells were present in the presumptive anterior lateral line (J; arrowhead). **(K, L)** Quantification of Pax2a+ cells reveals a significant increase in the number of Pax2a+ cells in the facial (**K**) and glossopharyngeal and vagal placodes (**L**) of the transplanted sides versus contralateral sides (Wilcoxon matched-pairs signed rank test: **P<0.01; error bars: standard error of mean; n=8 embryos). Abbreviations: f, facial placode; g+v glossopharyngeal/vagal placode; ov, otic vesicle. Scale bars: 50 μm (A, I); 25 μm (G).

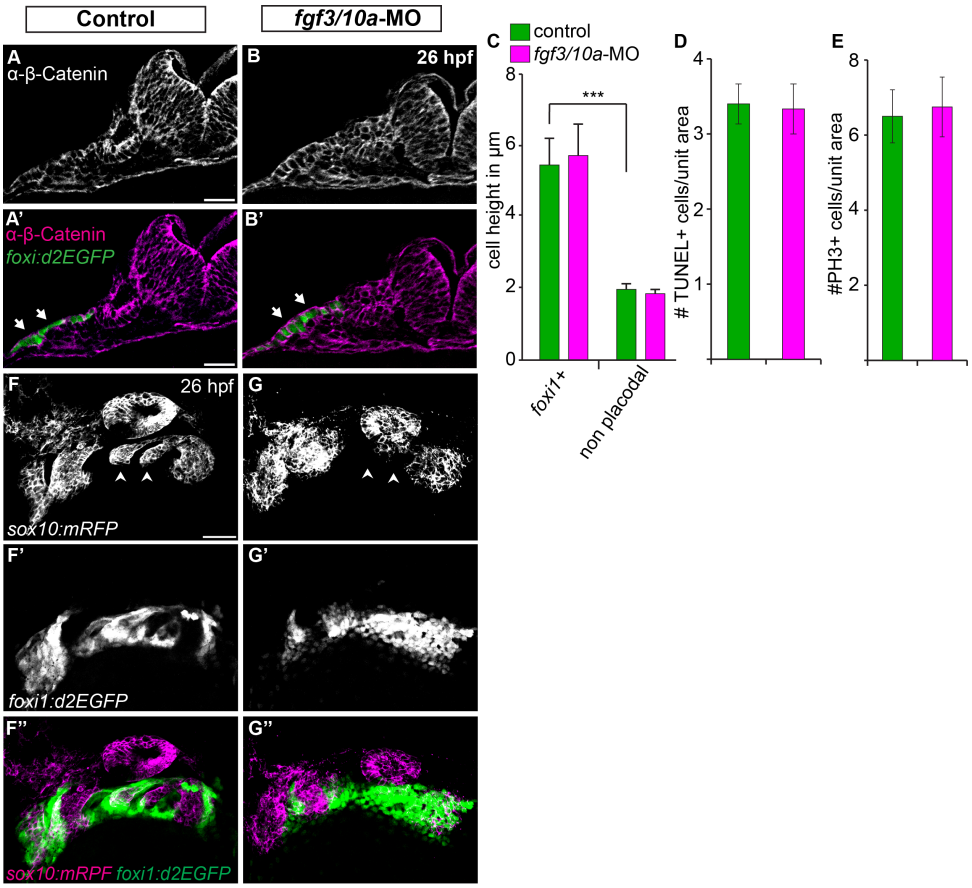

Figure 41: Fgf3 and Fgf10a are not required during EB placode induction, proliferation, and survival, but they are required for the EB placode and NC interaction.

(A, B) Confocal projections of TgBAC(*foxi1:d2EGFP*) (green) 26 hpf zebrafish embryos immunostained for β-Catenin (magenta). Images show unilateral transverse sections at the level of the glossopharyngeal/vagal placode (arrows). Note columnar morphology of the epithelial cells lateral to the otic vesicle in control (A) and *fgf3+10a*-MO embryos (B). **(C)** Average cell height of *foxi1:d2EGFP*+ cells measured in µm was unchanged in fgf3/10a-MO injected embryos compared to controls, measurement non-placodal cells medial to the *foxi1*+ cells are significantly shorter (Error bars: standard error of mean. ANOVA multiple comparison with Sidak's correction; ***P<<0.001; n≥25 cells from 5 individual embryos per condition). **(D, E)** Comparison of TUNEL+ cells or PH3+ cells per unit area of the prospective EB placodes between control and *fgf3+10a*-MO injected 18 hpf embryos reveals no change in cell death or proliferation at this stage (n≥8 embryos per condition). **(F, G)** Confocal projections of 26hpf embryos derived from crossing *Tg*(*sox10*(*7.2*)*:mrfp*) to TgBAC(*foxi1:d2EGFP*) parents. Control conditions show properly formed branchial arches (F; arrowheads), and mature placodes assembling within corridor like structures (F', F''). In *fgf3+10a*-MO embryo, a subset of branchial arches is absent (G; arrowheads); however the anterior and posterior most NC derived structures are still present. Foxi1+ placodal ectoderm is present, albeit not properly organized at this stage (G', G''). Scale bars: 25µm (A, A'); 50µm (F).

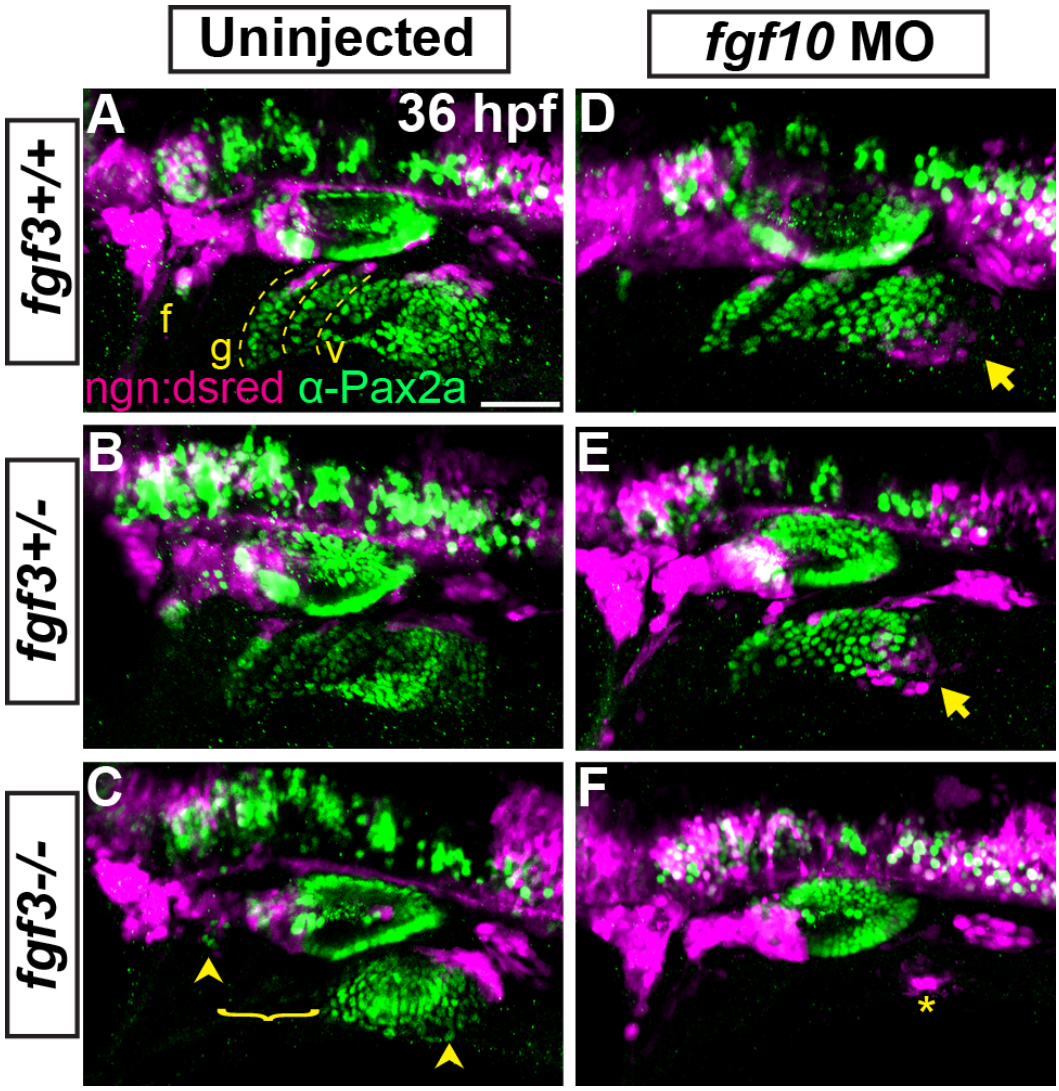

Figure 42: Fgf3 and Fgf10a are required for placode maturation and neurogenesis.

(A-F) Uninjected and *fgf10a*-MO injected progeny from *fgf3+/-;*TgBAC(*neurog1-DSRed*) crosses were collected at 36 hpf and immunolabeled for Pax2a and DSRed to visualize EB placodes and migrating neuroblasts, respectively. Wild-type (A) and *fgf3+/-* (B) panels shows *neurog1:DSRed*+ cells undergoing neurogenesis (magenta) at the dorsal aspect of the mature Pax2a+ EB placodes (green; dotted line). *fgf3-/-* embryos show a loss of properly formed Pax2a+ EB placodes in the region of the prospective glossopharyngeal and three small vagal ganglia and a concurrent loss of *neurog1:DSRed*+ cells in this region (C; bracket); however, the facial and large vagal placode/ganglia are still present (arrowheads). Analysis of *fgf10a*-MO injected wild-type (D) and *fgf3+/-* (E) embryos reveal ectopic neurogenesis as marked by *neurog1:DSRed*+ cells ventral to the posterior most aspect of the vagal placode (arrow). *fgf3-/-;fgf10*-MO embryos show a complete loss Pax2a expression in EB placodes and an absence of neurogenesis, except for a few *neurog1:DSRed*+ cells near the region of the large vagal ganglia (F; asterisk). Abbreviation: *ngn:dsred*, TgBAC(*neurog1-DSRed*); f, facial placode; g, glossopharyngeal placode; v, vagal placodes. Scale bar: 50 μm.

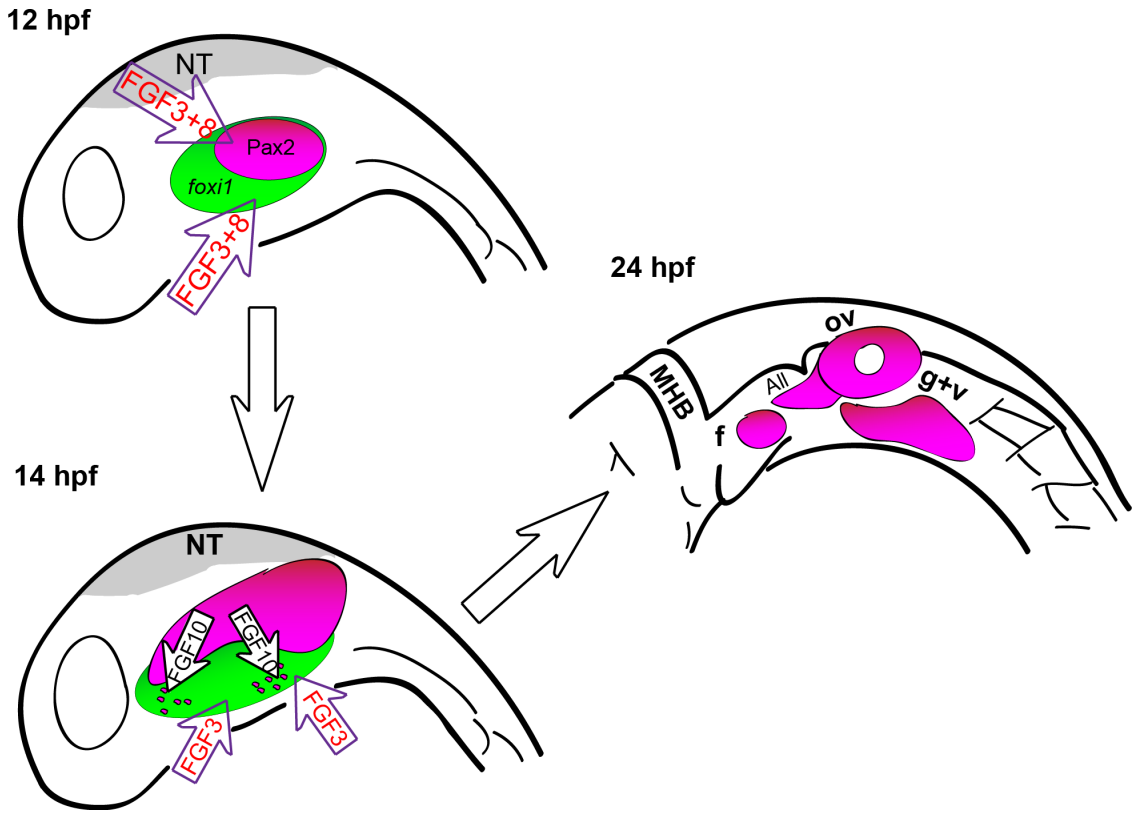

Figure 43: A model for EB placode development in zebrafish.
Before 12 hpf, Fgf3 and Fgf8 specify cells of the posterior placodal area that will give rise to the otic and EB placodes. Shortly after, between 14 and 22 hpf, Fgf10a, expressed by the anterior lateral line precursors and the forming otic vesicle, and Fgf3, expressed by the endoderm, are required for EB placode development by promoting the expression of Pax2a and Sox3 in a subset of cells of the Foxi1+ placodal competent ectoderm. By 24 hpf, EB placodes are fully developed. Abbreviations: NT, neural tube; MHB, midbrain hindbrain boundary; f, facial placode; ov, otic vesicle; All, anterior lateral line; g+v, glossopharyngeal/vagal placode.

CHAPTER 5: DISCUSSION

The work described in this dissertation builds upon former placode developmental studies and reveals new mechanisms by which the early posterior placode precursors gradually obtain unique identities and form discrete structures (Figure 44). During early neurula stages, approximately 11 hpf, Fgf signals from the neural plate and head mesoderm promote formation of the multipotent Pax2a/8+ PPA domain that gives rise to the otic placode, anterior lateral line, and contributes cells to EB placodes. Shortly after the PPA is specified at 12 hpf, Wnt signaling from the neural tube promotes otic commitment in the posteromedial PPA, by driving high levels of Pax2a/8 expression. We speculate that, in parallel with other factors, these differential levels of Pax2a/8 modulate cellular behaviors that contribute to segregation and subsequent morphogenesis of otic or EB progenitors. Subsequently, (14-24 hpf) signals from the PPA, including Fgf10a from the nascent lateral line system and Fgf3 from the endoderm promote EB placode development through controlling expression of Sox3 and Pax2a in placodal competent Foxi1+ non-neural ectoderm.

5.1 The PPA is spatially biased at 12 hpf

What are the origins of the posterior placodes? Previous fate maps of the PPA generated in chick and Xenopus embryos suggested that there is a high degree of overlap with precursors of the otic and EB placodes (Pieper et al., 2011; Streit, 2002). In addition these studies indicated that precursors of the otic placode undergo extensive cell movements during development (Streit, 2002). These studies, however, were preformed using vital dye injections, which label

large numbers of cells often in adjacent precursor domains. Due to these technical limitations, we proposed that the fate-maps generated using the aforementioned methods were not very precise. Using the genetic and imaging advantage of the zebrafish system, we accurately label 2-3 cells in a tissue specific manner to generate a highly resolved fate-map of the PPA.

Our studies challenge the previous assertions of the origins and cellular behaviors of PPA progenitors (Ohyama and Groves, 2004a; Pieper et al., 2011; Streit, 2002). In contrast to the study indicating extensive movements of placode precursor cells during development, we find that cells of the PPA are already spatially biased during early neurulation stages, and there are only rare instances of dramatic cellular relocation events. Additionally, our fate mapping and ablation experiments show that the majority of the EB placode precursors occupy a discrete domain at this stage, with the Pax2+ cells destined to become the otic and lateral line organs. The differences seen between our and earlier studies are likely due to the inconsistency in the number and location of labeling placode progenitor cells. The fate-mapping methods described in this dissertation can be applied to other aspects of stem cell biology in order to determine early patterning and origins of different tissues, and to follow progenitor cells.

5.2 Pax2a levels in development and disease

Another unexplored question in the filed is what intrinsic factors drive segregation of pan-placodal precursors into different domains. Here we show several lines of evidence that relative levels of transcription factor Pax2 can influence cell fate of otic and EB progenitors. Two secreted signals regulate Pax2

expression in the PPA: Fgf is required to initiate Pax2 expression, whereas Wnt signaling controls differential levels of Pax2. Pax2 misexpression and partial knockdown experiments reveal a bias for cells of the PPA such that high levels of Pax2 promote incorporation into the ear, whereas cells with low Pax2 expression resolve to the EB placodes. Interestingly Pax2 is seen in other tissues with intricate cellular morphologies (Eccles et al., 2002). For instance, Pax2 and Pax8 are among the first markers of the pronephros; and proper levels of Pax2 is critical during development in these tissues as well (Bouchard, 2002; Eccles et al., 2002). Heterozygous mutations of the Pax2 gene in humans leads to renal coloboma syndrome, a congenital disease where some patients display eye and kidney abnormalities and to a lesser extent high frequency hearing loss and CNS defects (Alur et al., 2010; Schimmenti, 2011). In addition high levels of Pax2 plays a critical role during the formation of the midbrain hindbrain boundary (Picker et al., 2002; Shima et al., 2009). A detailed investigation of the downstream Pax effectors, and how graded levels of these factors result in different cellular behaviors is important for future understanding of the Pax genes' role in disease and development.

The ability of different transcription factor levels to drive cellular fates in vivo has been reported previously (Acar et al., 2006; Manuel et al., 2006). In particular, during sensory organ formation in Drosophila the transcription factor Senseless has been shown to act as a proneural factor at high levels, synergizing with basic helix loop helix proteins, whereas at low levels it can act as a repressor (Acar et al., 2006). Also, Pax6 has been shown to influence fate of

cortical progenitors in mice with ectopically increased levels of Pax6 resulting in early exit of cycling neuro-progenitors (Manuel et al., 2006). Similarly, in otic and EB development, different levels of Pax2 can direct cell fate decisions in multipotent progenitors. Studies in chick, investigating the role of Pax2 in otic assembly, show that improper levels (both increased or decreased) of this factor will result in mislocalization or loss of critical adhesion molecules N-CAM and N-cadherin needed for morphogenesis of the otic vesicle (Christophorou et al., 2010). Gene dosage of Pax2 is important during organogenesis in other species: Pax2 haploisufficiency results in renal-coloboma syndromes in human, whereas in mouse Pax2 haploisufficiency leads to an analogous syndrome as well as improper formation of the inner ear and hearing deficits (Alur et al., 2010; Eccles et al., 2002; Schimmenti, 2011). Additionally misexpression of Pax2 is a hallmark of certain cancers in the adult, including the progression of renal tumors indicating a loss of cellular identity due to the misregulation of this transcription regulator (Davis et al., 2011).

5.3 Future directions in posterior placode research

In contrast to previous studies, (Phillips et al., 2004), our mosaic experiments showed a direct role of Wnt signaling during otic development in the zebrafish. In addition, cells that could not respond to Wnt had a propensity to contribute to the anterior lateral line domain, conceivably due to shifting from an otic to a more anterior PPA fate (Figure 33C). Loss of Wnt signaling during posterior placode development stages also results in an expanded facial placode (Figure 30E,F,I). Conversely, live time-lapse movies of the PPA in *pax2a:EGFP*

embryos treated with BIO exhibited a retraction of the anterior PPA into the otic vesicle (Figure 29) and α-Pax2a analysis of BIO treated embryos reveal a concomitant loss of the facial placode (Figure 26E,F,I). In light of my recent study defining the anterior lateral line as a source of Fgf signal required for facial placode development, it is likely that loss of Wnt signaling results in supernumerary cells in the anterior lateral line, increasing the Fgf10a signal from this structure; this in turn results in the observed explanation of Pax2a+ cells in the facial placode. Future studies are required to validate this hypothesis.

Another important future direction of cranial placode research is to understand how neuroblasts delaminate from the placodal epithelium. After the EB epithelium undergoes a neural programming, these neurogenic cells delaminate from the epithelium, escaping through breaks in the basement membrane to become migratory neuroblasts that ultimately condense in the underlying mesenchyme (Lassiter et al., 2013). This delamination process is different from the epithelial-to-mesenchymal transition (EMT) that is seen in other tissues, including the neural crest and some metastasizing cancer cells (Brabletz, 2012; Graham et al., 2007). For instance the canonical EMT molecules Slug, Twist and Snail are not expressed in delaminating placode cells (Graham et al., 2007). The mechanism of EB placodal delamination is currently unknown. The Fgf signaling pathway is poised to be a likely candidate for the initiation of the placodal delamination process, given its continuous requirement throughout all stages of EB development. Further studies aimed to better understand the biological processes involved in placodal delamination could reveal novel

mechanisms used by epithelial cells to acquire mesenchymal characteristics and invade distal tissues.

Defects in human cranial placode development result in a myriad of congenital defects including blindness, hearing and balance deficits, loss of smell, as well as hormone imbalance (Abdelhak et al., 1997; Baker and Bronner-Fraser, 2001). While cranial placode development has been actively studied in numerous lower vertebrate model organisms, human placode formation is largely understudied (Baker and Bronner-Fraser, 2001; Schlosser, 2006). Currently protocols are being developed for the use of human induced pluripotent stem cells (hiPSC) or human embryonic stem cells (hESC) as a source of tissue in which to study human placode development (Dincer et al., 2013). Additionally these protocols have the potential to become cell-based therapies for sensory-based diseases (Dincer et al., 2013). Using the insight gained from placode development studies in lower vertebrates and translating this information into hiPSC or mouse ESC fate direction, researchers have successfully generated placodal cell types. This includes the formation of adenohypophyseal placode derived hormone secreting cells, optic lens fibers, otic placode derived cell types including secretory cells, mechanosensory hair cells, and associated neurons, as well as trigeminal sensory neurons (Dincer et al., 2013; Koehler et al., 2013). To date no EB sensory neurons have been successfully derived from hiPSC, hESCs, or mouse ESCs. In the future, knowledge obtained from previous EB placode developmental studies, in conjunction with the work described in this dissertation, could be applied to direct hiPSCs or hESCs to an EB fate.

5.4 Conclusion

This body of work has addressed a number of outstanding questions in the area of placode development, including spatial bias of placode precursors and the intrinsic and extrinsic factors involved in placode development. Through the use of tissue specific fine fate mapping techniques and tissue specific ablations we have shown that the Pax2+ PPA is spatially biased and gives rise primarily to the otic and anterior lateral line, while the majority of EB placode precursors reside in a discrete domain. Our studies show that relative levels of Pax2/8 can influence placode segregation and tissue morphogenesis. The actions of Pax2 during these processes are regulated by extrinsic factors, Wnt and Fgf, in order to achieve the temporal and spatial resolution necessary for proper sensory structure formation. In addition, Fgf is responsible for inducing Pax2 and Sox3 in the nascent EB placodes, a process required for EB placode maturation and subsequent neurogenesis. Fgf and Wnt controlled levels of critical transcription factors could play vital roles in other biological processes such as cell commitment decisions, organ patterning, and tumorigenesis.

CHAPTER 5 FIGURES

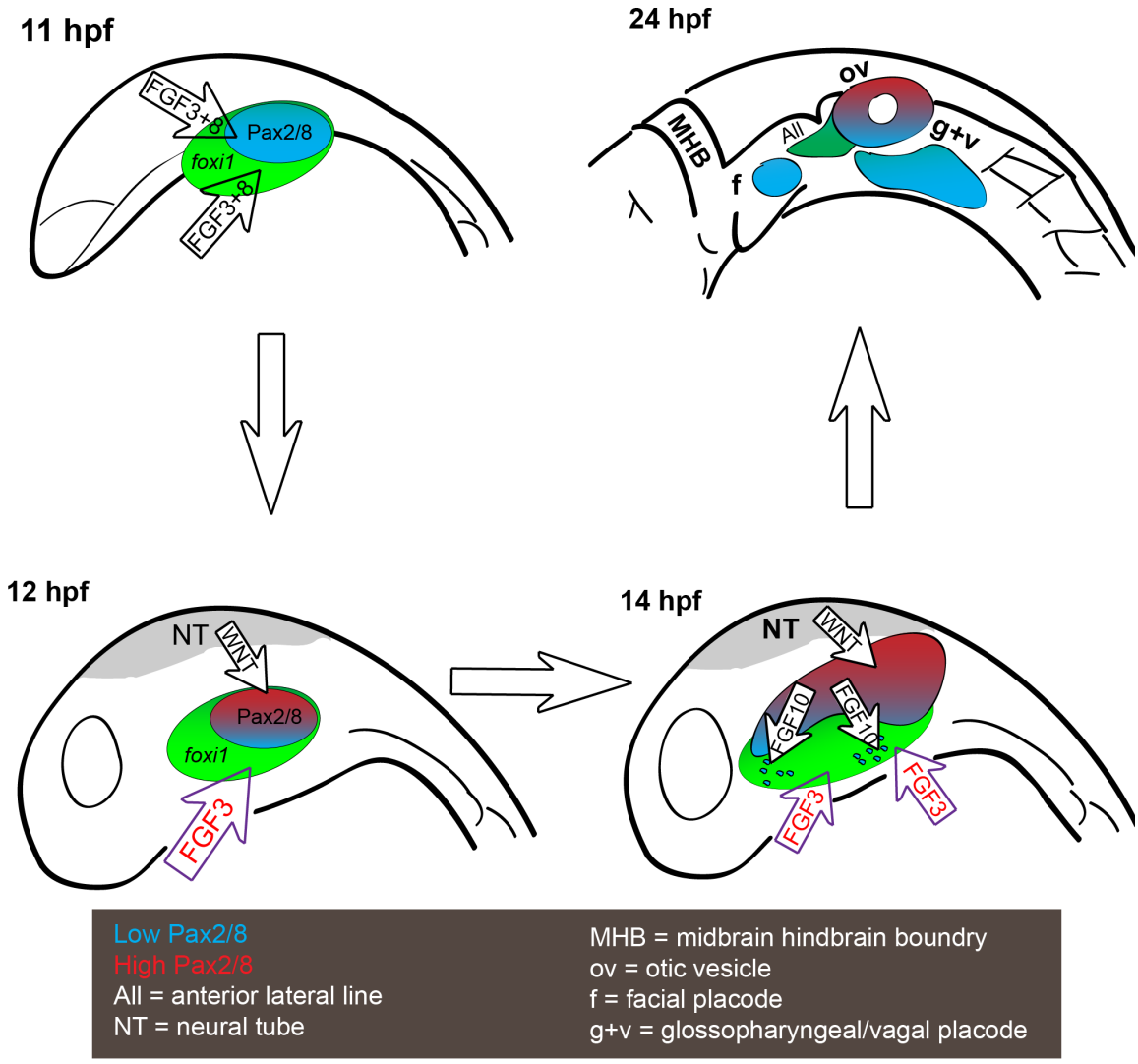

Figure 44: A model for formation of the posterior cranial placodes.
At 11 hpf (early neurula), Fgf3 and Fgf8 specify cells of the posterior placodal area that will give rise to the otic anterior lateral line and EB placodes by turning on Pax2/8 at initial low levels in a subset of foxi1+ placode competent ectoderm. Shortly after, WNT signaling from the neural tube promotes high levels of Pax2/8 to enforce an otic fate. Subsequently, between 14 and 22 hpf (segmentation stage), Fgf10a, expressed by the anterior lateral line precursors and the forming otic vesicle, and Fgf3, expressed by the endoderm, are required for EB placode development by promoting the expression of Pax2a and Sox3 in a subset of cells of the Foxi1+ placodal competent ectoderm. By 24 hpf, EB placodes are fully developed.

CHAPTER 6: APPENDIX

6.1 New transgenics to determine origins of the EB placodes

6.1.1 Background and rationale

Recent evidence indicates that all cranial placodes arise from a region of cephalic ectoderm, called pan-placodal ectoderm (PPE)(Ahrens and Schlosser, 2005; Streit, 2004b). In the zebrafish embryo, this horseshoe-shaped region of cephalic ectoderm, adjoining the forming neural plate and lateral to the neural crest, can be identified at the end of gastrulation (10 hpf) by expression of the transcription factors Eya1, Six4b, and Dlx3b (Figure 1B). Initially, precursors for different placodes are extensively intermingled; as development progresses, distinct regions of the PPE begin to express their own unique set of transcription factors as precursors segregate into discrete placodes. At 12 hpf in the developing zebrafish embryo, a distal subdomain of the PPE begins to express a paired box 2 gene Pax2a (Padanad and Riley, 2011), hereafter referred as the posterior placodal area or PPA (Figure 1C). It has been postulated that the PPA gives rise to both otic and EB placodes (Freter et al., 2008b; Ohyama and Groves, 2004a). My recent work described in Chapter 3 of this dissertation showed that this domain indeed gives rise to the otic placode and anterior lateral line; however, it only modestly contributes to the EB placodes (McCarroll et al., 2012). My findings challenge previous assertions that both the otic and EB placodes arise entirely from the PPA (Ahrens and Schlosser, 2005; Freter et al.,

2008b; Ohyama and Groves, 2004a). Thus, the origin of the EB placodes during embryonic development remains an outstanding question.

Findings from this dissertation revealed that only a small subset of cells in the 12 hpf Pax2a+ PPA contribute to the EB placodes. Experiments described in chapter 3 showed that the PPA gave rise to the otic placode while only 15% of labeled events marked EB placodes (Figure 9). Furthermore, we conducted experiments ablating specific regions of the PPA; these resulted in a loss of the otic placode, and a reduction but not complete loss of the EB placodes. Findings described in Chapter 4 show that the PPA supplies a necessary Fgf10a signal for EB placode maturation, however does not significantly contribute cells directly (Figure 40E, F). Thus, my data demonstrate that the majority of the EB placodal cells are not derived from the PPA. However, it is unclear if EB precursors are present at earlier times in the PPE or recruited later from the adjacent NNE. Our ongoing studies aim to resolve this question using new transgenic strains that will specifically mark PPA cells.

6.1.2 Experimental approach

Based on my preliminary data, we propose two possible models for the origin of EB placodes: **1)** EB placodes are entirely derived from the PPE; and **2)** a subset of the EB placodes originates from the PPE whereas the majority is derived from the NNE (Figure 45). The goal is to distinguish between these two models using newly generated transgenic lines that label individual placodal precursors. Using these reagents, we will generate a fate map of the PPE and

visualize dynamics of PPE cells using the newly generated transgenics. These studies will unambiguously determine the origin of EB placodes.

We are currently generating transgenic animals using recombined bacterial artificial chromosomes (BACs) and Tol2 transposon technology. BACs are large plasmids (100 - 300 kb) that often harbor regulatory regions necessary to closely recapitulate endogenous gene expression patterns (Giraldo and Montoliu, 2001). Recently a *Tol2* technology has been integrated with BAC transgenesis in zebrafish (Suster et al., 2011). *Tol2* is a transposable element which, when active, efficiently integrates (20-50% germ line integration rate) extrachromosomal fragments into the zebrafish genome as a single copy (Suster et al., 2011). Combining these two technologies allows efficient generation of transgenic zebrafish that closely recapitulates endogenous expression at physiologically relevant levels.

We have recently recombined BACs containing the *eya1* (148L10)*, six4b* (zH220D6)*, pax2a* (DKEY-254E7 and bZ15G12) *and dlx3b* (zH209K3T7) genes and a large portion of their respective promoters. We have generated three separate BAC clones in which the first exon (beginning at the endogenous ATG) of the *eya1* gene was replaced with either EGFP, photoconvertable mEos, or CreERt and in all cases the BAC backbone was modified to contain *Tol2* elements to facilitate germ line integration. Six4b and Dlx3b clones were generated in which the first exon of the respective gene was replaced with a nuclear localized Eos, and the first exon of the *pax2a* gene replaced with membrane GFP. In transient expression assays, Six4b, Pax2a, and Eya1

modified BACs closely recapitulated endogenous expression of their respective genes, indicating that they could provide useful tools for lineage analyses of the PPE and PPA cells. Dlx3b, however, did not exhibit a promising expression profile; based on this lack of endogenous expression further efforts to utilize the Dlx3b BAC were abandoned. We have microinjected these newly generated BACs along with transposase mRNA (induces *Tol2*-mediated integration) into single cell embryos to generate stable transgenic strains. We have identified germline founders for the *six4b:nlsEos*, and *eya1:d2EGFP* and *pax2a:memEGFP* (DKEY-254E7) BACs. Stable carriers of *eya1:d2EGFP* did not express early in the PPE, and expression of d2EGFP was not detected until 17hpf, which is too late for utilization in EB lineage studies. In addition, *pax2a:memEGFP* (DKEY-254E7) stable lines do not express EGFP in the EB placodes. We are still in a process of screening for *six4b:nlsEos* BAC germline carriers. Based on transient expression essays, integration of this BAC will produce a useful tool for EB lineage studies.

Once germ line carriers are identified, we will utilize my previously established fate-mapping techniques (McCarroll et al., 2012) to conduct PPE linage studies. We will use a confocal microscope laser to convert small groups of PPE cells (1-3) from green to red in *six4b:nlsEos* embryos. Initial location of the converted cells will be recorded, and embryos will be allowed to develop to 24 hpf (when placodes are fully developed). We will then record the final destination of these cells. In order to resolve PPE from NNE contribution to the EB placodes we will employ the use of a dark-to-red photoactivateable protein

PATagRFP (Subach et al., 2010). These experiments will be done in parallel by ubiquitously expressing PATagRFP in *six4b:nlsEos* embryos by mRNA injections, and regions of NNE (cells lateral to the *nlsEos* expressing PPE) will be photoconverted from dark to red. To determine NNE contribution to the EB placodes, embryos will be processed as described above. From these studies we will assemble a precise fate map of both PPE and/or NNE contribution to the EB placodes.

In addition, We will employ time-lapse microscopy to determine the migratory behavior of PPE and PPA cells: *six4b:nlsEos* positive PPE cells will be visualized from the onset of *six4b* expression (10 hpf; Figure 1B) until the placodes have fully segregated (24 hpf; Figure 1A). Embryos will then be fixed and stained with placode specific antibodies to verify placode identity. From these studies we will determine the origin of the EB placodes and reveal the cellular dynamics involved in their formation. We do not anticipate technical difficulties, as we have successfully utilized live imaging and photoconversion in my previous studies (McCarroll et al., 2012).

6.1.3 Results and discussion

Generation of recombined BACs using the Suster et al., protocol is an efficient and powerful tool to generate reporter lines that recapitulate endogenous expression of the relevant gene of interest. The BACs recombined here were generated as tools for studying cranial placode development, and the use of *six4b:nlsEos* for this effort is still to be determined. Unfortunately, some of the

stable transgenic lines generated by these methods have not been fruitful: *eya1:d2EGFP* transgenic is not expressed during early stages of placode development and the *pax2a:memGFP* BACs were not expressed in EB placodes, Initially we reasoned that because DKEY-254E7 Pax2a BAC clone lacked the 3' non-coding genomic sequence it was likely missing enhancer elements required for expression in the EB placodes. However, *pax2a:memEGFP* BAC (bZ15G12) transgene did include both upstream and downstream non-coding regions, but still lacked expression in the EB placodes in transient expression assays. This suggests that enhancers that regulate Pax2 expression in EB placodes may lie further upstream or downstream of the *pax2a* coding sequence. Previous work in mice analyzing multiple enhancer elements of the Pax2 gene required for its expression in the midbrain hindbrain boundary showed that multiple regulatory elements were required for initial Pax2 expression, and different combinations of these elements was required for the maintenance of Pax2 during later stages of midbrain hindbrain boundary formation (Pfeffer et al., 2002). This taken together with our unsuccessful attempts to generate a Pax2a reporter line that recapitulates endogenous expression patterns indicates complex regulation of this gene. It is possible that a small promoter fragment, a single enhancer element, or even a recombinant BAC will not be sufficient to reproduce some aspects of the endogenous Pax2a expression. Recent advances in genome editing (CRISPR/Cas9 & TALEN) and knock in technology may be the next reasonable approach to generate a Pax2a reporter in zebrafish (Auer et al., 2013).

Transient injections of the *six4b:nlsEos* recombinant BAC clone showed expression in the PPE. Thus, it is possible that *six4b:nlsEos* transgenic will be a useful tool to investigate the origin of EB placodes. We are in the process of screening BAC injected founders for germ line transmission; once a founder(s) is identified, we will validate the transgene expression in the PPE. Once validated, this strain will be utilized in our lineage studies as outlined above.

6.2 Lack of a cranial neural crest contribution to the EB ganglia in zebrafish

6.2.1 Background and rationale

In the developing vertebrate head, components of the PNS arise from two cell populations, the cranial placodes and the cranial neural crest. The cranial placodes can give rise to peripheral neurons while the neural crest can contribute both neurons and peripheral neuron-associated glia known as Schwann cells. The anatomy of the cranial nerves in amniotes consists of 2 lobes (proximal and distal) where in general the proximal lobe is of neural crest origin and the distal is of placode origin (D'Amico-Martel and Noden, 1983). Notably, functional components of the EB ganglia are also segregated based on embryonic origin, with the viscerosensory component of these cranial nerves of placode lineage while the ontogeny of the parasympathetic ganglia is neural crest (Coppola et al., 2010).

In teleosts, however, there has been no report of parasympathetic ganglia associated with the facial ganglia, and these fish lack salivary glands, indicating that viscerosensory components of the EB ganglia predates parasympathetics during evolution (Nilsson and Holmgren, 1994). Given that the parasympathetics of the facial nerve do not exist in the zebrafish and that these structures are of neural crest origin, we set out to determine if the neural crest contributes neurons to the EB ganglia in the zebrafish. We utilized a combination of lineage tracing experiments using genetically encoded photoconvertable molecules and imaging of neural crest reporter lines co-labeled with EB placode and subsequent ganglia specific markers to determine if the cranial neural crest contributes to the EB ganglia in zebrafish.

6.2.2 Experimental approach

All of the neurons within the visceroreflex circuit, including the EB ganglia neurons, express the transcription factors Phox2a and Phox2b (Dauger et al., 2003). Sox10 expression can identify the neural crest (Kucenas et al., 2008). In our laboratory, we have established transgenic strains that label both EB ganglia (*phox2b:EGFP*) and the cranial neural crest progenitors (*sox10:nlsEos* and *sox10:mRFP*). In addition, differentiated neurons can be labeled with anti-Elav (anti-Hu) antibody. Using these tools we performed a series of experiments to specifically label neural crest precursors and then imaged these embryos after the EB ganglia has formed.

We crossed the *sox10:nlsEos* transgenic to the *phox2b:EGFP* to generate double transgenics to label both neural crest and EB ganglia. We utilized my previously established fate-mapping techniques (McCarroll et al., 2012) to conduct neural crest linage studies. We used a confocal microscope laser to convert groups of neural crest cells from green to red in *sox10:nlsEos* embryos at 12 hpf (pre-migratory stage of neural crest). Initial location of the converted cells was recorded, and embryos were allowed to develop to 3 dpf (when the EB ganglia is developed). In addition we also crossed the *phox2b:EGFP* transgenic to the *sox10:mRFP* line to obtain double transgenics to label both neural crest in red and EB ganglia in green and fixed samples at 5 dpf. We recorded the final destination of these cells and co-labeled with pan-neuronal specific marker α-HU. From these studies we will determine if the neural crest contributes to the EB ganglia.

6.2.3 Results and discussion

Lineage tracing of neural crest cells using *sox10:nlsEos* embryos photoconverted at 12 hpf and fixed and stained with anti-Hu and 3 dpf revealed no contribution of the cranial neural crest to the EB ganglia, including the facial ganglia. However, *sox10*+ cells were seen to co-localize with the more anteriolateral trigeminal ganglia (data not shown). Because anti-HU is a pan-neuronal marker, we wanted to more specifically label the EB ganglia. To accomplish this, further lineage studies were performed by crossing *phox2b:EGFP* animals to *sox10:mRFP* transgenics to generate double

transgenic progeny. Embryos were allowed to develop to 5 dpf and imaged for phox2b and sox10 expression (Figure 46). These crosses revealed no contribution of sox10+ cells to the EB ganglia, albeit a few RFP+ cells in the large vagal ganglion which was consistently seen (Figure 46B; arrow).

Utilizing neural crest and EB ganglia specific reporters, these studies reveal little to no neural crest contribution to the neurons of the EB ganglia during larval stages of zebrafish development. This is different from EB ganglia development in amniotes where two separate lobes of the EB ganglia originate from either the placodes (distal) or the neural crest (proximal). Because there is no evidence that the zebrafish posses a separate parasympathetic component to its EB ganglia system, it is likely that the neural crest was recruited later in evolution to give rise to the more proximal parasympathetic component of this visceroreflex circuit.

A recent study laid claim that a large portion of the facial ganglia in the zebrafish contained cells of neural crest lineage (Kague et al., 2012). Based on our lineage work, and what is know about the evolution and anatomy of the EB ganglia in teleosts, we do not think that this is the case. We did however identify sox10+ cells in the trigeminal ganglia, which overlap with the facial ganglia during larval stages of development. Given that Kague et al., used a pan-neuronal marker to analyze the cranial ganglia, and the difficult to distinguish individual ganglia at this stage, it is likely that the trigeminal ganglia was mistaken for the facial ganglia.

CHAPTER 6 FIGURES

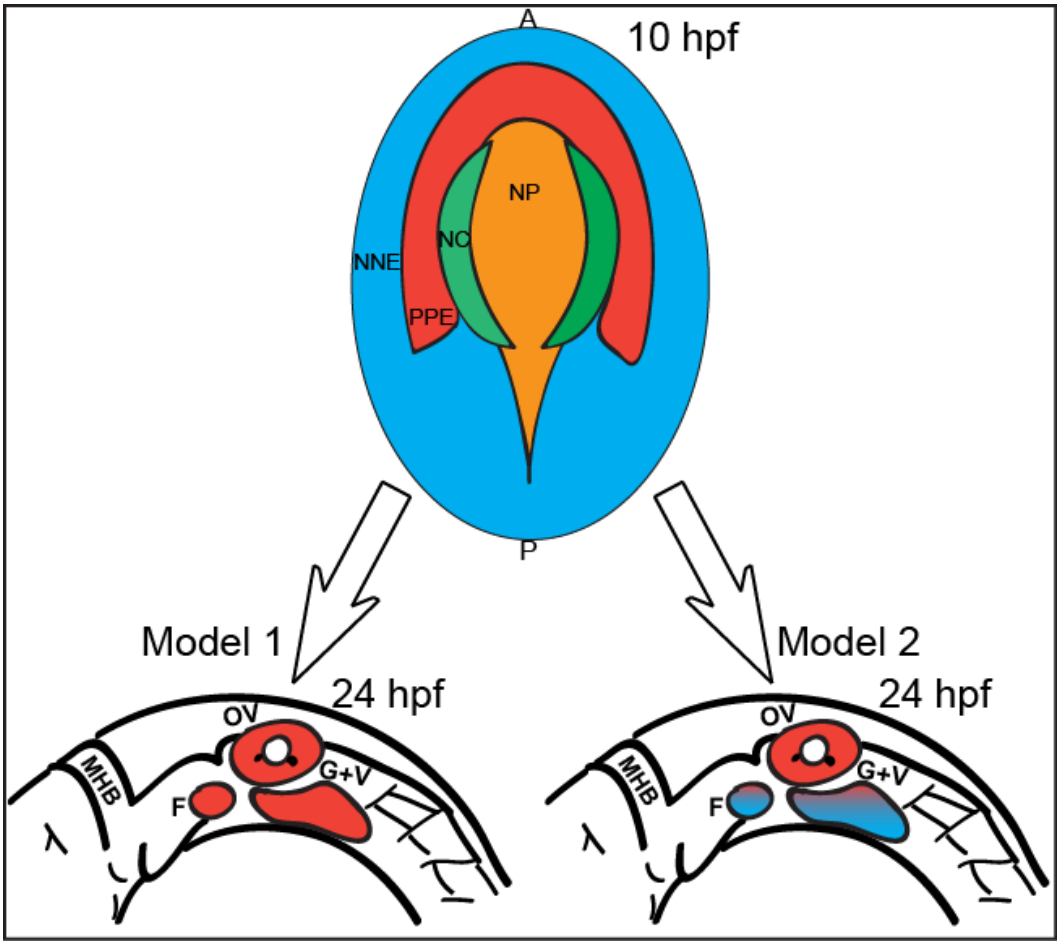

Figure 45: Two potential origins of the epibranchial placodes.
In model one, the EB placodes are derived from the PPE. In the second model, a subset of the EB placodes arises from the PPE while the majority originates from the NNE. Abbreviations: OV, otic vesicle, F, facial placode; G+V, glossopharyngeal, and vagal placodes; MHB, midbrain hindbrain boundary.

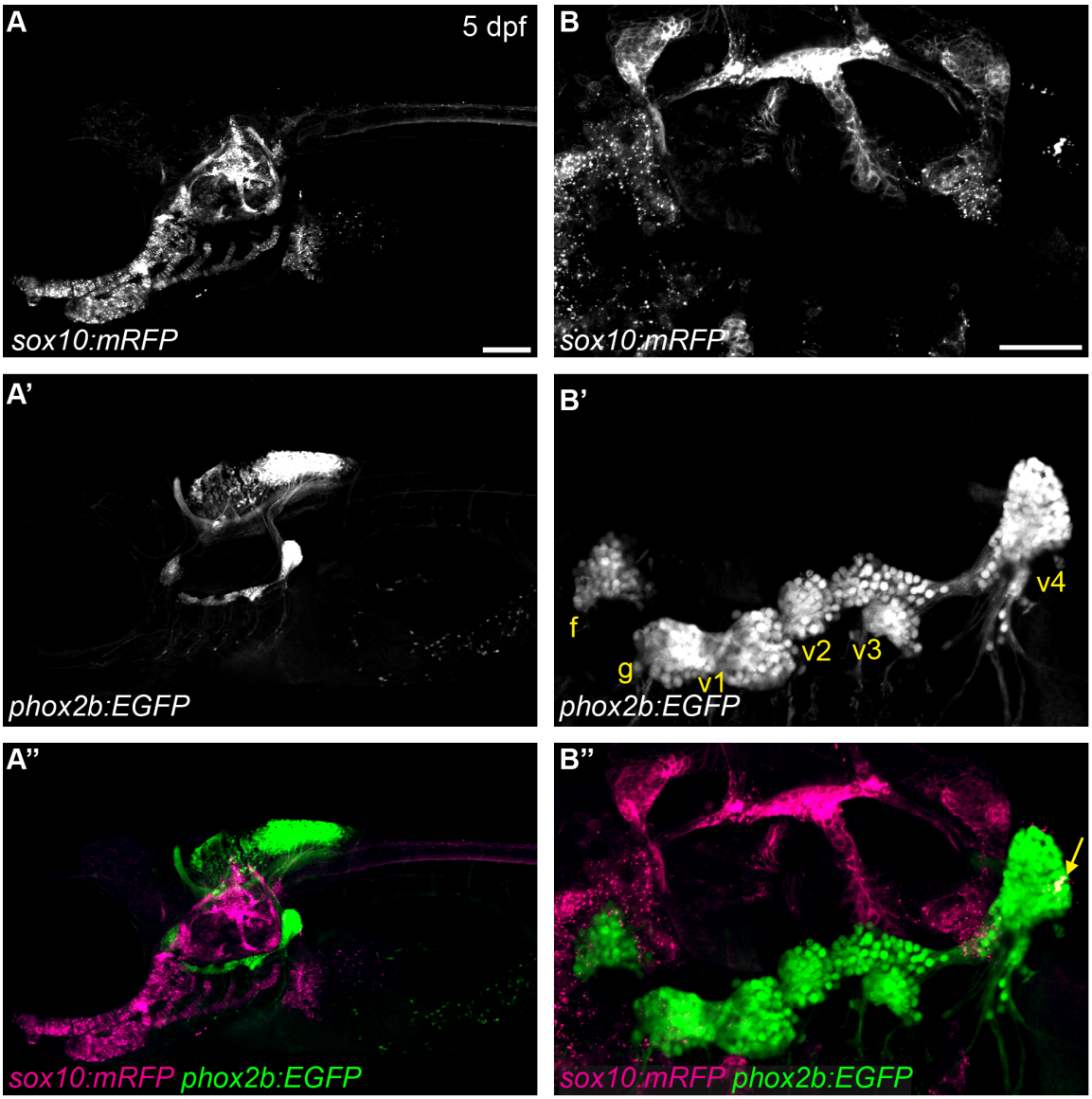

Figure 46: Neural crest does not contribute to the epibranchial ganglia in zebrafish.

(A, B) Confocal projection of a 5 dpf zebrafish larva expressing the *sox10*+ neural crest reporter (magenta) and the *phox2b*+ EB ganglia reporter (green). 10X magnification (A) illustrates the *phox2b*+ hindbrain neurons and the EB ganglia of the viscerosensory circuit and the craniofacial structures of the *sox10*+ neural crest. 40X magnification of the EB ganglia reveals no neural crest contribution to the EB ganglia, albeit a small number of cells in the large vagal ganglia that co-label for *sox10* and *phox2b* (arrow). Abbreviations: f, facial; g, glossopharyngeal; v1-v3, small vagal; v4, large vagal. Scale bars: (A) 100μm, (B) 50μm.

REFERENCES

Abdelhak, S., Kalatzis, V., Heilig, R., Compain, S., Samson, D., Vincent, C., Weil, D., Cruaud, C., Sahly, I., Leibovici, M., et al. (1997). A human homologue of the Drosophila eyes absent gene underlies Branchio-Oto-Renal (BOR) syndrome and identifies a novel gene family. *Nat. Genet.* 15, 157–164.

Abello, G., Khatri, S., Radosevic, M., Scotting, P., Giraldez, F. and Alsina, B. (2010). Independent regulation of Sox3 and Lmx1b by FGF and BMP signaling influences the neurogenic and non-neurogenic domains in the chick otic placode. *Dev. Biol.* 339, 166–178.

Abelló, G., Khatri, S., Giráldez, F. and Alsina, B. (2007). Early regionalization of the otic placode and its regulation by the Notch signaling pathway. *Mech. Dev.* 124, 631–645.

Abramoff, M. D., Magalhaes, P. J. and Ram, S. J. (2004). image processesing with image j. *Biophotonics Int.* 11, 36–42.

Abu-Elmagd, M., Ishii, Y., Cheung, M., Rex, M., Le Rouëdec, D. and Scotting, P. J. (2001a). cSox3 Expression and Neurogenesis in the Epibranchial Placodes. *Dev. Biol.* 237, 258–269.

Abu-Elmagd, M., Ishii, Y., Cheung, M., Rex, M., Le Rouëdec, D. and Scotting, P. J. (2001b). cSox3 Expression and Neurogenesis in the Epibranchial Placodes. *Dev. Biol.* 237, 258–269.

Acampora, D., Gulisano, M., Broccoli, V. and Simeone, A. (2001). Otx genes in brain morphogenesis. *Prog. Neurobiol.* 64, 69–95.

Acar, M., Jafar-Nejad, H., Giagtzoglou, N., Yallampalli, S., David, G., He, Y., Delidakis, C. and Bellen, H. J. (2006). Senseless physically interacts with proneural proteins and functions as a transcriptional co-activator. *Development* 133, 1979–1989.

Ahrens, K. and Schlosser, G. (2005). Tissues and signals involved in the induction of placodal Six1 expression in Xenopus laevis. *Dev. Biol.* 288, 40–59.

Alur, R. P., Vijayasarathy, C., Brown, J. D., Mehtani, M., Onojafe, I. F., Sergeev, Y. V., Boobalan, E., Jones, M., Tang, K., Liu, H., et al. (2010). Papillorenal Syndrome-Causing Missense Mutations in PAX2/Pax2 Result in Hypomorphic Alleles in Mouse and Human. *PLoS Genet.* 6, e1000870.

Alvarez, Y., Alonso, M. T., Vendrell, V., Zelarayan, L. C., Chamero, P., Theil, T., Bösl, M. R., Kato, S., Maconochie, M., Riethmacher, D., et al. (2003). Requirements for FGF3 and FGF10 during inner ear formation. *Development* 130, 6329–6338.

Amiel, J., Laudier, B., Attié-Bitach, T., Trang, H., de Pontual, L., Gener, B., Trochet, D., Etchevers, H., Ray, P., Simonneau, M., et al. (2003). Polyalanine expansion and frameshift mutations of the paired-like homeobox gene PHOX2B in congenital central hypoventilation syndrome. *Nat. Genet.* 33, 459–461.

Andermann, P., Ungos, J. and Raible, D. W. (2002). Neurogenin1 defines zebrafish cranial sensory ganglia precursors. *Dev. Biol.* 251, 45–58.

Auer, T. O., Duroure, K., De Cian, A., Concordet, J.-P. and Del Bene, F. (2013). Highly efficient CRISPR/Cas9-mediated knock-in in zebrafish by homology-independent DNA repair. *Genome Res.*

Bailey, A. P., Bhattacharyya, S., Bronner-Fraser, M. and Streit, A. (2006). Lens specification is the ground state of all sensory placodes, from which FGF promotes olfactory identity. *Dev. Cell* 11, 505–517.

Bajoghli, B., Aghaallaei, N., Heimbucher, T. and Czerny, T. (2004). An artificial promoter construct for heat-inducible misexpression during fish embryogenesis. *Dev. Biol.* 271, 416–430.

Baker, C. V. H. and Bronner-Fraser, M. (2001). Vertebrate Cranial Placodes I. Embryonic Induction. *Dev. Biol.* 232, 1–61.

Bancroft, M. and Bellairs, R. (1977). Placodes of the chick embryo studied by SEM. *Anat. Embryol. (Berl.)* 151, 97–108.

Barraud, P., Seferiadis, A. A., Tyson, L. D., Zwart, M. F., Szabo-Rogers, H. L., Ruhrberg, C., Liu, K. J. and Baker, C. V. H. (2010). Neural crest origin of olfactory ensheathing glia. *Proc. Natl. Acad. Sci.* 107, 21040–21045.

Beard, J. (1885). *The system of branchial sense organs and their associated ganglia in ichthyopsida: a contribution to the ancestral history of vertebrates...* n. pub.

Begbie, J., Brunet, J. F., Rubenstein, J. L. and Graham, A. (1999). Induction of the epibranchial placodes. *Development* 126, 895–902.

Begbie, J., Ballivet, M. and Graham, A. (2002). Early Steps in the Production of Sensory Neurons by the Neurogenic Placodes. *Mol. Cell. Neurosci.* 21, 502–511.

Beites, C. L., Kawauchi, S., Crocker, C. E. and Calof, A. L. (2005). Identification and molecular regulation of neural stem cells in the olfactory epithelium. *Exp. Cell Res.* 306, 309–316.

Belov, A. A. and Mohammadi, M. (2013). Molecular mechanisms of fibroblast growth factor signaling in physiology and pathology. *Cold Spring Harb. Perspect. Biol.* 5,.

Bhat, N. and Riley, B. B. (2011). Integrin-α5 Coordinates Assembly of Posterior Cranial Placodes in Zebrafish and Enhances Fgf-Dependent Regulation of Otic/Epibranchial Cells. *PLoS ONE* 6, e27778.

Bhattacharyya, S., Bailey, A. P., Bronner-Fraser, M. and Streit, A. (2004). Segregation of lens and olfactory precursors from a common territory: cell sorting and reciprocity of Dlx5 and Pax6 expression. *Dev. Biol.* 271, 403–414.

Bok, J., Raft, S., Kong, K.-A., Koo, S. K., Dräger, U. C. and Wu, D. K. (2011). Transient retinoic acid signaling confers anterior-posterior polarity to the inner ear. *Proc. Natl. Acad. Sci.* 108, 161–166.

Bouchard, M. (2002). Nephric lineage specification by Pax2 and Pax8. *Genes Dev.* 16, 2958–2970.

Bouchard, M., Souabni, A. and Busslinger, M. (2004). Tissue-specific expression of cre recombinase from the Pax8 locus. *genesis* 38, 105–109.

Brabletz, T. (2012). EMT and MET in Metastasis: Where Are the Cancer Stem Cells? *Cancer Cell* 22, 699–701.

Bricaud, O. and Collazo, A. (2006). The transcription factor six1 inhibits neuronal and promotes hair cell fate in the developing zebrafish (Danio rerio) inner ear. *J. Neurosci.* 26, 10438.

Brown, A. S. and Epstein, D. J. (2011). Otic ablation of smoothened reveals direct and indirect requirements for Hedgehog signaling in inner ear development. *Development* 138, 3967–3976.

Brown, S. T., Wang, J. and Groves, A. K. (2005). Dlx gene expression during chick inner ear development. *J. Comp. Neurol.* 483, 48–65.

Brugmann, S. A., Pandur, P. D., Kenyon, K. L., Pignoni, F. and Moody, S. A. (2004a). Six1 promotes a placodal fate within the lateral neurogenic ectoderm by functioning as both a transcriptional activator and repressor. *Development* 131, 5871–5881.

Brugmann, S. A., Pandur, P. D., Kenyon, K. L., Pignoni, F. and Moody, S. A. (2004b). Six1 promotes a placodal fate within the lateral neurogenic ectoderm by functioning as both a transcriptional activator and repressor. *Development* 131, 5871–5881.

Brunet, J. F. and Pattyn, A. (2002). Phox2 genes–from patterning to connectivity. *Curr. Opin. Genet. Dev.* 12, 435–440.

Buj-Bello, A., Buchman, V. L., Horton, A., Rosenthal, A. and Davies, A. M. (1995). GDNF is an age-specific survival factor for sensory and autonomic neurons. *Neuron* 15, 821–828.

Burgess, W. H. and Maciag, T. (1989). The Heparin-Binding (Fibroblast) Growth Factor Family of Proteins. *Annu. Rev. Biochem.* 58, 575–602.

Canning, C. A., Lee, L., Luo, S. X., Graham, A. and Jones, C. M. (2008). Neural tube derived Wnt signals cooperate with FGF signaling in the formation and differentiation of the trigeminal placodes. *Neural Develop.* 3, 35.

Chapman, S. C., Sawitzke, A. L., Campbell, D. S. and Schoenwolf, G. C. (2005). A three-dimensional atlas of pituitary gland development in the zebrafish. *J. Comp. Neurol.* 487, 428–440.

Chien, A. J., Conrad, W. H. and Moon, R. T. (2009). A Wnt survival guide: from flies to human disease. *J. Invest. Dermatol.* 129, 1614–1627.

Chow, R. L., Altmann, C. R., Lang, R. A. and Hemmati-Brivanlou, A. (1999). Pax6 induces ectopic eyes in a vertebrate. *Development* 126, 4213–4222.

Christophorou, N. A. D., Mende, M., Lleras-Forero, L., Grocott, T. and Streit, A. (2010). Pax2 coordinates epithelial morphogenesis and cell fate in the inner ear. *Dev. Biol.* 345, 180–190.

Clancy, J. A., Deuchars, S. A. and Deuchars, J. (2012). The wonders of the Wanderer. *Exp. Physiol.*

Coppola, E., Rallu, M., Richard, J., Dufour, S., Riethmacher, D., Guillemot, F., Goridis, C. and Brunet, J.-F. (2010). Epibranchial ganglia orchestrate the development of the cranial neurogenic crest. *Proc. Natl. Acad. Sci.* 107, 2066–2071.

Crump, J. G., Maves, L., Lawson, N. D., Weinstein, B. M. and Kimmel, C. B. (2004). An essential role for Fgfs in endodermal pouch formation influences later craniofacial skeletal patterning. *Development* 131, 5703–5716.

Culbertson, M. D., Lewis, Z. R. and Nechiporuk, A. V. (2011). Chondrogenic and Gliogenic Subpopulations of Neural Crest Play Distinct Roles during the Assembly of Epibranchial Ganglia. *PLoS ONE* 6, e24443.

Cunliffe, H., McNoe, L., Ward, T., Devriendt, K., Brunner, H. and Eccles, M. (1998). The prevalence of PAX2 mutations in patients with isolated

colobomas or colobomas associated with urogenital anomalies. *J. Med. Genet.* 35, 806.

D'Amico-Martel, A. and Noden, D. M. (1983). Contributions of placodal and neural crest cells to avian cranial peripheral ganglia. *Am. J. Anat.* 166, 445–468.

Dailey, L., Ambrosetti, D., Mansukhani, A. and Basilico, C. (2005). Mechanisms underlying differential responses to FGF signaling. *Cytokine Growth Factor Rev.* 16, 233–247.

Dauger, S., Pattyn, A., Lofaso, F., Gaultier, C., Goridis, C., Gallego, J. and Brunet, J. F. (2003). Phox2b controls the development of peripheral chemoreceptors and afferent visceral pathways. *Development* 130, 6635.

Davis, S. W. and Camper, S. A. (2007). Noggin regulates Bmp4 activity during pituitary induction. *Dev. Biol.* 305, 145–160.

Davis, J. L., Matsumura, L., Weeks, D. A. and Troxell, M. L. (2011). PAX2 Expression in Wilms Tumors and Other Childhood Neoplasms.

Dincer, Z., Piao, J., Niu, L., Ganat, Y., Kriks, S., Zimmer, B., Shi, S.-H., Tabar, V. and Studer, L. (2013). Specification of Functional Cranial Placode Derivatives from Human Pluripotent Stem Cells. *Cell Rep.* 5, 1387–1402.

Drerup, C. M. and Nechiporuk, A. V. (2013). JNK-Interacting Protein 3 Mediates the Retrograde Transport of Activated c-Jun N-Terminal Kinase and Lysosomes. *PLoS Genet* 9, e1003303.

Dude, C. M., Kuan, C.-Y. K., Bradshaw, J. R., Greene, N. D. E., Relaix, F., Stark, M. R. and Baker, C. V. H. (2009). Activation of Pax3 target genes is necessary but not sufficient for neurogenesis in the ophthalmic trigeminal placode. *Dev. Biol.* 326, 314–326.

Dutta, S., Dietrich, J.-E., Aspöck, G., Burdine, R. D., Schier, A., Westerfield, M. and Varga, Z. M. (2005). pitx3 defines an equivalence domain for lens and anterior pituitary placode. *Development* 132, 1579–1590.

Eccles, M. R., He, S., Legge, M., Kumar, R., Fox, J., Zhou, C., French, M. and Tsai, R. W. S. (2002). PAX genes in development and disease: the role of PAX2 in urogenital tract developments. *Int. J. Dev. Biol.* 46, 535–544.

Eiraku, M., Takata, N., Ishibashi, H., Kawada, M., Sakakura, E., Okuda, S., Sekiguchi, K., Adachi, T. and Sasai, Y. (2011). Self-organizing optic-cup morphogenesis in three-dimensional culture. *Nature* 472, 51–56.

Eisthen, H. L., Delay, R. J., Wirsig-Wiechmann, C. R. and Dionne, V. E. (2000). Neuromodulatory Effects of Gonadotropin Releasing Hormone on Olfactory Receptor Neurons. *J. Neurosci.* 20, 3947–3955.

Enomoto, H. (2013). The cellular origin of the enteric nervous system.

Erickson, T., Scholpp, S., Brand, M., Moens, C. B. and Jan Waskiewicz, A. (2007). Pbx proteins cooperate with Engrailed to pattern the midbrain-hindbrain and diencephalic-mesencephalic boundaries. *Dev. Biol.* 301, 504–517.

Faber, S. C., Dimanlig, P., Makarenkova, H. P., Shirke, S., Ko, K. and Lang, R. A. (2001). Fgf receptor signaling plays a role in lens induction. *Development* 128, 4425–4438.

Fode, C., Gradwohl, G., Morin, X., Dierich, A., LeMeur, M., Goridis, C. and Guillemot, F. (1998). The bHLH Protein NEUROGENIN 2 Is a Determination Factor for Epibranchial Placode–Derived Sensory Neurons. *Neuron* 20, 483–494.

Freter, S., Muta, Y., Mak, S.-S., Rinkwitz, S. and Ladher, R. K. (2008a). Progressive restriction of otic fate: the role of FGF and Wnt in resolving inner ear potential. *Development* 135, 3415–3424.

Freter, S., Muta, Y., Mak, S.-S., Rinkwitz, S. and Ladher, R. K. (2008b). Progressive restriction of otic fate: the role of FGF and Wnt in resolving inner ear potential. *Development* 135, 3415–3424.

Freter, S., Fleenor, S. J., Freter, R., Liu, K. J. and Begbie, J. (2013). Cranial neural crest cells form corridors prefiguring sensory neuroblast migration. *Development* 140, 3595–3600.

Furthauer, M. (2004). Fgf signalling controls the dorsoventral patterning of the zebrafish embryo. *Development* 131, 2853–2864.

Ghysen, A. and Dambly-Chaudière, C. (2004). Development of the zebrafish lateral line. *Curr. Opin. Neurobiol.* 14, 67–73.

Gibbs, M. A. (2004). Lateral Line Receptors: Where Do They Come from Developmentally and Where Is Our Research Going? *Brain. Behav. Evol.* 64, 163–181.

Giraldo, P. and Montoliu, L. (2001). Size matters: use of YACs, BACs and PACs in transgenic animals. *Transgenic Res.* 10, 83–103.

Glasgow, E., Karavanov, A. A. and Dawid, I. B. (1997). Neuronal and Neuroendocrine Expression oflim3,a LIM Class Homeobox Gene, Is

Altered in Mutant Zebrafish with Axial Signaling Defects. *Dev. Biol.* 192, 405–419.

Glavic, A., Gómez-Skarmeta, J. L. and Mayor, R. (2002). The homeoprotein Xiro1 is required for midbrain-hindbrain boundary formation. *Development* 129, 1609–1621.

Goldfarb, M. (2005). FIBROBLAST GROWTH FACTOR HOMOLOGOUS FACTORS: EVOLUTION, STRUCTURE, AND FUNCTION. *Cytokine Growth Factor Rev.* 16, 215–220.

Gonzalez, C., Almaraz, L., Obeso, A. and Rigual, R. (1994). Carotid body chemoreceptors: from natural stimuli to sensory discharges. *Physiol. Rev.* 74, 829–898.

Gospodarowicz, D. and Moran, J. S. (1975). Mitogenic effect of fibroblast growth factor on early passage cultures of human and murine fibroblasts. *J. Cell Biol.* 66, 451–457.

Graham, A., Blentic, A., Duque, S. and Begbie, J. (2007). Delamination of cells from neurogenic placodes does not involve an epithelial-to-mesenchymal transition. *Development* 134, 4141–4145.

Grandel, H., Draper, B. W. and Schulte-Merker, S. (2000). dackel acts in the ectoderm of the zebrafish pectoral fin bud to maintain AER signaling. *Development* 127, 4169–4178.

Grifone, R., Demignon, J., Houbron, C., Souil, E., Niro, C., Seller, M. J., Hamard, G. and Maire, P. (2005). Six1 and Six4 homeoproteins are required for Pax3 and Mrf expression during myogenesis in the mouse embryo. *Development* 132, 2235–2249.

Grocott, T., Tambalo, M. and Streit, A. (2012). The peripheral sensory nervous system in the vertebrate head: A gene regulatory perspective. *Dev. Biol.*

Groves, A. K. and Fekete, D. M. (2012). Shaping sound in space: the regulation of inner ear patterning. *Development* 139, 245–257.

Halder, G., Callaerts, P. and Gehring, W. J. (1995). Induction of ectopic eyes by targeted expression of the eyeless gene in Drosophila. *Science* 267, 1788–1792.

Hammond, K. L. and Whitfield, T. T. (2011). Fgf and Hh signalling act on a symmetrical pre-pattern to specify anterior and posterior identity in the zebrafish otic placode and vesicle. *Development*.

Hammond, K. L., Loynes, H. E., Folarin, A. A., Smith, J. and Whitfield, T. T. (2003). Hedgehog signalling is required for correct anteroposterior patterning of the zebrafish otic vesicle. *Development* 130, 1403–1417.

Hammond, K. L., van Eeden, F. J. M. and Whitfield, T. T. (2010). Repression of Hedgehog signalling is required for the acquisition of dorsolateral cell fates in the zebrafish otic vesicle. *Development* 137, 1361–1371.

Hanafusa, H., Torii, S., Yasunaga, T. and Nishida, E. (2002). Sprouty1 and Sprouty2 provide a control mechanism for the Ras/MAPK signalling pathway. *Nat. Cell Biol.* 4, 850–858.

Hans, S., Liu, D. and Westerfield, M. (2004a). Pax8 and Pax2a function synergistically in otic specification, downstream of the Foxi1 and Dlx3b transcription factors. *Development* 131, 5091.

Hans, S., Liu, D. and Westerfield, M. (2004b). Pax8 and Pax2a function synergistically in otic specification, downstream of the Foxi1 and Dlx3b transcription factors. *Development* 131, 5091.

Hans, S., Christison, J., Liu, D. and Westerfield, M. (2007). Fgf-dependent otic induction requires competence provided by Foxi1 and Dlx3b. *BMC Dev. Biol.* 7, 5.

Hans, S., Irmscher, A. and Brand, M. (2013). Zebrafish Foxi1 provides a neuronal ground state during inner ear induction preceding the Dlx3b/4b-regulated sensory lineage. *Development* 140, 1936–1945.

Harden, M. V., Pereiro, L., Ramialison, M., Wittbrodt, J., Prasad, M. K., McCallion, A. S. and Whitlock, K. E. (2012). Close association of olfactory placode precursors and cranial neural crest cells does not predestine cell mixing. *Dev. Dyn.* 241, 1143–1154.

Harding, M. J. and Nechiporuk, A. V. (2012). Fgfr-Ras-MAPK signaling is required for apical constriction via apical positioning of Rho-associated kinase during mechanosensory organ formation. *Development* 139, 3130–3135.

Harris, J. A., Cheng, A. G., Cunningham, L. L., MacDonald, G., Raible, D. W. and Rubel, E. W. (2003). Neomycin-Induced Hair Cell Death and Rapid Regeneration in the Lateral Line of Zebrafish (Danio rerio). *JARO J. Assoc. Res. Otolaryngol.* 4, 219–234.

Harrison, R. G. (1936). Relations of symmetry in the developing ear of Amblystoma punctatum. *Proc. Natl. Acad. Sci. U. S. A.* 22, 238.

Herzog, W. (2004). Fgf3 signaling from the ventral diencephalon is required for early specification and subsequent survival of the zebrafish adenohypophysis. *Development* 131, 3681–3692.

Herzog, W., Zeng, X., Lele, Z., Sonntag, C., Ting, J.-W., Chang, C.-Y. and Hammerschmidt, M. (2003). Adenohypophysis formation in the zebrafish and its dependence on sonic hedgehog. *Dev. Biol.* 254, 36–49.

Holzschuh, J., Wada, N., Wada, C., Schaffer, A., Javidan, Y., Tallafuß, A., Bally-Cuif, L. and Schilling, T. F. (2005). Requirements for endoderm and BMP signaling in sensory neurogenesis in zebrafish. *Development* 132, 3731–3742.

Hoppler, S. and Kavanagh, C. L. (2007). Wnt signalling: variety at the core. *J. Cell Sci.* 120, 385–393.

Itoh, N. (2007). The Fgf families in humans, mice, and zebrafish: their evolutional processes and roles in development, metabolism, and disease. *Biol. Pharm. Bull.* 30, 1819–1825.

Itoh, N. and Konishi, M. (2007). The zebrafish fgf family. *Zebrafish* 4, 179–186.

Itoh, N. and Ornitz, D. M. (2004). Evolution of the Fgf and Fgfr gene families. *Trends Genet.* 20, 563–569.

Kague, E., Gallagher, M., Burke, S., Parsons, M., Franz-Odendaal, T. and Fisher, S. (2012). Skeletogenic Fate of Zebrafish Cranial and Trunk Neural Crest. *PloS One* 7, e47394.

Karlstrom, R. O., Talbot, W. S. and Schier, A. F. (1999). Comparative synteny cloning of zebrafish you-too: mutations in the Hedgehog target gli2 affect ventral forebrain patterning. *Genes Dev.* 13, 388–393.

Katz, D. M., Adler, J. E. and Black, I. B. (1987). Catecholaminergic primary sensory neurons: autonomic targets and mechanisms of transmitter regulation. *Fed. Proc.* 46, 24–29.

Kiefer, P., Strahle, U. and Dickson, C. (1996). The zebrafish Fgf-3 gene: cDNA sequence, transcript structure and genomic organization. *Gene* 168, 211–215.

Kil, S.-H., Streit, A., Brown, S. T., Agrawal, N., Collazo, A., Zile, M. H. and Groves, A. K. (2005). Distinct roles for hindbrain and paraxial mesoderm in the induction and patterning of the inner ear revealed by a study of vitamin-A-deficient quail. *Dev. Biol.* 285, 252–271.

Kimmel, C. B., Ballard, W. W., Kimmel, S. R., Ullmann, B. and Schilling, T. F. (1995). Stages of embryonic development of the zebrafish. *Am. J. Anat.* 203, 253–310.

Knecht, A. K. and Bronner-Fraser, M. (2002). Induction of the neural crest: a multigene process. *Nat. Rev. Genet.* 3, 453–461.

Koehler, K. R., Mikosz, A. M., Molosh, A. I., Patel, D. and Hashino, E. (2013). Generation of inner ear sensory epithelia from pluripotent stem cells in 3D culture. *Nature* 500, 217–221.

Kozlowski, D., Murakami, T., Ho, R. and Weinberg, E. (1997). Regional cell movement and tissue patterning in the zebrafish embryo revealed by fate mapping with caged fluorescein. *J. Biochem. Cell Biol.* 75, 551–562.

Krauss, S., Johansen, T., Korzh, V. and Fjose, A. (1991). Expression of the zebrafish paired box gene pax [zf-b] during early neurogenesis. *Development* 113, 1193.

Kucenas, S., Takada, N., Park, H.-C., Woodruff, E., Broadie, K. and Appel, B. (2008). CNS-derived glia ensheath peripheral nerves and mediate motor root development. *Nat. Neurosci.* 11, 143–151.

Kwon, H.-J., Bhat, N., Sweet, E. M., Cornell, R. A. and Riley, B. B. (2010). Identification of Early Requirements for Preplacodal Ectoderm and Sensory Organ Development. *PLoS Genet.* 6, e1001133.

Ladher, R. K. (2000). Identification of Synergistic Signals Initiating Inner Ear Development. *Science* 290, 1965–1967.

Ladher, R. K. (2005). FGF8 initiates inner ear induction in chick and mouse. *Genes Dev.* 19, 603–613.

Ladher, R. K., O'Neill, P. and Begbie, J. (2010). From shared lineage to distinct functions: the development of the inner ear and epibranchial placodes. *Development* 137, 1777–1785.

Lassiter, R. N. T., Dude, C. M., Reynolds, S. B., Winters, N. I., Baker, C. V. H. and Stark, M. R. (2007). Canonical Wnt signaling is required for ophthalmic trigeminal placode cell fate determination and maintenance. *Dev. Biol.* 308, 392–406.

Lassiter, R. N. T., Stark, M. R., Zhao, T. and Zhou, C. J. (2013). Signaling mechanisms controlling cranial placode neurogenesis and delamination. *Dev. Biol.*

Lee, S. A., Shen, E. L., Fiser, A., Sali, A. and Guo, S. (2003). The zebrafish forkhead transcription factor Foxi1 specifies epibranchial placode-derived sensory neurons. *Development* 130, 2669.

Lee, Y., Grill, S., Sanchez, A., Murphy-Ryan, M. and Poss, K. D. (2005). Fgf signaling instructs position-dependent growth rate during zebrafish fin regeneration. *Development* 132, 5173.

Léger, S. and Brand, M. (2002). Fgf8 and Fgf3 are required for zebrafish ear placode induction, maintenance and inner ear patterning. *Mech. Dev.* 119, 91–108.

Li, H.-S., Yang, J.-M., Jacobson, R. D., Pasko, D. and Sundin, O. (1994). Pax-6 Is First Expressed in a Region of Ectoderm Anterior to the Early Neural Plate: Implications for Stepwise Determination of the Lens. *Dev. Biol.* 162, 181–194.

Li, B., Kuriyama, S., Moreno, M. and Mayor, R. (2009). The posteriorizing gene Gbx2 is a direct target of Wnt signalling and the earliest factor in neural crest induction. *Dev. Camb. Engl.* 136, 3267–3278.

Litsiou, A., Hanson, S. and Streit, A. (2005). A balance of FGF, BMP and WNT signalling positions the future placode territory in the head. *Development* 132, 4051.

Lleras-Forero, L., Tambalo, M., Christophorou, N., Chambers, D., Houart, C. and Streit, A. (2013). Neuropeptides: Developmental Signals in Placode Progenitor Formation. *Dev. Cell* 26, 195–203.

Ma, Q., Chen, Z., Barrantes, I. del B., Pompa, J. L. de la and Anderson, D. J. (1998). neurogenin1 Is Essential for the Determination of Neuronal Precursors for Proximal Cranial Sensory Ganglia. *Neuron* 20, 469–482.

Mackereth, M. D., Kwak, S. J., Fritz, A. and Riley, B. B. (2005). Zebrafish pax8 is required for otic placode induction and plays a redundant role with Pax2 genes in the maintenance of the otic placode. *Development* 132, 371.

Mahoney Rogers, A. A., Zhang, J. and Shim, K. (2011). Sprouty1 and Sprouty2 limit both the size of the otic placode and hindbrain Wnt8a by antagonizing FGF signaling. *Dev. Biol.* 353, 94–104.

Manuel, M., Georgala, P. A., Carr, C. B., Chanas, S., Kleinjan, D. A., Martynoga, B., Mason, J. O., Molinek, M., Pinson, J., Pratt, T., et al. (2006). Controlled overexpression of Pax6 in vivo negatively autoregulates the Pax6 locus, causing cell-autonomous defects of late cortical progenitor proliferation with little effect on cortical arealization. *Development* 134, 545–555.

Maroon, H., Walshe, J., Mahmood, R., Kiefer, P., Dickson, C. and Mason, I. (2002). Fgf3 and Fgf8 are required together for formation of the otic placode and vesicle. *Development* 129, 2099–2108.

Marques, S. R., Lee, Y., Poss, K. D. and Yelon, D. (2008). Reiterative roles for FGF signaling in the establishment of size and proportion of the zebrafish heart. *Dev. Biol.* 321, 397–406.

Martin, B. L. and Kimelman, D. (2011). Canonical Wnt signaling dynamically controls multiple stem cell fate decisions during vertebrate body formation. *Dev. Cell* in press,.

Martin, B. L. and Kimelman, D. (2012). Canonical Wnt Signaling Dynamically Controls Multiple Stem Cell Fate Decisions during Vertebrate Body Formation. *Dev. Cell* 22, 223–232.

Matteoli, G. and Boeckxstaens, G. E. (2012). The vagal innervation of the gut and immune homeostasis. *Gut*.

McAvoy, J. W., Chamberlain, C. G., de Longh, R. U., Hales, A. M. and Lovicu, F. J. (1999). Lens development. *Eye* 13, 425–437.

McCabe, K. L. and Bronner-Fraser, M. (2008). Essential role for PDGF signaling in ophthalmic trigeminal placode induction. *Development* 135, 1863–1874.

McCabe, K. L. and Bronner-Fraser, M. (2009). Molecular and tissue interactions governing induction of cranial ectodermal placodes. *Dev. Biol.* 332, 189–195.

McCabe, K. L., Sechrist, J. W. and Bronner-Fraser, M. (2009). Birth of ophthalmic trigeminal neurons initiates early in the placodal ectoderm. *J. Comp. Neurol.* 514, 161–173.

McCarroll, M. N., Lewis, Z. R., Culbertson, M. D., Martin, B. L., Kimelman, D. and Nechiporuk, A. V. (2012). Graded levels of Pax2a and Pax8 regulate cell differentiation during sensory placode formation. *Development*.

McMahon, A. P. and Moon, R. T. (1989). int-1--a proto-oncogene involved in cell signalling. *Dev. Camb. Engl.* 107 Suppl, 161–167.

Memi, F., Abe, P., Cariboni, A., MacKay, F., Parnavelas, J. G. and Stumm, R. (2013). CXC Chemokine Receptor 7 (CXCR7) Affects the Migration of GnRH Neurons by Regulating CXCL12 Availability. *J. Neurosci.* 33, 17527–17537.

Metz, H. and Wray, S. (2010). Use of Mutant Mouse Lines to Investigate Origin of Gonadotropin-Releasing Hormone-1 Neurons: Lineage Independent of the Adenohypophysis. *Endocrinology* 151, 766–773.

Modrell, M. S., Bemis, W. E., Northcutt, R. G., Davis, M. C. and Baker, C. V. H. (2011). Electrosensory ampullary organs are derived from lateral line placodes in bony fishes. *Nat. Commun.* 2, 496.

Mohammadi, M., Olsen, S. K. and Ibrahimi, O. A. (2005). Structural basis for fibroblast growth factor receptor activation. *Cytokine Growth Factor Rev.* 16, 107–137.

Nannapaneni, R., Behari, S., Todd, N. V. and Mendelow, A. D. (2005). Retracing "Ondine's Curse". [Miscellaneous Article]. *Neurosurg. August 2005* 57, 354–363.

Nechiporuk, A. and Raible, D. W. (2008). FGF-Dependent Mechanosensory Organ Patterning in Zebrafish. *Science* 320, 1774–1777.

Nechiporuk, A., Linbo, T. and Raible, D. W. (2005). Endoderm-derived Fgf3 is necessary and sufficient for inducing neurogenesis in the epibranchial placodes in zebrafish. *Development* 132, 3717.

Nechiporuk, A., Linbo, T., Poss, K. D. and Raible, D. W. (2006). Specification of epibranchial placodes in zebrafish. *Development* 134, 611–623.

Nikaido, M., Doi, K., Shimizu, T., Hibi, M., Kikuchi, Y. and Yamasu, K. (2007a). Initial specification of the epibranchial placode in zebrafish embryos depends on the fibroblast growth factor signal. *Dev. Dyn.* 236, 564–571.

Nikaido, M., Doi, K., Shimizu, T., Hibi, M., Kikuchi, Y. and Yamasu, K. (2007b). Initial specification of the epibranchial placode in zebrafish embryos depends on the fibroblast growth factor signal. *Dev. Dyn.* 236, 564–571.

Nilsson, S. and Holmgren, S. (1994). *Comparative Physiology and Evolution of the Autonomic Nervous System*. 1st ed. Harwood Academic Publishers.

Nissen, R. M., Yan, J., Amsterdam, A., Hopkins, N. and Burgess, S. M. (2003). Zebrafish foxi one modulates cellular responses to Fgf signaling required for the integrity of ear and jaw patterning. *Development* 130, 2543.

Northcutt, R. G. and Muske, L. E. (1994). Multiple embryonic origins of gonadotropin-releasing hormone (GnRH) immunoreactive neurons. *Brain Res. Dev. Brain Res.* 78, 279–290.

Norton, W. H. J., Ledin, J., Grandel, H. and Neumann, C. J. (2005). HSPG synthesis by zebrafish Ext2 and Extl3 is required for Fgf10 signalling during limb. *Development* 132, 4963–4973.

Nusse, R. and Varmus, H. E. (1982). Many tumors induced by the mouse mammary tumor virus contain a provirus integrated in the same region of the host genome. *Cell* 31, 99–109.

Nüsslein-Volhard, C. and Wieschaus, E. (1980). Mutations affecting segment number and polarity in Drosophila. *Nature* 287, 795–801.

Ohyama, T. and Groves, A. K. (2004a). Generation of Pax2-Cre mice by modification of a Pax2 bacterial artificial chromosome. *Genesis* 38, 195–199.

Ohyama, T. and Groves, A. K. (2004b). Expression of mouse Foxi class genes in early craniofacial development. *Dev. Dyn.* 231, 640–646.

Ohyama, T., Mohamed, O. A., Taketo, M. M., Dufort, D. and Groves, A. K. (2006). Wnt signals mediate a fate decision between otic placode and epidermis. *Development* 133, 865–875.

Padanad, M. S. and Riley, B. B. (2011). Pax2/8 proteins coordinate sequential induction of otic and epibranchial placodes through differential regulation of foxi1, sox3 and fgf24. *Dev. Biol.* 351, 90–98.

Padanad, M. S., Bhat, N., Guo, B. and Riley, B. B. (2012). Conditions that influence the response to Fgf during otic placode induction. *Dev. Biol.* 364, 1–10.

Pardal, R. and López-Barneo, J. (2002). Low glucose–sensing cells in the carotid body. *Nat. Neurosci.* 5, 197–198.

Park, B. Y. and Saint-Jeannet, J. P. (2008). Hindbrain-derived Wnt and Fgf signals cooperate to specify the otic placode in Xenopus. *Dev. Biol.* 324, 108–121.

Pfeffer, P. L., Gerster, T., Lun, K., Brand, M. and Busslinger, M. (1998). Characterization of three novel members of the zebrafish Pax2/5/8 family: dependency of Pax5 and Pax8 expression on the Pax2. 1 (noi) function. *Development* 125, 3063.

Pfeffer, P. L., Payer, B., Reim, G., Magliano, M. P. di and Busslinger, M. (2002). The activation and maintenance of Pax2 expression at the mid-hindbrain boundary is controlled by separate enhancers. *Development* 129, 307–318.

Phillips, B. T., Bolding, K. and Riley, B. B. (2001). Zebrafish fgf3 and fgf8 Encode Redundant Functions Required for Otic Placode Induction. *Dev. Biol.* 235, 351–365.

Phillips, B. T., Storch, E. M., Lekven, A. C. and Riley, B. B. (2004). A direct role for Fgf but not Wnt in otic placode induction. *Development* 131, 923.

Picker, A., Scholpp, S., B\öhli, H., Takeda, H. and Brand, M. (2002). A novel positive transcriptional feedback loop in midbrain-hindbrain boundary

development is revealed through analysis of the zebrafish pax2. 1 promoter in transgenic lines. *Development* 129, 3227.

Pieper, M., Eagleson, G. W., Wosniok, W. and Schlosser, G. (2011). Origin and segregation of cranial placodes in< i> Xenopus laevis</i>. *Dev. Biol.* 257–275.

Purves, D., Augustine, G. J., Fitzpatrick, D., Katz, L. C., LaMantia, A.-S., McNamara, J. O. and Williams, S. M. (2001). The Otolith Organs: The Utricle and Sacculus.

Quinn, J. C., West, J. D. and Hill, R. E. (1996). Multiple functions for Pax6 in mouse eye and nasal development. *Genes Dev.* 10, 435–446.

Radosevic, M., Robert-Moreno, A., Coolen, M., Bally-Cuif, L. and Alsina, B. (2011). Her9 represses neurogenic fate downstream of Tbx1 and retinoic acid signaling in the inner ear. *Development* 138, 397–408.

Raible, F. and Brand, M. (2001). Tight transcriptional control of the ETS domain factors Erm and Pea3 by Fgf signaling during early zebrafish development. *Mech. Dev.* 107, 105–117.

Ramón-Cueto, A. and Avila, J. (1998). Olfactory ensheathing glia: properties and function. *Brain Res. Bull.* 46, 175–187.

Reifers, F., Bohli, H., Walsh, E. C., Crossley, P. H., Stainier, D. and Brand, M. (1998). Fgf8 is mutated in zebrafish acerebellar (ace) mutants and is required for maintenance of midbrain-hindbrain boundary development and somitogenesis. *Development* 125, 2381–2395.

Reisine, H., Simpson, J. I. and Henn, V. (1988). A Geometric Analysis of Semicircular Canals and Induced Activity in Their Peripheral Afferents in the Rhesus Monkey. *Ann. N. Y. Acad. Sci.* 545, 10–20.

Riccomagno, M. M. (2005). Wnt-dependent regulation of inner ear morphogenesis is balanced by the opposing and supporting roles of Shh. *Genes Dev.* 19, 1612–1623.

Riccomagno, M. M., Takada, S. and Epstein, D. J. (2005). Wnt-dependent regulation of inner ear morphogenesis is balanced by the opposing and supporting roles of Shh. *Genes Dev.* 19, 1612–1623.

Rinkwitz, S., Bober, E. and Baker, R. (2001). Development of the vertebrate inner ear. *Ann. N. Y. Acad. Sci.* 942, 1–14.

Ruf, R. G., Xu, P.-X., Silvius, D., Otto, E. A., Beekmann, F., Muerb, U. T., Kumar, S., Neuhaus, T. J., Kemper, M. J., Raymond, R. M., et al. (2004). SIX1

mutations cause branchio-oto-renal syndrome by disruption of EYA1–SIX1–DNA complexes. *Proc. Natl. Acad. Sci. U. S. A.* 101, 8090–8095.

Sagasti, A., O'Brien, G. S., Rieger, S., Martin, S. M., Cavanaugh, A. M. and Portera-Cailliau, C. (2009). Two-photon axotomy and time-lapse confocal imaging in live zebrafish embryos. *J. Vis. Exp.*

Sahly, I., Andermann, P. and Petit, C. (1999). The zebrafish eya1 gene and its expression pattern during embryogenesis. *Dev. Genes Evol.* 209, 399–410.

Saint-Germain, N. (2004). Specification of the otic placode depends on Sox9 function in Xenopus. *Development* 131, 1755–1763.

Sakaguchi, T., Kuroiwa, A. and Takeda, H. (2001). A novel sox gene, 226D7, acts downstream of Nodal signaling to specify endoderm precursors in zebrafish. *Mech. Dev.* 107, 25–38.

Sato, N., Meijer, L., Skaltsounis, L., Greengard, P. and Brivanlou, A. H. (2003). Maintenance of pluripotency in human and mouse embryonic stem cells through activation of Wnt signaling by a pharmacological GSK-3-specific inhibitor. *Nat. Med.* 10, 55–63.

Schimmenti, L. A. (2011). Renal coloboma syndrome. *Eur. J. Hum. Genet.*

Schlessinger, J. (2000). Cell Signaling by Receptor Tyrosine Kinases. *Cell* 103, 211–225.

Schlosser, G. (2003). Hypobranchial placodes in Xenopus laevis give rise to hypobranchial ganglia, a novel type of cranial ganglia. *Cell Tissue Res.* 312, 21–29.

Schlosser, G. (2005). Evolutionary origins of vertebrate placodes: insights from developmental studies and from comparisons with other deuterostomes. *J. Exp. Zoolog. B Mol. Dev. Evol.* 304, 347–399.

Schlosser, G. (2006). Induction and specification of cranial placodes. *Dev. Biol.* 294, 303–351.

Schlosser, G. and Ahrens, K. (2004). Molecular anatomy of placode development in Xenopus laevis. *Dev. Biol.* 271, 439–466.

Schlosser, G. and Northcutt, R. G. (2000). Development of neurogenic placodes in Xenopus laevis. *J. Comp. Neurol.* 418, 121–146.

Schwob, J. E. (2002). Neural regeneration and the peripheral olfactory system. *Anat. Rec.* 269, 33–49.

Shima, T., Znosko, W. and Tsang, M. (2009). The characterization of a zebrafish mid-hindbrain mutant, mid-hindbrain gone (mgo). *Dev. Dyn.* 238, 899–907.

Siegfried, E. and Perrimon, N. (1994). Drosophila wingless: a paradigm for the function and mechanism of Wnt signaling. *BioEssays News Rev. Mol. Cell. Dev. Biol.* 16, 395–404.

Simeone, A., Acampora, D., Gulisano, M., Stornaiuolo, A. and Boncinelli, E. (1992). Nested expression domains of four homeobox genes in developing rostral brain. *Nature* 358, 687–690.

Sjödal, M., Edlund, T. and Gunhaga, L. (2007). Time of Exposure to BMP Signals Plays a Key Role in the Specification of the Olfactory and Lens Placodes Ex Vivo. *Dev. Cell* 13, 141–149.

Solomon, K. S. and Fritz, A. (2002). Concerted action of two dlx paralogs in sensory placode formation. *Development* 129, 3127–3136.

Solomon, K. S., Kudoh, T., Dawid, I. B. and Fritz, A. (2003). Zebrafish foxi1 mediates otic placode formation and jaw. *Development* 130, 929–940.

Spemann, H. (1901). Uber Correlationen in der Entwickelung des Auges. *Verh. Anat. Ges.* 61–79.

Steventon, B., Mayor, R. and Streit, A. (2012). Mutual repression between Gbx2 and Otx2 in sensory placodes reveals a general mechanism for ectodermal patterning. *Dev. Biol.* 367, 55–65.

Stoick-Cooper, C. L., Weidinger, G., Riehle, K. J., Hubbert, C., Major, M. B., Fausto, N. and Moon, R. T. (2006). Distinct Wnt signaling pathways have opposing roles in appendage regeneration. *Development* 134, 479–489.

Stooke-Vaughan, G. A., Huang, P., Hammond, K. L., Schier, A. F. and Whitfield, T. T. (2012). The role of hair cells, cilia and ciliary motility in otolith formation in the zebrafish otic vesicle. *Development* 139, 1777–1787.

Streit, A. (2002). Extensive cell movements accompany formation of the otic placode. *Dev. Biol.* 249, 237–254.

Streit, A. (2004a). Early development of the cranial sensory nervous system: from a common field to individual placodes. *Dev. Biol.* 276, 1–15.

Streit, A. (2004b). Early development of the cranial sensory nervous system: from a common field to individual placodes. *Dev. Biol.* 276, 1–15.

Subach, F. V., Patterson, G. H., Renz, M., Lippincott-Schwartz, J. and Verkhusha, V. V. (2010). Bright Monomeric Photoactivatable Red

Fluorescent Protein for Two-Color Super-Resolution sptPALM of Live Cells. *J. Am. Chem. Soc.* 132, 6481–6491.

Sun, S. K., Dee, C. T., Tripathi, V. B., Rengifo, A., Hirst, C. S. and Scotting, P. J. (2007). Epibranchial and otic placodes are induced by a common Fgf signal, but their subsequent development is independent. *Dev. Biol.* 303, 675–686.

Suster, M. L., Abe, G., Schouw, A. and Kawakami, K. (2011). Transposon-mediated BAC transgenesis in zebrafish. *Nat. Protoc.* 6, 1998–2021.

Takuma, N., Sheng, H. Z., Furuta, Y., Ward, J. M., Sharma, K., Hogan, B. L., Pfaff, S. L., Westphal, H., Kimura, S. and Mahon, K. A. (1998). Formation of Rathke's pouch requires dual induction from the diencephalon. *Development* 125, 4835–4840.

Theveneau, E., Steventon, B., Scarpa, E., Garcia, S., Trepat, X., Streit, A. and Mayor, R. (2013). Chase-and-run between adjacent cell populations promotes directional collective migration. *Nat. Cell Biol.* 15, 763–772.

Thisse, B. and Thisse, C. (2005). Functions and regulations of fibroblast growth factor signaling during embryonic development. *Dev. Biol.* 287, 390–402.

Tripathi, V.-B., Ishii, Y., Abu-Elmagd, M. M. and Scotting, P. J. (2009). The surface ectoderm of the chick embryo exhibits dynamic variation in its response to neurogenic signals. *Int. J. Dev. Biol.* 53, 1023–1033.

Tsai, B. P., Hoverter, N. P. and Waterman, M. L. (2012). Blending hippo and WNT: sharing messengers and regulation. *Cell* 151, 1401–1403.

Valenta, T., Hausmann, G. and Basler, K. (2012). The many faces and functions of ?-catenin. *EMBO J.* 31, 2714–2736.

Vemaraju, S., Kantarci, H., Padanad, M. S. and Riley, B. B. (2012). A Spatial and Temporal Gradient of Fgf Differentially Regulates Distinct Stages of Neural Development in the Zebrafish Inner Ear. *PLoS Genet.* 8, e1003068.

Vendrell, V., Carnicero, E., Giraldez, F., Alonso, M. T. and Schimmang, T. (2000). Induction of inner ear fate by FGF3. *Development* 127, 2011–2019.

Von Bartheld, C. S. (2004). The terminal nerve and its relation with extrabulbar "olfactory" projections: Lessons from lampreys and lungfishes. *Microsc. Res. Tech.* 65, 13–24.

Von Kupffer, C. (1891). The development of the cranial nerves of vertebrates. *J. Comp. Neurol.* 1, 246–264.

Wada, H., Dambly-Chaudière, C., Kawakami, K. and Ghysen, A. (2013). Innervation is required for sense organ development in the lateral line system of adult zebrafish. *Proc. Natl. Acad. Sci.* 110, 5659–5664.

Wakamatsu, Y. (2011). Mutual repression between Pax3 and Pax6 is involved in the positioning of ophthalmic trigeminal placode in avian embryo. *Dev. Growth Differ.* 53, 994–1003.

Waldman, E. H., Castillo, A. and Collazo, A. (2007). Ablation studies on the developing inner ear reveal a propensity for mirror duplications. *Dev. Dyn.* 236, 1237–1248.

Wang, K., Zhang, Y., Li, X., Chen, L., Wang, H., Wu, J., Zheng, J. and Wu, D. (2008). Characterization of the Kremen-binding site on Dkk1 and elucidation of the role of Kremen in Dkk-mediated Wnt antagonism. *J. Biol. Chem.* 283, 23371–23375.

Washausen, S., Obermayer, B., Brunnett, G., Kuhn, H.-J. and Knabe, W. (2005). Apoptosis and proliferation in developing, mature, and regressing epibranchial placodes. *Dev. Biol.* 278, 86–102.

Wawersik, S., Purcell, P., Rauchman, M., Dudley, A. T., Robertson, E. J. and Maas, R. (1999). BMP7 Acts in Murine Lens Placode Development. *Dev. Biol.* 207, 176–188.

Weinstein, D. C. and Hemmati-Brivanlou, A. (1997). Neural induction in Xenopus laevis: evidence for the default model. *Curr. Opin. Neurobiol.* 7, 7–12.

Westerfield, M. (2000). *The Zebrafish Book. A Guide for the Laboratory Use of Zebrafish (Danio rerio)*. 4th ed. Eugene, OR: University of Oregon Press.

Whitlock, K. E. and Westerfield, M. (2000). The olfactory placodes of the zebrafish form by convergence of cellular fields at the edge of the neural plate. *Development* 127, 3645–3653.

Wilson, P. A. and Hemmati-Brivanlou, A. (1995). Induction of epidermis and inhibition of neural fate by Bmp-4. *Nature* 376, 331–333.

Winklbauer, R. (1989). Development of the lateral line system in Xenopus. *Prog. Neurobiol.* 32, 181–206.

Wray, S. (2002). Development of gonadotropin-releasing hormone-1 neurons. *Front. Neuroendocrinol.* 23, 292–316.

Wray, S., Grant, P. and Gainer, H. (1989). Evidence that cells expressing luteinizing hormone-releasing hormone mRNA in the mouse are derived from progenitor cells in the olfactory placode. *Proc. Natl. Acad. Sci.* 86, 8132–8136.

Wright, T. J. and Mansour, S. L. (2003). Fgf3 and Fgf10 are required for mouse otic placode induction. *Development* 130, 3379–3390.

Xu, P.-X., Adams, J., Peters, H., Brown, M. C., Heaney, S. and Maas, R. (1999). Eya1-deficient mice lack ears and kidneys and show abnormal apoptosis of organ primordia. *Nat. Genet.* 23, 113–117.

Xu, H., Dude, C. M. and Baker, C. V. H. (2008). Fine-grained fate maps for the ophthalmic and maxillomandibular trigeminal placodes in the chick embryo. *Dev. Biol.* 317, 174–186.

Yamamoto, H., Ihara, M., Matsuura, Y. and Kikuchi, A. (2003). Sumoylation is involved in beta-catenin-dependent activation of Tcf-4. *EMBO J.* 22, 2047–2059.

Zeiske, E., Kasumyan, A., Bartsch, P. and Hansen, A. (2003). Early development of the olfactory organ in sturgeons of the genus Acipenser: a comparative and electron microscopic study. *Anat. Embryol. (Berl.)* 206, 357–372.

Zelarayan, L. C., Vendrell, V., Alvarez, Y., Domínguez-Frutos, E., Theil, T., Alonso, M. T., Maconochie, M. and Schimmang, T. (2007a). Differential requirements for FGF3, FGF8 and FGF10 during inner ear development. *Dev. Biol.* 308, 379–391.

Zelarayan, L. C., Vendrell, V., Alvarez, Y., Domínguez-Frutos, E., Theil, T., Alonso, M. T., Maconochie, M. and Schimmang, T. (2007b). Differential requirements for FGF3, FGF8 and FGF10 during inner ear development. *Dev. Biol.* 308, 379–391.

Zhang, Y., Knosp, B. M., Maconochie, M., Friedman, R. A. and Smith, R. J. H. (2004). A Comparative Study of Eya1 and Eya4 Protein Function and Its Implication in Branchio-oto-renal Syndrome and DFNA10. *J. Assoc. Res. Otolaryngol.* 5, 295–304.

Zhang, X., Ibrahimi, O. A., Olsen, S. K., Umemori, H., Mohammadi, M. and Ornitz, D. M. (2006). Receptor specificity of the fibroblast growth factor family. The complete mammalian FGF family. *J. Biol. Chem.* 281, 15694–15700.

McCarroll, Matthew Nicholas

Massachusetts General Hospital &
Harvard Medical School
Department of Medicine
Cardiovascular Research Center
149 13th Street
Charlestown MA 02129
Cellular phone: 971 221 4642
lab phone: 617 726 6470
email: mccarroll79@gmail.com

Education

2008-2014	Ph.D. in Cell and Developmental Biology Oregon Health & Science University, Portland, OR.
June 2005	B.S. in Micro and Molecular Biology Portland State University, Portland, OR.
June 2002	Transfer Credits Rogue Community College, Grants Pass, OR.

Research Experience

Present	Massachusetts General Hospital & Harvard Medical School, Charlestown, MA Cardiovascular Research Center Postdoctoral Fellow *High-throughput behavioral screening assays*
2009-2014	Oregon Health & Science University, Portland, OR Department of Cell and Developmental Biology Graduate Student *Development of cranial sensory systems in zebrafish*
2008-2009	Oregon Health & Science University, Portland, OR Department of Biochemistry Graduate Student *Monoketone analogs of curcumin play a role in inhibiting the Fanconi Anemia pathway*
2005-2008	Oregon Health & Science University, Portland, OR Vaccine and Gene Therapy Institute Research Assistant II *HIV accessory protein VPU's role in immune evasion*

2004-2005 Oregon Health & Science University, Portland, OR
Vaccine and Gene Therapy Institute
Research Assistant I
Immunofluorescent Imaging of KSHV latency proteins in infected human endothelial cells

Awards

2010-2012 Program in Molecular and Cellular Bioscience graduate training grant T32 NIH

2013 Oregon Health & Science University Brain Institute graduate fellowship

2013 Honorable mention for best graduate student talk. Northwest Developmental Biology Meeting, Friday Harbor, WA.

Professional Societies

2009 Member, American Association for the Advancement of Science

2009 Member, Society for Developmental Biology

Teaching and Mentoring Experience

2003-2004 Oregon Museum of Science and Industry, Portland, OR.
Science educator in life sciences exhibit: Answered general questions from visitors, put together workshops to assist young students in learning basic biological concepts.

2011 Oregon Health & Science University, Portland, OR.
Equity Summer Research Program: Taught a summer intern student basic molecular biology techniques in my thesis lab, assisted this student in constructing and presenting a poster presentation.

2012 Oregon Health & Science University, Portland, OR.
Saturday Academy: Designed course work to instruct high school students about the basics of embryonic neural development, this lecture was accompanied by a lab section where the students were exposed to current research techniques used to study neural development.

Publications

1. **McCarroll MN**, Nechiporuk AV. Fgf3 and Fgf10 work in concert to promote maturation of the epibranchial placodes. *Plos One*. **8**, e85087. 2013.

2. Harding M, **McCarroll MN**, McGraw H, Nechiporuk A. (in review) Ear and lateral line of vertebrates: organization and development (version 3.0). *John Wiley & Sons*, *Ltd.* 2013.

3. **McCarroll MN**, Lewis ZR, Culbertson MD, Martin BL, Kimelman D, Nechiporuk A. (2012). Graded levels of Pax2a and Pax8 regulate cell differentiation during sensory placode formation. *Development*. 2012 Aug:10:1242.
This article was recommended by Faculty of 1000 Biology.

4. Igor Landais, Sanne Hiddingh, Aiming Sun, **Matthew McCarroll**, Mitchell S. Turker, James P. Snyder and Maureen E. Hoatlin. (2009). Monoketone analogs of curcumin, a new class of Fanconi anemia pathway inhibitors. *Mol Cancer*. 2009 Dec;8:133.

4. Douglas JL, Viswanathan K, **McCarroll MN**, Gustin JK, Früh K, Moses AV. (2009). Vpu directs the degradation of the human immunodeficiency virus restriction factor BST-2/Tetherin via a βTrCP-dependent mechanism. *J Virol*. 2009 Aug;83(16):7931-47. Epub 2009 Jun 10.

Presentations

1. **McCarroll MN**, Nechiporuk A. Fgf3 and Fgf10 work in concert to induce the epibranchial placodes. 2013, Northwest Developmental Biology Meeting, Friday Harbor, WA.

2. **McCarroll MN**, Lewis ZR, Culbertson MD, Martin BL, Kimelman D, Nechiporuk A. Graded levels of Pax2a and Pax8 regulate cell differentiation during sensory placode formation. 2012, International Conference on Zebrafish Development and Genetics, Madison, WI.

3. **McCarroll MN**, Lewis ZR, Culbertson MD, Martin BL, Kimelman D, Nechiporuk A. Graded levels of Pax2a and Pax8 regulate cell differentiation during sensory placode formation. 2012, Northwest Developmental Biology Meeting, Friday Harbor, WA.

4. Landais I, **McCarroll MN**, Sun S, Turker M, Lloyd S, Snyder JP, Hoatlin ME. Identification of potent inhibitors of the Fanconi anemia pathway using a novel cell-free assay. Platform presentation, *Keystone Symposium on Targeted Cancer Therapies*, March 2009, Whistler, Canada.

5. Douglas JL, Viswanathan K, **McCarroll MN**, Gustin JK, Früh K, Moses AV. HIV Vpu Complexes with βTrCP to Direct the Degradation of the Virus Release Inhibitor BST-2 (Tetherin). *11th annual International Meeting of the Institute of Human Virology*, September 2008, Baltimore, Maryland.

CELL & DEVELOPMENTAL BIOLOGY

Ph.D. Thesis Defense:

Origin of Cranial Sensory Systems

Matthew N McCarroll
Alex Nechiporuk Lab
Oregon Health & Science University

Friday, January 17, 2014
2:00 PM
Vollum Institute M1441